The role of N-Hydroxypipecolic acid in plant resistance

Inaugural-Dissertation

zur Erlangung des Doktorgrades
der Mathematisch-Naturwissenschaftlichen Fakultät
der Heinrich-Heine-Universität Düsseldorf

vorgelegt von

Anika Schnake
aus Bremen

Düsseldorf, März 2024

aus dem Institut für Molekulare Ökophysiologie der Pflanzen
der Heinrich-Heine-Universität Düsseldorf

Gedruckt mit der Genehmigung der
Mathematisch-Naturwissenschaftlichen Fakultät der
Heinrich-Heine-Universität Düsseldorf

Berichterstatter:

1. Prof. Dr. Jürgen Zeier

2. Prof. Dr. Laura Rose

Tag der mündlichen Prüfung: 08.07.2025

Summary

In the defense against pathogens, plants have developed a multi-layered immune system based on a complex signaling network. The establishment of defense reactions against pathogens in plants is controlled by defense related metabolites and plant hormones. Major players in this complicated network are the phenolic compound salicylic acid (SA) and the recently discovered secondary metabolite N-hydroxypiplecolic acid (NHP). Both compounds accumulate at the local site of a pathogen infection and in systemic parts of plants and thereby trigger changes in plants metabolome which can lead to a local or systemic acquired resistance (LAR or SAR) against the attacking pathogen. The role of SA has been studied extensively in mono- and dicotyledonous plant species, but the role of NHP is not fully elucidated yet. The aim of this thesis is to gain further inside in role of NHP in plant immunity.

To identity the role of NHP in local in systemic immune responses of mono- and dicotyledonous plant species, the infection with suitable pathogens of two monocotyledonous and two dicotyledonous plant species was studied. Via GC-MS analyses the metabolite accumulation after infections was evaluated in time-courses and showed the accumulation of NHP after the infection in all studied plant species. Furthermore, the exogenous application of NHP was shown to lead to an induced resistance in the monocotyledonous model organism *Brachypodium distachyon* and in dicotyledonous crop plants (cucumber and tobacco). Additionally, the establishment of SAR in the monocot *B. distachyon* was demonstrated in parallel with a local and systemic accumulation of SA and NHP suggesting similar mechanisms in the induction of local and systemic immune responses of *B. distachyon* and the studied dicotyledonous plant species. Although diverse strategies to accumulate NHP have been identified in the studied mono- and dicotyledonous plant species, the here presented results suggest a conserved function of NHP in plants immunity.

Plant pathogens developed diverse lifestyle and infection strategies to infest their hosts and dependent on these strategies are categorized as biotrophic, hemibiotrophic or necrotrophic pathogens. While biotrophic pathogens feed on living plant tissue and therefore dependent on a living plant host, necrotrophic pathogens in contrast kill their hosts to feed on lysed plant cells. Hemibiotrophic pathogens have an initial biotrophic phase and then switch to a necrotrophic phase. So far, the biosynthesis of NHP and its immune inducing function against biotrophic and hemibiotrophic pathogens has been demonstrated in the dicotyledonous plant

model organism *Arabidopsis thaliana*, but the role of NHP in the defense against pathogens with a necrotrophic lifestyle is not clear. Therefor this thesis aimed to investigate the role of NHP in the plant defense against pathogens with various lifestyle and infection strategies using *A. thaliana* as model organism.

GC-MS analyses of the with biotrophic (oomycete), hemobiotrophic (bacteria or fungi) and necrotrophic (fungi) pathogens infected *A. thaliana* plants revealed a NHP accumulation in local and systemic leaves. To investigate if NHP also covers resistance to those pathogens exogenous NHP was applied to *A. thaliana* plants. It was demonstrated that NHP induces resistance in *A. thaliana* against pathogens with biotrophic, hemibiotrophic and necrotrophic lifestyles. It was further demonstrated that bacterial and fungal infections of *A. thaliana* leaves trigger an efficient SAR against hemibiotrophic and necrotrophic fungi dependent on a functional SA and NHP signaling pathways. Studies have shown that SA induced defense responses induce resistance to biotrophic and hemibiotrophic pathogens. This study indicates that NHP in contrast plays an important role of in the defense against pathogens of all investigated lifestyles including the necrotrophic pathogen *Botrytis cinerea*. Via fluorescence microscopy this study further showed that callose deposition are formed in *A. thaliana* leaves after NHP treatments which might contribute to the mechanisms of NHP induced resistance against the investigated pathogens with various lifestyles.

This study supports that the establishment of local and systemic defense responses of plants against pathogens requires the interplay of the small metabolites SA and NHP. It has been demonstrated in several studies that SA induced defense responses are regulated by NON-EXPRESSOR OF PR GENES 1 (NPR1) proteins. The direct binding of NPR1 with SA was demonstrated in recent studies. Since SA and NHP exhibit similar structural characteristics and NHP was demonstrated to induce SA-independent but NPR1-dependent activation of immunty it was investigated if a Strep-NPR1 protein expressed in *Escherichia coli* can bind NHP by the same mechanisms as it binds SA. The here presented results demonstrate that NPR1 does not bind NHP. These findings suggest the existence of yet unknown mechanisms in the NHP induced activation of SA-independent NPR1 mediated immune responses.

Zusammenfassung

Zur Abwehr von Krankheitserregern haben Pflanzen ein vielschichtiges Immunsystem entwickelt, das auf einem komplexen Signalnetzwerk beruht. Die Einleitung von Abwehrreaktionen gegen Krankheitserreger in Pflanzen wird durch abwehrrelevante Sekundärmetabolite und Pflanzenhormone gesteuert. Hauptakteure in diesem komplizierten Netzwerk sind die Phenolverbindung Salicylsäure (SA) und der kürzlich entdeckte Sekundärmetabolit N-Hydroxypiplecolsäure (NHP). Beide Verbindungen reichern sich am lokalen Ort einer Pathogeninfektion und in systemischen Pflanzenteilen an und lösen dadurch Veränderungen im Metabolom der Pflanzen aus, die zu einer lokalen oder systemischen erworbenen Resistenz (LAR oder SAR) gegen das angreifende Pathogen führen können. Die Rolle von SA wurde bei monokotylen und dikotylen Pflanzenarten eingehend untersucht, die Rolle von NHP ist jedoch noch nicht vollständig geklärt. Ziel dieser Arbeit ist es, die Rolle der NHP in der Pflanzenimmunität besser zu verstehen.

Um die Rolle der NHP bei lokalen und systemischen Immunantworten von ein- und zweikeimblättrigen Pflanzenarten zu ermitteln, wurde die Infektion mit geeigneten Pathogenen von zwei monokotylen und zwei dikotylen Pflanzenarten untersucht. Durch GC-MS Analysen wurde die Akkumulation von ausgewählten Metaboliten nach der Infektion in Zeitverläufen untersucht und zeigte die Akkumulation von NHP nach der Infektion in allen untersuchten Pflanzenarten. Darüber hinaus wurde gezeigt, dass die exogene Zugabe von NHP zu einer induzierten Resistenz in dem monokotylen Modellorganismus *Brachypodium distachyon* und in dikotylen Nutzpflanzen (Gurke und Tabak) führt. Außerdem wurde die Etablierung der SAR im monokotylen *B. distachyon* parallel zu einer lokalen und systemischen Akkumulation von SA und NHP nachgewiesen, was auf ähnliche Mechanismen bei der Induktion lokaler und systemischer Immunreaktionen von *B. distachyon* und den untersuchten dikotylen Pflanzenarten schließen lässt. Obwohl bei den untersuchten mono- und dikotylen Pflanzenarten unterschiedliche Strategien zur Akkumulation von NHP identifiziert wurden, deuten die hier vorgestellten Ergebnisse auf eine konservierte Funktion von NHP in den pflanzlichen Abwehrmechanismen hin.

Pflanzenpathogene haben verschiedene Lebens- und Infektionsstrategien entwickelt, um ihre Wirte zu befallen und abhängig von diesen Strategien werden sie in biotrophe, hemibiotrophe oder nekrotrophe Pathogene eingeteilt. Während sich biotrophe Erreger von lebendem

Pflanzengewebe ernähren und daher auf einen lebenden Pflanzenwirt angewiesen sind, töten nekrotrophe Erreger dagegen ihre Wirte ab, um sich von lysierten Pflanzenzellen zu ernähren. Hemibiotrophe Erreger durchlaufen zunächst eine biotrophe Phase und gehen dann in eine nekrotrophe Phase über. Bisher wurde die Biosynthese von NHP und seine immuninduzierende Funktion gegen biotrophe und hemibiotrophe Pathogene in dem dikotylen Pflanzenmodellorganismus *Arabidopsis thaliana* nachgewiesen, die Rolle von NHP bei der Abwehr von Pathogenen mit nekrotropher Lebensweise ist jedoch unklar. Ziel dieser Arbeit war es daher, die Rolle der NHP bei der pflanzlichen Abwehr von Pathogenen mit unterschiedlicher Lebensweise und Infektionsstrategien am Beispiel von *A. thaliana* zu untersuchen.

GC-Analysen der mit biotrophen (Oomyceten), hemobiotrophen (Bakterien oder Pilze) und nekrotrophen (Pilze) Krankheitserregern infizierten *A. thaliana* Pflanzen ergaben eine NHP-Akkumulation in lokalen und systemischen Blättern im Infektionsverlauf. Um zu untersuchen, ob NHP auch die Resistenz gegen diese Krankheitserreger abdeckt, wurde exogenes NHP auf *A. thaliana* Pflanzen appliziert. Es wurde gezeigt, dass NHP in *A. thaliana* eine Resistenz gegen Krankheitserreger mit biotropher, hemibiotropher und nekrotropher Lebensweise induziert. Ferner wurde gezeigt, dass bakterielle und pilzliche Infektionen von *A. thaliana* Blättern eine effiziente SAR gegen hemibiotrophe und nekrotrophe Pilze auslösen, die von funktionierenden SA- und NHP-Signalwegen abhängt. Studien haben gezeigt, dass SA-induzierte Abwehrreaktionen eine Resistenz gegen biotrophe und hemibiotrophe Krankheitserreger auslösen. Diese Studie zeigt, dass NHP dagegen eine wichtige Rolle bei der Abwehr von Pathogenen aller untersuchten Lebensformen einschließlich nekrotropher Pathogene spielt. Mittels Fluoreszenzmikroskopie konnte in dieser Studie außerdem gezeigt werden, dass sich in den Blättern von *A. thaliana* nach NHP-Behandlungen Kalloseablagerungen bilden, welche zu den Mechanismen der NHP induzierten Resistenz gegen die untersuchten Krankheitserreger mit unterschiedlichen Lebensweisen beitragen könnten.

Diese Studie belegt, dass die Etablierung lokaler und systemischer Abwehrreaktionen von Pflanzen gegen Krankheitserreger das Zusammenspiel der Metaboliten SA und NHP erfordert. In mehreren Studien wurde nachgewiesen, dass SA-induzierte Abwehrreaktionen durch NON-EXPRESSOR OF PR GENES 1 (NPR1) Proteine reguliert werden. Auch die direkte Bindung von

SA an NPR1 wurde in kürzlich veröffentlichten Studien nachgewiesen. Da SA und NHP ähnliche strukturelle Eigenschaften aufweisen und NHP nachweislich eine SA-unabhängige NPR1-Aktivierung auslöst, wurde untersucht, ob ein in *Escherichia coli* exprimiertes Strep-NPR1 Protein NHP über die gleichen Mechanismen wie SA binden kann. Die hier vorgestellten Ergebnisse zeigen, dass NPR1 nicht NHP bindet, wie bereits in früheren Studien gezeigt wurde. Diese Ergebnisse deuten auf noch unbekannte Mechanismen bei der NHP-induzierten Aktivierung von SA-unabhängigen NPR1-vermittelten Immunantworten hin.

Content

1. Introduction

1.1. The broad spectrum of biotic plant stressors

Plants live in fast changing environments and through their sessile lifestyle are exposed to several abiotic stressors such as changing nutrient availability, temperature or light conditions. Additionally, plants are exposed to biotic stress such as the interaction with insects, microorganism, or other plants. Part of biotic stressors for plants is a broad spectrum of phytopathogenic microbes that use different feeding strategies in the interaction with their hosts. Plant pathogens are classified as biotrophic, necrotrophic and hemibiotrophic depending on their feeding strategies. Biotrophic pathogens grow in association with living host cells, utilizing their hosts metabolism to grow without causing injury to the host cells. In contrast, by producing phytotoxins necrotrophic pathogens kill their host cells to feed on the nutrients of the lysed tissue. However, many phytopathogens exhibit both lifestyles which is described as hemibiotrophy. Hemibiotrophic pathogens have an initial biotrophic phase, which varies in length, and a following switch to necrotrophy (Agrios, 1988). A detailed introduction to the lifestyle strategies of *Arabidopsis thaliana* infecting pathogens is given in PART II.

To defend against pathogens of various lifestyles plants evolved a multi-layered immune system that acts against the pathogens attack (Thordal-Christensen 2003, Jones and Dangl 2006, Spoel and Dong 2012). If a pathogen successfully overcomes the constitutive and inducible defense barriers of a host plant and therefore can cause disease, the interaction between pathogen and host is described as a compatible interaction (Glazebrook 2005). The outcome of a plant and microbe interaction is described as incompatible if the plants immune system successfully defends itself against the attack (Glazebrook 2005). In many plant microbe interactions, the successful infection of a pathogen fails due to the lacking adaption of the pathogen to the host as a fitting nutrient source which is described as non-host resistance (Thordal-Christensen 2003).

1.2. Principles of the innate plant immunity

To defend against pathogens plants developed constitutive and inducible defense barriers. Constitutive or structural barriers include trichomes on leaves and stem, chemicals that are constitutively present on the plant's surface, a distinct cuticle or particular cell wall reinforcements (Thordal-Christensen 2003, Vorwerk et al. 2004, Spoel and Dong 2012). These first constitutive barriers can be highly effective in the defense against herbivores. Handley and colleagues (2005) for example showed that a high trichome density on *A. thaliana* leaves negatively affects the oviparity, feeding and larval nutrition of the diamondback moth *Plutella xylostella*. Several studies have additionally demonstrated that constitutive barriers like the host surface topography and chemical composition are effective plant defense strategies against attacking microbes (Gow 1993). Hansjakob and his team (2011), for example, showed that the powdery mildew fungi *Blumeria graminis* fails to form appressoria on maize plants based on the composition of very-long-chain aldehydes in cuticular waxes. Likewise, changes of the *A. thaliana* cell wall composition confer enhanced resistance against *Botrytis cinerea* infections (Manabe et al. 2011), demonstrating that the success of a microbial pathogen can rely on the composition of the plants' cuticle waxes (Hansjakob et al. 2011).

In addition to these constitutive barriers, plants are equipped with inducible defense strategies against attacking microbes. The host's first action of induced defense starts when the pathogen is recognized by pattern recognition receptors (PRRs) on the host's cell surface (Ngou et al. 2022). These receptors can detect conserved pathogen-/damage-/microbe-/herbivore-associated molecular patterns (PAMP/DAMP/MAMP/HAMPs) via extracellular domains (Ngou et al. 2022) and are further recognized as PAMPs. Known PRRs are either receptor-like proteins (RLPs) or receptor-like kinases (RLKs) which are both localized at the plasma membrane and need co-receptors to transmit an immune signal (Boutrot and Zipfel 2017). Plant PRR proteins can perceive a wide range of PAMPs from bacteria, fungi, oomycetes, viruses and parasitic plants including peptides, lipids, peptidoglycans, polysaccharides, chitin and oligo-galacturonides (Ngou et al. 2022). *A. thaliana* for example recognizes the bacterial peptide flg22 via the LRR-RLKs AtFLS2 (Chinchilla et al. 2006). Moreover, in *A. thaliana* the lysin motif containing RLP *At*LYM1/3 recognizes peptidoglycans from bacterial cell walls (Willmann et al. 2011) whereas the lysin motif containing RLK *At*LYM2/4/5 perceives chitin from fungal cell walls (Wan et al. 2008). If PAMPs are detected

by PRRs, the host plant initiates a PAMP-triggered immunity (PTI), trying to halt and terminate the attacking pathogen's growth (Figure 1, Jones and Dangl, 2006, Ngou et al. 2022).

Successful pathogens suppress PTI by secreting effector proteins in the plants apoplast (Figure 1, Jones and Dangl, 2006). These effectors, also so called Avr proteins are encoded by *avirulence* (*Avr*) genes can interfere with PTI, resulting in an effector-triggered susceptibility (ETS) (Figure 1, Jones and Dangl, 2006). The Pseudomonas AvrPtoB effector for example is an E3 ubiquitin ligase that induces the degradation of FLS2 which is essential for flg22 triggered PTI in plants (Göhre et al. 2008). Thereby the effectors of Pseudomonas bacteria disable the plant to induce PTI by FLS2 recognition and establish the ETS. Likewise, the NIS1 effector of *Colletotrichum* fungi disrupts the plants' PTI signaling by targeting the receptor kinase complexes in *A. thaliana* and several other dicotylous and monocotyledonous plant species (Irieda et al. 2019).

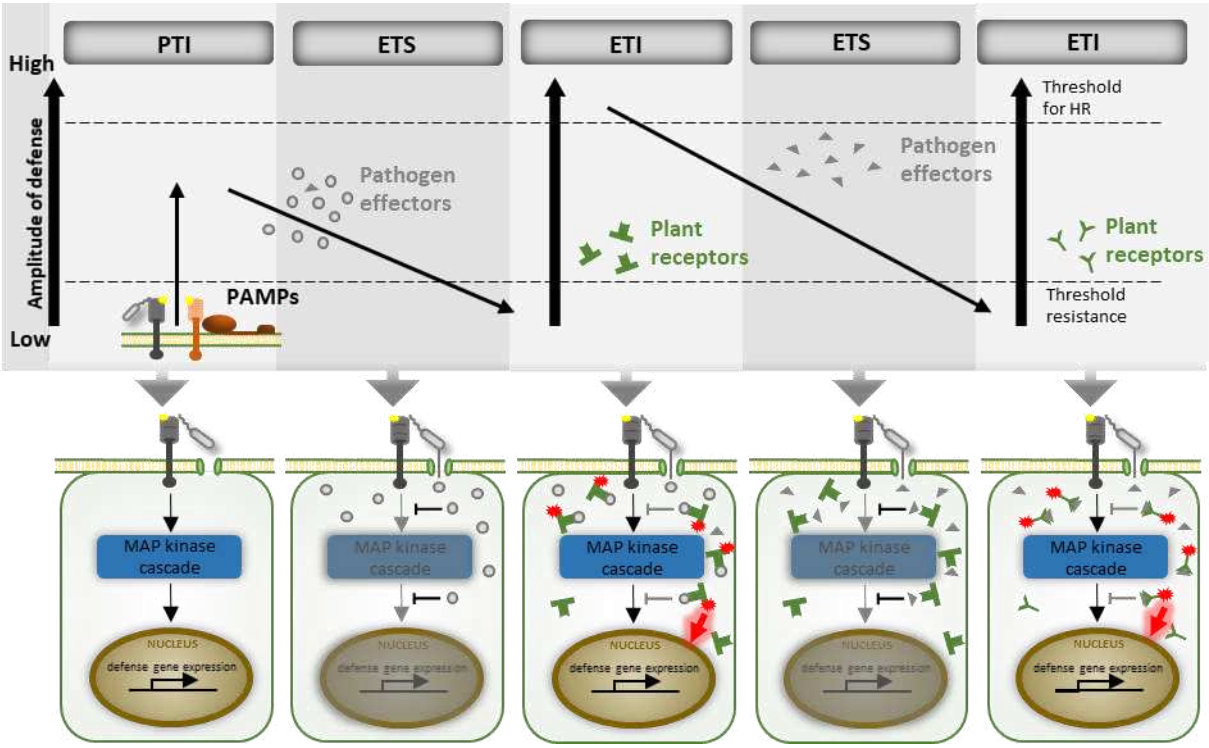

Figure 1: The zigzag model illustrating the amplitude of disease resistance and susceptibility of the plants immune system in the defence against pathogens. The host's first action of defense starts when the pathogen is recognized by PRRs on the host's cell surface. PRRs detect PAMPs. If PAMPs are detected, the host plant initiates a PTI, trying to halt and terminate the pathogen's growth. Pathogenic effector proteins can interfere with PTI, resulting in an ETS. Pathogens effectors that try to conquer PTI can be recognized by specific receptor proteins inside host cell, which are frequently encoded by *R* genes. This recognition leads to an ETI in the host which often results in localized cell death, limiting the spread of the infections. This Suppl. Figure 3s designed after Jones and Dangl (2006).

Abbrevations: PRRs = pattern recognition receptors; PAMP = pathogen-associated molecular pattern; PTI = PAMP-triggered immunity; ETS = an effector-triggered susceptibility; R = Resistance; ETI = effector-triggered immunity

Pathogens' effectors that try to conquer PTI are recognized by intracellular nucleotide-binding leucine-rich repeat (NB-LRR) receptor proteins, which are frequently encoded by resistance (*R*) genes (Jones and Dangl, 2006). This recognition leads to an effector-triggered immunity (ETI) in the host (Jones and Dangl, 2006). ETI results in localized cell death, often induced through the production of reactive oxygen species, called the hypersensitive response (HR) and is associated with the accumulation of defense related phytohormones (Ngou et al. 2022). Hence, the ETI is a faster and stronger version of the PTI. Recently, several NB-LRR receptor proteins have been identified in plants that can induce ETI by detecting effector proteins of bacteria, fungi, oomycetes, viruses, parasitic plants and herbivores (Ngou et al. 2022). The Pseudomonas AvrB effector is for example recognized intracellularly by *A. thaliana* TAO1 and RPM1, resulting in the activation of the ETI (Grant et al. 1995, Ashfield et al. 2004). Similarly, the effectors ATR1 and ATR5 of the oomycete *Hyaloperonospora arabidopsidis* (*Hpa*) are recognized by *A. thaliana* RPP1 and RPP5 respectively to trigger ETI in the host (Krasileva et al. 2010, Bailey et al. 2011).

Plants PRRs and R proteins trigger overlapping and unique signaling to deploy tightly regulated defense mechanisms against an attacking microbe, while being suppressed by the microbes Avr effectors (Ngou et al. 2022). Therefore, while the pathogen is under selection for new Avr isolates that conquer PTI and ETI, the host is under selection for individuals that have evolved *R* gene variants that can re-establish PTI and ETI (Thomma et al. 2011). Thus, plants and phytopathogens are in constant state of coevolution.

1.3. Systemic acquired resistance

The perception of pathogens by plant receptors activates conserved signaling to trigger a wide range of defense mechanisms at the site of infection (Glazebrook 2005). In addition to local PTI and ETI induced defense responses against a pathogen, the whole plant shoot is set into a state of elevated resistance, recognized as systemic acquired resistance (Mishina and Zeier 2007). Upon a local pathogen attack the expression of SAR associated genes and synthesis of defense related metabolites is activated in local and distal tissue (Bernsdorff et al. 2016). Thereby, plants in the SAR state can react faster and more effective to subsequent pathogen attacks (Mishina and Zeier 2007). In the following paragraphs relevant regulators in local plant

defense and SAR will be further discussed. A detailed introduction for the SAR in plants is given in PART I and PART II.

1.4. Regulators in local and systemic plant immunity

Upon the induction of the SAR state, plants express over 3,000 defense-associated genes in untreated systemic leaves triggering the accumulation of a diverse spectrum of primary and secondary metabolites (Gruner et al. 2013). Whereat primary metabolites are described as required for the plant development, secondary metabolites are not essential for these processes and their production is induced upon challenging conditions, such as an infection with pathogens (Dixon 2001). The small secondary metabolites, N-hydroxypipecolic acid (NHP) and salicylic acid (SA) accumulate in local plant tissue infected with biotrophic or hemibiotrophic pathogens and control the following establishment of SAR in distal leaves (Hartmann and Zeier 2019), while other accumulating secondary metabolites like phytoalexins possess direct antimicrobial effects (Bednarek and Osbourn 2009, Ahuja et al. 2012). In the following paragraphs further insight into the role of crucial regulators in plant immunity is given.

1.4.1. Salicylic acid (SA)

Since the early 1990s, when researchers discovered high SA levels in pathogen infected tobacco and cucumber plants (Malamy et al. 1990, Métraux et al. 1990) and the crucial role of SA in SAR in tobacco plants against TMV (Gaffney et al. 1993), SA has emerged as one the best studied metabolites in plant immunity. Upon the perception of an attacking pathogen, plants induced SA synthesis via the isochorismate synthase (ICS) and phenylalanine (Phe) ammonia-lyase (PAL) pathways. Both SA synthesis pathways originate from the shikimate pathway intermediate chorismite (CA) and are initiated in chloroplasts. In the first step of the PAL pathway chorismate mutase (CM) converts CA to prephenic acid (Pre) which after a few intermediate steps, including phenylpyruvate and phenylalanine, in this pathway is converted to Phe. Generated Phe is then converted to *trans*-cinnamic acid (*trans*-CiA) by the PAL enzyme while releasing NH_3 (Rohde et al. 2004). Via β-oxidation by 3-hydroxyacyl-CoA dehydrogenase and peroxisomal protein 1 (AIM1), *trans*-CiA can be further converted to benzoic acid (BA) as observed in *A. thaliana* and rice (Dempsey et al. 2011, Xu et al. 2017, Bussell et al. 2014). The synthesized benzoic acid is proposed to be converted to SA by benzoic acid 2-hydroxylase

(BA2H) (Dempsey et al. 2011). In model the organism *A. thaliana,* the pathogen induced SA synthesis is, however, facilitated via the ICS pathway to 90 % and only to 10 % via the PAL pathway, revealing a dispensable role for SA synthesized via the PAL pathway in the defense induced SA accumulation (Wildermuth et al. 2001, Garcion et al.2008).

In the first step of the ICS pathway, ICS1 converts CA to isochorismate (IC) in the chloroplast. Upon a pathogen infection the ICS1 expression was found to be upregulated in local and distal leaves (Wildermuth et al. 2001). Moreover, Wildermuth and colleges (2001) demonstrated that in *A. thaliana* a knockout of the ICS1 encoding gene *SA induction deficient 2* (*sid2*) results in the loss of SA accumulation. The ICS1 generated IC is transported from the chloroplast to the cytosol by ENHANCED DISESE SUSCEPTIBILITY 5 (EDS5) (Rekhter et al. 2019) (Figure 2). After pathogen contact, UV-C light treatment or exogenous SA application of *A. thaliana*, *EDS5* expression is induced (Nawrath 2002) and *A. thaliana eds5* knockout mutants show an enhanced susceptibility to Pseudomonas bacteria (Rogers and Ausubel et al. 1997), demonstrating the important role of EDS5 in plant immunity. In the cytosol the EDS5 generated IC is conjugated with glutamate to isochorismate-9-glutamate by avrPphB Susceptible 3 (PBS3) (Figure 2; Torrens-Spence et al. 2019). Nobuta and colleagues (2007) showed that *PBS3* expression, correlating with *ICS1* expression*,* is pathogen induced in *A. thaliana* and that the *pbs3* knockout mutant is compromised in the perception of SA, demonstrating a crucial role of PBS3 in SA mediated defense responses as a part of the SA biosynthesis machinery. In the final step of the ICS pathway SA is generated by spontaneously decays of isochorismate-9-glutamate (Torrens-Spence et al. 2019, Rekhter et al. 2019).

Modification of SA

To modulate and finetune the SA level during immune responses, SA can be modified resulting in inactive storage forms of SA (Dempsey et al. 2011). The glycosylation of SA leads to generation of SA 2-O-β-D-glucoside (SAG) or salicylate-glucose-ester (SGE) which are stored in the vacuole and thereby reduce the toxic effect of high SA levels synthesized in the cytosol (Dempsey et al. 2011). In *A. thaliana* the SA glycosyltransferases (SAGT) UGT74F1, UGT74F2 and UGT76B1 have been identified to facilitate the glycosylation of SA to SAG, whereas UGT74F2 generates SAG and SGE but is more active in SGE glycosylation (Dean and Delaney et al. 2008, Thompson et al. 2017). As recently demonstrated, UGT76B1 converts SA to SAG and facilitates the glycosylation of NHP to NHPG (Bauer et al. 2021). Another proposed SA

storage mechanism in *A. thaliana* is the hydroxylation of SA. Thereby, the SA hydroxylases SA 3-hydroxylase (S3H) and SA 5-hydroxylase (S5H) can convert SA to 2,3-dihydroxybenzoic acid (2,3-DHBA) and 2,5-dihydroxybenzoic acid (2,5-DHBA), respectively (Zhang et al. 2013, Zhang et al. 2017). These hydroxylated SA forms can be further glycosylated by UGT89A2 and UGT76D1 in *A. thaliana* (Chen et al. 2017, Huang et al. 2018). Although it was proposed that DHBAs might be SA storage forms and others might activate PR proteins independent of SA in *A. thaliana*, the role of DHBA and their glycosides in plant defense is not fully understood yet (Bartsch et al. 2010). In addition to glycosylation and hydroxylation SA can be methylated to MeSA by plants which enables SA a better membrane permeability and volatility (Chen et al. 2003).

SA mediated defense signaling

In the cytosol generated SA can directly bind to the SA receptor NONEXPRESSOR OF PR GENES1 (NPR1), which is then translocated to the nucleus to activate the expression of *PATHOGENESIS-RELATED* (*PR)* genes (Delaney et al. 1994, Wu et al. 2012, Ding et al.2018). Theses PR proteins are small proteins that can reduce disease in pathogen attacked host plants. It is proposed that some PR proteins exhibit direct antimicrobial features, but the targets of several PR-proteins have not yet been identified (van Loon et al. 2006). A detailed introduction to the mechanisms of NPR1 in plant immunity is given in PART III.

Several research groups showed that *A. thaliana* mutants with defects in SA biosynthesis and perception fail to establish SAR and are highly susceptible to pathogens caused by a disrupted PTI and ETI signal transduction and the impaired expression of PR proteins demonstrating the crucial role of SA in plant immunity (Gaffney et al. 1993, Nawrath and Métraux 1999, Wildermuth et al. 2001, Vlot et al. 2009, Bernsdorff et al. 2016). Early research by Gaffney and colleagues (1993) showed that genetic engineered tobacco plants that are unable to accumulate SA fail to manifest SAR, suggesting that SA plays a major role in the signal transduction of SAR and might be the mobile SAR signal. Grafting experiments of genetic engineered tobacco rootstocks that are unable to accumulate SA, were however able to induce SAR in wildtype scions, ruling out a role of SA as mobile SAR signal (Vernooij et al. 1994).

1.4.2. N-hydroxypipecolic acid (NHP)

The small metabolite NHP was just recently identified as a crucial player in local and systemic plant immunity (Hartmann et al. 2018, Chen et al. 2018). The accumulation of the biosynthetic NHP precursor pipecolic acid (Pip) after pathogen infection has been reported in several plant species decades ago (Pálfi and Dézsi 1968) but in 2012 Pip was first described as immune enhancing metabolite and required for SAR (Návarová et al. 2012). In *A. thaliana* the Pip induced resistance response seemed to depend on a functional FLAVIN-DEPENDENT MONOOXYGENASE1 (FMO1) protein and further metabolite analyses via GC-MS- and GC-FTIR confirmed that FMO1 converts Pip to NHP (Bernsdorff et al.2016, Hartmann et al. 2018). Several studies have investigated and elucidated the NHP biosynthesis pathway in the last decade.

Upon an attack of a pathogen, plants undergo changes in their metabolism to provide resources for defense responses resulting in an accumulation of amino acids like lysine (Figure 2; Vogel-Adghough et al. 2013, Zeier 2021). In its natural L-form, L-lysin can be converted to its corresponding α-oxoacid, ε-amino-a-ketocaproic acid (KAC) by the α-aminotransferase AGD2-LIKE DEFENSE RESPONSE PROTEIN1 (ALD1) which transfers the α-NH2 group of L-lysine to an acceptor like pyruvate (Hartmann et al. 2017, Zeier 2021). The ALD1 generated KAC spontaneously cyclizes to 1,2-dehydropipecolic acid (1,2-DP) and its tautomer 2,3-DP by water loss (Hartmann et al. 2017, Zeier 2021). These DP intermediates are further reduced to Pip by the NAD(P)H-dependent ketimine reductase SAR-DEFICIENT4 (SARD4). The NHP biosynthesis steps catalyzed by ALD1 and SARD4 are proposed to be located in the plastid while the final step of the NHP biosynthesis is suggested to be facilitated in the cytosol (Huang et al. 2019, Zeier et al. 2021). In this final step, FMO1 converts Pip to NHP via FAD- and NAD(P)H dependent hydroxylation (Hartmann et al. 2018, Chen et al. 2018). It is proposed that NHP is further glycosylated to finetune and modify NHP accumulation in defense reactions (Mohnike et al. 2021). Bauer et al. 2021 discovered that the UGT76B1, which glycosylates SA to SAG, mediates the glycosylation of NHP to an NHP-*O*-β-D-glucoside (NHPG) as well. Another proposed storage form of NHP is an NHP-glucose-ester (NHPGE) which was recently identified in *A. thaliana* leaf extracts via LC-MS-MS (Hartmann and Zeier 2019, Holmes et al. 2021).

NHP mediated defense signaling

Intensive research has demonstrated an upregulated *FMO1* and *ALD1* gene expression correlating with the accumulation of NHP and Pip after pathogen infection in local and systemic *A. thaliana* leaves (Návarová et al. 2012, Hartmann et al. 2018). The *A. thaliana ald1* and *fmo1* knockout mutants have been demonstrated to fail pathogen induced local and systemic accumulation of NHP and are unable to establish SAR (Bernsdorff et al. 2016, Hartmann et al. 2018, Song et al. 2004). The SAR state can be established in the *A. thaliana* wildtype Col-0 and rescued in *ald1* and *fmo1* plants by exogenous application of NHP, emphasizing an important role for NHP in local and systemic defense responses (Hartmann et al. 2018, Yildiz et al. 2021). It has been shown that local *Psm* infected leaves of *ald1* mutants can deploy defense responses in the local leaf, however in distal leaves transcriptional defense responses associated with SAR and SA accumulation are not established (Hartmann et al. 2018). Furthermore, Hartmann and colleagues revealed a fast NHP accumulation in systemic leaves prior to a SA accumulation after a local pathogen attack, indicating that NHP is transported to the systemic leaves and might not be synthesized *de novo* systemically. Hence, NHP is hypothesized as mobile SAR signal that is transported to systemic leaves where it triggers SA accumulation for a full systemic transcriptional reprogramming in SAR (Zeier 2021). Exogenous NHP leads to upregulation of biosynthesis genes indicating a feedback loop in its own biosynthesis.

1.4.3. Regulation and perception of the SA and NHP signaling pathways

In plants the accumulation of the small metabolites SA and NHP are crucial for an effective defense response to an attacking pathogen. In contrast to the *A. thaliana* wildtype, the *sid2* and *fmo1* knockout mutants are highly susceptible to (hemi)biotrophic pathogens and functional ICS1 and FMO1 enzymes are essential for a full SAR response in distal leaves (Bernsdorff et al. 2016, Hartmann 2018). Moreover, exogenously applied SA leads to an upregulation of the NHP biosynthesis genes *ALD1*, *SARD4* and *FMO1* while exogenously applied NHP results in the transcriptional upregulation of SA biosynthesis genes like ICS1 and EDS5, indicating a strong interplay between the SA und NHP biosynthesis pathways (Hartmann et al.2018, Hartmann et al.2019). Hence, several modulators for the positive and negative regulation of synergistic SA and NHP biosynthesis have been identified.

The direct interaction partners ENHANCED DISEASE SUSCEPTIBILITY 1 (EDS1) and PHYTOALEXIN DEFICIENT 4 (PAD4) transmit R protein induced defense responses in *A. thaliana* (Feys et al. 2001, Jing et al. 2011, Rietz et al. 2011, Zeier et al. 2021). The *eds1* and *pad4* deficient *A. thaliana* mutants showed reduced activation of SA and NHP biosynthesis genes like *ICS1*, *ALD1* and *FMO1* and are thus insufficient the accumulation of SA and NHP (Feys et al. 2001, Jing et al. 2011, Rietz et al. 2011, Hartmann et al. 2018, Zeier 2021). Moreover, Chang and colleagues (2019) showed that EDS1 is protected from degradation by PBS3 which is part of the SA biosynthesis machinery and thereby demonstrates a direct interplay of EDS1 with the SA biosynthesis. Independent of SA, EDS1 was also found to be involved in transcriptional regulation of *FMO1*, demonstrating the EDS1 interplay with the NHP biosynthesis (Bartsch et al. 2006). Likewise, PAD4 was shown to promote the Pip and NHP amplification loop, modulating the NHP accumulation in *A. thaliana* defense against pathogens (Návarová et al. 2012, Hartmann et al. 2018). Hence, EDS1 and PAD4 were identified as positive regulators of SA and NHP biosynthesis.

Other identified modulators in plant resistance that positively regulate SA and NHP biosynthesis synergistically are the transcription factors, SYSTEMIC ACQUIRED RESISTANCE DEFICIENT 1 (SARD1) and CALMODULIN-BINDING PROTEIN 60-LIKE G (CBP60g) (Huang et al. 2020). Redundant calmodulin binding transcription activator (CAMTA) transcription factors in contrast negatively regulate SARD1 and CBP60g and thereby negatively regulate the pathogen induced SA and NHP biosynthesis (Sun et al. 2020, Kim et al. 2020). After a pathogen infection CAMTA transcription factors, SARD1 and CBP60g regulate the expression of EDS1 and PAD4 in *A. thaliana* contributing to the SA and NHP homeostasis during the defense against the attacking pathogen (Sun et al. 2015). Other transcription factors positively regulate one pathway while they negatively regulate another pathway. The WRKY transcription factor 33 (WRKY33) for example negatively regulates SA accumulation and signaling (Birkenbihl et al. 2012, Liu et al. 2015), and positively regulates Pip accumulation by direct binding to the *ALD1* promoter in *A. thaliana* (Wang et al. 2018), revealing a complex network that finetunes the activation of the SA and NHP biosynthesis pathways. However, transcription factors in many cases are involved in the regulation of several signaling pathways in plant defense. WRKY33 for example is not only involved in the SA and NHP pathway regulation, but also regulates *PAD3* expression and thereby the accumulation of the phytoalexin camalexin (Mao et al. 2011). Likewise, EDS1 and PAD4 were shown to regulate pathogen inducible processes in

plants independent of the SA and NHP pathways, like the accumulation of phytoalexins and tocopherols in *A. thaliana* after a pathogen infection (Jirage et al. 1999, Song et al. 2004, Stahl et al. 2019). Moreover, studies of WRKY33 deficient and WRKY33 overexpressing mutants indicate a regulation of the jasmonic acid (JA)/ethylene (ET)- and abscisic acid (ABA)-mediated signaling by WRKY33 (Liu et al. 2015, Sham et al. 2017).

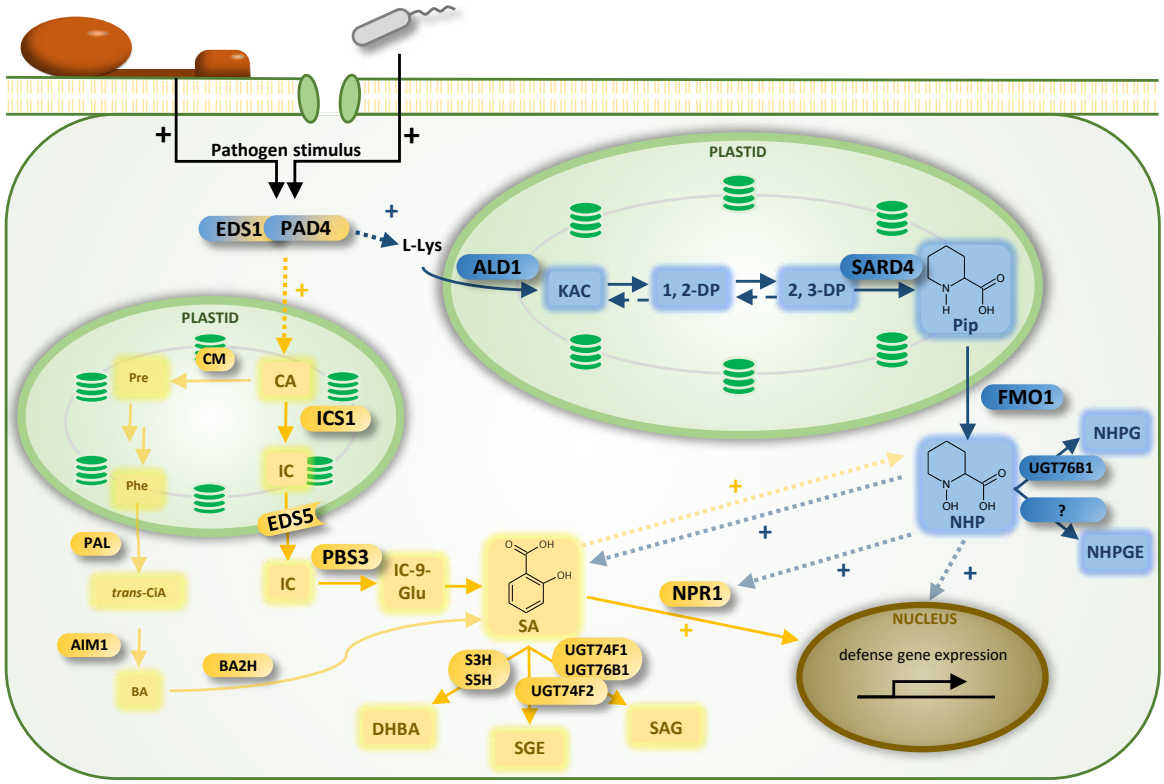

Figure 2: The biosynthesis pathways of SA and NHP and their interplay in the *A. thaliana* resistance.
Upon the perception of an attacking biotrophic or hemibiotrophic fungal or bacterial pathogen, EDS1 and PAD4 stimulate the SA (yellow) and NHP (blue) biosynthesis pathways. SA synthesis is induced via the ICS pathway (bright yellow) to 90% and via the PAL pathways (light yellow) to 10 % (Wildermuth et al. 2001). Both pathways originate from CA and are initiated in chloroplasts. In the PAL pathway, CA is converted to Pre by CM which is further converted to Phe over a few intermediate steps. Phe is transferred to the cytosol and converted to *trans*-CiA by PAL. AIM1 then converts *trans*-CiA to BA, which is further converted to SA by the BA2H. In the ICS pathway, CA is converted to IC by ICS1, which is then transported from the chloroplast to the cytosol via EDS5. In the cytosol IC is conjugated with glutamate to IC-9-Glu isochorismate-9-glutamate via the PBS3. Spontaneously decays of IC-9-Glu then generate SA. SA can be further modified. Examples are the hydroxylation by S3H or S5H to DHBAs or the glycosylation via UGTs to SGE and SAG. In the first step of the NHP biosynthesis pathway (blue), lysin is converted to KAC by ALD1. Generated KAC spontaneously cyclizes to 1,2-DP and 2,3-DP which ware further reduced to Pip by SARD4. In the final step, Pip is converted to NHP by FMO1 in the cytosol. NHP can be further glycosylated to NHPG or NHPGE. Continuous lines indicate biosynthesis pathways, dashed lines indicate positive/negative regulation.
Abbreviations: SA = salicylic acid; NHP = N-hydroxypipecolic acid; EDS1 = ENHANCED DISEASE SUSCEPTIBILITY 1; PAD4 = PHYTOALEXIN DEFICIENT 4; ICS = isochorismate synthase; Phe = phenylalanine; PAL = Phe ammonia-lyase; CA = chorismite; CM = chorismate mutase; Pre = prephenic acid ; *trans*-CiA = *trans*-cinnamic acid; AIM1 = 3-hyhroxyacyl-CoA dehydrogenase and peroxisomal protein 1; BA = benzoic acid; BA2H = benzoic acid 2-hydroxylase; IC = isochorismate, EDS5 = ENHANCED DISESE SUSCEPTIBILITY 5; IC-9-Glu = isochorismate-9-glutamate; PBS3 = avrPphB Susceptible 3; S3H = SA 3-hydroxylase, S5H = SA 5-hydroxylase; 2,x-DHBA = 2,x-dihydroxybenzoic acid; SGE = salicylate-glucose-ester, SAG = SA 2-O-β-D-glucoside; UGT = UDP-dependent glycosyl transferase; KAC = ε-amino-a-ketocaproic acid; ALD1 = AGD2-LIKE DEFENSE RESPONSE PROTEIN1; DP = dehydropipecolic acid; SARD4 = SAR-DEFICIENT4; Pip = Pipecolic acid, FMO1 = FLAVIN-DEPENDENT MONOOXYGENASE1, NHPG = NHP-*O*-β-D-glucoside; NHPGE = NHP-glucose-ester

Downstream of the SA and NHP biosynthesis, the accumulation of both metabolites activates local and systemic defense responses that are essential for SAR establishment. Yildiz and her team (2021) demonstrated the crucial role of NPR1 in the NHP induced local and systemic defense against (hemi)biotrophic pathogens in *A. thaliana*. The importance of NPR1 in plant defense was discovered in a *A. thaliana* mutant screening for mediators of SA perception and revealed that the *npr1* mutant fails to activate *PR1* gene expression resulting in an insufficient establishment of local or systemic defense responses (Cao et al. 1994, Shah et al. 1997). Shortly after the identification of NPR1, it was described as bonafide receptor for SA in the perception of SA induced expression of *PR* genes (Delaney et al. 1994, Wu et al. 2012, Ding et al. 2018). The crucial role of NHP and SA in the NPR1 dependent activation of PR gene expression might lead to the assumption that NPR1 acts as receptor for SA and NHP in plant defense. Yildiz and colleagues (2021) showed that the exogenous application of NHP leads to an elevated *PR* gene expression which was demonstrated to be disrupted in *sid2* and *npr1* mutant plants (Yildiz et al. 2021). These recent findings support the current model for SAR, which draws the role of NHP as mobile signal that is translocated from the point of infection to systemic leaves where it triggers the accumulation of SA. The perception of SA by NPR1 then leads to the essential expression of *PR* genes in SAR, which is thus dependent on a functional SA and NHP biosynthesis.

1.4.4. Jasmonic acid (JA), ethylene (ET) and abscisic acid (ABA) in the crosstalk of phytohormones

In plants the phytohormone JA plays a major role in immune responses after wounding and herbivory but it is also involved in the defense against pathogens (Wasternack and Hause 2013). The first steps of the JA biosynthesis take place in the chloroplast where α-linolenic acid is released from the chloroplast membrane by lipoxygenases and is further converted to 12-cis-oxo-phytodienoic-acid (OPDA) over intermediate steps involving an allene oxide synthase and an allene oxide cyclase (Feußner and Wasternack, 2002, Wasternack and Hause 2013). Generated OPDA is transported to the peroxisome where it is converted to JA by several intermediate steps facilitated by the OPDA reductase 3, CoA-ligation and beta-oxidation (Wasternack and Hause 2013). The synthesized JA is finally transported from the peroxisome to the cytosol.

In the cytosol JA must be conjugated with isoleucine to activate JA dependent transcriptional responses (Staswick 2007, Wasternack and Hause 2013). In the nucleus JA-Ile is recognized by the SCF^{COI1}-JAZ receptor complex consisting of the F-box protein CORONATINE-INSENSITIVE1 (COI1) and JASMONATE ZIM-DOMAIN (JAZ) proteins (Staswick 2007, Wasternack and Hause 2013). The formation of the JA-Ile-SCF^{COI1}-JAZ complex leads to the ubiquitination of JAZ proteins followed by the degradation of the 26S proteasome resulting in the activation of JA dependent transcriptional responses (Staswick 2007, Chini et al. 2007, Katsir et al. 2008, Wasternack and Hause 2013). In the absence of JA-Ile, JAZ proteins function as repressors of these JA dependent transcriptional responses (Thines et al. 2007, Thatcher et al. 2016). The JA dependent transcriptional defense splits in the MYC branch which is activated by wounding or herbivory and the JA/ethylene (ET) branch which is activated in plants after the infection of necrotrophic pathogens (Pieterse et al. 2009, Wasternack and Hause 2013). Although the JA signaling pathway is only activated by necrotrophic pathogens, it has been shown that JA is involved in the *A. thaliana* resistance against hemibiotrophic Pseudomonas bacteria, caused by the antagonistic regulation of the SA and JA signaling pathways (Gupta et al.2000, Clarke et al. 2000). In *coi1* mutant *A. thaliana* plants, that fail to activate JA dependent transcriptional responses, the SA dependent defense responses are hyperactivated resulting in an enhanced resistance against hemibiotrophic bacteria (Kloek et al. 2001). Likewise, an JA pathway activating elicitor treatment in tobacco revealed an inhibition of SA dependent gene expression demonstrating the conserved JA/SA antagonism in plant defense (Vidal et al. 1997).

In early responses of plants to a pathogen infection the production of the adenosyl-methionine derivate ET is enhanced and leads to the activation of defense responses (Abeles et al. 2012). In plants ET is moreover involved in the response to abiotic stress factors and in several developmental and physiological processes like germination, ripening and senescence (Bleecker and Kende 2000). In the successful plant defense against necrotrophic pathogens, it is suggested that JA and the gaseous plant hormone ET interact synergistically (van Loon et al. 2006). Microarray studies showed that half of the genes that were induced by ET treatment were likewise induced by JA treatment (Xu et al. 1994). In response to an *A. thaliana* infection with the necrotrophic fungi *Alternaria brassicicola* for example, ET and JA signaling are both required for the expression of *PLANT DEFENSIN 1.2* (*PDF1.2*) which is involved in the production of a defensin with antifungal effects (Xu et al. 1994, Penninckx et al. 1996, Kunkel

and Brooks 2002). The microarray study by Xu and colleagues (1994) however also revealed independent regulation of separate sets of genes by JA and ET and suggests that ET and SA mutually activate the expression of a set of genes. Furthermore, the *PR* gene expression in *A. thaliana* does not require functional ethylene signaling but upon ET exposure the SA induced expression of *PR1* is potentiated demonstrating a positive influence of ET on SA mediated defense responses (Lawton et al. 1994). Revealing the complex mechanisms underlying the regulation of phytohormones in the defense against pathogens, PR1 levels are increased in ET deficient mutants by ET indicating a negative regulation of SA mediated responses (Lawton et al. 1994). The limited data on the ET and SA interplay therefore supports negative as well as positive regulation between those pathways, which might enable plants to finetune defense response against pathogens (Kunkel and Brooks 2002).

In contrast to the intensively studied phytohormones JA, ET, SA or even NHP only little is known about the role of the phytohormone ABA in plants' defense against pathogens. The production of ABA is mainly associated with drought stress and other abiotic stressors in plants however research of the last 15 years revealed ABA as a major regulator of pathogen virulence (Kumar et al. 2019). From carotenoids derived ABA regulates the stomata closure in plants (Nambara and Marion-Poll 2005). Thereby ABA mediated stomatal closure prevents water loss to cope with abiotic stressors and provides a structural barrier against biotic attackers (Mauch-Mani and Mauch 2005, Kumar et al. 2019). Although ABA is rapidly produced in the first hour after pathogen infection in *A. thaliana*, the highest ABA levels were detected 48 hours post infection (hpi) (Gruner et al. 2013) suggesting a role for ABA in later infection stages. The interplay of ABA with other defense related pathways during pathogen infections has been demonstrated and reveals a role of ABA besides stomatal closure in defense resistance (Mauch-Mani and Mauch 2005). In *A. thaliana* high ABA concentrations strongly decrease the transcriptional levels of JA or ET responsive genes, which leads to a hypersensitivity against necrotrophic pathogens (Anderson et al. 2004). Corresponding, *A. thaliana* mutants deficient in ABA signaling showed an increase of the transcriptional levels of these JA or ET responsive genes pointing to an antagonistic interaction between the ABA and the JA/ET pathways (Anderson et al. 2004). Moreover, in tomato and rice an antagonistic regulation of the ABA and SA signaling pathways was observed (Thaler et al. 2004, Xu et al. 2013). The ABA/SA antagonism was demonstrated in *A. thaliana* since it was shown that SA protects its own bonafide receptor NPR1 form degradation while ABA mediates NPR1 from

degradation (Ding et al. 2016). Furthermore, exogenous ABA treatment was reported to suppress the biosynthesis of terpenoid phytoalexins (Henfling et al. 1980).

1.4.5. Phytoalexins

Phytoalexins are small secondary metabolites that are produced by plants upon the recognition of an invading pathogen and exhibit antimicrobial activities (VanEtten et al. 1994, Pedras et al. 2011). Phytoalexins that are constitutively produced and therefore are not related to the induced defense are referred to as phytoanticipins (VanEtten et al. 1994). Hence, it is possible that a substance is classified as phytoalexin in one species and as phytoanticipin in another species (Pedras et al. 2011).

In Brassicaceae over 40 phytoalexins have been identified with a particular prominence of tryptophan (Trp) derived indole alkaloids (Pedras et al. 2011, Ahuja et al. 2012). After an infection with bacteria, fungi or oomycetes, in *A. thaliana* the accumulation of phytoalexins like camalexin and other small indolic metabolites like ICA is induced (Glawischnig 2007). The biosynthesis of camalexin and ICA in the indolic secondary metabolism starts with the conversion of Trp to indole-3-acetaldoxime (IAOx) catalyzed by the two cytochrome P450 enzymes CYP79B2 and CYP79B3 (Zhao et al. 2002). From IAOx several pathways branch in the indolic secondary metabolism of *A. thaliana* to form camalexin, ICA, indole glucosinolates and other low molecular weight indoles in the defense against pathogens (Glawischnig 2007, Bender and Celenza, 2009; Sønderby et al., 2010; Bednarek, 2012). In the camalexin derived branch IAOx is converted to Indole-3-acetonitrile (IAN) by the cytochrome P450 enzyme CYP71A13 (Nafisi et al. 2007). However, another synthesis pathway from IAOx to IAN was demonstrated where Indol-3-ylmethylglucosinolateis is formed as an intermediate and can be hydrolysed to IAN (Kim et al. 2008, Pfalz et al. 2011). IAN is further converted to Cys-IAN by yet unknown mechanisms (Schuhegger et al. 2006). In the last steps of the camalexin biosynthesis, PAD3 converts Cys-IAN to Dihydrocamalexic acid (DHCA) and DHCA to camalexin (Schuhegger et al. 2006, Böttcher et al. 2009).

In Arabidopsis camalexin is one and best studied phytoalexins with direct antimicrobial activity via membrane-disruption (Pedras et al. 2011). Camalexin accumulates prominently in *A. thaliana* leaves infected with hemibiotrophic bacteria or necrotrophic fungi (Kliebenstein et al. 2005, Schuhegger et al. 2007, Glawischnig 2007). However, in the camalexin deficient *A. thaliana pad3* mutants, bacterial growth assays revealed a dispensable role of camalexin in

the resistance against hemibiotrophic Pseudomonas bacteria (Glazebrook and Ausubel 1994). Camalexin is rather suggested to play a major role in the *A. thaliana* resistance against necrotrophic fungi like *A. brassicicola*, *Botrytis cinerea*, and *Leptosphaeria maculans* or the hemibiotrophic oomycete *Phytophthora brassicae* (Thomma et al. 1999, Bohman et al. 2004, Ferrari et al. 2007, Schlaeppi et al. 2010). The influence of camalexin on the plant's resistance however relies on the specific plant pathogen interaction since plant pathogens like *Sclerotinia sclerotiorum* and *B. cinerea* have been demonstrated to detoxify camalexin for their advantage and the level of camalexin induction is dependent on the infected ecotype (Pedras et al. 2011).

In the ICA derived synthesis branch IAOx is converted to IAN which is converted to Indole-3-carbaldehyde (ICHO) by CYP71B6 (Böttcher et al. 2014). The *ARABIDOPSIS* ALDEHYDE OXIDASE 1 (AAO1) then catalyzes the conversion of ICHO to ICA (Böttcher et al. 2014). After a pathogen challenge generated ICA is esterified to the cell wall to form a barrier against invading pathogens (Forcat et al.2010) and is involved in β-aminobutyric acid induced defense priming (Gamir et al. 2012). A direct antimicrobial effect of ICA has however not been demonstrated yet but ICA derivatives like the brassicanals were identified to exhibit antimicrobial effects of phytoalexins (Pedras et al. 2011). ICA accumulation has been observed in the exudates of Arabidopsis roots infected with the necrotrophic oomycete *Pythium sylvaticum* (Bednarek et al. 2005). Additionally, ICA accumulates in *A. thaliana* in local and systemic leaves after a local Pseudomonas infection (Stahl et al. 2016). Stahl and colleagues (2016) however demonstrated that the systemic accumulation of ICA is dependent on a functional SAR signaling mediated by SA and NHP and is therefore not relevant for SAR establishment but a consequence of SAR. Like camalexin, ICA and its derivates contribute to the *A. thaliana* resistance against necrotrophic fungi (Pastor-Fernández et al. 2019, Böttcher et al. 2014). Hence, accumulating ICA in Pseudomonas induced SAR might prime plants for the defense against fungal pathogens. Besides camalexin and ICA several metabolites in the indolic secondary metabolism have been identified as resistance inducing metabolites in many different plant species (Pedras et al.2011).

In addition to those indolic secondary metabolites and their derivates with antimicrobial activities, the oxidative burst contributes to the defense against pathogens in plants with direct destructive effects on microbes (Bolwell and Daudi 2009). Upon the recognition of an attacking pathogen via PAMPs or Avr proteins, the accumulation of reactive oxygen species

(ROS) such as superoxide (O_2^-) or hydrogen peroxide (H_2O_2) leading to an oxidative burst have been observed (Auh and Murphy 1995, Grant et al.2000, Torres et al. 2006). Virulent pathogens that escape the PAMP or Avr mediated recognition of plants trigger the production of ROS in a much lower amplitude than avirulent, recognized pathogens, indicating a role for ROS in the introduction of defense against pathogens (Torres et al. 2006).

Besides the destructive effects on pathogens, the accumulation of ROS leads to the hypersensitive response (HR) in plants which results in cell death (Torres et al. 2006). The HR can thereby detract (hemi)biotrophic pathogens from their feeding source leading to an enhanced resistance or support necrotrophic pathogens in cell lyses leading to an enhanced susceptibility (Torres et al. 2006). Whether a pathogens growth is terminated by the destructive effects of ROS on the pathogen or by the plants' establishment of the HR is not fully understood and may be dependent on the specific pathogen-host interaction.

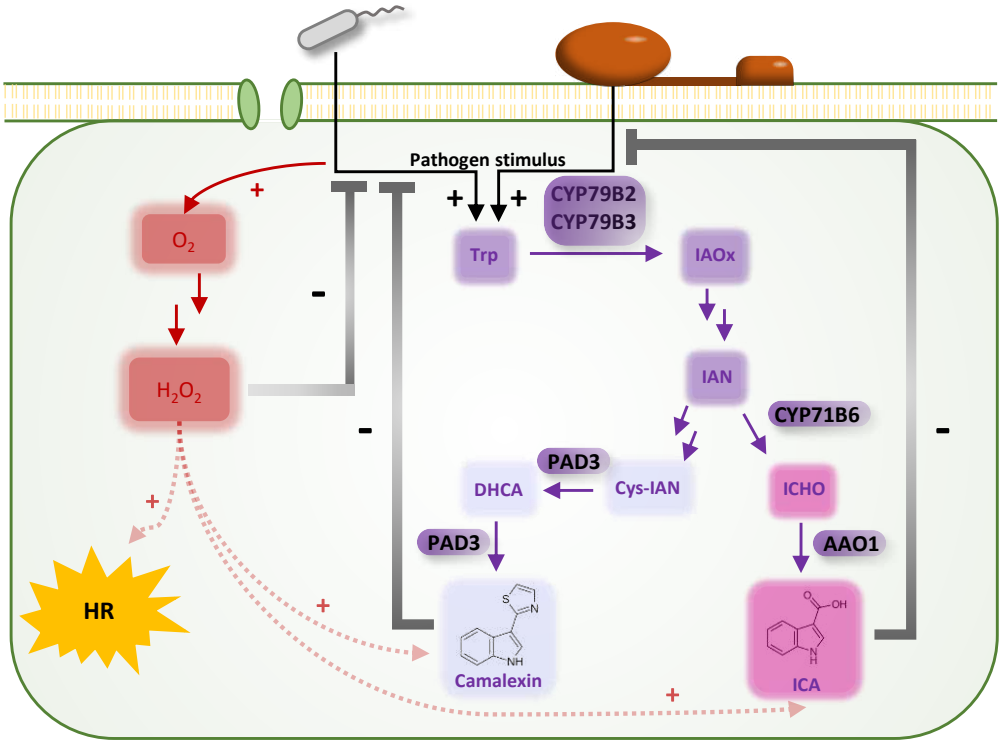

Figure 3: Simplified scheme of the camalexin and ICA biosynthesis pathways and reactive oxygen species induced defense responses. A pathogen stimulus activates these biosynthetic pathways and Trp is converted to IAOx by CYP79B2/CYP79B3. Over intermediate steps generated IAOx can be converted to IAN. In the camalexin derived biosynthesis branch (blue) IAN is converted to Cys-IAN which is further converted to DHCA by PAD3. The last step of the camalexin biosynthesis from DHCA to camalexin is as well facilitated by PAD3. In the ICA branch (pink) IAN is converted to ICHO by CYP71B6 which is then further converted to ICA by AAO1. A pathogen stimulus can as well lead to the recruitment of reactive oxygen species in the chloroplast inducing the expression of defense genes, the HR at the site of infection and the biosynthesis of Trp derived phytoalexins.
Abbreviations: Trp = tryptophan; IAOx = Indole-3-acetaldoxime; IAN = Indole-3-acetonitrile; ICHO = Indole-3-carbaldehyde; ICA = Indole-3-carboxylic acid; I3M = Indole-3-methyl-GSL; DHCA = R-Dihydro-camalexicacid; AAO1 = *ARABIDOPSIS* ALDEHYDE OXIDASE 1; PAD3 = PHYTOALEXIN DEFICIENT 3; CYP = Cytochrome P450; HR = hypersensitive response

In the defense against pathogen the interaction of ROS with defense related signaling pathways has been observed. In this manner, ROS and SA were demonstrated to act antagonistically in the regulation of the expansion of cell death at the site of infection (Torres et al. 2005). Moreover, ROS can be sensed by the ET receptor ETR1 to mediate the closure of stomata (Desikan et al. 2005) and additionally functions as an intermediate in ABA signaling during the closure of stomata (Pei et al. 2000). Furthermore, moderate levels of ROS were shown to induce the expression of the transcription factor WRKY33 conferring enhanced resistance towards *Chig* in *A. thaliana* (Sewelam et al. 2014).

1.5. Aims and form of this thesis

As described, SA and NHP are the major players in SAR (Hartmann and Zeier 2019). The interplay of SA and NHP in plant immunity activates diverse signaling pathways in local and systematic responses to an infection with pathogens, including the accumulation of phytoalexins and other indolic compounds (Zeier et al. 2021). To further elucidate the role of NHP in plant immunity, this thesis aims

I. to identify the role of NHP in local and systemic immune responses of mono- and dicotyledonous plant species in an infection with suitable pathogens.

II. to investigate the role of NHP in the *A. thaliana* defense against necrotrophic pathogens.

III. to investigate if NPR1 is a possible NHP receptor.

To investigate these aims this thesis is further divided in three parts whereat each part will engage one of these expressed aims.

2. PART I: The biosynthesis and immune function of NHP in mono- and dicotyledonous plants

2.1. Introduction

Since most of the in Part I presented results were published in the Schnake et al. 2020 paper, the introduction only states research available before this publication. As indicated in the discussion other studies have focused on comparable issues since our publication in 2020.

2.1.1. The conserved role of SA and NHP in the immune response of plants

In plant defense phytohormones act in diverse roles as they can exhibit direct antimicrobial effects against pathogens, can strengthen cell walls to form barriers against these microbial attackers or can induce and regulate the expression of defense genes (Ahuja et al. 2012, Berens et al. 2017, Chezem et al. 2017). In plants, SA and JA are the major phytohormones associated with defense responses against pathogens (Shigenaga and Argueso 2016, Berens et al. 2017). Whereat SA is a positive regulator of defense against biotrophic or hemibiotrophic pathogens, JA is a positive regulator of defense against pathogens with a necrotrophic lifestyle (Glazebrook 2005). However, most of the research on phytohormone regulation and crosstalk was conducted in the model organism *A. thaliana* and the applicability to other dicotyledonous and monocotyledonous plants is questionable. In dicotyledonous plants like tobacco, cucumber or *A. thaliana* for example, SA is mostly synthesized via the ICS pathway and neglectable amounts of SA are synthesized via the PAL pathway, but in soybeans ICS and PAL synthesized SA accumulates in equal levels (Pallas et al. 1996, Smith-Becker et al. 1998, Wildermuth et al. 2001, Shine et al. 2016). Moreover, studies of PAL deficient rice mutants indicated that the PAL pathway might be the major source of SA synthesis in monocotyledonous plants (Duan et al. 2014, Tonnessen et al. 2015). Attacking pathogens that are able to overcome the plants defense by interrupting the plants' SA biosynthesis are restricted to a host spectrum with similar regulatory mechanisms in the SA biosynthesis due to the great differences in the SA biosynthesis between various plant species (Djamei et al. 2011). These diverse mechanisms in the SA biosynthesis in different plant species however also reflect major differences in defense mechanisms of mono- and dicotyledonous plant species.

The accumulation of SA upon an infection with a biotrophic or hemibiotrophic pathogen was, additionally to *A. thaliana*, observed in dicots like potato, tobacco, pepper and strawberry (Halim et al. 2007, Vogel-Adghough et al. 2013, Kim and Hwang 2014, Yang et al.2011, Grellet-Bournonville et al. 2012), but not yet in monocots like rice or wheat (Balmer et al. 2012). An exception was demonstrated in a recent study by Lenk and colleagues (2019) in which a slight SA accumulation in leaf exudates of the monocot *H. vulgare* after an infection with Pseudomonas bacteria was observed, reflecting no unanimity in the role of SA in the pathogen induced immune responses of monocotyledonous plants in the current state of research. However, the exogenous application of SA or SA analogs was shown to induce resistance in monocots and dicots against a broad spectrum of biotrophic and hemibiotrophic pathogens (Grellet-Bournonville et al. 2012, Sugano et al. 2013, Ueno et al. 2015, Yang et al. 2011). This indicates a conserved role of SA as positive regulator in the immunity of monocots and dicots against biotrophic and hemibiotrophic pathogens even though the regulation of SA biosynthesis and accumulation does not underly these conserved mechanisms (Berens et al. 2017). Consistently, the SA receptor NPR1 is conserved in monocots and dicots revealing conserved mechanisms in the SA perception in angiosperms (Li et al.2004, Qiu et al. 2007, Yuan et al. 2007). In agreement, the in dicots well elucidated SA/JA antagonism was recently confirmed in wheat (Ding et al. 2016). The application of JA or its derivates was shown to induce resistance against necrotrophic pathogens in the dicotyledonous species *A. thaliana* and *Medicago truncatula*, and in the monocot rice (Spoel et al. 2007, Gaige et al. 2010, Taheri et al. 2010).

In mutants of dicots like Arabidopsis or tobacco that are deficient in SA biosynthesis full establishment of SAR fails, demonstrating the importance of SA in the systemic immunity of these plant species (Gaffney et al. 1993, Nawrath and Métraux 1999, Bernsdorff et al. 2016). Although, the successful establishment of SAR in barley and rice has been reported decades ago (Sticher 1997), the contemporary knowledge about the role of SA in the mechanisms of SAR in monocots is rare. For a long time, SA was discussed as the mobile signal in SAR which travels from local to systemic leaves where it activates immune responses for the defense against subsequent attacking pathogens. Rasmussen and his team (1991) for example detected SA in phloem exudates of cucumber leaves infected with Pseudomonas bacteria proposing a role for SA as mobile signal in SAR. In the same study, a time course analysis revealed that the actual SAR signal must act prior to the observed systemic SA accumulation

in cucumbers (Rasmussen et al. 1991). Additionally, grafting experiments with tobacco demonstrated that SA is not the mobile SAR activating signal (Vernooij et al. 1994). Since then, several metabolites like methyl salicylate, dehydroabietinal, azelaic acid and glycerol-3-phosphate have been proposed to act as mobile SAR signal but recently the lysine-derived metabolite NHP has emerged as possible SAR inducer (Shah and Zeier 2013, Hartmann et al. 2018, Hartmann und Zeier 2018, Chen et al. 2018, Hartmann et al. 2019).

The small metabolite NHP was first identified in the dicot model organism *A. thaliana* (Hartmann et al. 2018, Chen et al. 2018). Upon an infection with Pseudomonas bacteria the naturally occurring metabolite NHP accumulates in local and systemic *A. thaliana* leaves, while NHP is not produced in uninfected plants (Hartmann et al. 2018). The exogenous application of NHP enhances the *A. thaliana* resistance against hemibiotrophic *Psm* bacteria and the biotrophic oomycete *Hpa* revealing the resistance inducing function of NHP against a broad spectrum of pathogens (Chen et al. 2018, Hartmann et al. 2018). Additionally, NHP treatment of *A. thaliana* leaves resulted in an elevated resistance of systemic leaves indicating NHP could act as long-distance signal in SAR (Chen et al. 2018).

Recent phylogenetic studies based on *A. thaliana* sequences of genes involved in the NHP biosynthesis revealed homologs of these genes in a broad spectrum of monocotyledonous and dicotyledonous plant species promising a conserved function of NHP in SAR across the plant kingdom (Hartmann et al. 2018, Holmes et al. 2019). In agreement, the NHP precursor metabolite Pip has been identified to accumulate upon pathogen contact in several mono- and dicotyledonous plants, including Arabidopsis, soybean, tobacco, rice and barley (Návarová et al. 2012, Aliferis et al. 2014, Abeysekara et al. 2016, Vogel-Adghough et al. 2013, Adam et al., 2018, Palfi and Dezsi 1968, Lenk et al.2019). However, in *A. thaliana* Pip induces SAR in an FMO1 dependent manner, indicating that NHP and not Pip is the SAR inducing metabolite (Návarová et al. 2012, Bernsdorff et al. 2016). So far, the accumulation of NHP upon contact with a pathogen and its resistance inducing function were only determined in the dicotyledonous species Arabidopsis, tomato and tobacco (Hartmann et al. 2018, Holmes et al. 2019). These findings indicate an important role of the NHP biosynthesis pathway in immune responses to pathogens of monocotyledonous plant species that might be comparable to the role of the NHP biosynthesis pathway illustrated in dicotyledonous plants. Further research is necessary though to confirm this assumption.

To finetune SA and NHP mediated defense responses, plants like *A. thaliana* were shown to modify the phytohormones to establish homeostasis (described in detail in 1.4.). Only little is known about these mechanisms in other dicots and monocots though. In the monocot rice, infection with a blast fungus leads to the accumulation of SAG but not to SA accumulation indicating an important role for SAG in rice immunity on the basis of the prevention of SA accumulation (Umemura et al. 2009). Derivates of NHP were first identified in *A. thaliana* but comparable mechanisms in other angiosperms remain to be investigated.

2.1.2. Aims

In *A. thaliana*, SA and NHP synergistically confer resistance against a broad spectrum of phytopathogens. However, in *A. thaliana* NHP alone is sufficient to induce the SAR state and positively affects local and systemic SA accumulation (Hartmann et al. 2018, Chen et al. 2018). Holmes and colleagues (2019) demonstrated the Pseudomonas induced accumulation of NHP in the dicot crop plant including tomato, tobacco, and mustard indicating a conserved role of NHP in dicots. Additionally, the pathogen induced accumulation of Pip and the identification of homologs of the *A. thaliana* NHP biosynthesis genes in various monocotyledonous and dicotyledonous plant species indicate a putative functional NHP biosynthesis pathway in these species (Návarová et al. 2012, Aliferis et al. 2014, Abeysekara et al. 2016, Vogel-Adghough et al. 2013, Adam et al., 2018, Palfi and Dezsi 1968, Lenk et al.2019, Hartmann et al.2018, Holmes et al. 2019). However, it remains unknown if NHP-associated immune responses are present in mono- and dicotyledonous plants.

Hence, this study aims to investigate the biosynthesis and immune function of NHP in local and systemic immune responses of mono- and dicotyledonous plant species. Therefore, two dicotyledonous (*Cucumis sativus*, *Nicotiana tabacum*) and two monocotyledonous (*Brachypodium distachyon*, *Hordeum vulgare*) species were infected with suitable hemibiotrophic fungal and bacterial pathogens and metabolite analyses were conducted. To gain further insight into the mechanisms of SAR, the metabolite analyses was additionally performed on local and systemic leaves and petiole exudates of cucumbers infected with bacteria. Moreover, the immune inducing effect of NHP was tested in the investigated dicotyledonous plant species and in *B. distachyon*. Since it is not known whether the in dicots identified molecular mechanisms of SAR and especially the role for SA in systemic immunity, can be applied to monocot plant species (Balmer et al. 2012, Dey et al. 2014), this study

additional aims to gain insight into the mechanisms of local and systemic resistance in monocots. Therefore, the systemic response of *B. distachyon* to a local bacterial infection was analyzed on the metabolite level and SAR establishment was tested with second bacterial infection of systemic leaves.

2.2. Results

2.2.1. *Pseudomonas syringae* pv. lachrymans induced metabolite accumulation in local and systemic *Cucumis sativus* leaves and petiole exudates

To evaluate the changes of resistance related metabolites in *C. sativus* after a pathogen attack, the first fully grown leaf of 3-week-old *C. sativus* plants were spray inoculated with a *Psl* solution (OD_{600} = 0.2) or with 10 mM $MgCl_2$ as a control treatment. To investigate the transport of metabolites to systemic leaves in *C. sativus*, petiole exudates (PE) were collected at the stems of the local inoculated and at the stems of the systemic, untreated leaves (Figure 4.A, 4.B). Like other Cucurbitaceae species, *C. sativus* is widely known for bleeding high amounts of phloem sap upon wounding which were rapidly collected with a filter paper (Figure 4.B). Samples were collected 1 dpi, 3 dpi and 5 dpi and analyzed via GC-MS to quantify resistance related metabolites in inoculated local and untreated systemic leaves and PE as well as the corresponding controls. The quantified amounts of defense related metabolites in leaves and PE are not comparable since the density of the PE were equaled to the density of water and might therefore not reflect correct amounts.

The defense related metabolite SA and its glucosides SAG and SGE were selected for quantification in *Psl* and $MgCl_2$ treated *C. sativus* plants. The results of the GC-MS analyses showed that a *Psl* inoculation elevated SA levels significantly in local leaves as well as in local and systemic PE samples compared to the $MgCl_2$ treatment, starting 3 dpi (Figure 4.C). However, the SA levels detected in systemic leaves of *Psl* treated plants equaled the SA levels detected in systemic leaves of $MgCl_2$ treated plants at all sampling timepoints (Figure 4.C). In *Psl* sprayed leaves significantly higher SA amounts were quantified than in $MgCl_2$ sprayed leaves 3 dpi (1.86 µg g^{-1} FW) and 5 dpi (1.30 µg g^{-1} FW) (Figure 4.C). In local PE samples of *Psl* treated plants, significantly higher SA levels were detected than in samples of $MgCl_2$ treated plants 3 dpi and 5 dpi. Thereby, in local PE samples of *Psl* treated plants sampled 3 dpi (5.33 µg g^{-1} FW) a significantly higher SA level was quantified than in local PE samples of *Psl* treated plants sampled 5 dpi (3.22 µg g^{-1} FW) (Figure 4.C). Systemic PE samples of *Psl* treated plants exhibited significantly higher SA levels than systemic PE samples of $MgCl_2$ treated plants at 3 dpi. Furthermore, in systemic PE samples of plants that were inoculated with *Psl*, detected SA levels were about half of those quantified in local PE samples (local PE, 3 dpi, *Psl* = 5.33 µg

g^{-1} FW; systemic PE, 3 dpi, *Psl* = 3.04 µg g^{-1} FW). No significant differences between the SA levels in systemic PE samples of plants that were inoculated with *Psl* samples 3 dpi and 5 dpi were identified (Figure 4.C).

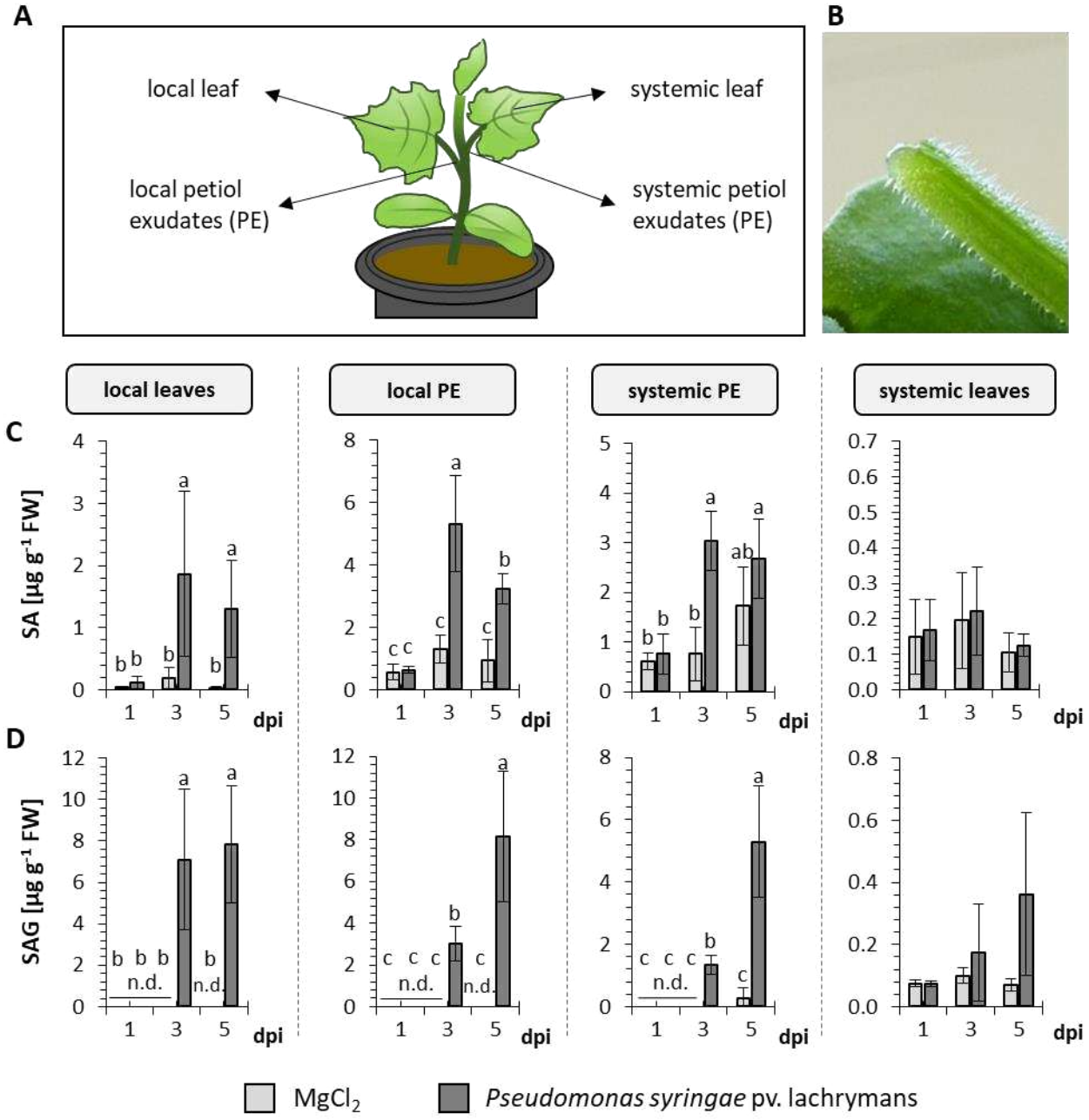

Figure 4: Accumulation of SA derived metabolites over time in *Pseudomonas syringae* pv. lachrymans (*Psl*) infected *Cucumis sativus* leaves, distal leaves and petiole exudates. Three-week-old C. sativus plants were spray-inoculated with a *Psl* solution (OD_{600}=0.2, containing 0.005% SilwetR L-77) or with 10 mM $MgCl_2$ containing 0.005% SilwetR L-77 (mock treatment). Leave and phloem samples were taken 1, 3, and 5 dpi. (**A**) Leaf samples were taken at the local inoculated leaves and the systemic, untreated leaves. Petiol exudate (PE) samples were taken at the stem site of the local and systemic leaves. (**B**) When a branch of the stem to a leaf was cut, PE starts to flow out of the branch. Exudates were collected at the site of the stem using a filter paper. One plant thereby served as one biological replicate for local and systemic leaf and PE samples. For each treatment and sampling timepoint at least four and maximal five individual replicates were used (n ≥ 4). All samples were analyzed via GC-MS and in the resulting chromatograms (**C**) SA and (**D**) SAG were quantified. If a metabolite was not detected with the here used TMS derivatization method, it is indicated as not detected (n.d.). Bars represent mean values ± standard deviation. Letters above the bars show statistical differences determined with a Kruskal-Wallis test in SPSS.

In *A. thaliana* the glycosylation of SA results in the formation of two conjugates: SAG and SGE (Dempsey et al. 2011). In *C. sativus* only the SA and its conjugate SAG were quantifiable, while SGE was not detected in *C. sativus* leaves or PE. Starting 3 dpi the SAG amounts were significantly elevated after a *Psl* inoculation in comparison to a $MgCl_2$ inoculation in local leaves, local and systemic PE samples but not in systemic leaves (Figure 4.D). Independent of the treatment, 1 dpi no SAG was detected in local leaves and PE samples, but low levels of SAG were detected 1 dpi in systemic leaves of $MgCl_2$ and *Psl* treated plants (< 0.09 µg g^{-1} FW) (Figure 4.D). In leaves and PE of $MgCl_2$ treated plants, significantly lower SAG amounts than in leaves and PE of *Psl* treated plants were detected 3 dpi and 5 dpi (Figure 4.D). Additionally, SAG was detected in significantly higher amounts in local PE samples of *Psl* inoculated plants sampled 5 dpi (8.15 µg g^{-1} FW) when compared to the detected amounts in local PE samples of *Psl* inoculated plants collected 3 dpi (3.02 µg g^{-1} FW) (Figure 4.D). In systemic PE samples of $MgCl_2$ treated *C. sativus* plants, SAG was only detected 5 dpi in 2 out of 5 samples. However, in systemic PE of *Psl* inoculated plants a significantly higher level of SAG than in systemic PE of $MgCl_2$ treated plants was quantified 3 dpi and 5 dpi (Figure 4.D). As observed in local PE samples, the SAG amounts detected 5 dpi in systemic PE samples of *Psl* treated plants (5.29 µg g^{-1} FW) were significantly higher than the quantified SAG amounts in systemic PE samples of *Psl* treated plants 3 dpi (1.35 µg g^{-1} FW), indicating an accumulation of SAG after a *Psl* infection over time in local *C. sativus* leaves and PE (Figure 4.D). In response to all treatments, SAG levels of systemic leaves did not significantly differ from each other and were only detectable in low concentrations (below 0.7 µg g^{-1} FW), as examined for SA (Figure 4.D). Summarizing, these results indicate an accumulation of SA and SAG in *C. sativus* after a *Psl* infection starting 3 dpi in local leaves, and local and systemic PE but not in systemic leaves. In summary these results indicate a *Psl*-induced accumulation of SA and its derivate SAG in local leaves, local PE and systemic PE of *C. sativus* plants, but no SA or SAG accumulation was observed in systemic leaf samples.

In addition to SA and its conjugates, the biosynthesis of NHP and its conjugates was investigated via GC-MS in *C. sativus* plants after a *Psl* infection (Figure 5). The analyses revealed equal and constitutively high levels of the NHP precursor substance Pip after *Psl* or $MgCl_2$ treatments in local and systemic leaves and local and systemic PE at any sampling timepoint (Figure 5.A). Independent of the treatment, local and systemic PE samples that were collected 1 dpi showed a significantly lower amount of Pip than local and systemic PE samples

collected 3 dpi and 5 dpi (Figure 5.A). In local, *Psl* infected leaves Pip amounts of up to 15.14 µg g^{-1} FW were quantified 3 dpi, whereas Pip amounts of up to 43.40 µg g^{-1} FW were quantified already 1 dpi in systemic leaves (Figure 5.A), indicating a more important role of Pip in systemic than in local tissue that might be independent of the defense against pathogens in *C. sativus*.

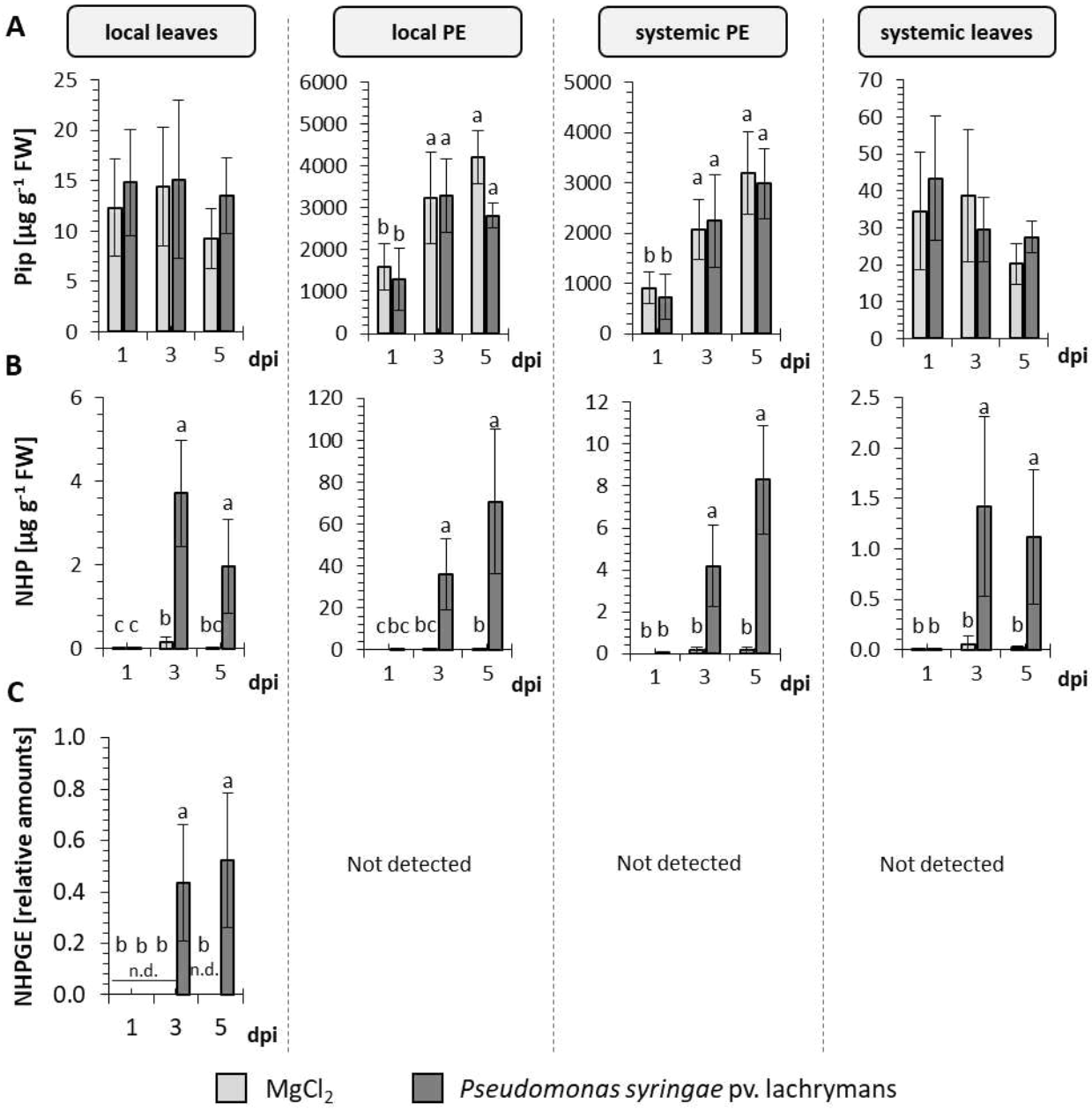

Figure 5: Time dependent accumulation of NHP derived metabolites in *Pseudomonas syringae* pv. lachrymans (*Psl*) infected *Cucumis sativus* leaves, distal leaves and petiole exudates. Three-week-old *C. sativus* plants were spray-inoculated with 10 mM $MgCl_2$ containing 0.005% SilwetR L-77 as control treatment or with a *Psl* solution (OD_{600}=0.2, containing 0.005% SilwetR L-77). Leave and phloem exudates (PE) samples were taken 1 dpi, 3 dpi, and 5 dpi. Leaf samples were taken at the local inoculated leaves and the systemic, untreated leaves. PE samples were taken at the stem site of the local and systemic leaves. Thereby, one plant served as one biological replicate for one local and systemic leaf and PE sample. For each treatment and sampling timepoint at least four and maximal five individual replicates were used (n ≥ 4). All samples were analyzed via GC-MS and (**A**) Pip and (**B**) NHP and (**C**) NHPGE were quantified in the resulting chromatogram. If a metabolite was not detected, it is indicated as not detected (n.d.). Bars represent mean values ± standard deviation. Letters above bars indicate the statistical differences investigated with a Kruskal-Wallis test in SPSS.

In comparison to the $MgCl_2$ treatment significantly higher levels of NHP were detected 3 dpi and 5 dpi in local and systemic leaves and PE of *Psl* treated *C. sativus* plants (Figure 5.B). In *C. sativus* leaves the highest NHP amounts were detected in local, inoculated tissue 3 dpi (3.71 µg g^{-1} FW) whereas in systemic, untreated leaves only 1.43 µg g^{-1} FW were detected 3 dpi (Figure 5.B). At the first sampling timepoint (1 dpi) no significant differences in the NHP level of $MgCl_2$ or *Psl* treated plants were measured in local and systemic leaves and PE (Figure 5.B) indicating that NHP accumulation starts between 1 dpi and 3 dpi with *Psl*. The NHP conjugate NHPGE was detected in local leaves 3 dpi and 5 dpi after a *Psl* inoculation but not in $MgCl_2$ treated leaves at any tested timepoint (Figure 5.C). In local PE, systemic PE and systemic leaves NHPGE was not detected (Figure 5.C). The recently in *A. thaliana* identified NHP conjugate NHPG (Holmes et al. 2021) was not detected in *C. sativus*.

Since the metabolite analyses revealed an existing Pip and NHP biosynthesis in *C. sativus*, homologs of the *A. thaliana ALD1* and *FMO1* genes were identified in the publicly available *C. sativus* genome via NCBI blast search to examine their expression during a *Psl* infection. For the expression analyses, the sampled and ground leave material of the local leaves that was used for the metabolite analyses before was used for RNA extraction, cDNA synthesis and subsequent semi-quantitative PCRs. For the semi-quantitative gene expression analyses only three of five replicates were used. Therefore, samples were chosen which displayed the mean detected amounts of Pip or NHP for each treatment at each sampling timepoint. The light intensities of the PCR products on a 2 % agarose gel were visualized by UV-light, photographed (Suppl. Figure 2) and measured using ImageJ. Measured light intensities of the bands were set

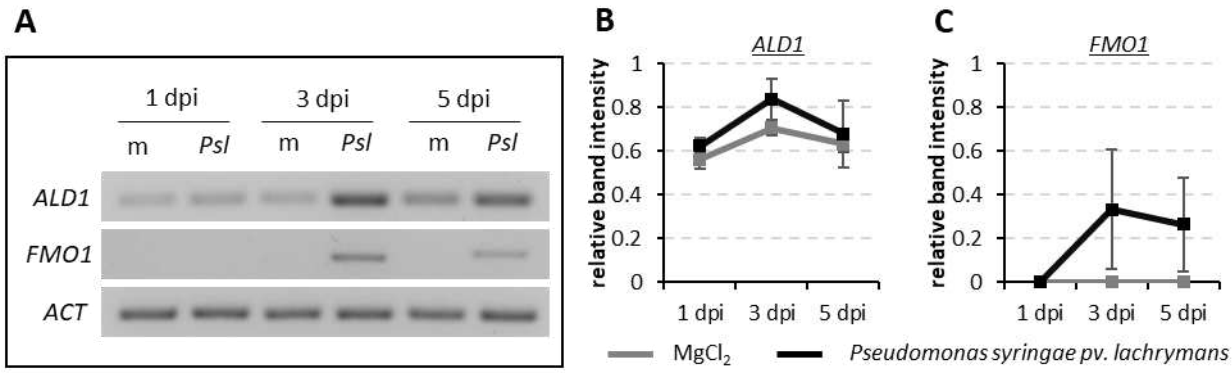

Figure 6: **Semi-quantitative expression analyses of *Cucucmis sativus* ACTIN, *ALD1* and *FMO1* in leaves treated with *Psl* or $MgCl_2$ via PCR**. (**A**) To assure an efficient cDNA synthesis PCRs with primers for the *C. sativus ACTIN* (*ACT*) gene were performed and evaluated on a 2 % agarose gel under UV-light. The PCR products of PCRs with *C. sativus ALD1* and *FMO1* primers were evaluated on a 2 % agarose gel under UV-light as well. The relative light intensity of the bands was determined, and mean values and the SEM were calculated for (**B**) *ALD1* and (**C**) *FMO1* for $MgCl_2$ or *Psl* treatments at 1 dpi, 3 dpi and 5 dpi (n = 3).

relative to the highest measured intensity on the gel to visualize differences and thereby draw a conclusion about the *ALD1* and *FMO1* gene expression. To assure a successful and efficient cDNA synthesis, a control PCR with *ACTIN* primers was performed (Figure 6.A). In semi-quantitative *ALD1* PCRs bands were observed in 1 dpi, 3 dpi and 5 dpi in $MgCl_2$ and *Psl* treated leaf samples (Figure 6.A, 6.B). The quantified relative band light intensity in *ALD1* PCRs revealed a slightly higher light intensity for *Psl* treated leaf samples compared to the light intensity of $MgCl_2$ treated leaves at all tested infection timepoints (Figure 6.B). In semi-quantitative *FMO1* PCRs, bands were only detected in samples of *Psl* treated *C. sativus* leaves that were harvested 3 dpi and 5 dpi but not in samples of $MgCl_2$ treated leaves (Figure 6.A, 6.C).

2.2.2. Metabolite changes in *Nicotiana tabacum* in response to *Pseudomonas syringae* pv. tabaci infection

To study the biosynthesis of NHP and SA in *N. tabacum* upon pathogen infection, four- to five-week-old plants were pressure infiltrated with a *Pseudomonas syringae* pv. tabaci (*Pstb*) solution (OD_{600} = 0.005) or 10 mM $MgCl_2$. Samples were taken 1 dpi, 2 dpi and 3 dpi and were analyzed via GC-MS.

In fully grown *N. tabacum* leaves SA levels were 1 dpi and 3 dpi significantly higher after *Pstb* treatment than in the $MgCl_2$ mock treatment (Figure 7.A). In samples which were collected 2 dpi differences between the treatments were not significant but in comparison of the treatments an elevated SA level was observed in *Pstb* treated plants (Figure 7.A). The highest amounts of SA (0.81 µg g^{-1} FW) were detected in *Pstb* treated *N. tabacum* leaves 1 dpi (Figure 7.A). Consequently, the investigated SA glycosides SAG and SGE were detected in significantly higher amounts after *Pstb* infections compared to the $MgCl_2$ treatments at all infection timepoints (Figure 7.B, C.C). In the $MgCl_2$ treated plants no SAG or SGE was detected (Figure 7.B, C.C). At 2 dpi the SAG level in *Pstb* infected *N. tabacum* leaves significantly elevates compared to 1 dpi and reaches a maximum concentration of 28.21 µg g^{-1} FW in *Pstb* infected leaves at 3 dpi (Figure 7.B). The detected amounts of SGE in *Pstb* infected leaves were significantly higher than those detected in $MgCl_2$ treated plants, but no significant elevation of the SGE level was observed over time (Figure 7.C). The maximum SGE concentration was

measured 3dpi in *Pstb* infected *N. tabacum* leaves (1.06 µg g^{-1} FW) (Figure 7.C). The calculated total SA levels show an elevating total SA concentration over time in *N. tabacum* leaves after a *Pstb* infection (Figure 7.D). However, the statistical analyses showed no statistical differences in total SA levels between the investigated infection time points or between the *Pstb* and $MgCl_2$ treatments which might related to the high variance between the samples (Figure 7.D). In brief, these results indicate a *Pstb* induced accumulation of SA and its derivates SAG and SGE in *N. tabacum*.

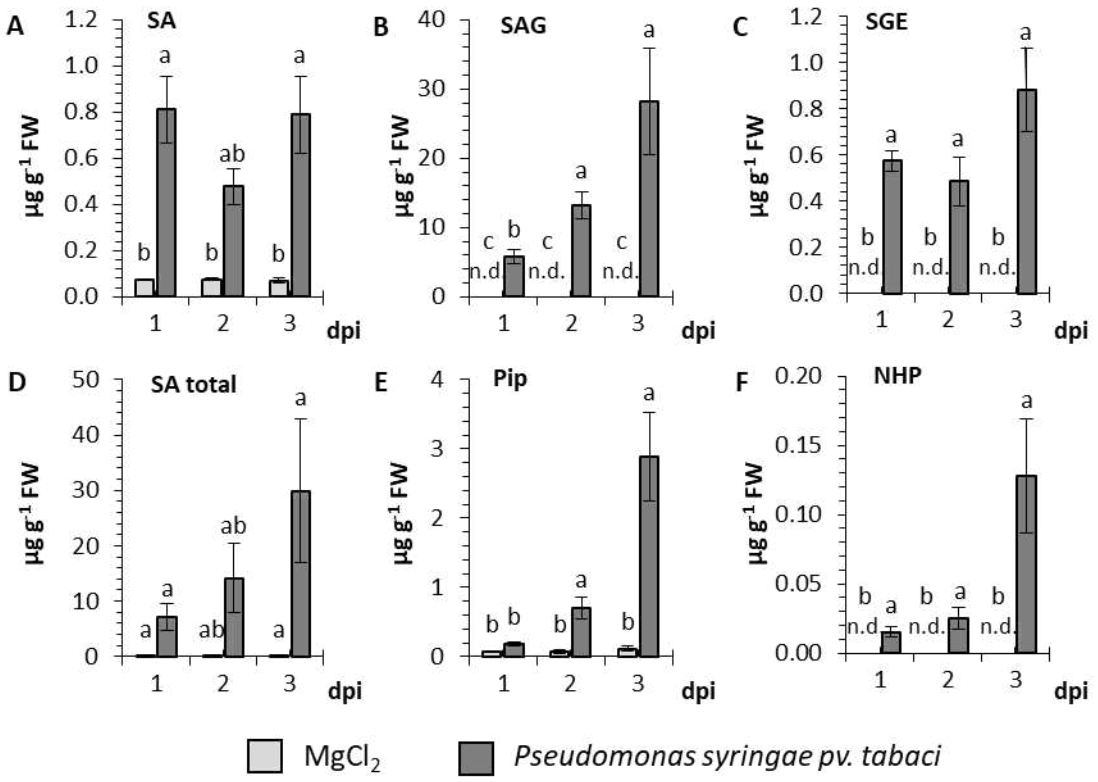

Figure 7: Accumulation of defense related metabolites in a *Nicotiana tabacum* - *Pseudomonas syringae* pv. tabaci (*Pstb*) infection-time course. Via GC-MS analyses total and relative amounts of (**A**) SA, (**B**) SAG, (**C**) SGE, (**D**) SA total, (**E**) Pip and (**F**) NHP were quantified in four- to five-week-old *N. tabacum* plants that were pressure infiltrated with a *Pstb* solution (OD_{600} = 0.005) (dark grey bars) or as a control treatment with 10 mM $MgCl_2$ (light grey bars) and sampled 1 dpi, 2 dpi and 3 dpi. If a metabolite was not detected with the here used TMS derivatization method, it is indicated as not detected (n.d.). Leaf samples of one plant served as one biological replicate. Per investigated timepoint and treatment five biological replicates were used (n = 5). Mean values ± standard deviations are represented by bars. Letters above bars indicate statistical differences determined by a Kruskal-Wallis test in SPSS.

The non-proteinogenic amino acid Pip was detected in low amounts up to 0.12 µg g^{-1} FW in $MgCl_2$ treated *N. tabacum* leaves and was detected in significantly higher levels in *Pstb* treated leaves 2 dpi (0.70 µg g^{-1} FW) and 3 dpi (2.89 µg g^{-1} FW) (Figure 7.D). The Pip levels detected 1 dpi showed no significant differences between the treatments, however a slightly higher Pip level was observed in the *Pstb* treatments compared to the $MgCl_2$ treatments (Figure 7.D). The defense related metabolite NHP was detected at all sampling timepoints between 1 dpi

and 3 dpi in *N. tabacum* leaves which were infected with *Pstb* but no NHP was detected in the leaves of the $MgCl_2$ control treatment (Figure 7.E). The highest NHP level was measured 3 dpi (0.13 µg g^{-1} FW) (Figure 7.E). These results demonstrate the importance of an accumulation of Pip and NHP upon a *Pstb* infections in *N. tabacum*.

2.2.3 Identification of unknown substances in *Brachypodium distachyon*

In the last decade *B. distachyon* emerged as model organism for monocotyledonous plant species (Fitzgerald et al. 2015). Its short life cycle, self-fertilization, small size and easy growth conditions also made *B. distachyon* a useable model organism source in plant-pathogen-interaction studies (Hong et al. 2011, Draper et al. 2001). In this study, the *B. distachyon* metabolite profile was investigated after the infection with *Xanthomonas translucens* (*Xtra*) bacteria to compare accumulation patterns after infections with the metabolite profile of dicotyledonous and monocotyledonous plant species and thereby contribute to uncover shared mechanisms in immune responses on the metabolite level of mono- and dicotyledonous plant species. Therefore, three leaves of five-week-old *B. distachyon* plants were infiltrated with a *Xtra* solution (OD_{600} = 0,05) or $MgCl_2$ as a control treatment and samples were taken 3 dpi. The infected leaf samples and respective controls were analyzed via GC-MS. In comparisons of the total ion chromatograms of pathogen infected *B. distachyon* leaves and respective controls, several accumulating substances were detected in the *Xtra* infected leave samples. Some of those substances were identified as commonly known plant metabolite in defense reactions (Figure 10, Figure 11). However, other accumulating substances had to be further identified by their mass spectra (Figure 8, Figure 9). A GC-MS mass-spectral library (Wiley275) of the National Institute of Standards and Technology (NIST) was therefore used to identify substance peaks by matching recorded mass spectra with spectra of the library.

Two peaks with a dominant fragment ion of m/z 290 accumulated in the selected 290 ion chromatogram of *Xtra* treated plants when compared with the mass spectra of mock treated plants (Figure 8.A). Both substances were identified as serotonin by the used mass-spectra library. The first accumulating peak (RT = 22.68) was identified as serotonin with 3 TMS groups and the second peak (RT = 24.83) as serotonin with 4 TMS groups. The detected fragment ions of these two peaks were compared with possible fragment ions of serotonin. The mass spectrum of the potential serotonin-3TMS revealed the molecular ion M+ of 392 and an ion

fragment of m/z 377 which correlated to the mass of M+ with a dissociated CH_3 group with a mass of 15 (Figure 8.C). Similarly, the mass spectrum of the potential serotonin-4TMS revealed the molecular ion M+ of m/z 464, which correlated with the M+ of serotonin-3TMS with an additional TMS group (MW = 73). The mass spectrum of the potential Serotonin-4TMS also showed an ion fragment of m/z 377 which correlated to the mass of the potential Serotonin-4TMS M+ with a dissociated CH_3 group (Figure 8.D).

In the mass spectrum of both serotonin peaks, the molecular ion of m/z 290 was identified (Figure 8.C, 8.D) which correlates with the molecular weight of serotonin with two TMS groups and a dissociated CH_3N (MW = 29 kDa) fragment, which can carry one (MW = 73) or two (MW = 146) TMS groups after derivatization (Figure 8.C, 8.D). If this fragment carries one TMS group, upon dissociation fragment ions of m/z 290 and m/z 102 will form which were both detected in the mass spectrum of the potential serotonin-3TMS (Figure 7.C). If this dissociated CH_3N fragment carried two TMS groups, upon dissociation the fragment ions of m/z 290 and m/z 174 would be generated. These fragment ions of m/z 290 and 174 were both detected in the mass spectrum of the potential serotonin-3TMS (Figure 7.D). Since the fragmentation pattern of these substances matches the serotonin-3TMS and serotonin-4TMS mass spectrum, they were identified as serotonin and are in the following referred to as serotonin-3TMS and serotonin-4TMS. In the here presented metabolite analyses entire relative serotonin amounts are indicated (Figure 11B).

Another substance that accumulated in *B. distachyon* after *Xtra* inoculation, when compared to the $MgCl_2$ mock treatment, was detected in the selected ion chromatogram (m/z 293) at RT 16.36 min (Figure 8.B). By comparing the mass spectrum of this substance with the used mass-spectra library, this substance was identified as potential phenylpyruvic acid (PPA) with an M+ of m/z 308 after TMS derivatization which was also detectable in the mass spectrum of this unknown substance (Figure 8.E). Additionally, a fragment ion of m/z 293 was higly abundant in the mass spectrum of peak m/z 293 which can be explained by the cleavage of a CH_3 group (MW = 15) of PPA with two TMS groups (MW = 308) (Figure 8.E). Hence, this substance was identified as putative PPA and will in the following be referred to as such.

At the retention time of 27.30 min and 27.64 min in the total ion chromatogram two substances of unknown character accumulated in *B. distachyon* upon a *Xtra* infection compared to a control sample chromatogram (Figure 9.A). In the mass spectrum of these

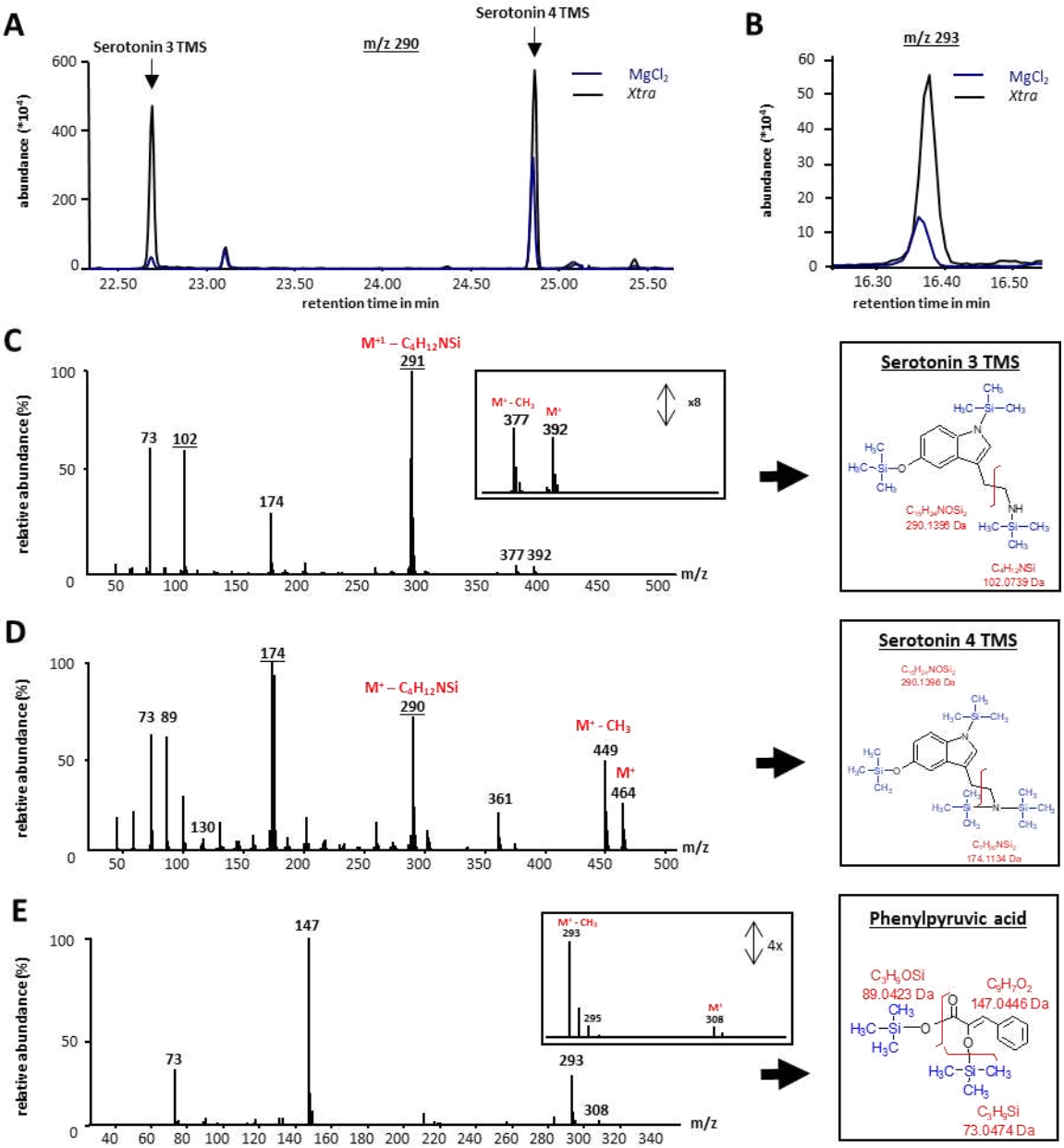

Figure 8: Identification of serotonin and phenylpyruvic acid (PPA) in *Xanthomonas translucens* (*Xtra*) infected *Brachypodium distachyon* leave samples. (**A**) The selected ion chromatogram (m/z 290) of a *Xtra* infected *B. distachyon* leave samples (black line) and respective $MgCl_2$ controls (blue line) harvested 3 dpi show the accumulation of two substances in *Xtra* infected samples at RTs of 22.68 min and 25.83 min. The investigated mass spectra revealed that (**C**) the first substance can be identified as serotonin with 3 TMS groups (M^+ = m/z 392) and (**D**) the second accumulating substance can be identified as serotonin with 4 TMS groups (M^+ = m/z 464). Likewise investigated was (**B**) the selected ion chromatogram (m/z 293) of a *Xtra* infected *B. distachyon* leave samples (black line) and respective $MgCl_2$ controls (blue line) harvested 3 dpi, which showed the accumulation of on unknown substance in *Xtra* infected samples at the RT of 16.36 min. (**E**) The respective mass spectrum of this unknown substance revealed characteristic ion fragments of PPA. A GC-MS mass-spectral library (Wiley275) was used to identify substance peaks by matching recorded mass spectra with spectra of the library.
Abbreviations: RT = retention time, TMS = trimethylsilyl

substances several ion fractions were identified (Figure 9.C, 9.E). In both substances ion fragments of m/z 267 and m/z 361 were detected in the mass spectrum (Figure 9.C, 9.E). The ion fragment of m/z 267 is associated with the SA or 2-Hydroxybenzioc acid molecule and the

fragment ion of m/z 361 is associated with sugars. Both of those ion fractions were also detected in the mass spectrum of SAG suggesting that the substances at RT 27.30 min and 27.64 min in the total ion chromatogram might be SA glycosides (Figure 9.C, 9.E).

By comparing the mass spectra of SAG and the two unknown substances the same ion fragments were detected in the chromatogram of a *Xtra* inoculated *B. distachyon* sample except for the ion fragment of m/z 355 which was only detected the mass spectra of the two unknown peaks and not in the mass spectrum of SAG (Figure 9.C, 9.E). Due to the same detected ion fragments in the mass spectra of SAG and the unknown substances it is assumed that the unknown substances have a SAG like structure. By comparisons of the mass spectra

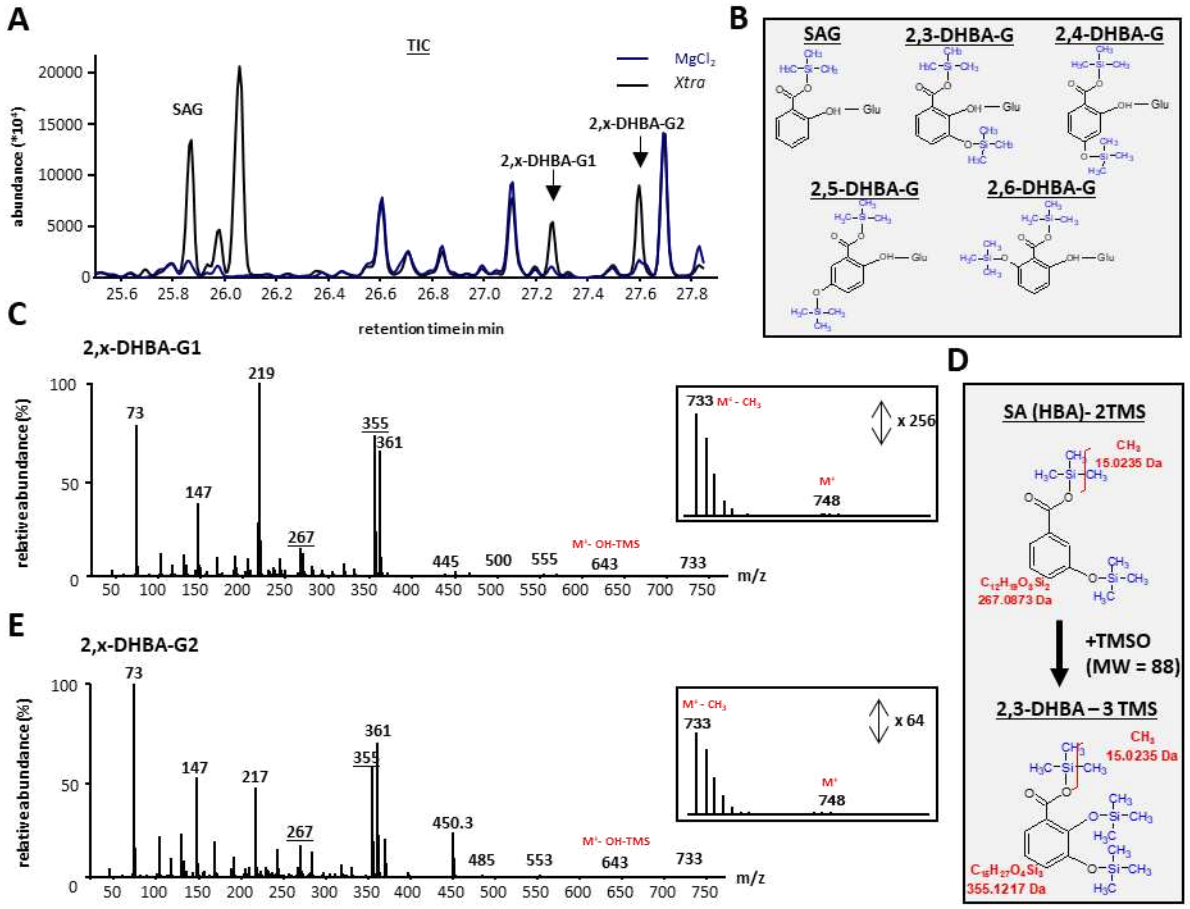

Figure 9: Identification of 2,x-DHBA-G1 and 2,x-DHBA-G2 in *Xanthomonas translucens* (*Xtra)* infected *Brachypodium dystachion* leave samples. (**A**) Total ion chromatogram of a *Xtra* infected *B. dystachion* leave samples (black line) and respective $MgCl_2$ controls (blue line) harvested 3 dpi show the accumulation in *Xtra* infected samples of SAG (RT = 25.88 min) and two other substances referred to as 2,x-2,X-DHBA-G1 (RT = 27.30 min) and 2,x-2,X-DHBA-G2 (RT = 27.64 minutes). The investigated mass spectra of (**C**) 2,x-2,X-DHBA-G1 and (**E**) 2,x-2,X-DHBA-G2 showed that both substances incorporate (**D**) the 2-Hydroxybenzoicacid structure (m/z 267) with an additional OH-group (m/z 15) containing a TMS group (m/z 73) of unknown position resulting in an m/z of 355. (**B**) Like SAG both investigated substances reveal a m/z of 361 which is associated with sugars and hence both determined substances are identified as 2,x-2,X-DHBA-Gs. A GC-MS mass-spectral library (Wiley275) was used to identify substance peaks by matching recorded mass spectra with spectra of the library.
Abbrevations: 2,X-DHBA-G = dihydroxybenzoicacid-glucoside, RT = retention time, TMS = trimethylsilyl

of both unknown substances with the used mass spectral library, both substances were identified as potential 2-6-Dihydroxybenzoic acid (Figure 9.B). Based on that, the detected ion fragment of m/z 355 in the unknown substances could represent the 2-Hydroxybenzoic acid structure (267) plus an OH-group (15) containing a TMS group (73) (Figure 9.D). As mentioned, both unknown peaks with m/z 355 also show an ion fragment at m/z 361 in the mass chromatogram which is commonly associated with sugars (Figure 9.D). This leads to the assumption that the peaks at RT 27.30 min and 27.64 min in the chromatogram might be 2,3- or 2,4 or 2,5 or 2,6-Dihydroxybezioc acid sugar derivates (Figure 9.B). Hence, the substance detected at a RT of 27.30 min is in the following referred to as 2,x-Dihydroxybenzoic acid glucoside 1 (2,x-DHBA-G1) and the substance detected at a RT of 27.64 min is in the following referred to as 2,x-DiHydroxybenzoic acid glucoside 2 (2,x-DHBA-G2).

2.2.4. Defense related metabolites accumulate in local and systemic *Brachypodium distachyon* leaves after *Xanthomonas translucens* infections

To investigate the local and systemic response of *B. distachyon* leaves to a bacterial *Xtra* infection on the metabolite level, three leaves of five-week-old plants were pressure infiltrated with a *Xtra* solution (OD_{600} = 0.05) or 10 mM $MgCl_2$ which served as a control treatment. Local and systemic leaf samples were harvested 1 dpi, 3 dpi and 5 dpi. The inoculated leaves were pooled as one replicate and three leaves systemic of these local leaves were pooled as one replicate for the performed GC-MS analyses (Figure 10.C).

The phytohormones SA, NHP and their derivates play a major role in the establishment of SAR in dicotylous plants (Hartmann and Zeier 2019, Zeier 2021). For this reason, these important defense substances were quantified in this study to reveal their role in the local and systemic defense of monocotyledonous plants against pathogens. The metabolite analyses of the conducted infection time course revealed significantly higher amounts of SA in local leaves that were treated with *Xtra* compared to the $MgCl_2$ treated leaves starting 3 dpi and reaching a maximum of 7.69 µg g^{-1} FW in *Xtra* treated leaves 5 dpi (Figure 10.A). At early infection stages (1 dpi) no significant differences were found in the measured SA in local leaves that were treated with *Xtra* or $MgCl_2$ (Figure 10.A). In systemic leaves of *Xtra* treated plants, a significantly higher amount of SA than in systemic leaves of $MgCl_2$ treated plants was only

measured 3 dpi but not 1 dpi or 5 dpi. The detected SA in systemic leaves of *Xtra* treated plants reached 3 dpi a maximum level of 1.18 µg g^{-1} FW which is approximately seven times less than the detected SA in local *Xtra* treated leaves (Figure 10.B). These results suggest an accumulation of SA in local *Xtra* infected and untreated systemic *B. distachyon* leaves.

In local *Xtra* treated leaves a significantly higher amount of the SA glucoside SAG was detected than in $MgCl_2$ treated leaves starting 3 dpi (Figure 10.A). In the progression of the *Xtra* infection, SAG was detected in significantly higher amounts in local *Xtra* treated leaves 5 dpi (438.92 µg g^{-1} FW) compared to the detected SAG amounts in local *Xtra* treated leaves 3 dpi (122.33 µg g^{-1} FW) (Figure 10.A). In systemic, untreated leaves equal amounts of SAG were detected 1 dpi, 3 dpi and 5 dpi in *Xtra* and $MgCl_2$ treated plants (Figure 10.B). The SA glucoside SGE was only detected in *Xtra* treated local leaves but not in $MgCl_2$ treated local or systemic leaves (Figure 10.A, G.B). In the local leaves of *B. distachyon* plants SAG was detected in significantly higher levels in *Xtra* treated leaves compared to $MgCl_2$ treated leaves 3 dpi and 5 dpi (Figure 10.A). Since, these results suggest that the SA derivates SAG and SGE accumulate in *B. distachyon* after an *Xtra* infection only in local infected leaves but not in systemic uninfected leaves.

In GC-MS chromatograms of *Xtra* treated *B. distachyon* leaf samples harvested 3 dpi, four substances were identified that were only detectable in low amounts in the chromatograms of $MgCl_2$ treated leaves. Two of these substances were further characterized as 2,x-DHBA-G1 and 2,x-DHBA-G2 which were both quantified in relative amounts since the correction factors of the included internal standards for these substances are unknown. The measured levels of 2,x-DHBA-G1 and 2,x-DHBA-G2 in local leaves are significantly higher in *Xtra* treated plants compared to $MgCl_2$ treated leaves at all infection timepoints that were studied (Figure 10.A). In the progression of the *Xtra* infection in local *B. distachyon* leaves, the levels of both DHBA glycosides significantly elevated constantly reaching a maximum 5 dpi (Figure 10.A). In systemic leaves, the 2,x-DHBA-G1 was detected in equal amounts in *Xtra* and $MgCl_2$ treated plants sampled 1 dpi but significantly higher level 2,x-DHBA-G1 were detected in systemic leaves of *Xtra* treated *B. distachyon* plants compared to $MgCl_2$ treated plants 3 dpi and 5 dpi (Figure 10.B). The 2,x-DHBA-G2 was detected in equal amounts in *Xtra* and $MgCl_2$ treated plants at all sampling timepoints (Figure 10.B).

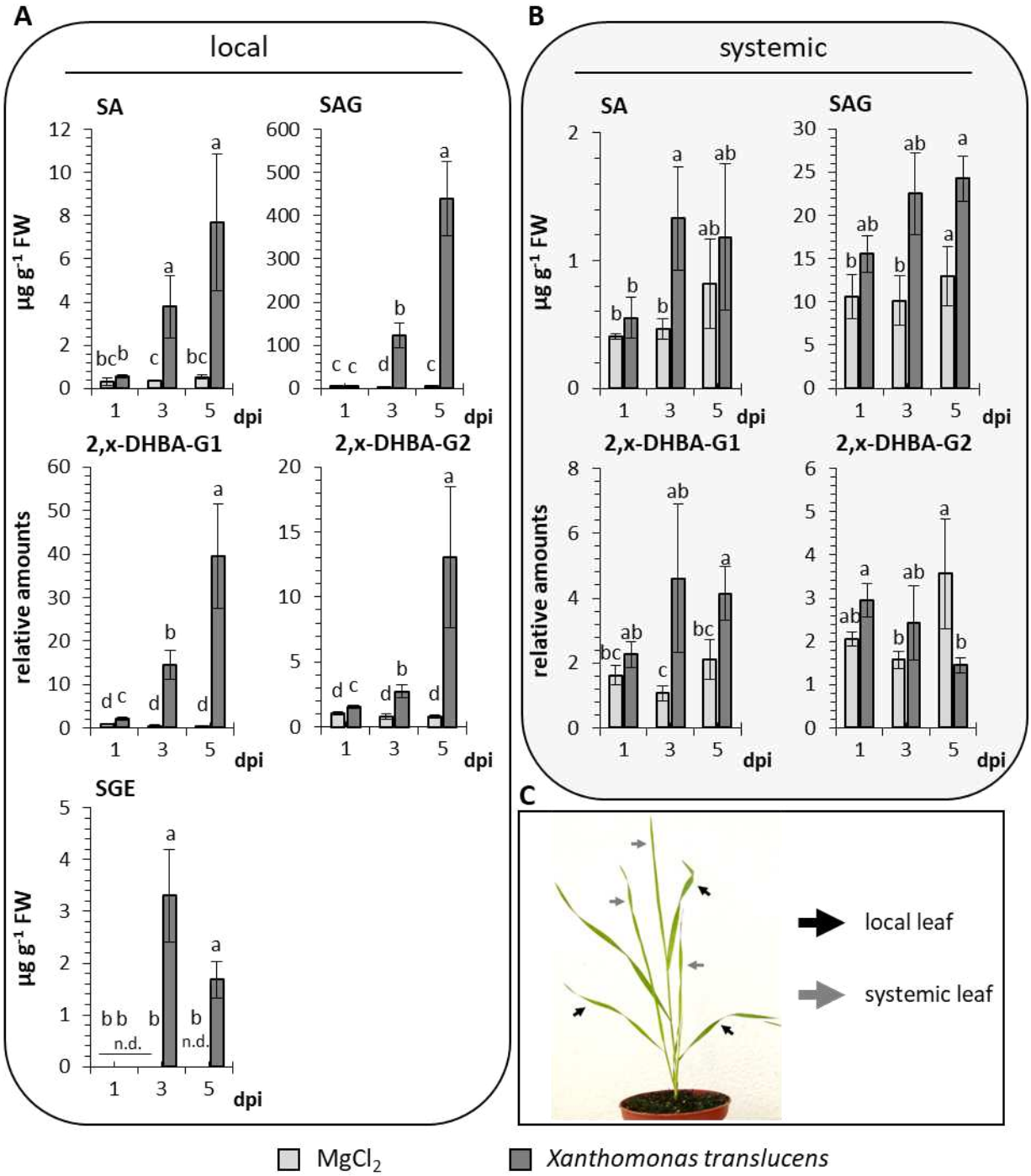

Figure 10: Time dependent accumulation of SA, SAG, 2,x-DHBA-G1, 2,x-DHBA-G1 and SGE in local *Xanthomonas translucens* (*Xtra*) and $MgCl_2$ treated systemic untreated leaves of *Brachypodium disatchyon* plants. (**C**) Three leaves of five-week-old *B. distachyon* plants were pressure infiltrated with a *Xtra* solution (OD_{600} = 0.05) or 10 mM $MgCl_2$ which served as a control treatment and local (black arrows) and systemic (grey arrows) leaf samples were harvested 1 dpi, 3 dpi and 5 dpi. For the performed GC-MS analyses, the three inoculated leaves of one plant were pooled as one local replicate and three untreated systemic leaves were respectively pooled as one replicate. For each treatment and sampling timepoint three individual replicates/plants were used (n = 3) for the GC-MS analyses of local (**A**, white background) and systemic (**B**, grey background) *B. distachyon* leaves. If a metabolite was not detected with the here used TMS derivatization method, it is indicated as not detected (n.d.). Presented bars show mean values ± standard deviation. Statistical differences were investigated with a Kruskal-Wallis test in SPSS and results are indicated by the letters above bars.

These results indicate a clear accumulation of 2,x-DHBA-G1 and 2,x-DHBA-G2 in B. *distachyon* after a *Xtra* infection in local infected leaves, while only a slight accumulation of 2,x-DHBA-G1 is indicated in systemic leaves (3dpi).

Another substance that was identified in the total ion chromatogram is serotonin which was as well quantified in relative amounts. In local, *Xtra* treated *B. distachyon* leaves a significantly higher level of serotonin was quantified than in $MgCl_2$ treated leaves starting 3 dpi whereat a further significant elevation of the serotonin level was detected in *Xtra* treated local leaves between 3 dpi and 5 dpi (Figure 11.A). In systemic *B. distachyon* leaves equal amounts of serotonin were detected in *Xtra* and $MgCl_2$ treated plants at all sampling timepoints (Figure 11.B). The fourth substance that was identified in the total ion chromatograms is PPA, which was also in quantified in relative amounts. The level of PPA in local *Xtra* treated leaves was 3 dpi significantly higher than in $MgCl_2$ treated leaves 3 dpi (Figure 11.A). Equal levels of PPA were measured in *Xtra* and $MgCl_2$ treated *B. distachyon* local leaves 1 dpi and 5 dpi (Figure 11.A). In systemic leaves no significant differences were detected between the *Xtra* and $MgCl_2$ treated plants (Figure 11.A). These findings indicate a role for serotonin and PPA in the local immune responses of *B. distachyon* against *Xtra* infection, while these metabolites do not seem to be engaged in systemic immune responses of this monocot.

The SAR inducer NHP and its precursor Pip were also detected in *B. distachyon.* In local, *Xtra* treated leaves a significantly higher amount of Pip was detected than in $MgCl_2$ treated leaves 3 dpi and 5 dpi, but 1 dpi equal amounts of Pip were measured in response to both treatments (Figure 11.A). A significant elevation of the Pip level was observed between 3 dpi (3.39 µg g^{-1} FW) and 5 dpi (8.96 µg g^{-1} FW) in local *Xtra* treated leaves (Figure 11.A). In systemic *B. distachyon* leaves no statistical differences between the control and *Xtra* treatments were observed between 1 dpi and 5 dpi (Figure 11.B). However, a slightly higher Pip level was observed 5 dpi in the systemic leaves of *Xtra* treated plants when compared to the systemic leaves of $MgCl_2$ treated plants (Figure 11.B).

The NHP was not detected in local leaves of $MgCl_2$ treated plants and was only detected in *Xtra* treated local leaves 3 dpi (0.54 µg g^{-1} FW) and 5 dpi (0.18 µg g^{-1} FW) (Figure 11.A). No elevation of NHP levels over time were observed during the progression of the *Xtra* infection (Figure 11.A). In systemic *B. distachyon* leaves of *Xtra* treated plants, NHP was only detected 3 dpi (0.05 µg g^{-1} FW) in two out of four replicates resulting in a high standard deviation (Figure

11.B). At all other testes timepoints (1 dpi, 5 dpi) no NHP was detected in the systemic leaves of $MgCl_2$ and *Xtra* treated plants (Figure 11.B). Summarizing these results indicate an induction of the NHP biosynthesis pathway in Brachypodium upon an *Xtra* infection in local infected and systemic uninfected leaves.

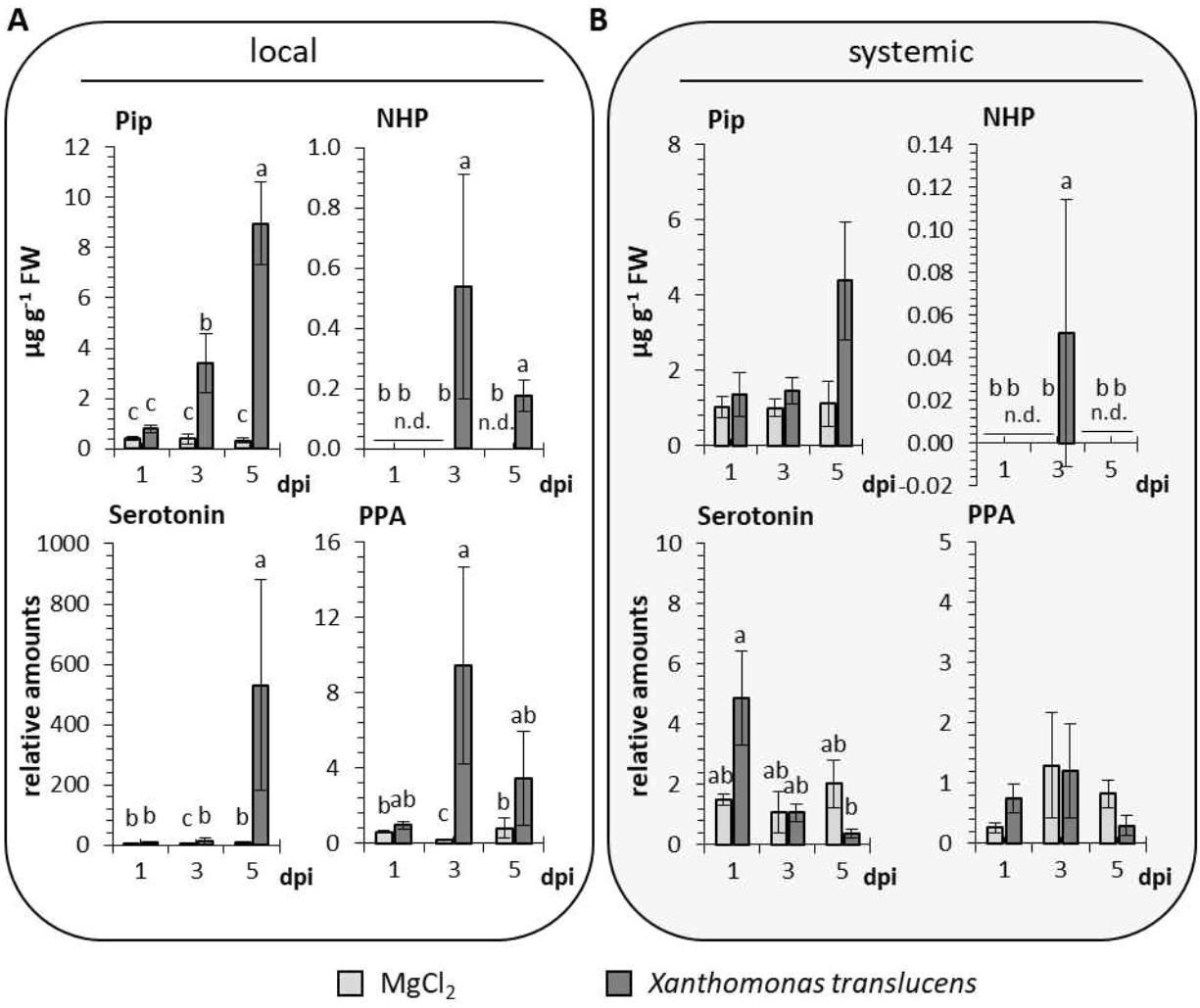

Figure 11: Time dependent accumulation of Pip, NHP, serotonin and PPA in local *Xanthomonas translucens* (*Xtra*) and $Mgcl_2$ treated and systemic untreated leaves of *Brachypodium distachyon* plants. Three leaves of five-week-old *B. distachyon* plants were pressure infiltrated with 10 mM $MgCl_2$ as a control treatment or with a *Xtra* solution (OD_{600} = 0.05). Local (**A**, white background) and systemic (**B**, grey background) leaf samples were harvested 1 dpi, 3 dpi and 5 dpi. The three inoculated leaves and the three untreated systemic leaves of one *B. distachyon* plant were respectively pooled as one replicate for the performed GC-MS analyses. Three individual replicates/plants were used for each treatment and sampling timepoint (n = 3). If the here used TMS derivatization method did not lead to the detection of an investigated metabolite, it is indicated as not detected (n.d.). Bars represent mean values ± standard deviation. Letters above bars indicate the statistical differences investigated with a Kruskal-Wallis test in SPSS.

2.2.5. Changes in the metabolite levels in *Brachypodium distachyon* after a *Magnaporthe grisea* infection

To gain further insight into the mechanisms of defense against pathogens in *B. distachyon*, changes in metabolite levels of *B. distachyon* after a fungi infection were investigated. Therefore, three- to four-week-old *B. distachyon* plants were sprayed with a *Mgri* spore solution (50 spores/µl) or H_2O as a control treatment. To establish high humidity for the best possible *Mgri* growth conditions, the plants were incubated in sealed plastic bags after spray inoculations. For the GC-MS analyses of *B. distachyon* leaves after a *Mgri* or H_2O treatment, samples were collected 2 dpi, 3 dpi and 4 dpi to investigate this plant-pathogen interaction during the biotrophic and necrotrophic growth stages of *Mgri* in *planta.*

In the H_2O treated *B. distachyon* leaves a basal SA level of approximately 0.5 µg g^{-1} FW was detected 2 dpi, 3 dpi and 4 dpi (Figure 12.A). An equal SA level was detected in H_2O and *Mgri* inoculated plants 2 dpi and 4 dpi (Figure 12.A). However, 3dpi significant higher amounts of SA were detected in *Mgri* treated *B. distachyon* leaves (1.18 µg g^{-1} FW) than in H_2O treated leaves (0.64 µg g^{-1} FW) (Figure 12.A). The investigated SA derivate SAG did not reveal any differences between the detected amounts of SAG in H_2O and *Mgri* treated plants at 2 dpi, 3dpi or 4 dpi (Figure 12.B). In contrast, the investigated SA derivate SGE was detected in significantly higher amounts in *Mgri* treated *B. distachyon* leaves (4.89 µg g^{-1} FW) than in H_2O treated leaves 4 dpi (3.47 µg g^{-1} FW) (Figure 12.C). Equal levels of SGE were observed in *Mgri* and H_2O treated leaves 2 dpi and 3 dpi (Figure 12.C). In short, these results indicate a slight SA accumulation in *B. distachyon* upon a *Mgri* infection, which does not seem to be associated with accumulation of the investigated SA derivates in this study.

The in *Xtra* infected *B. distachyon* leaves identified 2,x-DHBA-G1, 2,x-DHBA-G2, serotonin and PPA were also investigated in *B. distachyon* after the infection with *Mgri* to reveal differences in metabolite levels between the treatments. These substances are indicated in relative amounts since correction factors were not available. Noticeably, 2,x-DHBA-G1, 2,x-DHBA-G2 and PPA were detected in equal levels in *Mgri* and H_2O treated plants 2 dpi, 3 dpi and 4 dpi (Figure 12.D, J.E, J.I). Serotonin was also detected in equal amounts in *Mgri* and H_2O treated plants 2 dpi and 3 dpi but significantly higher amounts of serotonin were detected in *Mgri* treated plants than in H_2O treated plants 4 dpi (Figure 12.F). These findings suggest a role of

2,x-DHBA-G1, 2,x-DHBA-G2, serotonin and PPA in the defense reactions of *B. distachyon* against a *Mgri* infection in progressed *Mgri* infection stages.

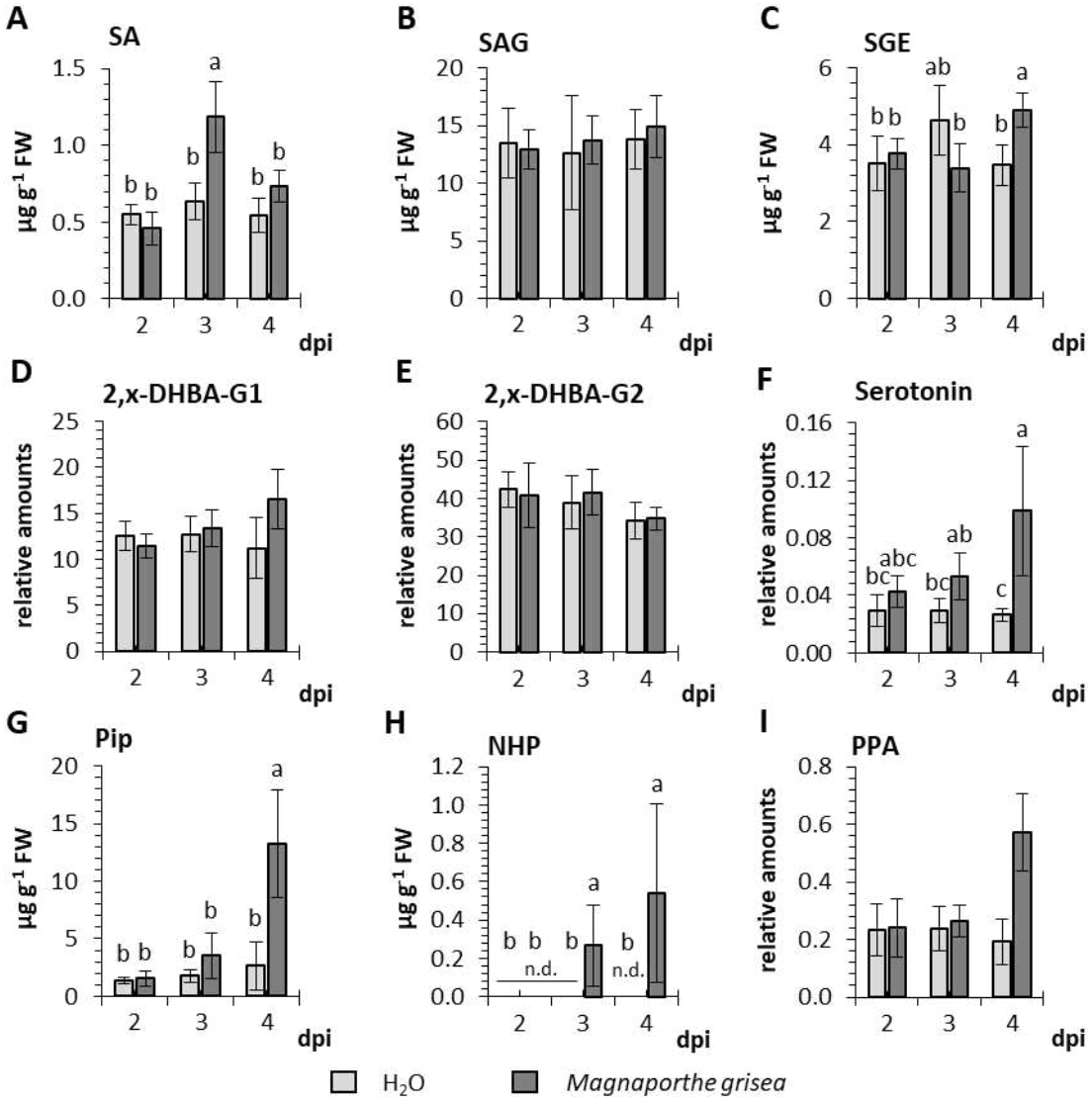

Figure 12: Time dependent accumulation of defense related metabolites in *Brachypodium distachyon* leaves infected with the fungal pathogen *Magnaporthe grisea* (*Mgri*). Total and relative amounts of (**A**) SA, (**B**) SAG, (**C**) SGE, (**D**) 2,x-DBHA-G1, (**E**) 2,x-DBHA-G2, (**F**) serotonin, (**G**) Pip, (**H**) NHP, (**I**) PPA were quantified via GC-MS analyses. Therefore, two leaves of 3- to 4-week-old *B. disatchyon* plants in the three-leaf-stage were sprayed with a *Mgri* spore solution (50 spores/µl) or H_2O as a control treatment and were contained in sealed plastic bags after inoculations. Samples for the GC-Ms analyses were taken 2 dpi, 3 dpi and 4 dpi whereat all infected leaves of one plant were pooled for one biological replicate. Bars represent mean values ± standard deviation for at least three biological replicates per sampled timepoint and treatment ($n \geq 3$). If a metabolite was not detected with the here used TMS derivatization method, it is indicated as not detected (n.d.). Statistical differences are indicated by the letters above bars and were investigated with a Kruskal-Wallis test in SPSS.

To investigate the NHP biosynthesis pathway Pip was quantified in *B. distachyon* after a *Mgri* infection. The GC-MS analyses revealed significantly higher amounts of Pip in *Mgri* treated leaves (2.64 µg g^{-1} FW) compared to H_2O treated leaves (0.27 µg g^{-1} FW) 4 dpi (Figure 12.G). A

basal level of Pip was detected 2 dpi and 3 dpi in *Mgri* and H_2O treated leaves but no significant differences between the treatments were found (Figure 12.G). The NHP was not detectable in H_2O inoculated *B. distachyon* plants and in *Mgri* inoculated plants that were sampled 2 dpi (Figure 12.H). However, NHP was detected 3 dpi (0.27 µg g^{-1} FW) and 4 dpi (0.54 µg g^{-1} FW) in *Mgri* treated leaves which thereby shows significantly higher levels of NHP after *Mgri* treatments than after H_2O treatments in *B. distachyon* (Figure 12.H). These results indicate the accumulation of Pip and NHP in *B. distachyon* upon *Mgri* infections and thereby indicates the pathogen induced activation of the NHP biosynthesis pathway, over Pip to NHP, in *B. distachyon* plants. Moreover, a parallel accumulation of SA and NHP in *B. distachyon* plants was observed after the infection with *Mgri*.

2.2.6. Metabolite analyses of *Hordeum vulgare* after a *Magnaporthe oryzae* infection

To study the interaction of monocotyledonous plants with pathogens on a metabolite level, *H. vulgare* plants were spray-inoculated with *Mory* or H_2O as a control treatment and analyzed via GC-MS. The *Mory* and control treatments of barley plants, as well as the sampling of leaf material 5 dpi were performed by Ulrich Schaffrath in the Department of Plant Physiology at RWTH Aachen University (Aachen, Germany).

The metabolite analyses showed equal amounts of SA in H_2O (0.07 µg g^{-1} FW) and *Mory* (0.083 µg g^{-1} FW) treated *H. vulgare* plants (Figure 13.A). The in this study investigated SA derivates SAG and SGE were not detected in *H. vulgare*. In summary, these results indicate a neglectable role of SA and its derivates in the immune response of *H. vulgare* after a *Mory* infection. However, the in *B. distachyon* identified 2,x-DHBA-G1 and 2,x-DHBA-G2 were detected in *H. vulgare* and revealed a significantly higher level of 2,x-DHBA-G1 and 2,x-DHBA-G2 in *Mory* inoculated plants than in H_2O inoculated *H. vulgare* plants (Figure 13.B, K.C), indicating an important role for these metabolites in the *H. vulgare* defense against *Mory*.

To investigate the NHP biosynthesis pathway in *H. vulgare,* Pip and NHP were quantified in *Mory* or H_2O treated plants 5 dpi. A significantly higher Pip level was detected in *Mory* treated (30.72 µg g^{-1} FW) than in H_2O (0.46 µg g^{-1} FW) treated *H. vulgare* plants (Figure 13.D). In H_2O inoculated plants no NHP was detected but in *Mory* inoculated plants 0.11 µg g^{-1} FW NHP were detected which thereby shows a significantly higher NHP level in *Mory* treated plants compared to H_2O treatments (Figure 13.E). This indicates an accumulation of Pip and NHP in *H. vulgare* which is induced by *Mory* infections.

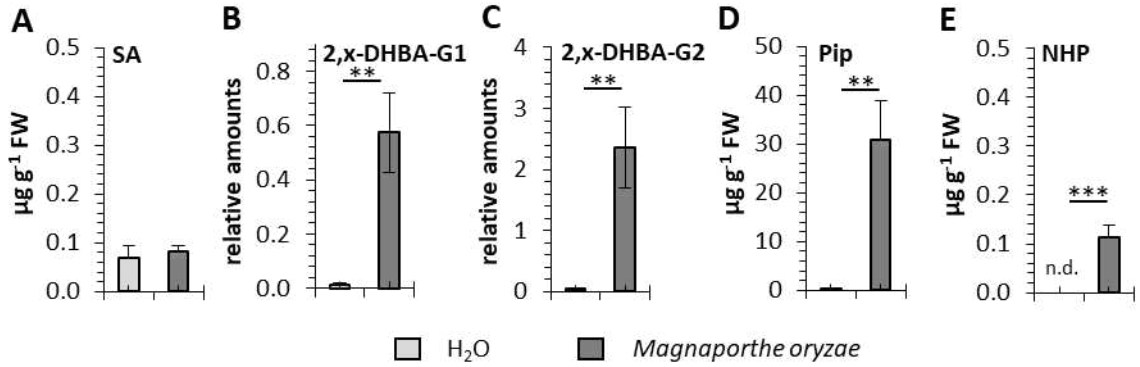

Figure 13: Accumulation of defense related metabolites in an *Hordeum vulgare* leaves upon a *Magnaporthe oryzae* (*Mory*) infection. Total and relative amounts of (**A**) SA, (**B**) 2,x-DBHA-G1, (**C**) 2,x-DBHA-G2, (**D**) Pip and (**E**) NHP were quantified via GC-MS. Therefore, leaves of *H. vulgare* plants were spray inoculated with a *Mory* spore solution (250 conidia/µl) or H_2O as a control treatment and sampled 5 dpi. Three biological replicates were sampled per treatment (n = 3) consisting of all infected leaves of one plant. Mean values ± standard deviation are represented by bars. If a metabolite was not detected with the here used TMS derivatization method, it is indicated as not detected (n.d.). Letters above bars indicate statistical differences determined by a Kruskal-Wallis test in SPSS. Infection assays were performed by Ulrich Schaffrath in the Department of Plant Physiology at RWTH Aachen University (Aachen, Germany).

2.2.7. The NHP induced resistance in dicotylous plants

The resistance inducing effect of NHP in *A. thaliana* has been the focus of recent studies (Hartmann et al. 2018, Chen et al. 2018), however only a few studies investigate the resistance inducing effect of NHP in other dicotyledonous plant species (Holmes et al. 2019). To test if exogenous NHP application can induce resistance in *C. sativus*, three-week-old plants were injected with 1 mM NHP or H_2O at the stem and were spray inoculated with a *Psl* solution (OD_{600} = 0.2) one day after the pretreatments. The number of *Psl* bacteria in the leaves was determined 3 dpi and 6 dpi in two independent experiments (Figure 14.A). For the macroscopic analyses of disease symptoms caused by *Psl*, pictures of NHP and H_2O pretreated plants were taken 6 dpi (Figure 14.B).

In *C. sativus* plants that were pretreated with H_2O a significant higher number of *Psl* bacteria was determined than in NHP pretreated plants 3 dpi and 6 dpi (Figure 14.A). In H_2O pretreated and *Psl* inoculated plants 3 dpi approximately 4 * 10^6 cfu were detected whereas in H_2O pretreated and *Psl* inoculated plants 6 dpi approximately 12 * 10^6 cfu were measured which shows a triplication of the number of bacteria between 3 dpi and 6 dpi in the two independent performed experiments (Figure 14.A). In NHP pretreated and *Psl* inoculated plants 3 dpi approximately 99 * 10^3 cfu and 6 dpi approximately 132 * 10^3 cfu were detected (Figure 14.A). This reveals approximately 46 times more bacteria in H_2O than in NHP pretreated leaves 3 dpi and 96 times more bacteria in H_2O than in NHP pretreated leaves 6 dpi which indicates a slower growth of *Psl* bacteria in NHP pretreated compared to H_2O pretreated plants. Macroscopically the leaves of H_2O pretreated and *Psl* inoculated plants showed yellowish chlorosis with necrotic spots 6 dpi while NHP treated leaves seemed green with only a few chlorotic spots (Figure 14.B). Additionally, the *Psl* inoculated and NHP treated plants macroscopically showed leaves with a healthy tension, but H_2O pretreated plants developed curled up leaf edges and showed signs of dehydration (Figure 14.B).

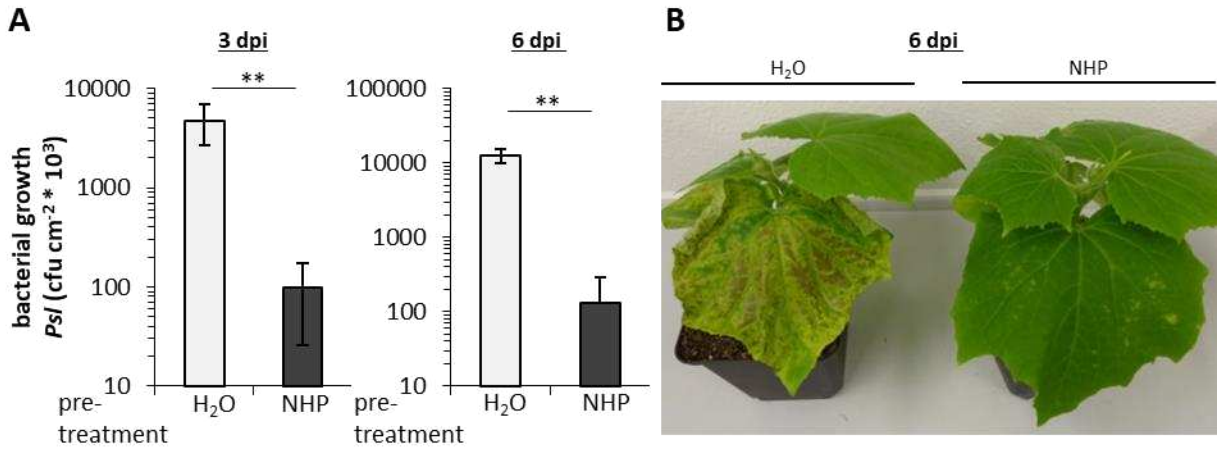

Figure 14: *Cucumis sativus* plants acquire systemic resistance to bacterial infections after a NHP injection in the stem. Three-week-old plants were injected with 1 mM NHP or H_2O as a control treatment at the stem and one day later the plants were spray inoculated with a *Psl* solution (OD_{600} = 0.2). (**A**) The number of *Psl* bacteria in the leaves was determined 3 dpi and 6 dpi in two independent experiments and is expressed as colony-forming units (cfu) per cm^2 leaf surface. Bars represent mean values ± standard deviation for five biological replicates (n = 5). Leaf samples of one *C. sativus* leaf served as one replicate. Statistically significant differences between bacterial growth in the pretreatments are indicated above bars with asterisks: ***P<0.001, **P<0.01 (two-tailed t-test). (**B**) For the macroscopic analyses of disease symptoms caused by *Psl*, pictures of NHP and H_2O pretreated plants were taken 6 dpi.

Holmes and colleagues (2019) examined the NHP resistance inducing effect in tomato. In the present study the resistance inducing effect of NHP was investigated in another Solanaceae species: *N. tabacum*. Therefore, four- to five-week-old *N. tabacum* plants were watered with

1 mM NHP or H_2O and inoculated with *Psm* (OD_{600} = 0.001) or *Pstb* (OD_{600} = 0.001) one day later. The *N. tabacum* resistance was assessed 3 dpi with *Psm* or *Pstb* by determination of bacterial growth in the inoculated leaves.

In leaves of *N. tabacum* plants that were pretreated with H_2O and inoculated with *Pstb* the number of bacterial determined in the leaves (97 * 10^4 cfu) was significantly, in total 2.3 times higher than the number of bacteria counted in the NHP pretreated and *Pstb* inoculated leaves (40 * 10^4 cfu) (Figure 15.A). The disease symptoms on leaves of H_2O and NHP pretreated plants were documented photographically 6 dpi when symptoms became macroscopically visible (Figure 15.B, M.D). The H_2O pretreated and *Pstb* inoculated *N. tabacum* leaves showed a slight

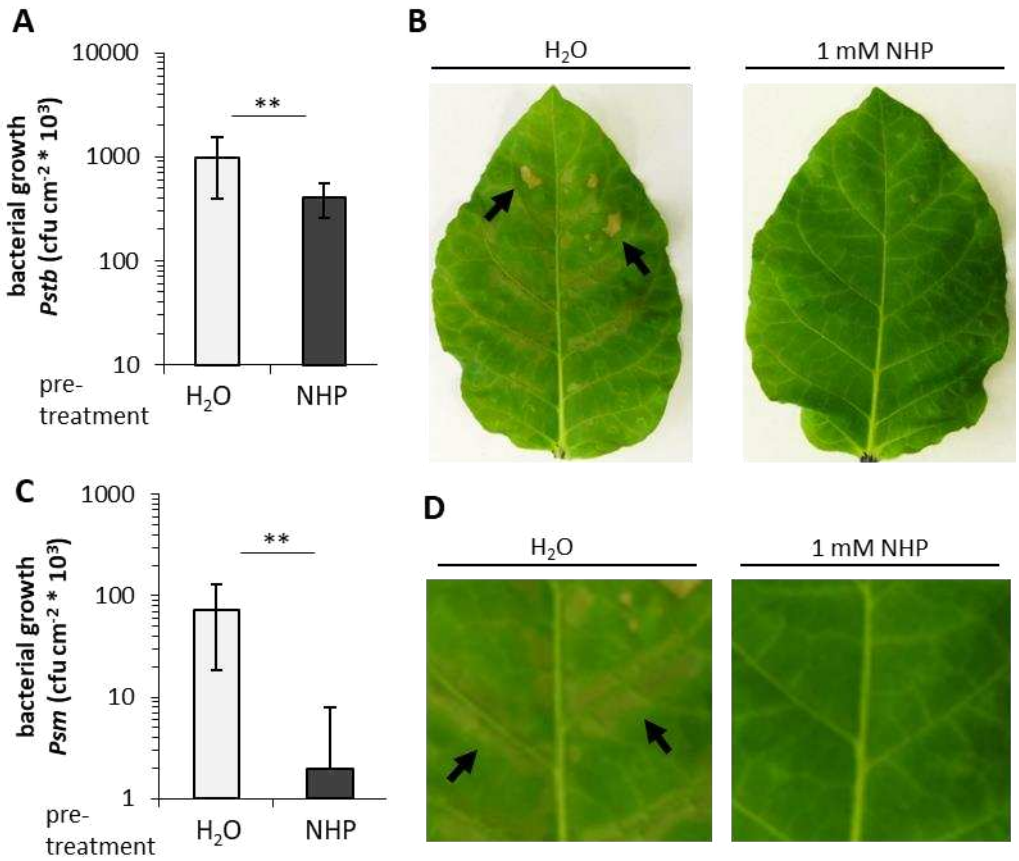

Figure 15: *Nicotiana tabacum* plants acquire systemic resistance to bacterial infections after a NHP injection in the stem. NHP or H_2O (control) were exogenously applied to four- to five-week-old *N. tabacum* plants via the soil and leaves of pretreated plants were infiltrated (**A**) with *Pstb* (OD_{600} = 0.001) or (**C**) with *Psm* (OD_{600} = 0.001) one day later. The resistance of *N. tabacum* plants was assessed 3 dpi by determination of bacterial growth in the inoculated leaves. Mean values ± standard deviation for four biological replicates in *Pstb* and at least five biological replicates in *Psm* experiments are represented by the bars (*Pstb* n = 4; *Psm* n ≥ 5). One replicate consisted of leaf samples from one plant. A two-tailed *t*-test was performed to determine statistically significant differences between bacterial growth in the pretreatments. Results are indicated above bars with asterisks: ***P<0.001, **P<0.01. (**B**) For the macroscopic analyses of disease symptoms in *N. tabacum* caused by *Pstb*, pictures of leaves of NHP and H_2O pretreated plants were taken 6 dpi. (**D**) Close up views show developing necrosis alongside the leaf veins of H_2O pretreated, but not of NHP pretreated leaves.

chlorosis compared to the fully green leaves of NHP pretreated and *Pstb* inoculated leaves 6 dpi (Figure 15.B). Additionally, developing necrosis alongside the leaf veins of H_2O pretreated and *Pstb* inoculated *N. tabacum* leaves (Figure 15.D) and some necrotic spots between the leaf veins were observed (Figure 15.B) while no necrosis was observed on NHP pretreated and *Pstb* inoculated leaves (Figure 15.B, M.D). To test, if the immune inducing effect of NHP in *N. tabacum* is applicable to other *N. tabacum*-pathogen interactions the same experiment was performed using *Psm* instead of *Pstb* bacteria. In leaves of *N. tabacum* plants that were pretreated with H_2O and inoculated with *Psm* the bacterial number ($7.3 * 10^4$ cfu) was 33.7 times higher and thereby significantly higher than the number of bacteria counted in the NHP pretreated and *Psm* inoculated leaves ($0.2 * 10^4$ cfu) (Figure 15.C). These results show significant induction of resistance by exogenous NHP application in *N. tabacum* against *Pseudomonas* infections.

2.2.8. NHP treatments and bacterial infections induce a state of resistance in *Brachypodium distachyon*

To compare the mechanisms of chemical and pathogen induced resistance of dicots and monocots, resistance was induced chemically by NHP application (Figure 16) and SAR was induced with *Xtra* bacteria in *B. distachyon* (Figure 17). To study the NHP induced resistance, two fully grown leaves of three-week-old *B. distachyon* plants were pressure infiltrated with a 1 mM NHP solution or with H_2O as a control treatment. The NHP and H_2O pretreated leaves were pressure infiltrated with *Xtra* (OD_{600} = 0.005). Samples were taken 3 days after *Xtra* infections to assess the resistance of *B. distachyon* (Figure 16.A) and the progression of the infection in NHP and H_2O pretreated leaves was macroscopically documented 3 dpi and 8 dpi (Figure 16.B). In H_2O pretreated and *Xtra* infected leaves an average of $12 * 10^6$ cfu were measured 3 dpi while in NHP pretreated and *Xtra* infected leaves $1.8 * 10^6$ cfu and thereby significantly less than in H_2O pretreated leaves were observed 3 dpi (Figure 16.A). The *Xtra* inoculated leaves of NHP pretreated *B. distachyon* plants showed slight pressure marks as a result of the used application method by infiltration 3 dpi but apart from those, the leaves appeared green and undamaged (Figure 16.B). In contrast, the H_2O pretreated *B. distachyon* leaves developed yellow or brown, dehydrated lesions at *Xtra* infiltration sites at 3 dpi (Figure 16.B). Until 8 dpi, NHP pretreated and *Xtra* infected leaves macroscopically showed slight chlorosis but predominantly still undamaged and green leaves whereas H_2O pretreated and

Xtra infected leaves showed strong chlorosis and beginning necrosis which spread from the infiltration sites to the entire leaf (Figure 16.B).

To further compare the resistance inducing effect of NHP in Brachypodium plants against bacterial and fungal pathogens the same experimental setup was reproduced with an *Magnaporthe grisea* (*Mgri*) infection. The H_2O or NHP pretreated plants were sprayed with a *Mgri* spore solution (50 spores/µl) one day after pretreatments to compare the NHP induced resistance in *B. distachyon* against. Prior to that, the successful infection of *Mgri* in *B. distachyon* was verified macro- and microscopically (Suppl. Figure 3).

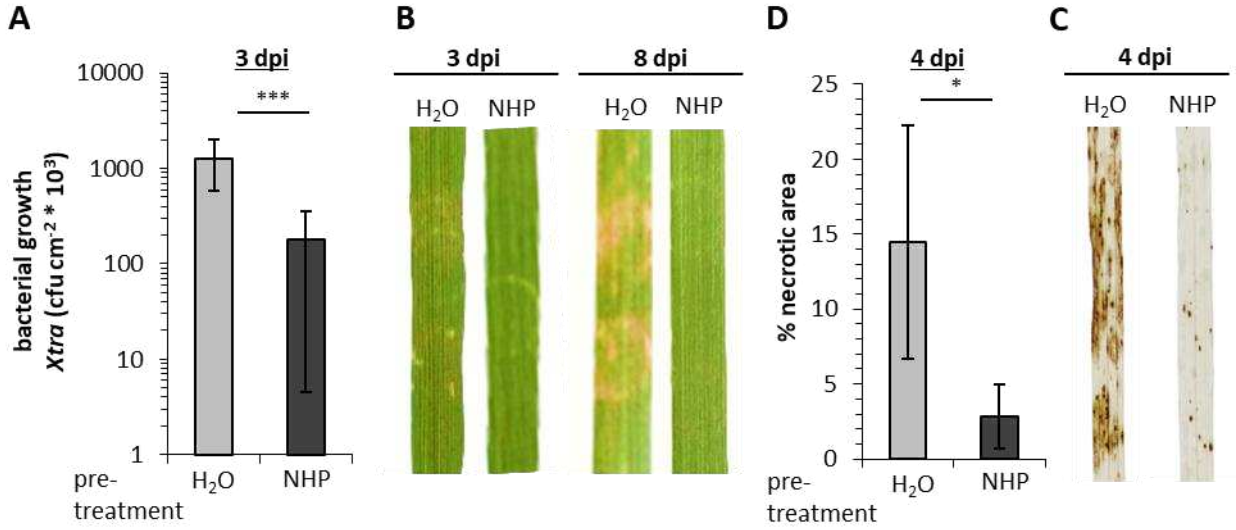

Figure 16: NHP induces acquired resistance in *Brachypodium distachyon* against *Xanthomonas translucens* (*Xtra*) and *Magnaporthe grisea* (*Mgri*) infections. Two fully grown leaves of three-week-old *B. distachyon* plants were pressure infiltrated with a 1 mM NHP solution or H_2O as a control treatment. The NHP and H_2O pretreated leaves were one day later pressure infiltrated with *Xtra* (OD_{600} = 0.005) or sprayed with a *Mgri* solution (50 spores/µl). (**A**) Bacterial numbers in leaves were assessed as colony-forming units (cfu) per cm^2 leaf surface at 3 dpi. For each pretreatment nine individual replicates/plants were used (n = 9). (**B**) Pictures of NHP and H_2O pretreated leaves were taken 3 dpi and 8 dpi for the macroscopic analyses of bacterial disease symptoms in *B. distachyon*. (**C**) The *B. distachyon* resistance against *Mgri* in NHP and H_2O pretreated leaves was assessed 4 dpi. Sampled leaves were destained and the necrotic area per leaf surface was determined in % as a measure of disease severity. Four individual replicates/plants were used for each investigated pretreatment (n = 4). (**D**) Pictures of NHP and H_2O pretreated leaves were taken 4 dpi for the macroscopic analyses of fungal disease symptoms in *B. distachyon*. Statistically significant differences in bacterial growth (A) or leaf necrotic areas (C) between NHP- and H_2O-pretreated plants were determined with a two-tailed t-test. Asterisks (***P<0.001, *P<0.05) are indicated above bars that represent mean values ± standard deviation.

Leaves that were pretreated with H_2O or NHP and were one day later inoculated with *Mgri* one day later. They were sampled four days after *Mgri* treatments and the necrotic areas of *B. distachyon* leaves were measured to assess the *B. distachyon* resistance (Figure 16.D, O.C). The results revealed approximately five times larger necrotic are in H_2O pretreated and *Mgri* infected leaves (14.5 % necrotic leaf area) than in NHP pretreated and *Mgri* infected leaves (2.9 % necrotic leaf area). Thus, the statistical analyses determined significantly more necrotic leaf area in H_2O than in NHP pretreated *B. distachyon* leaves (Figure 16.D). The macroscopic

analyses of H_2O or NHP pretreated, *Mgri* infected leaves, that were harvested 4 dpi and subsequently bleached showed small dark brown necrotic spots on NHP pretreated leaves while the H_2O pretreatment resulted in dark brown lesion covering large areas of the leaves (Figure 16.C). Summarizing, these results indicate an elevated resistance of *B. distachyon* against *Xtra* and *Mgri* after NHP pretreatments when compared to the H_2O control treatments.

To compare the mechanisms of SAR in monocots and dicots, SAR was established in *B. distachyon*. Therefore, two fully grown leaves of three-week-old plants were challenge infiltrated with *Xtra* (OD_{600} = 0.05) or a 10 mM $MgCl_2$ solution and two days later one systemic leaf of each plant was infiltrated with *Xtra* (OD_{600} = 0.005) (Figure 17.A). For assessment of *B. distachyon* resistance in systemic leaves the growth of *Xtra* bacteria was determined 3 dpi. In systemic, *Xtra* treated leaves of *B. distachyon* plants whose local leaves were treated with $MgCl_2$, approximately 34 * 10^6 cfu were detected 3 dpi while in plants whose local leaves were treated with *Xtra,* approximately 9.5 * 10^6 cfu were detected in systemic *Xtra* infiltrated leaves 3 dpi (Figure 17.B). This shows 3.6 times more *Xtra* growth in the systemic leaves of plants which local leaves were infiltrated with $MgCl_2$ than in plants which local leaves were infiltrated with *Xtra*. Macroscopically the local $MgCl_2$ infiltrated *B. distachyon* leaves seemed

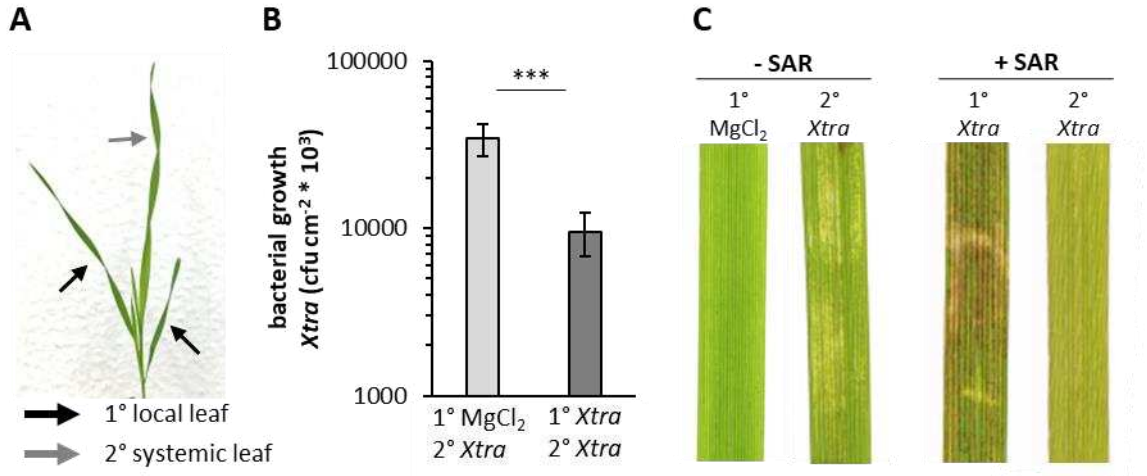

Figure 17: A *Xanthomonas translucens* (*Xtra*) infection induces resistance in systemic *Brachypodium distachyon* leaves against subsequent bacterial infections. (**A**) To trigger SAR, two fully grown leaves (black arrows) of three-week-old *B. distachyon* plants were pressure infiltrated with *Xtra* (OD_{600} = 0.05) or a 10 mM $MgCl_2$ solution. Two days later one systemic leaf (grey arrow) was infiltrated with *Xtra* (OD_{600} = 0.005). (**B**) Bacterial numbers in systemic *B. distachyon* leaves were assessed 3 dpi as colony-forming units (cfu) per cm^2 leaf surface. Six individual replicates/plants were used for each pretreatment (n = 6). Bars represent mean values ± standard deviations. Differences in systemic bacterial growth between *Xtra* and $MgCl_2$ treated plants were tested for statistical significance with a two-tailed t-test and asterisks (***P<0.001) are indicated above bars. (**C**) Pictures of systemic *Xtra* infected leaves and *Xtra* and $MgCl_2$ pretreated leaves were taken 3 dpi for the macroscopic analyses of *Xtra* caused disease symptoms in *B. distachyon*.

undamaged and fully green (Figure 17.C). The local *Xtra* infiltrated leaves however showed chlorosis and necrosis which spread from the infiltration sites to the entire leaf (Figure 17.C). The systemic leaves of *B. distachyon* plants with a local $MgCl_2$ treatment showed chlorotic areas at the inoculation sites 3 dpi while systemic leaves of plants with local *Xtra* treatments showed no signs of chlorosis or damage at the same sampling timepoint (Figure 17.C). Additionally, the statistical analyses revealed a significantly higher number of *Xtra* bacteria in $MgCl_2$ and *Xtra* inoculated plants than in *Xtra* and *Xtra* inoculated plants (Figure 17.B) indicating the successful establishment of SAR in *B. distachyon*.

2.3. Discussion

2.3.1. The pathogen induced NHP biosynthesis is a conserved feature in the immune response of mono- and dicotyledonous plants

The pathogen induced accumulation and immune inducing function of the L-lysin derived small metabolite NHP was first discovered in *A. thaliana* (Hartmann et al. 2018, Chen et al. 2018). Recent phylogenetic studies indicate a functional NHP biosynthesis pathway in several monocotyledonous and dicotyledonous plant species suggesting highly conserved mechanisms in disease resistance of the angiosperm lineage (Hartmann et al. 2018, Homes et al. 2019). Consistently, the NHP precursor Pip has been identified in several monocots and dicots (Návarová et al. 2012, Aliferis et al. 2014, Abeysekara et al. 2016, Vogel-Adghough et al. 2013, Adam et al., 2018, Palfi and Dezsi 1968, Lenk et al.2019). Holmes and colleagues (2019) discovered the pathogen induced accumulation of NHP in the dicotyledonous crop plants tomato, tobacco, and mustard upon inoculation with non-host *P. syringae* strains. This study demonstrates the accumulation of Pip and NHP in the dicots *C. sativus* (Figure 5) and *N. tabacum* (Figure 8) after an infection with *P. syringae* bacteria and in the monocots *B. distachyon* after a *Xtra* (Figure 11) and *Mgri* (Figure 12) infection and *H. vulgare* after a *Mory* infection (Figure 13). In the corresponding Schnake et al. (2020) publication we additionally showed the accumulation of NHP in soybean and tomato after an infection with Pseudomonas bacteria and in tomato after an infection with the oomycete *Phytophthora infestans*. Hence, this study shows major contribution to the current finding that NHP accumulation can be triggered by bacterial, oomycete, and fungal pathogens in dicotyledonous as well as in monocotyledonous plant species.

In untreated *B. distachyon*, *H. vulgare* and *N. tabacum* plants no NHP was detected and in untreated *C. sativus* leaves only small amounts of NHP were detected (Figure 5, 8, 11, 12) indicating that angiosperms exhibit low NHP levels in the absence of a biotic stressor. In *A. thaliana* constitutive accumulation of high amounts of NHP results in retarded plant growth (Guerra et al. 2020, Sun et al. 2020) suggesting that low levels of NHP in unstressed plants set the conditions for proper plant growth. The negative influence of naturally accumulating NHP on the plant's growth reveals a scenario in which a plant must balance between defense and growth.

In case of a pathogenic attack, the NHP biosynthesis is activated in *A. thaliana* to initiate defense responses and, as typical for a signaling molecule, the NHP concentration decreases

in the infected plant tissue over time (Hartmann et al. 2018, Hartmann and Zeier 2019). Similarly, in this study the fast induction of NHP biosynthesis was observed in all investigated plant species. However, only in *C. sativus* infected with *Psl* and in *B. distachyon* infected with *Xtra* a decrease of NHP levels was observed over the performed infection time-courses (Figure 5). In *N. tabacum* infected with *Pstb*, in *H. vulgare* plants infected with *Mory* and in *B. distachyon* infected with *Mgri* the NHP levels were only increasing after infections in the performed infection time-courses (Figure 8, 12, 13). Given the fact that a decrease of NHP was observed in *B. distachyon* after a *Xtra* infection, a decrease in NHP levels in *B. distachyon* after a *Mgri* infection at later, here not investigated sampling timepoints is to expect and can therefore be assumed to take place after infections in *N. tabacum* and *H. vulgare* as well. Hence, the inducible character of the small metabolite NHP can be verified in the here investigated angiosperms.

In *A. thaliana* the decrease of NHP levels is associated with an increase of NHP derivates like the glycosylation to NHPG or NHPGE (Chen et al. 2018, Hartmann and Zeier 2019). In this study NHP derivates were only identified in *C. sativus* (Figure 5). After a *Psl* infection, NHPGE was detected in local infected *C. sativus* leaves (Figure 5). Since a decrease of NHP in the infection time course of *B. distachyon* infected with *Xtra* was observed but no NHP derivates were detected, it is either to assume that NHPG and NHPGE levels were below the detection level or that *B. distachyon* might modify NHP with yet unknown mechanisms. In the latter case, NHP derivates might have not been detectable with the used GC-MS method.

2.3.2. Angiosperms exhibit different strategies to accumulate NHP

In *A. thaliana* the direct biosynthetic precursor of NHP is Pip (Hartmann et al. 2018). The pathogen inducible character of Pip was identified in several plant species including dicots like tobacco, soybean and potato or monocots like rice and barley (Aliferis et al. 2014, Abeysekara et al. 2016, Vogel-Adghough et al. 2013, Adam et al., 2018, Palfi and Dezsi 1968, Lenk et al. 2019). In this study the pathogen induced accumulation of Pip was demonstrated in tobacco and in the monocots *B. distachyon* and barley (Figure 10 - 13). In Schnake et al. (2020) we additionally demonstrated the pathogen induced accumulation of Pip in soybean infected with suitable Pseudomonas bacteria and in tomato after infections with the oomycete *P. infestans* or *Pst* bacteria. In most of the until today investigated species a low basal Pip level below one µg g^{-1} FW was detected (Hartmann et al. 2018, Figure 7, K). The only exception

represents the cucumber, since highly elevated basal Pip levels between 10 and 25 µg g^{-1} FW were detected in the GC-MS analyses of *C. sativus* leaves (Figure 5). Moreover, after *Psl* infections the Pip level did not elevate in cucumber leaves any further (Figure 5). In comparison to other investigated plant species, in *B. distachyon* relatively high basal Pip levels between 1 and 2 µg g^{-1} FW were detected and *B. distachyon* showed a slower Pip than NHP accumulation after infections with hemibiotrophic bacteria or fungi (Figure 11).

Based on the outlined findings three different types of NHP induction after a pathogen infection are proposed to exist in different plants. The first type, like *A. thaliana*, tobacco, tomato, soybean, and barley, accumulate Pip and NHP in parallel upon an infection with a hemibiotrophic pathogen (Hartmann et al. 2018, Schnake et al. 2020). In plants like *A. thaliana* and soybean this pathogen induced accumulation of Pip is strongly associated with the transcriptional induction of *ALD1* gene expression (Návarová et al. 2012, Abeysekara et al. 2016). In Arabidopsis the inducible ALD1 expression and the biosynthesis of Pip and further NHP have been shown to be regulated by the same set of immune regulatory genes like EDS1 and PAD4 supporting the model of a parallel pathogen induced induction of Pip and NHP accumulation in plants (Návarová et al. 2012, Hartmann et al. 2018, Sun et al. 2018, Sun et al. 2020, Wang et al. 2018, Kim et al. 2020).

The second type is represented by the cucumber in this study. In contrast to the first type of NHP biosynthesis induction, in cucumbers constitutively high levels of ALD1 transcripts were observed in combination with constitutively high basal Pip levels (Figure 6). Upon a *Psl* infection, *C. sativus* plants showed elevated *ALD1* transcript levels, but in the NHP biosynthesis pathway only the *FMO1* expression is induced by *Psl*, making NHP the pathogen induced component in the plant's immune response (Figure 6). Furthermore, these constitutive high basal Pip levels in *C. sativus* preclude Pip from the role as a mediator of resistance since this would result in a constitutively activated immunity in *C. sativus* plants. In agreement, *A. thaliana FMO1* deficient mutants were unable to induce resistance after an exogenous Pip application but induced resistance when NHP was applied exogenously to the plants (Hartmann et al. 2018). Thus, high Pip levels in plants like cucumbers supposably serve as steady source for a rapid NHP biosynthesis in the case of a pathogen infection.

The third type of NHP biosynthesis induction is a combination of both before described types. Like *B. distachyon*, plants of this type induce Pip and NHP in parallel upon a pathogenic attack and relatively high basal Pip level might encourage a fast NHP accumulation (Figure 11).

Noticeably, basal Pip levels in *H. vulgare* were comparable with those detected in Arabidopsis or tobacco indicating that dicots and monocots evolved several types of pathogen induced NHP biosynthesis (Figure 13, Figure 7, Hartmann et al. 2018). This strategic divergence in the pathogen induced NHP biosynthesis demonstrates the major importance of NHP in conserved mechanisms in the immune response in angiosperms.

2.3.3. The immune inducing function of NHP in the interplay with SA in mono- and dicotyledonous plants

The immune inducing function of NHP was first demonstrated in *A. thaliana* and confers the plant a primed state of immunity which induces resistance against biotrophic and hemibiotrophic pathogens like *Hpa* or *Psm* (Hartmann et al. 2018, Chen et al. 2018). In this study the NHP induced resistance was demonstrated in *C. sativus* against hemibiotrophic *Psl* bacteria (Figure 14), in *N. tabacum* against hemibiotrophic *Pstb* and *Psm* bacteria (Figure 15) and in *B. distachyon* against hemibiotrophic *Xtra* bacteria and *Mgri* fungi (Figure 16). These results indicate the function of NHP as immune inducer in monocotyledonous and dicotyledonous plant species. Consistently, Holmes and colleagues (2019) demonstrated the NHP induced resistance in tomato against *Pst* DC3000 infections and in pepper against *Xanthomonas euvesicatoria* infections. In addition, Zhang et al. (2021) showed the immune inducing function of NHP in the monocot wheat against the filamentous fungi *Fusarium graminearum*. These recent findings support the role for NHP as a conserved immune inducer in angiosperms and reveals its efficient immune inducing function against a broad spectrum of biotrophic and hemibiotrophic oomycete, bacteria and fungi.

Chen et al. (2018) demonstrated that the infiltration of local *A. thaliana* leaves with an NHP solution results in the activation of SAR in systemic leaves against *Psm* bacteria, making NHP a candidate for the searched long-distance signal in SAR. Even though Pip has been discussed as long-distance signal in SAR, the same study revealed no establishment of SAR in systemic leaves of *A. thaliana* after a local Pip treatment of the same plants (Chen et al. 2018). In agreement, defense priming associated with SAR is completely absent in *ALD1* or *FMO1* deficient *A. thaliana* mutants (Návarová et al. 2012, Bernsdorff et al. 2016). In the SA deficient *sid2* mutant on the other hand SAR and NHP associated defense priming are inhibited, but not completely absent (Bernsdorff et al. 2016, Hartmann et al. 2018). Furthermore, Pip has been shown to positively influence SA mediated immune responses in an *FMO1* dependent manner

(Bernsdorff et al. 2016). This finally suggests a close interplay between SA and NHP in the successful establishment of SAR in *A. thaliana* (Hartmann and Zeier 2019). The here conducted metabolite analyses agrees with these current findings in *A. thaliana*, since NHP and SA accumulated in parallel in the performed infection time courses in tobacco and *B. distachyon* (Figure 4, 5, 7, 10, 11). Additionally, in the Schnake et al. (2020) publication we demonstrated the pathogen induced mutual accumulation of SA and NHP in soybean and tomato.

Noticeably, no SA accumulation was observed in *H. vulgare* after *Mory* infections in this study (Figure 13). Although significant Pip and NHP accumulation was detected in *H. vulgare* after *Mory* infections, the SA level stayed below 0.1 µg g^{-1} FW in infected plants and the respective control plants (Figure 13). Likewise, *H. vulgare* plants infected with the biotrophic fungi *Blumeria graminis* f. sp. *hordei* do not accumulate SA (Hückelhoven et al. 1999). In these *B. graminis* infected barley plants the expression of PR genes was verified though, indicating barley plants might use yet unknown mechanisms in resistance to activate immune responses that are associated with SA in other plant species (Hückelhoven et al. 1999). The immune inducing effect of exogenous SA treatments in barley was however demonstrated to be effective against *B. graminis* infections, indicating conserved mechanism in SA mediated activation of immune responses (Beßer et al. 2000, Kogel et al. 1995, Lenk et al. 2018). A *B. graminis* infection of local barley leaves was in addition sufficient to establish SAR against a *B. graminis* infection in systemic leaves (Hwang and Heitefuss 1982, Sticher et al. 1997). Since *B. graminis* infections in *H. vulgare* do not trigger SA accumulation in local leaves while SAR is established in systemic leaves, the existence of at least one more signaling component other than SA that involved in the establishment of SAR in barley is indispensable.

The role of SA in SAR of other monocotyledonous plant species is however uncertain. In this study only a slight SA accumulation (up to 1.5 µg g^{-1} FW) was detected in *B. distachyon* after *Mgri* infections while after *Xtra* infection in *B. distachyon* leaves explicitly higher SA levels of approximately 8 µg g^{-1} FW (5 dpi) were detected (Figure 11A, J). In *H. vulgare* no SA accumulation was observed after *Mory* infections in this study and after *B. graminis* infections in previous studies (Hückelhoven et al. 1999). In contrast, a recent study demonstrated the accumulation of SA in very low levels in *H. vulgare* plants after an infection with suitable Pseudomonas bacteria and the establishment of SAR by these bacteria (Lenk et al. 2019). In combination these findings indicate a pathogen specific SA signaling response in monocotyledonous plant species which may not allow the application of strict rules for the

role of SA in immune responses of monocots. This assumption supports the existence of at least one more signaling component other than SA that involved in the establishment of SAR in monocotyledonous plant species.

The here presented metabolite analyses of barley and *B. distachyon* suggest that NHP signaling might be involved in the establishment of SAR in monocots. In addition to the *Xtra* and *Mgri* induced local Pip and NHP accumulation in *B. distachyon*, the accumulation of defense related metabolites in systemic leaves after a local *Xtra* infection was investigated. The results reveal a systemic accumulation of NHP and SA in *Xtra* inoculated local leaves and systemic untreated leaves, which was not the case for any other investigated metabolite in *B. distachyon* (Figure 11A, 11B). These findings suggest that SA and NHP are both involved in the full establishment of SAR in *B. distachyon* in the same manner as in *A. thaliana* (Zeier 2021). Additionally, the infiltration of local *B. distachyon* leaves with NHP induced resistance in the same leaves against infections with *Xtra* bacteria or *Mgri* fungi (Figure 16). Remarkably, the treatment of local *B. distachyon* leaves with *Xtra* bacteria resulted in a comparable induction of resistance in systemic leaves against infections with *Xtra* (Figure 15). These findings indicate a central role for NHP in local and systemic immune responses in *B. distachyon*. In agreement, Lenk and his team (2019) demonstrated the sufficient Pip induced resistance in *H. vulgare* against infections with hemibiotrophic *Xtra* pathovar *cerealis* bacteria. Likewise, resistance can be induced by exogenous NHP treatments in wheat and is associated with the deposition of callose (Zhang et al. 2021). In rice, overexpression of the ALD1 gene leads to the induced resistance against *Mory* fungi (Jung et al. 2016) which is comparable to the NHP induced resistance observed here in *B. distachyon* and suggests a role for NHP in the SAR in rice as well. Given that NHP seems to activate the SAR state in barley, wheat, *B. distachyon* and rice it is to assume that the role of NHP in SAR is conserved in monocots. This assumption is highly supported by the identification of NHP biosynthesis genes in several monocots in recent phylogenetic studies (Hartmann et al. 2018, Holmes et al. 2019).

2.3.4. Pathogen-specific accumulation of defense associated metabolites after pathogen infection in monocotyledonous plant species

In this study, a pathogen specific SA accumulation was observed in *B. distachyon* (Figure 10). Further results in this study support a pathogen specific accumulation of defense associated

metabolites in monocotyledonous plant species. The SA associated metabolites (2,x-DHBA-G1, 2,x-DHBA-G2) and derivates (SAG, SGE) accumulate only after *Xtra* infection, but no significant accumulation of these metabolites was detected in *B. distachyon* leaves after *Mgri* infections (Figure 10, 12). In *Mory* infected *H. vulgare* plants no SAG or SGE were detected, however 2,x-DHBA-G1 and 2,x-DHBA-G2 accumulated significantly in *Mory* infected leaves (Figure 13). In *A. thaliana* the SA derivates SAG and SGE are known as SA storage forms which are rapidly generated by the plant to prohibit high, toxic SA levels and to thereby finetune the plants defense response (Dempsey et al. 2017). The SA associated metabolites 2,x-DHBA-G1 and 2,x-DHBA-G2 were identified in this study by comparisons of GC-MS chromatograms of *B. distachyon* leaf samples of infected and control plants. Both metabolites were identified as 2-Hydroxybenzoic acids like SA with an additional OH-group of unknown position and a sugar derivate (Figure 9). In the immune response of plants SA and DHBAs like 2,5-DHBA are thought to have complementary roles since they activate the expression of different sets of PR genes (Bellés et al. 1999). SA and DHBAs were shown to exhibit toxic features when accumulating at high concentrations. However, the plant can bypass toxic effects by sugar conjugation (Bartsch et al. 2010). A recent study revealed the major contribution of DHBA glycosides to the SA homeostasis during immune responses to *Pst* infections in *A. thaliana* (Huang et al. 2018). Hence, the identified 2,x-DHBA-G1 and 2,x-DHBA-G2 might likewise contribute to the homeostasis of SA and DHBAs in in *B. distachyon* and *H. vulgare* in a pathogen specific manner.

Another SA associated metabolite identified in *B. distachyon* this study is PPA, which was identified in several plant families before but still has unknown function in the plant's metabolism (Kindl et al. 1969, Jarvis et al. 2000). The phenylpropanoids structure is a metabolic precursor for several compounds in plants including coumarins, flavonoids and lignin. Most of these phenylpropanoid derived compounds incorporate cinnamic acid in their structure. However, some phenylpropanoid derived compounds are a result of shortening of the side chain of this cinnamic acid structure, including intermediates of the SA biosynthesis pathway (Jarvis et al. 2000). In this study, PPA accumulated significantly in *B. distachyon* plants after *Xtra* but only slightly and not significantly after *Mgri* infections (Figure 11, 12). Additionally, no PPA was detected in *H. vulgare* after *Mory* infections (Figure 13). Assuming an involvement of PPA in the SA biosynthesis as precursor of SA, it seems consistent that in this study no PPA or SA accumulation was observed in *H. vulgare*. In the same matter, only a

slight accumulation of PPA in *B. distachyon* after *Mgri* seems consistent with the along going observed weak accumulation of SA (Figure 12). In agreement, SA and PPA co-accumulation was detected in *Xtra* infected *B. distachyon* leaves 3 dpi (Figure 11). Given that PPA accumulation can be associated with SA accumulation, these results support a pathogen specific induction of the SA biosynthesis pathway in monocotyledonous plants like *B. distachyon* and *H. vulgare*.

A further metabolite that was identified in the metabolite profile of *B. distachyon* is serotonin. Serotonin was identified in several mono- and dicotyledonous plant species in previous studies and might in those species act as phytohormone in plant development (Smith 1977, Roychoudhury 2021). In this study the serotonin accumulation in leaves in *B. distachyon* infection time-courses with *Xtra* bacteria was observed, but serotonin did not significantly accumulate in leaves after *B. distachyon* infections with *Mgri* (Figure 11, 12). These results indicate a pathogen specific accumulation of serotonin in *B. distachyon*. In *H. vulgare* no serotonin was detected in *Mory* infected or control leaf samples (Figure 13), however under the previously formed assumption this might be based on a pathogen specific *H. vulgare* defense response and serotonin might accumulate in this monocot after infections with other pathogens. The current state of research in this matter offers no evidence for a pathogen induced serotonin accumulation in *H. vulgare* though. In the here investigated dicotyledonous plant species, cucumber and tobacco, no serotonin was detected in infected and control leaf samples. However, the basal level of serotonin in several healthy mono- and dicotyledonous plant species including rice, wheat, potato and spinach has been demonstrated (Huang and Mazza 2011). In the same study, no basal serotonin levels were detected in *H. vulgare* seedlings and seeds (Huang and Mazza 2011), agreeing with the here presented results of the metabolite analyses of *H. vulgare* (Figure 13).

In addition to serotonins stimulating role in plant development, it serves as an antioxidant by countering the accumulation of ROS through interactions with the phenylpropanoid pathway, in which serotonin serves as an amine substrate for the formation of hydroxycinnamic acid amides (Bajwa et al. 2015, Roychoudhury 2021). Some of these hydroxycinnamic acid amides are also integrated in the cell wall of plants whereby they serve as mechanical barriers against pathogens (Keller et al. 1996, Hahlbrock and Scheel 1989). These mechanisms have also been observed for serotonin, which in integrated into the cell walls of rice plants and thereby provides protection against *Bcin* infections (Ishihara et al. 2008). The accumulation of

serotonin after a pathogen attack in plants like *B. distachyon* could therefore serve as regulation of ROS accumulation and formation of mechanical barriers, enabling plants to response appropriately to attacking pathogens. In agreement, it has been shown that the exogenous application of serotonin can induce a cell death and cell wall strengthening associated resistance in rice against a *Mgri* pathovar (Fujiwara et al. 2010). In the defense against the fungal pathogen *Stagonospora nodorum*, serotonin might additionally act as a phytoalexin in wheat by the promotion of the generation of the mycotoxin alternariol (Fall and Solomon 2013).

In contrast, only little is known about the role of serotonin in dicotylous plants. It has been demonstrated that low basal serotonin levels can be detected in the dicotyledonous model organism *A. thaliana*, however several studies investigated the role of the serotonin derivate melatonin in plant growth and plant resistance of dicotyledonous plant species (Pelagio-Flores et al. 2011, Lee et al. 2014, Zhu et al. 2021). In this matter, a recent study demonstrated that melatonin is an important regulatory factor in JA, phytoalexin and ROS associated defense responses against *Bcin* in *A. thaliana* (Zhu et al. 2021). Hence, the suggested roles for serotonin in monocotyledonous plant species like rice match the suggested role for melatonin in dicotyledonous species like Arabidopsis, indicating shared mechanisms in the pathogen induced biosynthesis of hydroxycinnamic acid amides. The serotonin accumulation however seems not only pathogen specific in monocotyledonous plants but is rather highly dependent on the specific plant-pathogen interaction system, since serotonin can not be detected in all angiosperms and was detected in this study only in *B. distachyon* after *Xtra* infection, but not after *Mgri* infections.

2.3.5. NHP potentially is the long-distance signal in SAR

A controversial aspect of SAR has since its discovery been the achievement of long-distance signaling from an infected leave to distal plant tissue (Shah and Zeier 2013). Recently, NHP has emerged as the secondary metabolite that is required for SAR establishment in the dicotyledonous model organism *A. thaliana* (Hartmann et al. 2018, Hartmann und Zeier 2019, Chen et al. 2018). In Arabidopsis, the immune inducing systemic effects of local NHP infiltrations against bacterial infections in systemic leaves were observed (Chen et al. 2018) indicating long-distance travels of NHP from the infiltrated to distal leaves in plants. Likewise, NHP application of the stem side of a tomato leaflet induces resistance in untreated leaflets

of the same leaf (Holmes et al. 2019). Furthermore, Holmes and colleagues (2019) demonstrated the activation of the SAR state in distal leaf tissue of tomato and tobacco after the local *Agrobacterium*-mediated expression of the *A. thaliana* NHP biosynthetic genes. Although these studies support the role for NHP as mobile SAR signal, the experimental setups do not resolve the question whether NHP achieves long distance communication via cell-to-cell signal propagation or by direct transfer from infected to distal tissue.

Therefore, the phloem exudates (PE) of *Psl* infected cucumber plants and respective control treatments were investigated via GC-MS analyses in this study (Figure 4, 5). The PEs of cucumbers have been under investigation in this matter in previous studies with the focus on the role of SA as long-distance signal in SAR (Métraux et al. 1990). Hence, it has been demonstrated that SA accumulates in local leaves and PE of *C. sativus* plant that were infected with *Colletotrichum lagenarium* or the tobacco mosaic virus (Métraux et al. 1990). Furthermore, this SA accumulation occurs in parallel with a sufficient induction of resistance in systemic leaves of cucumbers (Métraux et al. 1990). Transportable characteristics of SA were also tested by the application of radiolabeled SA to cucumber leaves. The results suggested a transport of SA to the distant cucumber leaves but the authors at the same time do not rule out the existence of another, primary SAR signal (Meuwly et al. 1995). Consistently, Rasmussen and colleagues (1991) observed the activation of the SAR state in systemic leaves of Pseudomonas infected *C. sativus* plants prior to the accumulation of SA in the PE of systemic leaves and therefore suggested this primary SAR signal might activate the SA accumulation in systemic cucumber leaves.

The here presented results, confirm the SA accumulation and its derivate SAG, in *Psl* inoculated *C. sativus* leaves and the PE of these leaves (Figure 4). However, no SA accumulation was detected in systemic leaves of *Psl* infected *C. sativus* plants and in comparison to the respective control treatments only a slight SA accumulation was observed in systemic PE (Figure 4). In contrast, the accumulation of NHP after *Psl* infections was observed in local leaves, local PE, as well as in systemic PE and systemic leaves of *C. sativus* plants (Figure 5). These results agree with the before suggested role for NHP as long-distance signal in the communication of SAR in plants. The NHP precursor Pip was detected in constitutively high levels in PE samples and did not accumulate after a *Psl* infection in cucumber (Figure 5). Hu et al. (2016) identified Pip as a constituent of the phloem in cucumbers and Pip might thus serve as steady source for the pathogen induced NHP

biosynthesis in the phloem. In this assumption, it is likely that NHP as the primary SAR signal achieves long distance communication via cell-to-cell signal propagation rather than by direct transfer from infected to distal tissue. In disagreement, Yildiz and colleagues (2021) demonstrated that D9 labeled NHP which is infiltrated in an *A. thaliana* leaf is detectable in distal leaves, verifying that NHP can in fact travel from an inoculated to an uninfected leaf. The current data in this matter thus suggests a combined model in which NHP accumulates in local leaves and is transported to systemic leaves via the phloem. Accumulating NHP in the phloem and systemic leaves promotes the transcriptional response of the NHP biosynthesis enzymes resulting a strong accumulation of Pip and NHP in systemic leaves.

In this study it was demonstrated that an NHP treatment of *B. distachyon* leaves induces resistance in systemic leaves against an *Xtra* infection in a comparable degree as a local *Xtra* infection induced resistance to a following infection of systemic leaves in the monocotyledonous model organism (Figure 16, 21). Additionally, the local and systemic response of *B. distachyon* to a *Xtra* infection was investigated via GC-MS and revealed a significant NHP accumulation in local and systemic leaves of *B. distachyon* plants (Figure 11). These findings suggest that NHP might serve as mobile SAR signal in mono- as well as in dicotyledonous plant species. It has been demonstrated that angiosperms share conserved mechanisms in JA and SA mediated immune responses against pathogens (Thaler et al. 2012). In *H. vulgare* SA does not accumulate after pathogen infection. Still, SAR is triggered by pathogen infections, indicating conserved SA-independent mechanisms in the activation of SAR in monocots (Hückelhoven et al. 1999, Hwang and Heitefuss 1982, Sticher et al. 1997). The conserved long-distance signal that activates SAR in mono- and dicotyledonous plant species might thus be NHP.

2.3.6. Conclusion

The here presented results demonstrate the pathogen induced NHP biosynthesis in various monocotyledonous and dicotyledonous plant species and indicate that angiosperms might have developed diverse strategies to accumulate NHP. Furthermore, an SAR associated immune inducing function of NHP was identified in the here investigated mono- and dicotyledonous plant species. Additionally, a functional SAR was demonstrated in the monocot model organism *B. distachyon* in parallel with a local and systemic accumulation of

SA and NHP indicating similar mechanisms in the induction of local and systemic immune responses of *B. distachyon* and the dicot model organism *A. thaliana* (Hartmann and Zeier 2019, Zeier 2021). The suggested role of NHP as mobile signal in SAR is further supported in this study by the systemic accumulation of NHP in leaves and PE of *Psl* infected cucumber plants.

3. PART II: The NHP resistance effect in *Arabidopsis thaliana* under the attack of hyphae growing pathogens with various lifestyles

3.1. Introduction

3.1.1. Lifestyle strategies of *Arabidopsis thaliana* infecting pathogens

A. thaliana or thale cress is an annual dicotyledonous plants species of the *Brassicaceae* plant family. Based on the short life cycle (six to eight weeks), high reproduction rate (more than 10 000 seeds per plant) and its simple cultivation, the small dicotyledonous *A. thaliana* represents the model organism for dicotyledonous plant species in several plant research areas (Meyerowitz 1987, Meinke et al. 1998). The *A. thaliana* genome is fully sequenced and consists of approximately 30 000 genes which are located on five chromosomes. Established manipulations of the *A. thaliana* genome by forward and reverse genetics have resulted in the distribution of *A. thaliana* mutants and ecotypes by institutions like The European Arabidopsis Stock Centre (NASC). The available knowledge, techniques, and mutant collections for *A. thaliana* make the dicotyledonous plant a suitable model organism for investigations of plant-pathogen interactions. Plants like *A. thaliana* are, under natural conditions, under the attack of a broad spectrum of phytopathogen that developed diverse strategies in the invasion of their hosts and in detraction of nutrients from their hosts (Glazebrook, 2005). Depending on their lifestyle strategies, plant infecting pathogens have thus been roughly classified in biotrophs, necrotrophs and hemibiotrophs (Glazebrook, 2005). Infection strategies of biotrophic, hemibiotrophic and necrotrophic pathogens that infect *A. thaliana* are in the following explained at the example of pathogens that are used in this study.

Biotrophy

Biotrophic pathogens that infect *A. thaliana*, such as *Hpa*, do not invade or destruct the host cells and feed from living plant tissue (Baxter et al. 2010). The biotrophic *Hpa* is a member of the group of oomycetes and as such can reproduce via oospores (sexual lifecycle) or via conidia (asexual lifecycle) (Slusarenko and Schlaich 2003). Oospores thereby represent the more robust reproduction structure and can overwinter in soil or plant tissue to infect new Arabidopsis plants in times of suitable conditions for infections (Coates and Beynon 2010). Further rounds of infections mostly occur by conidia (Slusarenko and Schlaich 2003).

If such a *Hpa* conidium lands on an *A. thaliana* leaf, it starts to germinate and forms an appressorium to penetrate the host cell. Appressoria formation is often observed at the junction of two adjoining epidermal cells whereby no cells are disrupted during the invasion of the penetration hyphae (Figure 18, Koch and Slusarenko 1990). Appressoria formed penetration hyphae then grow into the leaf intercellularly alongside the cell walls of epidermal cells. At this point usually the first haustoria are formed and extend into these epidermal cells (Figure 18, Koch and Slusarenko 1990, Coates and Beynon 2010). Haustoria are also referred to as feeding structure of *Hpa* and other oomycete and fungi since they are essential for the nutrient uptake of those pathogens (Catanzariti et al. 2007). This nutrient uptake is facilitated over an extrahaustorial membrane, which is established between the haustorial cell wall of *Hpa* and the hosts plasma membrane. Thereby *Hpa* haustoria do not breach the plasma membrane of a host cell and are thus not in direct contact with the plant cell (Soylu and Soylu 2003). The sequenced *Hpa* genome revealed that several genes that are necessary for the assimilation and fixation of nitrogen in other haustoria forming pathogens like *Phytophthora* species are not present in *Hpa* (Baxter et al. 2010) demonstrating the great dependency of *Hpa* on haustoria that facilitate the uptake of nutrients like nitrogen. In addition to nutrient uptake, haustoria are associated with cellular communications between the host and the pathogen in the establishment of a biotrophic relationship (Voegele and Mendgen 2003).

After the formation of the first haustoria, *Hpa* hyphae branch out intercellularly into the mesophyll, where several haustoria are formed (Figure 18, Koch and Slusarenko 1990, Slusarenko and Schlaich 2003). Hyphal tips of *Hpa* that grow close to stomata in the intercellular space develop into conidiophores, which emerge through the stomata and deploy their tree-shaped structure (Figure 18, Coates and Beynon 2010). This tree-shaped structure of *Hpa* conidiophores possess visual similarities with morning dew on *A. thaliana* leaves which is why *Hpa* infections are often referred to as downy or powdery mildew infections in *A. thaliana*. Oospores of *Hpa,* which are produced via sexual reproduction, are formed in the host's tissue. In the sexual reproduction cycle of *Hpa*, intercellularly growing hyphae differentiate into female oogonia and male antheridia. After fertilization the oogonia then develops an oospore (Slusarenko and Schlaich 2003, Coates and Beynon 2010). Conidiophores and oospores are under suitable conditions produced within a week and can infect new leaves or other plants (Coates and Beynon 2010). As an obligate biotroph, *Hpa* cannot be cultured *in vitro*, and its survival is dependent on a living Arabidopsis host.

In the defense against *Hpa*, the most effective defense strategy observed in *A. thaliana* is the induction of the HR which leads to cell-death of the *Hpa* infected cells (Glazebrook 2005). In SA signaling deficient *A. thaliana* mutants, like *eds1* or *pad4*, the establishment of HR fully or partially fails resulting in an enhanced susceptibility toward *Hpa* infections (Feys et al. 2001, Glazebrook 2005). These results demonstrate that the *A. thaliana* immune response against *Hpa* is dependent on SA mediated responses, however further research has revealed that SA-independent mechanisms are likewise involved in the *A. thaliana* defense against *Hpa* infections. In this matter, *A. thaliana ald1* and *fmo1* mutants with deficiencies in the NHP biosynthesis pathway were shown to exhibit an enhanced susceptibility toward *Hpa* infections (Hartmann et al. 2018). Likewise, exogenous NHP treatments induce resistance in *A. thaliana* against the biotrophic oomycete (Hartmann et al. 2018). The given data indicates the dependency of a proper *A. thaliana* immune response against *Hpa* infections on a functional SA and NHP signaling pathway.

Necrotrophy

In contrast to biotrophic pathogens that infect *A. thaliana*, necrotrophic pathogens, like *Bcin*, feed on lysed plant tissue (Glazebrook 2005). The fungi *Bcin* belongs to the group of ascomycetes and is a typical example of a necrotrophic pathogen, since it kills its hosts cells to further colonize and feed on them (Amselem et al. 2011). *Bcin* infects approximately 200 different plant species and thereby causes substantial economic losses every year, however the model organism *A. thaliana* is often used to study plants interaction with the necrotrophic fungi (Williamson et al. 2007, Dean et al. 2012). Infections with *Bcin* are mostly initiated by conidia that might land on an *A. thaliana* leaf by wind or rainfall (Schumacher and Tudzynski 2012). Conidia germinate on the leaf surface and develop a germ tube which directly penetrates a plant cell (Figure 18, Williamson et al. 1995). Epidermal cells are lysed by *Bcin*, which allows the necrotroph to colonize subepidermal cell layers intracellularly and establish the infection while causing necrosis (Figure 18). In comparison to the biotrophic *Hpa*, *Bcin* resembles rather complex reproductive mechanisms. During the asexual reproduction of *Bcin*, conidiophores carrying conidia are formed three to five days after the first infection with *Bcin* and emerge through lysed epidermal cells (Figure 18). During the sexual reproduction of *Bcin*, ascospores are formed by male microconidia and female apothecia. Additionally, *Bcin* forms

sclerotia as long-term survival structure, which are able to form new conidiophores under suitable environmental conditions for *Bcin* infections (Schumacher and Tudzynski 2012).

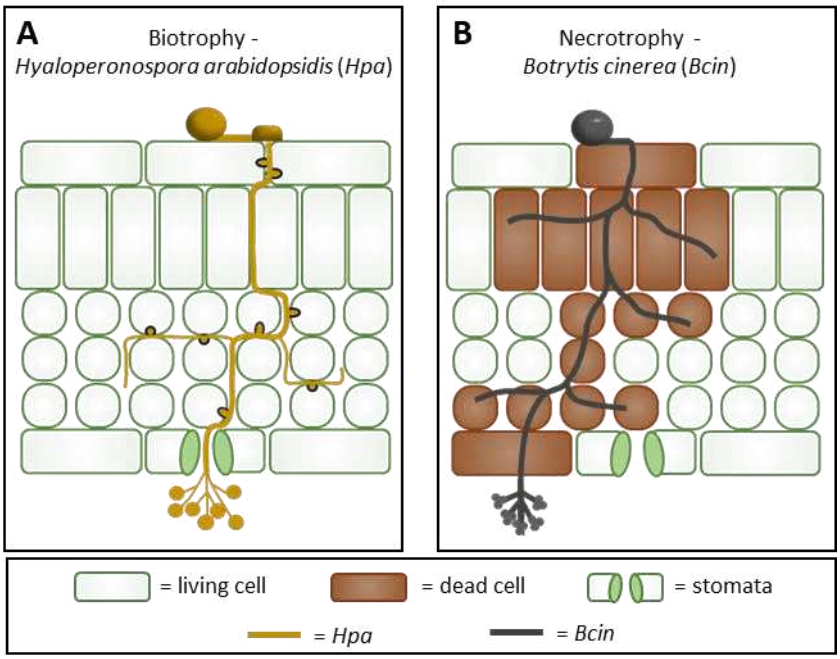

Figure 18: Life cycle of *Hyaloperonospora arabidopsidis* (*Hpa*) as an example of biotrophy and *Botrytis cinerea* (*Bcin*) as an example of necrotrophy. (**A**) When a *Hpa* conidium lands on the leaf surface it starts to form an appressorium in the junction of two epidermis cells. From the appressorium a penetration hyphae then grows into the leaf intercellularly, and hyphae start to branch and form haustoria in the mesophyll. *Hpa* haustoria reach into the plant cells without disrupting them and establish an extrahaustorial membrane (dark lines). Hyphal tips close to stomata in the intercellular space develop into conidiophores, which emerge through stomata. (**B**) When a *Bcin* conidium lands on the surface of a leaf, it forms a germ tube and penetrates an epidermis cell. The epidermal cell is lysed by *Bcin*, which allows the necrotroph to colonize subepidermal cell layers intracellularly and establish the infection while causing necrosis. Tree-shaped *Bcin* conidiophores, carrying fresh conidia, emerge through lysed cells.

Upon infections with necrotrophic pathogens the JA/ET signaling pathway is activated in plants (Wasternack and Hause 2013). Consistently, *A. thaliana* infections with *Bcin* have been demonstrated to induce the expression of JA and ET dependent genes like *PDF1.2* (Govrin and Levine 2002). Moreover, *A. thaliana* mutants with defects in the JA or ET signaling show an enhanced susceptibility towards *Bcin* infections compared to wildtype plants (Ferrari et al. 2007). Recent studies also identified WRKY33 as a key factor in the *A. thaliana* immunity towards *Bcin*. Among other signaling pathways the WRKY33 transcription factor regulates the pathogen induced ABA and camalexin accumulation (Liu et al. 2015). The *Bcin* induced accumulation of camalexin and the camalexin induced resistance against *Bcin* have been demonstrated in *A. thaliana* (Govrin and Levine 2002, Ferrari et al. 2003). Furthermore, *A. thaliana* mutants that are impaired in the camalexin biosynthesis, like *pad3* mutants, show increased susceptibility against infections with non-adapted *Bcin* isolates but not against

infections with host adapted *Bcin* isolates (Ferrari et al. 2003, Kliebenstein et al. 2005, Ferrari et al. 2007, Stefanato et al. 2009). The deficiency of *A. thaliana* mutants in the SA signaling however did not affect the resistance of *A. thaliana* towards *Bcin* infections (Ferrari et al. 2003, Ferrari et al. 2007). This demonstrates the importance of a functional JA, ET and camalexin signaling in *A. thaliana* immune responses against *Bcin* infections, while the SA signaling seems to be neglectable in this interaction.

Hemibiotrophy

Many plant infecting pathogens have developed an intermediate between the bio- and necrotrophic lifestyle: the hemibiotrophic lifestyle (Kabbage et al. 2015). This lifestyle consists of a biotrophic phase in which the pathogen needs a livings host to survive and feed on, followed by a switch to necrotrophy in which the host is killed to feed on lysed plant material (Glazebrook 2005). Arabidopsis infecting hemibiotrophic pathogens include a broad spectrum of bacteria, oomycetes and fungi with a multitude of strategies to achieve hemibiotrophy. It is suggested that hemibiotrophic fungi like *Chig* or *Sclero* use the biotrophic phase to establish the infection in plants (Vargas et al. 2012, Kabbage et al. 2015). During biotrophy defense responses of the plant are tolerated and accumulating defense responses might even trigger these fungi to switch to necrotrophy, a more effective infection strategy (Kabbage et al. 2015). The biotrophic phase of a fungal hemibiotrophic pathogen can be achieved by different strategies. The hemibiotrophic ascomycete *Chig* for example starts the infection of *A. thaliana* and other Brassicaceae with a conidium that lands on a leaf and germinates. After the formation of a short germ tube, an appressorium is formed and penetrates an epidermal plant cell with high pressure (Figure 19, De Silva et al. 2017). An infection peg penetrates the first epidermal cell and invaginates the host's plasma membrane whereby the cell wall of the host is not disrupted (Figure 19, O'Connell et al. 2004, De Silva et al. 2017). Thereby the entrance of *Chig* in the plant is successfully achieved and swollen, bulbous biotrophic hyphae (BH) arise from the infection peg (Figure 19, Yan et al. 2018). The BH exhibit haustoria like functions since they do not disrupt the cell walls of the host and this cell remains fully intact (Latunde-Dada et al. 1996, O'Connell et al. 2004). However, the growth of these BH is restricted to the first infected epidermal cell and represents the biotrophic phase of *Chig* in plants like *A. thaliana* (Figure 19, O'Connell et al. 2004). Three to four days after an infection with *Chig* of an *A. thaliana* plant filamentous necrotrophic hyphae (NH) start to develop (Yan et al. 2018). These

NH rapidly start to grow from BH and infect neighboring cells by intracellular growth (Figure 19, O'Connell et al. 2004, Yan et al. 2018). Thereby necrosis is caused in the infection site surrounding plant tissue approximately four to five days after a *Chig* infection (Figure 19, Yan et al. 2018). Acervuli start to grow out of necrotized tissue and produce conidiophores with conidia (Figure 19, O'Connell et al. 2004). Current available data mostly reports the reproduction of *Chig* via the described asexual life cycle (Figure 19), but sexual reproduction has also been observed in *Chig* pathovars and might be initiated under stress like the senescence of the host (De Silva et al. 2017). Homothallic and heterothallic *Chig* pathovars have been observed to form perithecia that produce ascospores inside of asci (De Silva et al. 2017).

The life cycle of the hemibiotrophic fungi *Sclero* exhibits substantial differences to the described *Chig* life cycle although both fungi share the hemibiotrophic pathogenic lifestyle (Kabbage et al. 2015). The initiating *Sclero* infection structure for an infection in plants like *A. thaliana* is scientifically not identified yet, however infections are frequently observed to be initiated by mycelium that grows into wounded plant tissue or forms appressoria in intact leave surfaces (Figure 19, Tariq and Jeffries 1984). *Sclero* appressoria are formed between two adjacent epidermal cells to penetrate the host (Figure 19). In the biotrophic infection phase *Sclero* then grows intercellularly without disruption the cell walls of hosts like *A. thaliana*. After a switch to the necrotrophic phase, *Sclero* hyphae grow intracellularly while the biotrophic stage is perpetuated in parallel at the edge of *Sclero* colonization (Figure 19, Kabbage et al. 2015). During the necrotrophic phase the hosts tissue is necrotized. In this necrotized tissue *Sclero* forms sclerotia, which are name giving for *Sclero* (Figure 19). Sclerotia have been observed to overwinter in the soil or in dead plant tissue and produce ascospore carrying apothecia or directly produce mycelium in more suitable environmental conditions for *Sclero* infections (Kabbage et al. 2015).

Previous research indicates that in *A. thaliana* infections with hemibiotrophic fungi like *Chig* and *Sclero*, the SA pathway seems to be of major importance for defense reaction of the plant in the biotrophic phase of the attacking pathogen, while JA and ET seem to mediate important immune responses in the plant during the necrotrophic phase of the pathogen (Narusaka et al. 2006, Guo and Stotz 2007). Hence, *A. thaliana* mutants with defects in the SA pathway showed increased susceptibility towards *Sclero* (Guo and Stotz 2007) and *Chig* (Liu et al. 2007, Gebauer et al. 2017) in independent studies. Guo and Stotz (2007) additionally

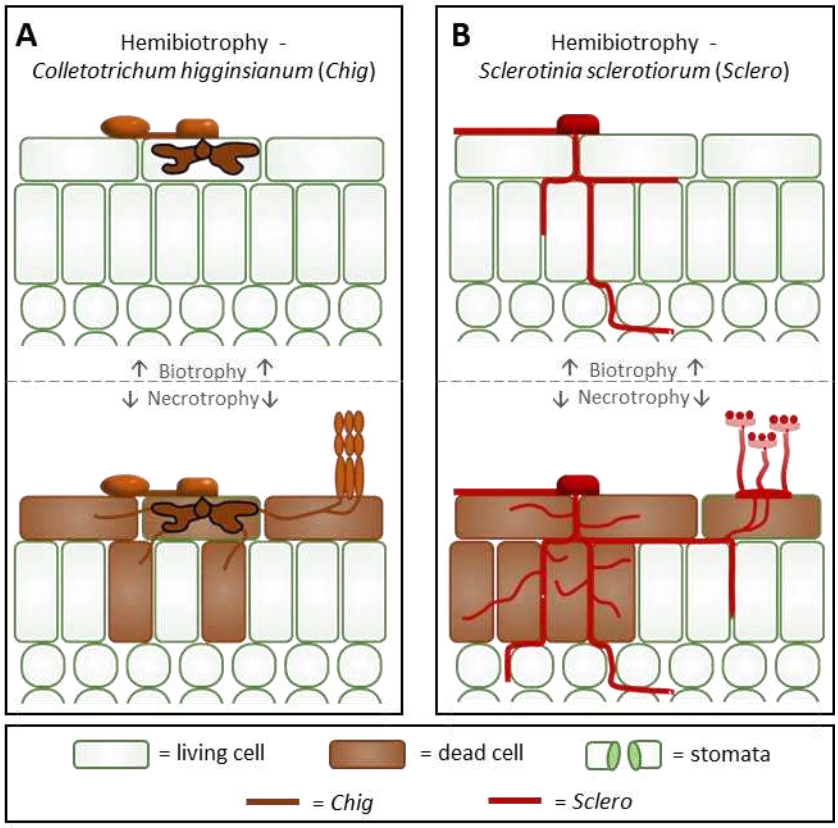

Figure 19: Life cycle of *Colletotrichum higginsianum* (*Chig*) and *Sclerotinia sclerotiorum* (*Sclero*) as an example of hemibiotrophy. (**A**) When a *Chig* conidium lands on a leaf surface it starts to form an appressorium, which penetrates an epidermal cell. In the biotrophic phase, the Chig penetration peg invaginates the hosts cell wall and grows swollen biotrophic hyphae, that do not disrupt cells, in the epidermis cell. In the necrotrophic phase, *Chig* starts to grow filamentous necrotrophic hyphae from the biotrophic hyphae. Necrotrophic hyphae *Chig* disrupt the first infected epidermis cell and neighbouring cells causing necrosis. Acervuli start to grow out of necrotized tissue and produce conidiophores with conidia. (**B**) *Sclero* infections are frequently observed to be initiated by mycelium that forms appressoria between two adjacent epidermal cells of a host. In the biotrophic phase, Sclero hyphae grow intercellularly without disrupting cell walls. After a switch to the necrotrophic phase, Sclero hyphae grow intracellularly while the biotrophic stage is perpetuated in paralle at the edge of Sclero colonization. In necrotized plant tissue Sclero forms sclerotia, which can grow fresh mycelium to infect new hosts.

demonstrated an increased susceptibility towards *Sclero* of *A. thaliana* mutants with defects in the JA/ET signaling pathway. In infections with *Chig* of *A. thaliana* mutants with defects in the JA signaling pathway, a wildtype-like disease development was observed, while *A. thaliana* ET mutants showed an increased susceptibility towards *Chig* compared to the Col-0 plants (Liu et al. 2007). Since *Sclero* maintains a biotrophic and necrotrophic phase in parallel and *Chig* establishes infections in a rather long biotrophic phase and then switches to the reproducing necrotrophic phase, JA is presumably more important in the *A. thaliana* immune responses against an establishing *Sclero* infection than an establishing *Chig* infection. However, agreeing with the assumption that JA is associated with necrotrophy, in later infection stages of *Chig* in

A. thaliana the accumulation of JA has been observed at later infection timepoints of the interaction (Riet et al. 2016).

The defense mechanisms of *A thaliana* against attacking hemibiotrophic pathogens were primarily investigated in the *A. thaliana* - *Pseudomonas syringae* model system for plan-pathogen interactions though. *P. syringae* are anaerobic gram-negative bacteria with polar flagella which can enter *A. thaliana* hosts through stomata or wounds. Once entered the plant, *P. syringae* bacteria multiply intercellularly and in later infection stages cause chlorosis and necrosis in infected plant tissue (Arnold and Preston 2019). During an infection of a plant, some *P. syringae* pathovars have been observed to produce coronatine which resembles the bioactive form of JA, JA-isoleucine. Thereby, the SA-signaling activated in the plant by the biotrophic growth of Pseudomonas bacteria is interrupted which is associated with the establishment of infection (Block et al. 2005, Katsir et al. 2008). This demonstrated that the SA signaling is essential for the *A. thaliana* resistance against *P. syringae* bacteria (Glazebrook 2005). Consistently, *A. thaliana* mutants with defects in the SA signaling like *sid2*, *eds1* or *pad4* show an increased susceptibility towards Pseudomonas infections (Mishina and Zeier 2006, Návarová et al. 2012, Bernsdorff et al. 2016). However, the constitutive activation of JA dependent defense responses has been shown to increase the *A. thaliana* resistance towards virulent *Psm* bacteria (Ellis et al. 2002). Hence, the *A. thaliana* resistance towards the here described hemibiotrophic bacteria and fungi seems to be dependent on a functional SA and JA signaling pathway.

3.1.2. NHP in the defense against pathogens with different lifestyles

In studies of plant resistance, the small metabolite NHP gained major attention in the last decade. The biosynthesis of NHP and its metabolic precursor Pip have been demonstrated to be induced upon the infection with hemibiotrophic pathogens in several plant species, including *A. thaliana* (Hartmann 2018, Holmes et al. 2019, Schnake et al. 2020). The immune inducing effect of NHP against these hemibiotrophic pathogens was additionally demonstrated in several angiosperms and indicates highly conserved mechanisms in NHP mediated defense responses in plants (Hartmann 2018, Holmes et al. 2019, Schnake et al. 2020). In *A. thaliana* exogenous treatment with NHP was sufficient to induce resistance towards infections with the biotrophic oomycete *Hpa* and the hemibiotrophic bacterium *Psm*

(Hartmann et al. 2018). After an infection of an *A. thaliana* leaf with *Psm* bacteria, NHP accumulation was moreover observed in local infected and in distal leaves, indicating an involvement of NHP in the establishment of SAR (Hartmann and Zeier 2019). In the current model for SAR based on research in *A. thaliana*, NHP as mobile SAR signal is translocated from the point of infection to systemic leaves where it triggers the accumulation of SA (Zeier 2021). Since SAR is strongly associated with SA mediated defense responses and those are effective against biotrophic and hemibiotrophic pathogens, it was assumed that SAR likewise induces resistance towards biotrophic and hemibiotrophic pathogens, but not towards necrotrophic pathogens (Glazebrook et al. 2005). Hence, the establishment of SAR in several angiosperms upon the infection with biotrophic Blumeria or Hyaloperonospora species and hemibiotrophic Pseudomonas, Colletotrichum or Fusarium species has been reported (Sticher 1997). Consitantly, it was demonstrated that the necrotrophic *Bcin* fails to stablish SAR (Govrin and Levine 2002, de Cremer et al. 2013). However, a recent study observed the establishment of an *fmo1* dependent egg extract induced SAR against infections with the necrotroph *Bcin* and the biotroph *Hpa* in *A. thaliana* (Alfonso et al. 2021), indicating NHP might play a role in systemic defense responses against pathogens with biotrophic and necrotrophic lifestyle strategies.

In support, Lenk and colleagues (2019) demonstrated that a treatment of barley leaves with the NHP precursor Pip induces resistance in systemic leaves against an infection with biotrophic fungi and hemibiotrophic bacteria, but only a slight induction of resistance was observed in systemic barley leaves after the infection with the necrotrophic fungi *Pyrenophora teres*. They additionally assumed that this Pip induced resistance in barley is not interfering with immune responses to necrotrophic pathogens. Confirming that systemically acquired resistance towards necrotrophic pathogens can be established, in tomato plants a mycorrhiza inoculation establishes sufficient defense responses against following *Bcin* infections (Sanmartín et al. 2020).

The same study demonstrates a callose priming in mycorrhiza challenged tomato plants which was relevant for the establishment of systemic resistance against *Bcin* (Sanmartín et al. 2020). Callose is deposited in plants cell walls to function as structural barrier against invading pathogens. The deposition of callose in cell walls in *A. thaliana* is associated with the primed state of SAR and has also been shown to be induced by SA treatments (Kohler et al. 2002). Zhang and colleagues (2021) revealed that exogenous NHP treatments of wheat plants induce

callose deposition in leaves and elevates the resistance of the monocot towards *Fusarium graminearum* infections significantly. The role of NHP in callose priming has however not been investigated in *A. thaliana* or other dicotyledonous plant species yet.

3.1.3. Aims

The *A. thaliana* – *Psm* pathosystem is frequently used to study plants defense responses against pathogens. However, pathogens that infect *A. thaliana* developed diverse lifestyles that trigger specific defense responses in the plant (Glazebrook 2005). The biosynthesis of NHP and its immune inducing function against biotrophic and hemibiotrophic pathogens in *A. thaliana* has been demonstrated, but the role of NHP in the defense against pathogens with a necrotrophic lifestyle is not clear.

Therefore this study aims to evaluate the metabolite profile of *A. thaliana* after the infection with biotrophic (*Hpa*), hemibiotrophic (*Chig*, *Sclero*) and necrotrophic (*Bcin*) hyphae growing pathogens and to compare accumulation patterns to the metabolite profile of the established *A. thaliana* – *Psm* pathosystem. Further, this study aims to understand the role of NHP in local and systemic defense responses against pathogens with a necrotrophic lifestyle phase. Therefore, the influence of an exogenous NHP treatment of *A. thaliana* Col-0 wildtype and mutant plants on the following infection with biotrophic, hemibiotrophic and necrotrophic pathogens is tested and the role of NHP in callose priming in *A. thaliana* is investigated. Additionally, the effect of SAR on pathogens with hemibiotrophic and necrotrophic lifestyles was investigated in Col-0 wildtype and *sid2* and *fmo1* mutant plants to further elucidate the role of NHP and SA in the defense against pathogens with a rather necrotrophic lifestyle.

3.2. Results

3.2.1. Metabolite changes over time in *Arabidopsis thaliana* upon the infection with …

3.2.1.1. … the biotrophic oomycete *Hyaloperospora arabidopsidis*

To investigate changes in the *A. thaliana* metabolite level after infections of pathogens with biotrophic, hemibiotrophic or necrotrophic lifestyles, in this study *A. thaliana* leaves were analyzed via GC-MS after an infection with the biotrophic oomycete *Hpa*. Therefore, four-week-old plants were sprayed with a *Hpa* spore solution (50 spores/µl), controls were treated likewise with H_2O. Samples were collected 3 dpi, 6 dpi and 9 dpi to monitor metabolite levels during the disease progression in *A. thaliana*.

Between 3 dpi and 9 dpi the GC-MS analyses revealed a basal SA level in H_2O sprayed *A. thaliana* leaves between 0.03 µg g^{-1} FW and 0.09 µg g^{-1} FW while the SA amounts detected in *Hpa* sprayed leaves were significantly higher at all sampling timepoints (Figure 20.A). In *Hpa* inoculated leaves the SA level reaches its maximum 3 dpi (0.55 µg g^{-1} FW) however only slightly lower SA amounts were detected 6 dpi (0.33 µg g^{-1} FW) and 9 dpi (0.46 µg g^{-1} FW) (Figure 20.A). The SA glucoside SAG was also detected in significantly higher amounts in *Hpa* inoculated *A. thaliana* leaves compared to the amounts that were detected in H_2O inoculated leaves at all sampling timepoints (Figure 20.B). Basal SAG levels of maximal 1.81 µg g^{-1} FW were measured in H_2O inoculated leaves (Figure 20.B). In *Hpa* infected leaves 3 dpi (15.98 µg g^{-1} FW) a significantly lower SAG level was detected than in leaves that were sampled 6 dpi (34.72 µg g^{-1} FW) and 9 dpi (59.11 µg g^{-1} FW) (Figure 20.B). The SA glucoside SGE was not detected between 3 dpi and 9 dpi in H_2O inoculated *A. thaliana* leaves but showed significant accumulation in *Hpa* inoculated leaves at all sampling timepoints (Figure 20.C). A maximal SGE amount of 2.62 µg g^{-1} FW was detected in *Hpa* infected leaves 3 dpi and only slightly less SAG was detected 6 dpi (1.11 µg g^{-1} FW) and 9 dpi (1.86 µg g^{-1} FW) in *Hpa* infected leaves (Figure 20.C). Summarizing SA and its glucosides SAG and SGE were detected in significantly higher amounts in *Hpa* inoculated than in H_2O inoculated leaves pointing to an accumulation of SA and its glucosides in *A. thaliana* upon a *Hpa* infection.

To investigate the NHP biosynthesis pathway the NHP precursor Pip was quantified in H_2O and *Hpa* inoculated *A. thaliana* leaves between 3 dpi and 9 dpi. In H_2O sprayed leaves a basal level

of maximal 0.41 µg g^{-1} FW (9 dpi) were detected but in *Hpa* sprayed leaves a significantly higher Pip level was detected at all sampling timepoints (Figure 20.D). The detected Pip amounts in *Hpa* infected leaves that were sampled 3 dpi (1.81 µg g^{-1} FW) are however significantly lower than the detected Pip amounts in *Hpa* infected leaves sampled 6 dpi (2.04 µg g^{-1} FW) and 9 dpi (4.25 µg g^{-1} FW) (Figure 20.D). The NHP was not detected in H_2O inoculated leaves but 3 dpi, 6 dpi and 9 dpi in *A. thaliana* leaves that were inoculated with *Hpa* (Figure 20.G). In *Hpa* inoculated leaves NHP levels between 0.11 µg g^{-1} FW (3 dpi) and 0.18 µg g^{-1} FW (9 dpi) were detected (Figure 20.G). The NHP glucosides NHPG and NHPGE were quantified in relative amounts since correction factors for the established standards were unknown. Both NHP glucosides were not detected at any sampling timepoint in H_2O inoculated *A. thaliana* leaves but were both detected in *Hpa* inoculated plants (Figure 20.H, P.I). In *Hpa* inoculated leaves 3 dpi (1.01 µg g^{-1} FW) a significantly lower NHPG amount was detected than 6 dpi (8.85 µg g^{-1} FW) and 6 dpi a significantly lower NHP amount was detected than 9 dpi (21.73 µg g^{-1} FW) (Figure 20.H). The NHP glucoside NHPGE was only detected 6 dpi and 9 dpi in *Hpa* inoculated plants and showed a significantly higher NHPGE level 9 dpi (0.24 µg g^{-1} FW) than 6 dpi (0.11 µg g^{-1} FW) (Figure 20.I). These results indicate the activation of the NHP biosynthesis pathway in *A. thaliana* upon the infection with the biotrophic *Hpa* resulting in an *Hpa* induced accumulation of Pip, NHP and the NHP glucosides NHPG and NHPGE.

To investigate indolic compounds in *A. thaliana* after *Hpa* infections, camalexin and ICA were quantified in the GC-MS runs of *Hpa* infected and H_2O treated leaves. In H_2O sprayed *A. thaliana* leaves camalexin and ICA were not detected (Figure 20.E, 20.F). In *Hpa* sprayed leaves however camalexin was detected in significantly higher amounts than in H_2O sprayed leaves at all sampling timepoints. The detected camalexin amounts in *A. thaliana* leaves were determined as significantly lower in *Hpa* inoculated leaves sampled 3 dpi (2.49 µg g^{-1} FW) than the camalexin amounts detected 9 dpi (9.29 µg g^{-1} FW) in *Hpa* inoculated leaves (Figure 20.E). No significant differences were identified between the camalexin amounts in *Hpa* treated leaves sampled 3 dpi and 6 dpi or 6 dpi and 9 dpi (Figure 20.E). Since ICA was not detected in H_2O inoculated *A. thaliana* leaves, the detected ICA level was significantly higher in *Hpa* than in H_2O treated leaves at all testes sampling timepoints (Figure 20.F). In *Hpa* inoculated leaves the ICA level showed no significant differences between 3 dpi and 9 dpi and reaches a maximum amount of 0.096 µg g^{-1} FW ICA 9 dpi in *Hpa* inoculated leaves (Figure 20.F).

Summarizing, these results indicate an accumulation of the indolic compounds camalexin and ICA upon a *Hpa* infection in *A. thaliana*.

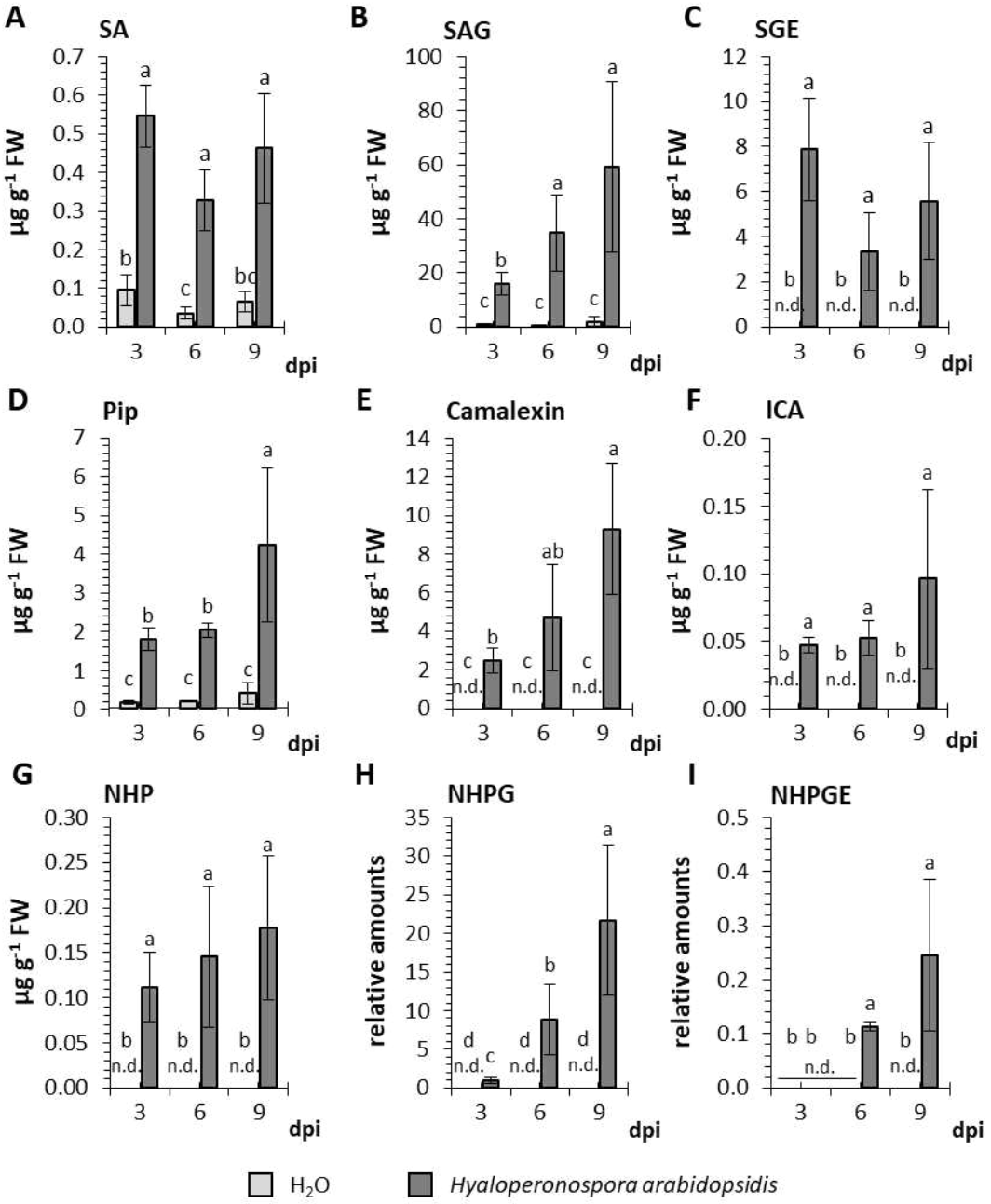

Figure 20: Accumulation of defense related metabolites in *Arabidopsis thaliana* induced by a *Hyaloperonospora arabidopsidis* (*Hpa*) infection. Five-week-old *A. thaliana* Col-0 plants were spray inoculated with a *Hpa* spore solution (50 spores/µl) or H_2O as a control treatment. Samples were taken 3 dpi, 6 dpi and 9 dpi for the GC-MS analyses whereat three fully grown, inoculated leaves of one plant were sampled as one biological replicate. In total four biological replicates per sampled timepoint and treatment were sampled and analyzed via GC-MS. In the GC-MS results total and relative amounts of (**A**) SA, (**B**) SAG, (**C**) SGE, (**D**) Pip, (**E**) camalexin, (**F**) ICA, (**G**) NHP, (**H**) NHPG and (**I**) NHPGE were quantified. Mean values ± standard deviation are represented by the bars. Not detected (n.d.) metabolites are indicated as such. Statistical differences between tested timepoints and treatments were determined in SPSS with a Kruskal-Wallis and are indicated by letters above bars.

3.2.1.2. … the hemibiotrophic bacteria *Pseudomonas syringae*

To study the *A. thaliana* defense reaction against pathogens of various lifestyles on a metabolite level, a GC-MS analyses of an infection time course of *A. thaliana* leaves inoculated with the hemibiotrophic bacteria *Psm* was performed. Therefore, three leaves of five-week-old *A. thaliana* Col-0 plants were infiltrated with $MgCl_2$ as a control treatment or a *Psm* solution (OD_{600} = 0.005). Sampling was performed 1 dpi, 2 dpi and 3 dpi and local as well as systemic samples were collected. Thereby, potentially important metabolites in SAR in *A. thaliana* were investigated.

In local $MgCl_2$ infiltrated *A. thaliana* leaves a maximum basal level of 0.28 µg g^{-1} FW SA (3 dpi) were detected (Figure 21.A). However, in local, *Psm* infiltrated leaves a significant higher amount of SA was detected than in $MgCl_2$ infiltrated leaves at all sampling timepoints (Figure 21.A). The maximum amount of SA was detected 1 dpi in *Psm* infiltrated leaves with 3.22 µg g^{-1} FW, which is significantly higher than the SA amounts detected 2 dpi (1.70 µg g^{-1} FW) and 3 dpi (1.71 µg g^{-1} FW) (Figure 21.A). In systemic leaves of local $MgCl_2$ infiltrated leaves equal basal SA levels like in local leaves were observed with a maximum detection of 0.31 µg g^{-1} FW SA (Figure 21.B). In systemic leaves of local *Psm* infiltrated *A. thaliana* leaves 2 dpi (0.85 µg g^{-1} FW) a significantly higher amount of SA was detected than 2 dpi in systemic leaves of local $MgCl_2$ infiltrated leaves (0.14 µg g^{-1} FW) (Figure 21.B). Equal amounts of SA were detected in systemic leaves of $MgCl_2$ and *Psm* infiltrated *A. thaliana* plants 1 dpi and 3 dpi (Figure 21.B).

The SA glucoside SAG was detected in significantly higher amounts in *Psm* than in $MgCl_2$ infiltrated *A. thaliana* plants 1 dpi, 2 dpi and 3 dpi (Figure 21.A). In local *Psm* infiltrated leaves 1 dpi (29.95 µg g^{-1} FW) a significantly lower SAG amount was detected than 2 dpi, and 2 dpi (126.15 µg g^{-1} FW) a significantly lower SAG amount was detected than 3 dpi (171.82 µg g^{-1} FW) in local leaves (Figure 21.A). In local $MgCl_2$ infiltrated leaves a basal SAG level between 0.95 µg g^{-1} FW (1 dpi) and 4.37 µg g^{-1} FW (3 dpi) was detected (Figure 21.A). In the systemic leaves of local $MgCl_2$ infiltrated plants the basal SAG level reached a maximum of 1.82 µg g^{-1} FW (3 dpi) (Figure 21.B). The SAG amounts detected in systemic leaves of *Psm* infiltrated plants 2 dpi (4.73 µg g^{-1} FW) and 3 dpi (22.22 µg g^{-1} FW) were significantly higher than the detected SAG amount in the control treatments at these sampling timepoints (Figure 21.B). However, equal SAG levels were detected in the systemic leaves $MgCl_2$ and *Psm* infiltrated plants 1 dpi (Figure 21.B).

The SA glucoside SGE was not detected in local $MgCl_2$ infiltrated leaves 1 dpi and 2 dpi but 3 dpi 0.16 µg g^{-1} FW SGE were detected in $MgCl_2$ infiltrated leaves (Figure 21.A). In *Psm* infiltrated leaves a significantly higher SGE level was detected than in $MgCl_2$ infiltrated *A. thaliana* leaves at all sampling timepoints whereat significantly higher SGE amounts were detected in *Psm* infiltrated leaves 1 dpi (15.23 µg g^{-1} FW) and 2 dpi (19.03 µg g^{-1} FW) than in *Psm* infiltrated leaves 3 dpi (7.43 µg g^{-1} FW) (Figure 21.A). In the systemic leaves of $MgCl_2$ infiltrated plants no SGE was detected at any sampling timepoint (Figure 21.B). In the systemic leaves of *Psm* infiltrated plants 1 dpi equally no SGE was detected while a significantly higher SGE amount was detected in systemic leaves of *Psm* infiltrated plants 2 dpi and 3 dpi than in systemic leaves of $MgCl_2$ infiltrated plants at those sampling timepoints.

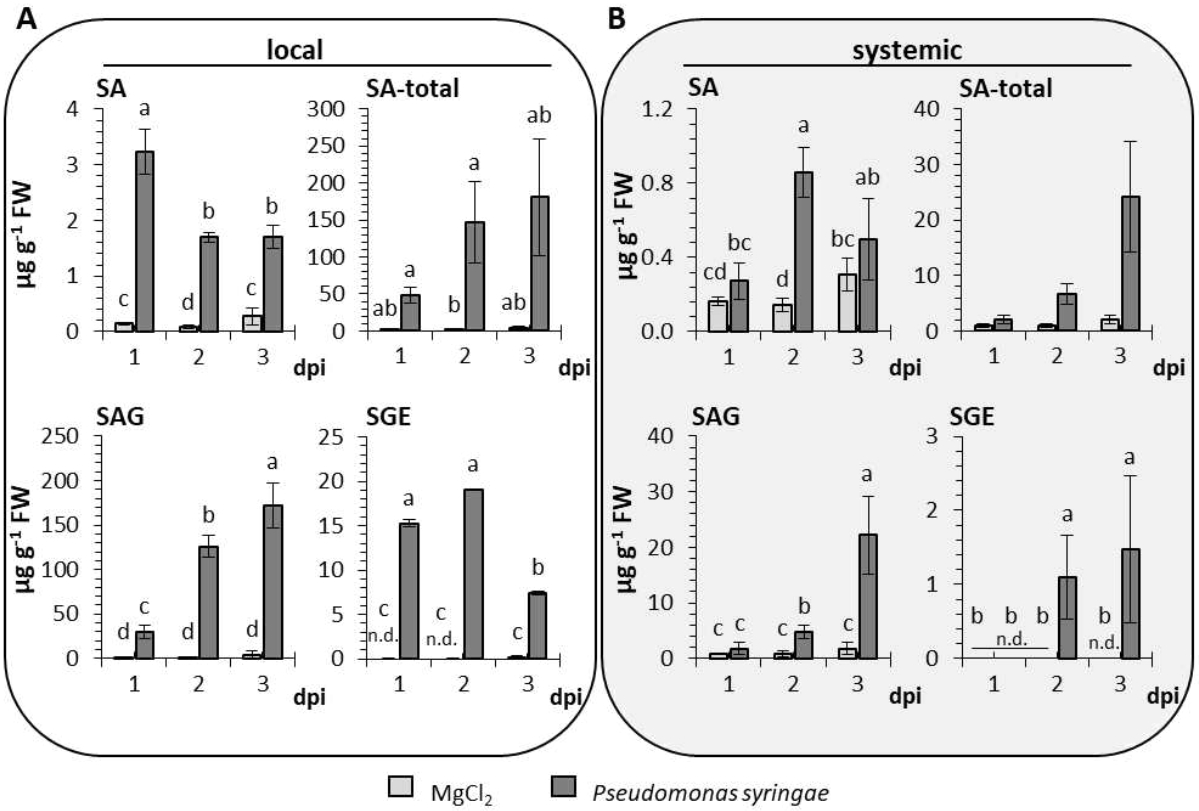

Figure 21: Local and systemic accumulation of SA and SA derivates in *Arabidopsis thaliana* after a *Pseudomonas syringae* (*Psm*) infection. Three fully grown leaves of five-week-old *A. thaliana* Col-0 plants were pressure infiltrated with a *Psm* solution (OD_{600} = 0.005) or a 10 mM $MgCl_2$ solution as a control treatment. Samples of local and systemic leaves were taken 1 dpi, 2 dpi and 3 dpi for the GC-MS analyses. In the resulting chromatograms of (**A**) local and (**B**) systemic leave samples of four replicates per treatment (n = 4) SA, SAG, SGE and total SA amounts were quantified and are expressed in µg g^{-1} FW. Not detected (n.d.) metabolites are marked as such. Bars represent mean values ± standard deviation. The statistical differences between tested timepoints and treatments were investigated with a Kruskal-Wallis test in SPSS and are represented by letters above bars. If no letters are given, no statistical differences were identified between the tested treatments and/or timepoints.

The total SA levels were estimated by summing up the detected amounts of SA, SAG and SGE for each tested timepoint and treatment. Hence the total SA levels show high standard deviation (Figure 21.A, 21.B). Only in local *Psm* infiltrated leaves 2 dpi (146.87 µg g^{-1} FW) a significantly higher amount of total SA was detected in comparison to the detected total SA amounts 2 dpi in $MgCl_2$ infiltrated leaves (1.36 µg g^{-1} FW) (Figure 21.A). In local *Psm* and $MgCl_2$ infiltrated leaves 1 dpi and 3 dpi equal amounts of total SA were detected (Figure 21.A). Likewise, no significant differences were found between the total SA levels in systemic leaves of *Psm* and $MgCl_2$ infiltrated plants at any sampling timepoint (Figure 21.B). In summary, these results might point to a SA accumulation and a following accumulation of its glucosides SAG and SGE in *A. thaliana* after a *Psm* infection. Moreover, this SA accumulation was not restricted to *Psm* treated leaves but was also observed in systemic leaves.

In addition to the phytohormone SA, the defense relevant metabolites Pip, NHP and NHP glucosides were quantified in local and systemic leaves of *Psm* or $MgCl_2$ infiltrated *A. thaliana* plants. The results revealed a basal Pip level between 0.27 µg g^{-1} FW (2 dpi) and 1.47 µg g^{-1} FW (3 dpi) in local $MgCl_2$ infiltrated leaves between the tested sampling timepoints 1 dpi and 3 dpi (Figure 22.A). In local *Psm* infiltrated *A. thaliana* leaves significantly higher Pip amounts were detected than in $MgCl_2$ infiltrated leaves at all sampling timepoints (Figure 22.A). The statistical analyses also revealed significantly lower Pip amounts in local *Psm* infiltrated leaves 1 dpi (16.19 µg g^{-1} FW) than in local *Psm* infiltrated leaves that were sampled 2 dpi (75.85 µg g^{-1} FW) and 3 dpi (77.35 µg g^{-1} FW) (Figure 22.A). In systemic leaves of *Psm* infiltrated plants only 3 dpi (17.13 µg g^{-1} FW) a significantly higher Pip level was detected than in systemic leaves of $MgCl_2$ infiltrated plants (1.27 µg g^{-1} FW) (Figure 22.B). Systemic leaves of *Psm* or $MgCl_2$ infiltrated plants that were sampled 2 dpi and 3 dpi showed equal Pip amounts (Figure 22.B). In the systemic leaves of $MgCl_2$ infiltrated plants basal Pip levels up to 1.27 µg g^{-1} FW (3 dpi) were detected, which is comparable to the basal Pip levels detected in local $MgCl_2$ infiltrated leaves (Figure 22.B).

The NHP was not detected in local and systemic leaves of $MgCl_2$ infiltrated plants and was detected in significantly higher amounts in local and systemic leaves of *Psm* infiltrated plants 1 dpi, 2 dpi and 3 dpi (Figure 22.A, R.B). In local *Psm* infiltrated leaves a significantly higher NHP level was detected 1 dpi (19.76 µg g^{-1} FW) and 2 dpi (26.43 µg g^{-1} FW) than in local *Psm* infiltrated leaves 3 dpi (7.52 µg g^{-1} FW) (Figure 22.A). In contrast, the NHP level detected in systemic leaves of *Psm* infiltrated plants was 2 dpi (3.53 µg g^{-1} FW) significantly higher than

1 dpi (0.49 µg g^{-1} FW) and 3 dpi (1.41 µg g^{-1} FW) (Figure 22.B). The quantified NHP amounts in systemic leaves of *Psm* infiltrated plants 3 dpi additionally showed significantly higher NHP levels than in systemic leaves of *Psm* infiltrated plants sampled 1 dpi (Figure 22.B).

As well as NHP, the investigated NHP glucosides NHPG and NHPGE were not detected in $MgCl_2$ infiltrated *A. thaliana* leaves or in systemic tissue (Figure 22.A, R.B). In local *Psm* infiltrated leaves the NHPG level was determined as significantly higher than in local $MgCl_2$ infiltrated leaves, revealing significantly higher NHPG amounts 2 dpi (210.70 µg g^{-1} FW) than 1 dpi (11.82 µg g^{-1} FW), and 3 dpi (645.55 µg g^{-1} FW) significantly higher NHPG amounts than 2 dpi in local *Psm* infiltrated leaves (Figure 22.A). In systemic leaves of *Psm* infiltrated *A. thaliana* plants no NHPG was detected 1 dpi, but significantly higher NHPG amounts were detected in systemic leaves of *Psm* infiltrated plants sampled 2 dpi (1.42 µg g^{-1} FW) and 3 dpi (7.15 µg g^{-1} FW) than in systemic leaves of $MgCl_2$ infiltrated plants at the same sampling timepoints (Figure 22.B). The statistical analyses also revealed significantly higher NHPG levels in systemic leaves of *Psm* infiltrated plants 3 dpi than in systemic leaves of *Psm* infiltrated plants 2 dpi (Figure 22.B).

The NHP glucoside NHPGE was detected in significantly higher levels in local *Psm* treated leaves than in local $MgCl_2$ treated leaves at all sampling timepoints (Figure 22.A). Thereby the NHPGE level in *Psm* infiltrated leaves was 2 dpi (26.43 µg g^{-1} FW) determined as significantly higher than 1 dpi (5.28 µg g^{-1} FW) and 3 dpi (17.72 µg g^{-1} FW) (Figure 22.A). In addition, 3 dpi significantly higher NHPGE levels were quantified in local *Psm* infiltrated leaves than 1 dpi in local *Psm* infiltrated leaves (Figure 22.A). In the systemic leaves of *Psm* infiltrated plants no NHPGE was detected 1 dpi (Figure 22.B). However, 2 dpi and 3 dpi significantly higher NHPGE levels were detected in systemic leaves of *Psm* infiltrated plants than in systemic leaves of $MgCl_2$ infiltrated plants (Figure 22.B). Equal NHPGE levels were determined in systemic leaves of *Psm* infiltrated plants that were sampled 2 dpi (2.61 µg g^{-1} FW) and 3 dpi (2.70 µg g^{-1} FW) (Figure 22.B). In summary the NHP biosynthesis pathway seems to be activated in *A. thaliana* upon a *Psm* infection in local and systemic leaves, indicating an elevation of the Pip, NHP, NHPG and NHPGE level in local and systemic tissue over time.

The tryptophan derived metabolites camalexin and ICA were as well quantified in *A. thaliana* after an infection with the hemibiotrophic *Psm* to investigate the role of the indolic secondary metabolism on the local and systemic pathogen response of *A. thaliana*. The phytoalexin camalexin was detected in significantly higher amounts in local *Psm* than in $MgCl_2$ infiltrated

leaves at all sampled infection timepoints between 1 dpi and 3 dpi (Figure 22.A). Thereby, in local *Psm* infiltrated leaves the estimated camalexin levels were 1 dpi (6.00 µg g^{-1} FW) significantly lower than 2 dpi (91.86 µg g^{-1} FW), and 2 dpi significantly lower than 3 dpi (165.82 µg g^{-1} FW). In local $MgCl_2$ infiltrated leaves in contrast no camalexin was detected 1 dpi and 2 dpi but 3 dpi a basal level of 0.44 µg g^{-1} FW camalexin was quantified (Figure 22.A).

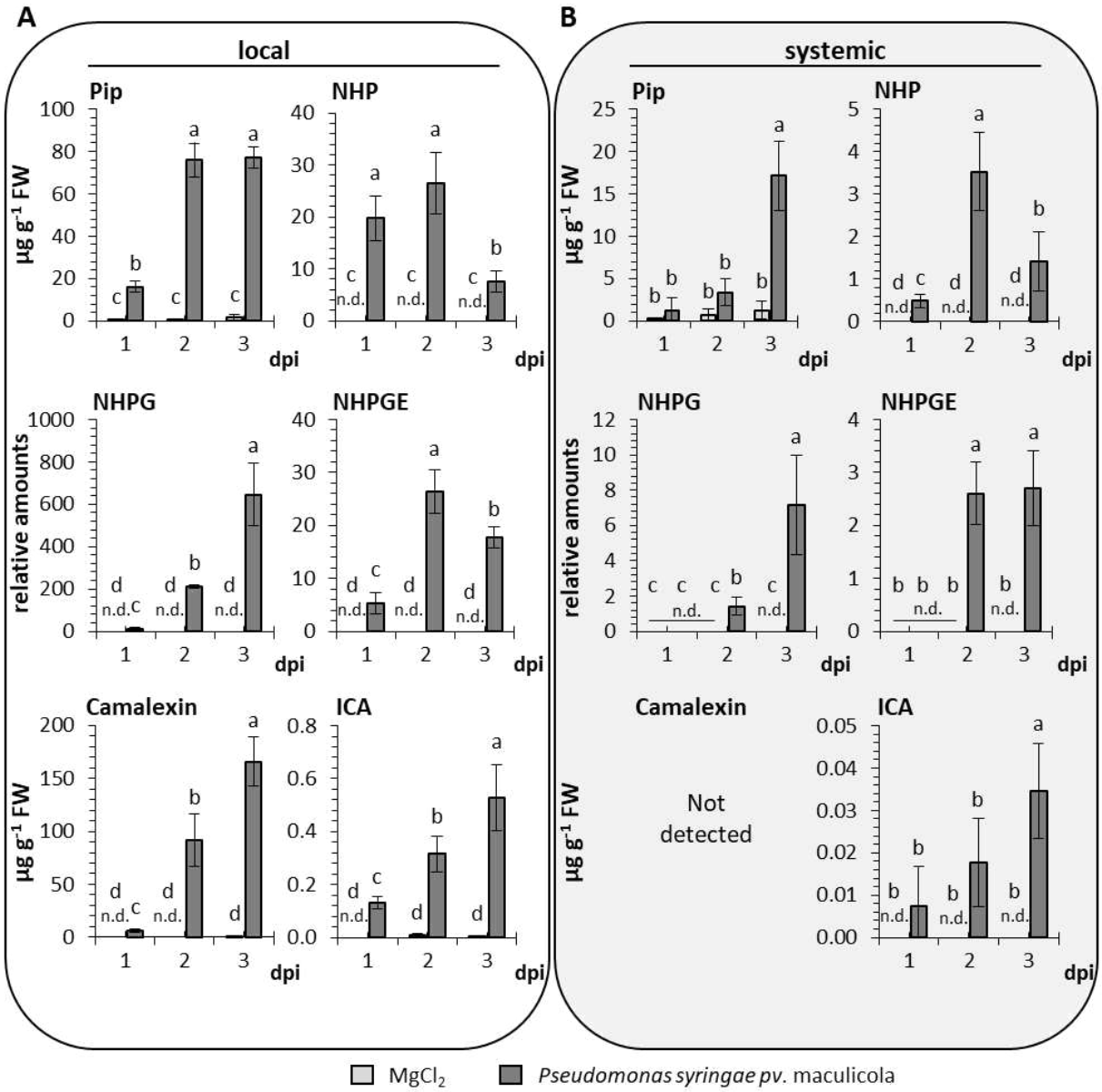

Figure 22: Accumulation of defense related metabolites in *Pseudomonas syringae* (*Psm*) infected and uninfected, systemic *Arabidopsis thaliana* leaves. Experimental procedures were performed as described in Figure 21. In the resulting chromatograms of (**A**) local and (**B**) systemic leave samples of four replicates per treatment (n = 4) Pip, NHP, NHPG, NHPGE, camalexin and ICA total and relative amounts were quantified and are expressed in µg g^{-1} FW. If a metabolite was not detected (n.d.) it is labelled as such. Bars represent mean values ± standard deviation. The statistical differences between tested timepoints and treatments investigated with a Kruskal-Wallis test in SPSS are represented by letters.

However, no camalexin was detected at any sampling timepoint in the infection time course in systemic leaves of *Psm* or $MgCl_2$ infiltrated *A. thaliana* plants (Figure 22.B).

The ICA was not detected in local $MgCl_2$ infiltrated leaves 1 dpi but 0.007 µg g^{-1} FW ICA were detected 2 dpi and 0.003 µg g^{-1} FW ICA 3 dpi in local $MgCl_2$ infiltrated leaves (Figure 22.A). Compared to the detected ICA amounts in $MgCl_2$ infiltrated *A. thaliana* leaves, in local *Psm* infiltrated leaves significantly higher amounts ICA were detected (Figure 22.A). The statistical analyses revealed significantly higher ICA levels in local *Psm* infiltrated leaves 2 dpi (0.32 µg g^{-1} FW) than 1 dpi (0.13 µg g^{-1} FW), and 3 dpi (0.53 µg g^{-1} FW) significantly higher ICA levels than 2 dpi (Figure 22.A). In the systemic leaves of $MgCl_2$ infiltrated plants no ICA was detected between 1 dpi and 3 dpi (Figure 22.B). As a probable result of high standard deviations, no significant differences in the ICA level in the systemic leaves of *Psm* and $MgCl_2$ infiltrated plants were detected 1 dpi and 2 dpi (Figure 22.B). Nevertheless, 3 dpi significantly higher ICA amounts were quantified in systemic leaves of *Psm* infiltrated *A. thaliana* plants (0.03 µg g^{-1} FW) than in systemic leaves of $MgCl_2$ infiltrated plants (0.00 µg g^{-1} FW) (Figure 22.B). These results might indicate that indoles like camalexin accumulate in *A. thaliana* after a *Psm* infection in local leaves but not or only in late infection stages in systemic leaves.

3.2.1.3. … the hemibiotrophic fungi *Colletrotrichum higginsianum*

The hemibiotrophic lifestyle is widely distributed among phytopathogens and comes along with diverse strategies of growth and survival (Glazebrook 2005, Horbach et al. 2011). To compare the metabolite changes in *A. thaliana* after infections with hemibiotrophic pathogens of different kingdoms, in this study the effect of an infection with the hemibiotrophic fungi *Chig* on the *A. thaliana* metabolite profile was investigated. Therefore four- to five-week-old *A. thaliana* plants were inoculated with droplets of a solution containing 500 *Chig* conidia/µl or H_2O as a control treatment. Samples were taken 2 dpi, 4 dpi, 6 dpi, 8 dpi and 10 dpi for the GC-MS analyses of selected defense related metabolites. To verify the successful *Chig* infection in *A. thaliana*, at each sampling timepoint additional samples were taken for the macro- and microscopic investigation of *Chig* caused disease symptoms and infection structure in planta (Suppl. Figure 4).

In the control treatments, analyzed leaves revealed a maximum basal SA level of 0.06 µg g^{-1} FW (10 dpi) between 2 dpi and 10 dpi (Figure 23.A). The *Chig* inoculated leaves

revealed significantly higher amounts of SA than H_2O inoculated leaves between 4 dpi and 10 dpi, but 2 dpi in *Chig* and H_2O inoculated *A. thaliana* leaves equal SA amounts were detected (Figure 23.A). In *Chig* treated leaves 4 dpi (0.08 µg g^{-1} FW) significant lower SA amounts were detected than in *Chig* treated *A. thaliana* leaves 6 dpi (0.24 µg g^{-1} FW), 8 dpi (0.44 µg g^{-1} FW) and 10 dpi (0.42 µg g^{-1} FW) (Figure 23.A).

To overview the total SA amounts in infected *A. thaliana* leaves, SAG and SGE were quantified in *A. thaliana* leaves after a *Chig* infection as well. The SA glucoside SAG was detected in amounts between 0.06 µg g^{-1} FW (4 dpi) and 0.96 µg g^{-1} FW (10 dpi) in H_2O inoculated leaves sampled between 2 dpi and 10 dpi (Figure 23.B). Equal SAG amounts were measured in H_2O and *Chig* inoculated leaves 2 dpi, but between 4 dpi and 10 dpi the SAG amounts in *Chig* inoculated leaves were significantly higher than the detected SAG amounts in H_2O inoculated leaves (Figure 23.B). In *Chig* inoculated leaves 4 dpi (1.04 µg g^{-1} FW) a significantly lower SAG level was detected than in *Chig* inoculated leaves 6 dpi (4.64 µg g^{-1} FW), 6 dpi a significantly lower SAG level was detected than 8 dpi (31.12 µg g^{-1} FW), and 8 dpi a significantly lower SAG level was detected than in *Chig* inoculated leaves 10 dpi (80.54 µg g^{-1} FW) (Figure 23.B). The SGE was 2 dpi not detected in H_2O or *Chig* inoculated *A. thaliana* leaves. Between 6 dpi and 10 dpi the SGE level in H_2O treated plants reached 10 dpi a maximum of 0.17 µg g^{-1} FW (Figure 23.C). The statistical analyses revealed significantly higher SGE level in *Chig* inoculated leaves than in H_2O inoculated leaves between 4 dpi and 10 dpi (Figure 23.C). Thereby, the SGE amounts in *Chig* inoculated *A. thaliana* leaves sampled 4 dpi (0.54 µg g^{-1} FW) and 6 dpi (0.71 µg g^{-1} FW) was determined as significantly lower than the detected SGE levels 8 dpi (3.12 µg g^{-1} FW) and 10 dpi (4.95 µg g^{-1} FW) in *Chig* inoculated leaves (Figure 23.C). Summarizing these results indicate an accumulation of SA and its storage forms SAG and SGE in *A. thaliana* upon a *Chig* infection with an observed elevation of the SA level during the progression of the *Chig* infection.

In the *A. thaliana* - *Chig* infection time course, the Pip, NHP and the NHP glucosides NHPG and NHPGE were quantified to investigate the NHP biosynthesis after an infection with the hemibiotrophic fungi. In H_2O inoculated leaves basal Pip level between 0.07 µg g^{-1} FW (4 dpi) and 0.25 µg g^{-1} FW (10 dpi) was detected (Figure 23.D). Between 4 dpi and 10 dpi, in *Chig* inoculated leaves a significantly higher Pip amount was quantified than in H_2O inoculated leaves while 2 dpi similar amounts were detected in *Chig* and H_2O inoculated leaves (Figure 23.D). In *Chig* inoculated leaves 4 dpi (0.36 µg g^{-1} FW) a significantly lower Pip level was

detected than In *Chig* inoculated *A. thaliana* leaves that were sampled 6 dpi (3.02 µg g^{-1} FW), 8 dpi (3.64 µg g^{-1} FW) and 10 dpi (5.89 µg g^{-1} FW) (Figure 23.D). The NHP was not detected in *A. thaliana* leaves that were treated with H_2O at any investigated timepoint of the infection (Figure 23.G). Moreover, no NHP was detected in *Chig* inoculated plants that were sampled 2 dpi (Figure 23.G). In *Chig* inoculated leaves that were sampled between 4 dpi and 10 dpi in contrast a significantly higher NHP level was detected than in H_2O inoculated leaves (Figure 23.G). The statistical analyses showed that in *Chig* inoculated plants 4 dpi (0.06 µg g^{-1} FW) a significantly lower NHP level was detected than in *Chig* inoculated plants sampled between 6 dpi and 10 dpi, and in *Chig* inoculated leaves 6 dpi (0.37 µg g^{-1} FW) a significantly higher NHP level was detected than in *Chig* inoculated leaves 8 dpi (0.13 µg g^{-1} FW) and 10 dpi (0.15 µg g^{-1} FW) (Figure 23.G).

The NHP glucosides NHPG and NHPGE were like NHP not detected in H_2O treated plants at any sampling timepoint (Figure 23.H). In *Chig* inoculated *A. thaliana* leaves in contrast significantly higher NHPG levels were detected than in $MgCl_2$ inoculated leaves between 6 dpi and 10 dpi whereat a significantly lower NHPG level was detected in *Chig* inoculated leaves 6 dpi (3.33 µg g^{-1} FW) than in *Chig* inoculated leaves 8 dpi (20.09 µg g^{-1} FW) and 10 dpi (16.93 µg g^{-1} FW) (Figure 23.H). In *Chig* inoculated leaves that were sampled 4 dpi mean NHPG amounts of 0.25 µg g^{-1} FW were quantified which revealed no significant differenced to the detected NHPG amounts in H_2O inoculated leaves 4 dpi (Figure 23.H). As mentioned, the NHP glucoside NHPGE was not detected in $MgCl_2$ inoculated *A. thaliana* between 2 dpi and 10 dpi (Figure 23.I). Furthermore, NHPGE was not detected in *Chig* inoculated leaved between 2 dpi and 6 dpi. However, in *Chig* inoculated leaves that were sampled 8 dpi (0.53 µg g^{-1} FW) and 10 dpi (0.52 µg g^{-1} FW) a significantly higher NHPGE level was detected than in $MgCl_2$ inoculated leaves at the same sampling timepoints (Figure 23.I). In conclusion, these results indicate an accumulation of Pip and NHP in *A. thaliana* after a *Chig* infection starting 4 dpi and a slightly time delayed accumulation of NHP glucosides starting 6 dpi.

The tryptophan derived metabolites camalexin and ICA were as well investigated during the *Chig* infection progression in *A. thaliana*. The phytoalexin camalexin was not detected in H_2O inoculated leaves sampled 2 dpi and 4 dpi but was detected in low levels up to 0.22 µg g^{-1} FW between 8 dpi and 10 dpi (Figure 23.E). However, in H_2O treated plants no significant differences in the camalexin levels were determined between the five sampling timepoints (Figure 23.E). Compared to the detected camalexin amounts in H_2O inoculated leaves, in *Chig*

inoculated leaves significantly higher camalexin amounts were quantified 6 dpi (12.16 µg g^{-1} FW), 8 dpi (34.43 µg g^{-1} FW) and 10 dpi (27.09 µg g^{-1} FW) while equal camalexin amounts were detected 2 dpi and 4 dpi in H_2O and *Chig* inoculated leaves (Figure 23.E). The ICA was detected in similar amounts at all sampling timepoints in H_2O inoculated leaves reaching a maximum of 0.01 µg g^{-1} FW 10 dpi. In *Chig* inoculated *A. thaliana*

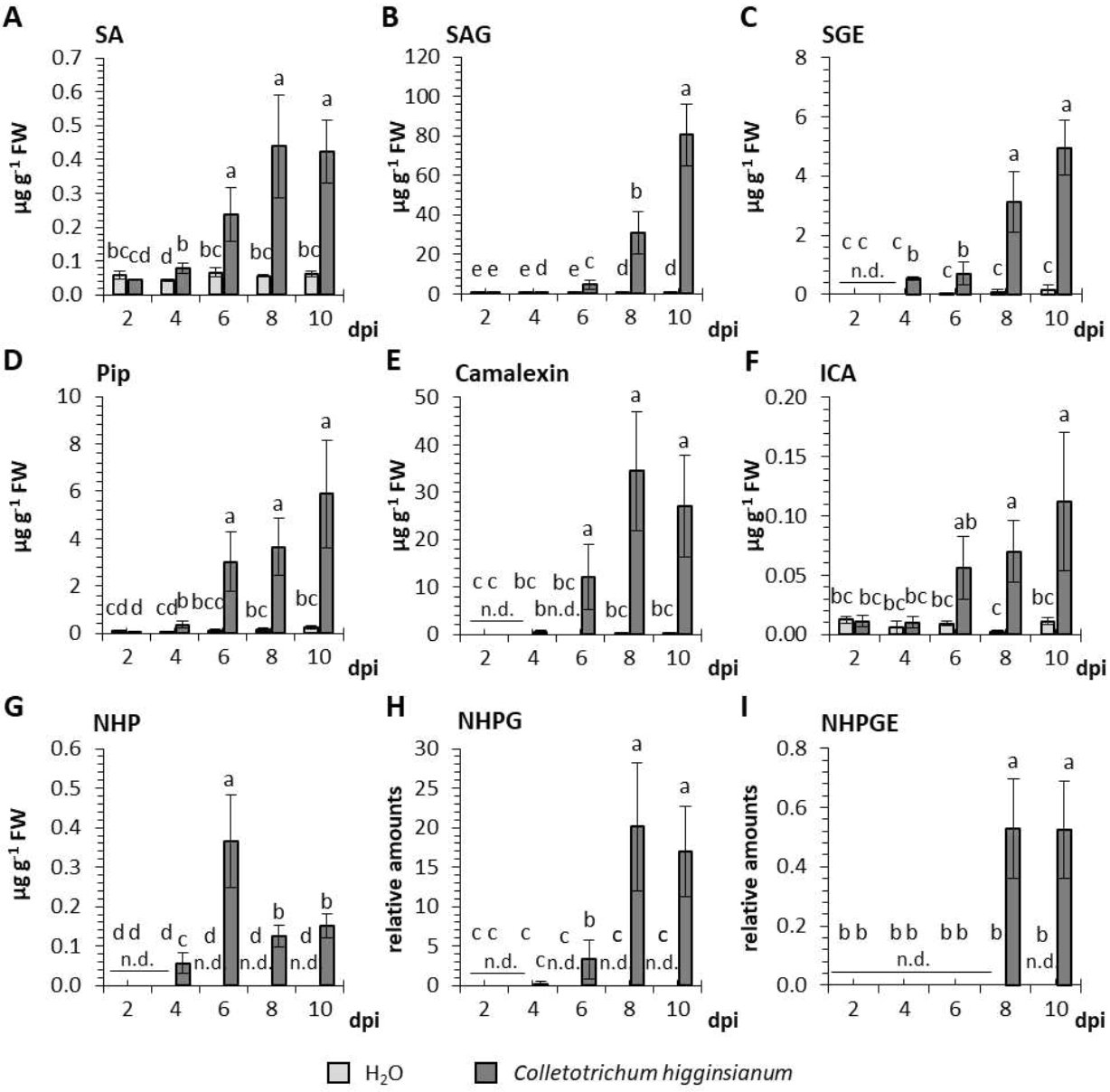

Figure 23: Defense related metabolites accumulate in *Arabidopsis thaliana* after a *Colletotrichum higginsianum* (*Chig*) infection timepoint-specific. Five-week-old *A. thaliana* Col-0 plants were used for the droplet inoculation of three fully grown leaves with a *Chig* spore solution (500 spores/µl) or H_2O as a control treatment. Samples were taken 2 dpi, 4 dpi, 6 dpi, 8 dpi and 10 dpi for the GC-MS analyses whereat the inoculated leaves of one plant were sampled as one biological replicate. Total and relative amounts of (**A**) SA, (**B**) SAG, (**C**) SGE, (**D**) Pip, (**E**) camalexin, (**F**) ICA, (**G**) NHP, (**H**) NHPG and (**I**) NHPGE were quantified via the GC-MS analyses in four biological replicates per sampled timepoint and treatment (n = 4). Bars represent mean values ± standard deviation. If a metabolite was not detected with the here used GC-MS analyses method, it is indicated as not detected (n.d.). Letters above bars indicate the statistical differences between tested timepoints and treatments which were investigated with a Kruskal-Wallis test in SPSS.

leaves significantly higher ICA levels than in H_2O inoculated leaves were only detected 8 dpi (0.07 µg g^{-1} FW) and 10 dpi (0.11 µg g^{-1} FW) (Figure 23.F). Between 2 dpi and 6 dpi equal amounts of ICA were quantified in *Chig* and H_2O treated leaves (Figure 23.F). These results might point to a camalexin accumulation after *Chig* infection in *A. thaliana* starting 6 dpi and an ICA accumulation after *Chig* infection in *A. thaliana* starting 8 dpi.

3.2.1.4. … the hemibiotrophic fungi *Sclerotinia sclerotiorum*

The hemibiotrophic lifestyle of pathogens is hard to identify since the duration of the biotrophic and necrotrophic phases can vary dependent on the host-pathogen interaction and genus of the pathogen (Kabbage et al. 2015). In this study, the effects on the *A. thaliana* metabolite level after an infection with the hemibiotrophic fungi *Sclero*, which has a rather short biotrophic phase and fast switch to necrotrophy while maintaining biotrophy at the edge of colonization, were investigated. Therefore five-week-old *A. thaliana* plants were inoculated with droplets of a *Sclero* inoculum or H_2O as a control treatment. For the GC-MS analyses of selected defense related metabolites samples were collected 1 dpi, 2 dpi, 3 dpi and 4 dpi.
The defense related phytohormone SA and its glucosides were selected for quantification in H_2O and *Sclero* inoculated leaves. In H_2O inoculated *A. thaliana* leaves a basal SA level between 0.68 µg g^{-1} FW (4 dpi) and 0.78 µg g^{-1} FW (2 dpi) were detected between 1 dpi and 4 dpi (Figure 24.A). Compared to the detected SA amounts in H_2O inoculated leaves statically equal SA amounts were detected in *Sclero* inoculated leaves between 1 dpi and 3 dpi, although slightly higher SA levels were observed in *Sclero* than in H_2O inoculated leaves that were sampled 2 dpi and 3 dpi (Figure 24.A). Only 4 dpi a significantly higher SA level was detected in *Sclero* inoculated leaves (1.76 µg g^{-1} FW) than in H_2O inoculated leaves (0.68 µg g^{-1} FW) (Figure 24.A). The SA glucoside SAG was as well detected in significantly higher amounts in *Sclero* (8.89 µg g^{-1} FW) than in H_2O (0.14 µg g^{-1} FW) inoculated leaves 4 dpi (Figure 24.B). Equal amounts of SAG were detected between 1 dpi and 3 dpi in *Sclero* suspension and H_2O inoculated *A. thaliana* leaves (Figure 24.B). Between 1 dpi and 3 dpi SAG amounts between 0.78 µg g^{-1} FW (1 dpi) and 0.94 µg g^{-1} FW (2 dpi) were detected in *Sclero* inoculated leaves and SAG amounts between 0.39 µg g^{-1} FW (3 dpi) and 0.49 µg g^{-1} FW (1 dpi) were detected in H_2O inoculated leaves (Figure 24.B). The SA glucoside SGE was not detected in H_2O treated leaves between 1 dpi and 4 dpi (Figure 24.C). In *Sclero* inoculated leaves no SGE was detected 1 dpi

and 2 dpi as well (Figure 24.C). However, a significantly higher SGE level was detected in *Sclero* inoculated leaves sampled 3 dpi (0.18 µg g^{-1} FW) and 4 dpi (0.42 µg g^{-1} FW) than in H_2O inoculated leaves that were sampled at the same timepoint (Figure 24.C). Summarizing these results indicate a significant accumulation of SA and SAG in *A. thaliana* starting 4 dpi with *Sclero* and a SGE accumulation starting 3 dpi in *Sclero* inoculated leaves.

In this study the metabolites Pip, NHP, NHPG and NHPGE were additionally selected for quantification in *A. thaliana* after a *Sclero* infection. In H_2O inoculated leaves Pip levels between 0.28 µg g^{-1} FW (2 dpi) and 0.37 µg g^{-1} FW (3 dpi) were detected in leaves that were sampled between 1 dpi and 4 dpi (Figure 24.D). In *Sclero* inoculated leaves a slightly higher Pip amount than in H_2O inoculated leaves 2 dpi (1.08 µg g^{-1} FW) and 3 dpi (2.15 µg g^{-1} FW) were detected, while 1 dpi equal amounts of Pip were detected in H_2O and *Sclero* inoculated leaves (Figure 24.D). However, compared to the detected Pip level in H_2O inoculated leaves a significantly higher Pip level was only detected in *Sclero* inoculated leaves 4 dpi (3.91 µg g^{-1} FW) (Figure 24.D). The NHP and its glucosides NHPG and NHPGE were not detected in H_2O treated leaves between 1 dpi and 4 dpi (Figure 24.G, T.H, T.I). In *Sclero* inoculated leaves no NHP was detected 1 dpi as well, but significantly higher NHP amounts were detected in *Sclero* inoculated leaves 2 dpi (0.09 µg g^{-1} FW), 3 dpi (0.11 µg g^{-1} FW) and 4 dpi (0.06 µg g^{-1} FW) than in H_2O inoculated leaves at the same sampling timepoints (Figure 24.G).

The NHP storage form NHPG was not detected in H_2O inoculated leaves as mentioned and was only detected 3 dpi in *Sclero* inoculated leaves (0.03 µg g^{-1} FW) (Figure 24.H). The statistical analyses revealed a significantly higher NHPG level in *Sclero* than in H_2O inoculated *A. thaliana* leaves 3 dpi (Figure 24.H). The NHP glucoside NHPGE was only detected in *Sclero* inoculated leaves 2 dpi (0.04 µg g^{-1} FW) and 3 dpi (0.05 µg g^{-1} FW) and therefore showed significantly higher NHPGE amounts in *Sclero* than in H_2O treated leaves at these sampling timepoints (Figure 24.I). Summarizing the GC-MS analyses suggests an accumulation of NHP in *A. thaliana* starting 2 dpi with *Sclero* attended with a NHPG and NHPGE accumulation between 2 dpi and 3 dpi and a significant Pip accumulation in *A. thaliana* after a *Sclero* inoculation 4 dpi.

Further selected defense related metabolites for quantification are the indoles camalexin and ICA. The phytoalexin camalexin was not detected in H_2O treated *A. thaliana* leaves between 1 dpi and 4 dpi (Figure 24.E). However, significantly higher camalexin levels were quantified in *Sclero* than in H_2O inoculated at all sampling timepoints (Figure 24.E). In *Sclero* inoculated

leaves the statistical analyses additionally revealed a significantly lower camalexin level 1 dpi (0.15 µg g^{-1} FW) than 2 dpi (19.01 µg g^{-1} FW) and 3 dpi (27.09 µg g^{-1} FW) while equal camalexin levels were detected in *Sclero* inoculated leaves 1 dpi and 4 dpi (10.22 µg g^{-1} FW) (Figure 24.E). Moreover, no significant differences in the camalexin level of *Sclero* inoculated leaves between 2 dpi and 4 dpi were observed (Figure 24.E). The ICA was also not detected in H_2O inoculated leaves at any sampling timepoint (Figure 24.F). Between 1 dpi and 4 dpi a

significant higher ICA level was detected in *Sclero* than in H_2O inoculated *A. thaliana* leaves (Figure 24.F). In *Sclero* inoculated leaves thereby the quantified ICA level was 1 dpi (0.02 µg g^{-1} FW) significantly lower than in *Sclero* inoculated leaves that were sampled 2 dpi (0.06 µg g^{-1} FW), 3 dpi (0.13 µg g^{-1} FW) and 4 dpi (0.23 µg g^{-1} FW) (Figure 24.F). These

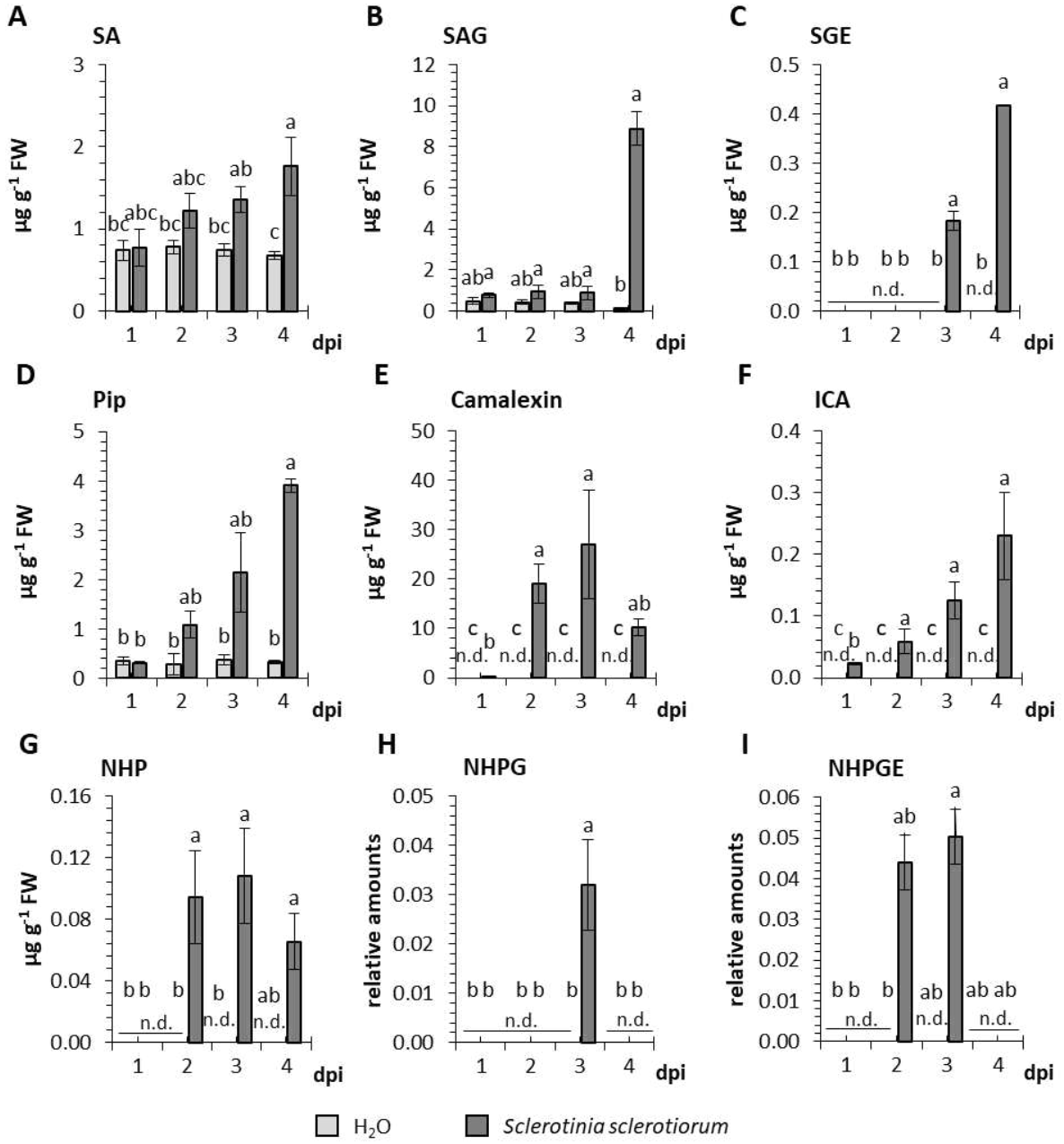

Figure 24: Time dependent accumulation of metabolites in *Arabidopsis thaliana* after an infection with *Sclerotinia sclerotiorum* (*Sclero*). Three fully grown leaves of five-week-old *A. thaliana* plants were droplet inoculated with a *Sclero* mycelium solution or H_2O as a control treatment. The inoculated leaves of one plant were sampled as one biological replicate 1 dpi, 2 dpi, 3 dpi and 4 dpi for the GC-MS analyses. In the GC-MS generated chromatograms total and relative amounts of (**A**) SA, (**B**) SAG, (**C**) SGE, (**D**) Pip, (**E**) camalexin, (**F**) ICA, (**G**) NHP, (**H**) NHPG and (**I**) NHPGE were quantified. Mean values ± standard deviation for three biological replicates per sampled timepoint and treatment (n = 3) are represented by bars. If a metabolite was not detected, it is indicated as not detected (n.d.). Statistical differences were determined with a Kruskal-Wallis test in SPSS and are indicated by letters above bars.

results point to a camalexin and ICA accumulation in *A. thaliana* after a *Sclero* infection starting 1 dpi.

3.2.1.5. … the necrotrophic fungi *Botrytis cinerea*

To investigate the *A. thaliana* defense at the metabolite level after an infection of pathogens with different lifestyle strategies, the infection of *A. thaliana* with the necrotrophic fungi *Bcin* was investigated in this study. Therefore, four- to five-week-old *A. thaliana* plants were inoculated with Mathur's medium as a control treatment or droplets of a *Bcin* solution (50 spores/µl). Samples were taken 1 dpi, 3 dpi and 5 dpi for the GC-MS analyses. To verify a successful *Bcin* infection in *A. thaliana*, at each timepoints additional samples were taken for the macro- and microscopic investigation of *Bcin* caused disease symptoms and infection structure in planta (Suppl. Figure 5).

In the GC-MS runs of *Bcin* and H_2O inoculated leaf samples, selected defense related metabolites like SA and SA glucosides were quantified. During the *Bcin* infection time course in *A. thaliana*, equal amounts of SA between 0.08 µg g^{-1} FW (H_2O, 3 dpi) and 0.20 µg g^{-1} FW (*Bcin*, 1 dpi) were detected in Mathur's medium and *Bcin* treated leaves (Figure 25.A). The SAG was detected in equal amounts of maximum 0.76 µg g^{-1} FW (5 dpi) in Mathur's medium inoculated leaves between 1 dpi and 5 dpi (Figure 25.B). In *Bcin* inoculated leaves 1 dpi equal amounts as in Mathur's medium inoculated leaves were detected (Figure 25.B). However, in *Bcin* inoculated leaves that were sampled 3 dpi (1.95 µg g^{-1} FW) and 5 dpi (3.90 µg g^{-1} FW) a slightly higher SAG level was detected than in Mathur's medium inoculated leaves, but no significant differences were determined between the treatments (Figure 25.B). The SGE was not detected in H_2O treated *A. thaliana* plants at any sampling timepoint and in *Bcin* treated plants 1 dpi (Figure 25.C). In *Bcin* inoculated leaves, SGE was detected in significantly higher amounts 3 dpi (0.20 µg g^{-1} FW) and 5 dpi (0.12 µg g^{-1} FW) than in Mathur's medium inoculated leaves at the same sampling timepoints (Figure 25.B). Summarizing, these results indicate no accumulation of SA, but a slight accumulation of the investigated SA glucosides in *A. thaliana* after a *Bcin* infection.

Further selected for quantification in *A. thaliana* were the defense related metabolites Pip, NHP and the NHP glucosides NHPG and NHPGE. The Pip was detected in basal levels between 0.11 µg g^{-1} FW (1 dpi) and 0.23 µg g^{-1} FW (5 dpi) in Mathur's medium inoculated leaves

(Figure 25.D). In comparison to Mathur's medium inoculated leaves a significantly higher Pip level was detected in *Bcin* inoculated leaves 3 dpi (1.96 µg g^{-1} FW) and 5 dpi (0.62 µg g^{-1} FW) while 1 dpi equal amounts of Pip were detected in Mathur's medium and *Bcin* inoculated leaves (Figure 25.D). The NHP and its glucosides NHPG and NHPGE were not detected in

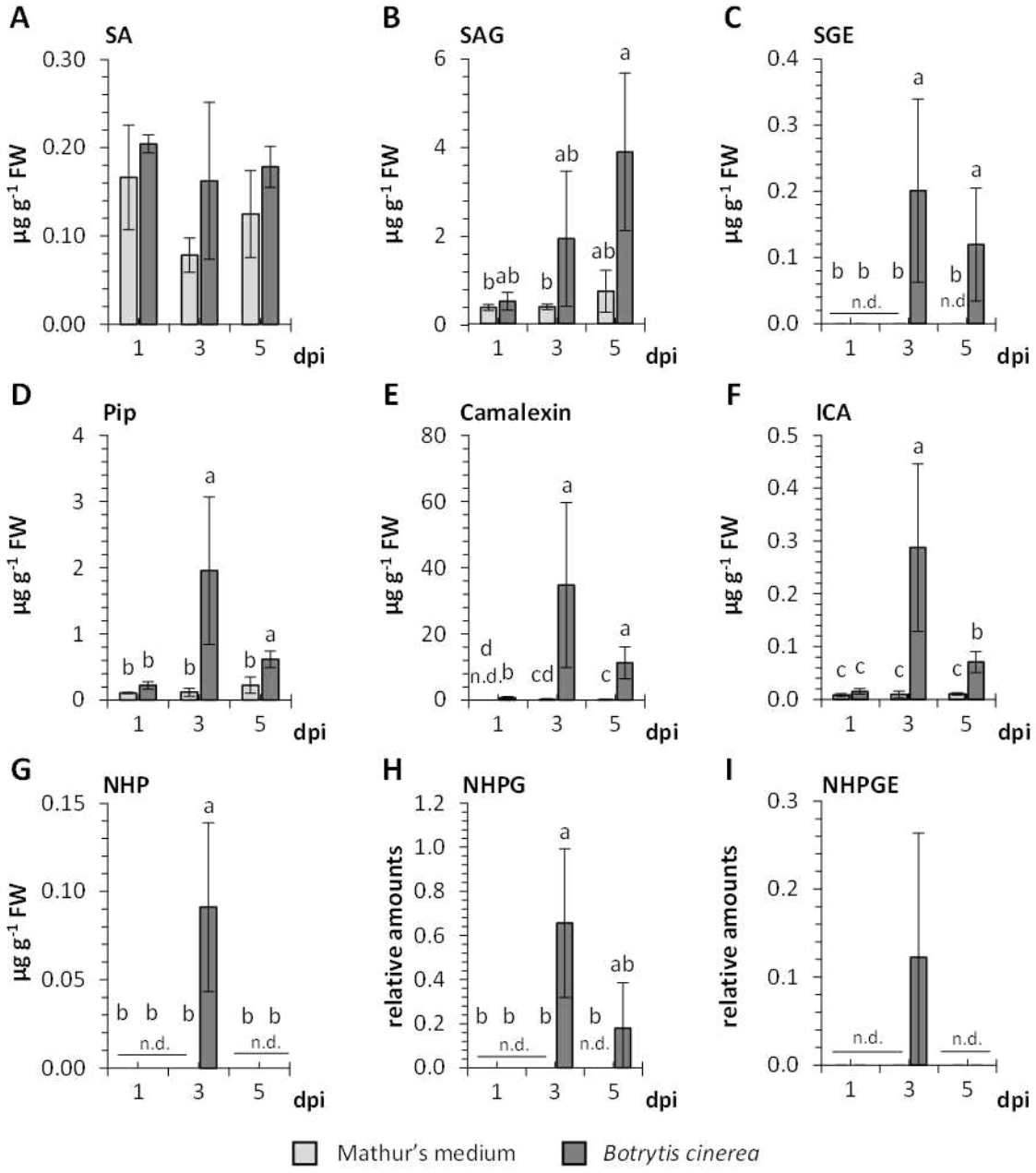

Figure 25: The plant's accumulation of defense related metabolites in the *Arabidopsis thaliana* - *Botrytis cinerea* (*Bcin*) pathosystem is time dependent. Three leaves of 4,5 weeks old *A. thaliana* Col-0 plants were droplet inoculated with a *Bcin* spore solution (50 spores/µl) or Mathur's medium as a control treatment. Samples were taken 1 dpi, 3 dpi and 5 dpi for the GC-MS analyses whereat all treated leaves of one plant were pooled for one biological replicate. After the GC-MS analyses total and relative amounts of (**A**) SA, (**B**) SAG, (**C**) SGE, (**D**) Pip, (**E**) camalexin, (**F**) ICA, (**G**) NHP, (**H**) NHPG and (**I**) NHPGE were quantified. Bars represent mean values ± standard deviation for four biological replicates per sampled timepoint and treatment (n = 4). If a metabolite was not detected with the here used GC-MS analyses method, it is indicated as not detected (n.d.). Statistical differences are indicated by the letters above bars and were investigated with a Kruskal-Wallis test in SPSS. If no letters are given, no statistical differences were identified between the tested treatments and/or timepoints.

Mathur's medium treated leaves between 1 dpi and 5 dpi (Figures 25.G, 25.H, 25.I). The NHP was not detected in *Bcin* treated plants 1 dpi and 5 dpi either but was detected in *Bcin* inoculated leaves 3 dpi (0.09 µg g^{-1} FW) in significantly higher amounts than in Mathur's medium inoculated leaves at the same sampling timepoint (Figure 25.G). The NHPG was only quantified in *Bcin* inoculated leaves that were sampled 3 dpi (0.66 µg g^{-1} FW) and 5 dpi (0.18 µg g^{-1} FW), revealing a significantly higher NHPG level in *Bcin* then in Mathur's medium inoculated leaves only 3 dpi (Figure 25.H). The NHP glucoside NHPGE was only detected in *Bcin* inoculated leaves 3 dpi (0.12 µg g^{-1} FW) but no significant differences to the Mathur's medium treatment were determined at this sampling timepoint (Figure 25.I). These results suggest a Pip accumulation in *A. thaliana* after a *Bcin* infection starting 3 dpi and a NHP accumulation only 3 dpi with *Bcin*. The quantification of the NHP glucosides points to a slight accumulation of NHPG and NHPGE in *A. thaliana* after a *Bcin* infection starting 3 dpi.
In Mathur's medium treated plants no camalexin was detected 1 dpi, but camalexin was detected 3 dpi (0.20 µg g^{-1} FW) and 5 dpi (0.15 µg g^{-1} FW) in Mathur's medium treatments. Compared to the detected camalexin amounts in Mathur's medium inoculated leaves, in *Bcin* inoculated leaves a significantly higher camalexin level was quantified at all sampling timepoints. Thereby, in *Bcin* inoculated leaves 1 dpi (0.77 µg g^{-1} FW) significant lower levels of camalexin were detected than 3 dpi (34.78 µg g^{-1} FW) and 5 dpi (11.27 µg g^{-1} FW). The ICA was detected in similar amounts of approximately 0.01 µg g^{-1} FW in H_2O inoculated leaves that were sampled between 1 dpi and 5 dpi, and in *Bcin* inoculated leaves sampled 1 dpi. In *Bcin* inoculated leaves that were sampled 3 dpi (0.29 µg g^{-1} FW) and 5 dpi (0.07 µg g^{-1} FW) significantly higher ICA amounts were detected than in the control treatments. The analyses of the selected indoles summarizing suggests a camalexin accumulation in *A. thaliana* after a *Bcin* inoculation starting 1 dpi and an ICA accumulation starting 3 dpi.

3.2.2. Comparison of the *Arabidopsis thaliana* metabolite profile after infections with pathogens of different lifestyles

To compare the *A. thaliana* defense reaction against pathogens with biotrophic, hemibiotrophic and necrotrophic lifestyles on a metabolite level, GC-MS analyses of infection time courses were performed. Therefore *A. thaliana* plants were infected with the biotrophic oomycete *Hpa*, the hemibiotrophic bacteria *Psm*, the hemibiotrophic fungi *Chig* and *Sclero*,

and the necrotrophic fungi *Bcin*. For a better comparison, the accumulation of selected defense related metabolites in *A. thaliana* after infections of pathogens with various lifestyles was compared at the timepoint of the highest detected amounts of each metabolite in each *A. thaliana* – pathogen infection time course (Table 1).

The comparison revealed similarities of the *A. thaliana* metabolite profile after infections with biotrophic and hemibiotrophic pathogens, since in interactions with *Hpa* (3 dpi), *Psm* (1 dpi), *Chig* (8 dpi) and *Sclero* (4 dpi) significantly higher SA amounts were detected in pathogen inoculated leaves than in the control treatments (Table 1). In control treatments *Bcin* inoculated leaves (5 dpi) equal SA levels were detected (Table 1). Compared to the investigated SA amounts detected in all other *A. thaliana* – pathogen interaction systems, in *A. thaliana* infections with the hemibiotrophic *Psm* (1 dpi) the highest SA amounts were detected (Table 1). The SA glucoside SAG was detected in significantly higher amounts in *A. thaliana* leaves infected with *Hpa* (9 dpi), *Psm* (3 dpi), *Chig* (10 dpi), *Sclero* (4 dpi) and *Bcin* (5 dpi) than in the respective control treatments at the same sampling timepoints (Table 1). Thereat, the highest SAG levels were as well detected in infections with the hemibiotrophic *Psm* (3 dpi) compared to the investigated SA levels detected in all other investigated infection systems (Table 1). Approximately 100 µg g^{-1} FW more SAG was detected in *A. thaliana* leaves infected with *Psm* than in leaves that were infected with *Hpa* or *Chig*, and the detected SAG levels in leaves infected with *Hpa* and *Chig* was approximately 10 times higher than the detected SAG levels in leaves infected with *Sclero* and *Bcin* (Table 1). The SA glucoside SGE was in control treatments only detected in *Chig* controls (10 dpi) but not in control treatments of other *A. thaliana* infection systems (Table 1). Compared to the investigated SGE levels detected in all other investigated infection systems the highest SGE levels were again detected in infections with *Psm* (2 dpi) (Table 1). Furthermore, the detected SGE amounts in leaves infected with *Hpa* and *Chig* were approximately 10 times higher than the SAG amounts detected in *Sclero* and *Bcin* infected leaves (Table 1). Taken together these results indicate a SA accumulation in *A. thaliana* infections with biotrophic and hemibiotrophic pathogens accompanied by an accumulation of SAG and SGE. In *A. thaliana* infections with the necrotrophic fungi *Bcin* no SA accumulation was observed and synthesized SA seemed be converted to SAG and SGE. Noticeably, the detected SAG and SGE amounts in *A. thaliana* infections with hemibiotrophic *Sclero*, which has a rather short biotrophic phase, were only slightly higher than the detected SA glycosides in *A. thaliana* infections with necrotroph *Bcin*.

The biosynthetic NHP precursor Pip was detected in significantly higher amounts in *A. thaliana* infections with biotrophic, hemibiotrophic and necrotrophic pathogens than in control treatments. In infections with *Psm* (3 dpi) the highest Pip levels were quantified compared to all other four infection systems (Table 1). Equal levels of Pip were detected in infections with the biotrophic *Hpa* (9 dpi) and the hemibiotrophic *Chig* (10 dpi) and *Sclero* (3 dpi) while in *Bcin* (3 dpi) infections only half of this Pip level was reached (Table 1). The defense inducer NHP was as well detected in significantly higher amounts in *A. thaliana* infections with biotrophic, hemibiotrophic and necrotrophic pathogens than in control treatments. Accurately, in control treatments of all five investigated *A. thaliana* infection systems no NHP was detected (Table 1). In comparison of all tested infection systems the highest NHP level was detected in *Psm* (2 dpi) infected plants (Table 1). Similar amounts of NHP were quantified in *Sclero* (3 dpi) and *Bcin* (3 dpi) infected *A. thaliana* plants and approximately twice of these NHP amounts were detected in *Hpa* (9 dpi) infections. Additionally, twice of the in *Hpa* infections detected NHP amounts were detected in *Chig* infections (6 dpi) (Table 1).

The NHP glucosides NHPG and NHPGE were as well as NHP not detected in control treatments of all investigated *A. thaliana* infection systems but were detected after the infections in *A. thaliana* leaves (Table 1). The lowest NHP glucoside amounts were detected in *A. thaliana* infections with *Sclero* (3 dpi) and only slightly higher amounts of NHPG and NHPGE were detected after infections with *Bcin* (3 dpi) (Table 1). Compared to the quantified NHPG amounts in *A. thaliana* after infections with *Sclero* and *Bcin*, in infections with *Hpa* (9 dpi) and *Chig* (8 dpi) more than 30 times higher NHPG amounts were quantified in infected leaves (Table 1). Additionally, the detected NHPGE levels in *A. thaliana* leaves after infections with *Hpa* (9 dpi) and *Chig* (8 dpi) were 2 – 10 times higher than the detected NHPGE levels in *Sclero* (3 dpi) and *Bcin* (3 dpi) infected leaves (Table 1). In comparison of all investigated *A. thaliana* infection systems, the by far highest NHPG and NHPE amounts were detected in *Psm* infected plants with 645.55 µg g^{-1} FW (3 dpi) NHPG and 26.43 µg g^{-1} FW (3 dpi) NHPGE (Table 1). In summary these results indicate the activation of the NHP biosynthesis pathway in *A. thaliana* after infections with biotrophic, hemibiotrophic and necrotrophic pathogen. However, lifestyle and pathogen specific mechanism might influence the degree of induction of the NHP biosynthesis and glycosylation.

The antimicrobial compounds camalexin and ICA were also selected for quantification in control treatments and infections with *Hpa*, *Psm*, *Chig*, *Sclero* and *Bcin*. In control treatments of *Hpa* and *Sclero* inoculations no camalexin and ICA was detected, while in the control treatments of *Psm*, *Chig* and *Bcin* inoculations a basal camalexin and ICA level was detected (Table 1). These differences are most likely caused by the varying sensitivity of the used GC-MS at different experimental timepoints. In *A. thaliana* leaves that were infected with *Hpa*, *Psm*, *Chig*, *Sclero* or *Bcin* significantly higher amounts of camalexin and ICA were detected than in leaves of the respective control treatments (Table 1). In *A. thaliana* infections with the biotroph *Hpa* (9 dpi) the lowest camalexin levels were detected compared to the detected camalexin levels in all other investigated *A. thaliana* infection systems (Table 1). After infections with *Chig* (8 dpi), *Sclero* (3 dpi) and *Bcin* (3 dpi) similar amounts of camalexin of approximately 30 µg g^{-1} FW were detected and in *A. thaliana* leaves that were infected with *Psm* (3 dpi) five times more camalexin was detected than in leaves infected with *Chig*, *Sclero* and *Bcin* (Table 1). Similarly, the highest amounts of ICA were detected in leaves infected with *Psm* with 0.53 µg g^{-1} FW (3 dpi) compared to the ICA amounts that were detected in *A. thaliana* after the infection of all other investigated pathogens (Table 1). Only half of the

Table 1: Comparison of accumulating defense related metabolites in the *Arabidopsis thaliana* after the infection with *Hyaloperonospora arabidopsidis*, *Pseudomonas syringae*, *Colletrotrichum higginsianum*, *Sclerotinia sclerotiorum* and *Botrytis cinerea* (*Bcin*). Infection time courses were performed as described in Figures 20-25. The accumulation of selected defense related metabolites in *A. thaliana* after infections of pathogens with various lifestyles (+) and the respective control treatment (-) was compared at the timepoint of the highest detected amounts of each metabolite in each *A. thaliana* – pathogen infection time course.

		SA		SAG		SGE		Pip		NHP		NHPG		NHPGE		Camalexin		ICA	
			µg/g FW ± SD		µg/g FW ± SD		µg/g FW ± SD		µg/g FW ± SD		µg/g FW ± SD		µg/g FW ± SD		µg/g FW ± SD		µg/g FW ± SD		µg/g FW ± SD
Hyaloperonospora arabidopsidis (*Hpa*)	-	3 dpi	0.1 ± 0.04	9 dpi	1.82 ± 1.97	3 dpi	n.d. ± 0.0	9 dpi	0.41 ± 0.27	9 dpi	n.d. ± 0.0	9 dpi	n.d. ± 0.0	9 dpi	n.d. ± 0.0	9 dpi	n.d. ± 0.0	9 dpi	n.d. ± 0.0
	+		0.55 ± 0.08		59.11 ± 31.55		2.62 ± 0.75		4.25 ± 1.98		0.18 ± 0.08		21.73 ± 9.78		0.24 ± 0.14		9.29 ± 3.39		0.10 ± 0.07
Pseudomonas syringae (*Psm*)	-	1 dpi	0.14 ± 0.03	3 dpi	4.37 ± 4.01	2 dpi	n.d. ± 0.0	3 dpi	1.47 ± 0.03	2 dpi	n.d. ± 0.0	3 dpi	n.d. ± 0.0	2 dpi	n.d. ± 0.0	3 dpi	0.44 ± 0.76	3 dpi	0.002 ± 0.004
	+		3.23 ± 0.40		171.82 ± 28.65		19.03 ± 2.92		77.35 ± 4.97		26.42 ± 5.94		645.55 ± 148.43		26.43 ± 4.15		165.82 ± 22.38		0.53 ± 0.13
Colletrotrichum higginsianum (*Chig*)	-	8 dpi	0.06 ± 0.004	10 dpi	0.96 ± 0.29	10 dpi	0.17 ± 0.17	10 dpi	0.25 ± 0.06	6 dpi	n.d. ± 0.0	8 dpi	n.d. ± 0.0	8 dpi	n.d. ± 0.0	8 dpi	0.06 ± 0.11	10 dpi	0.01 ± 0.003
	+		0.44 ± 0.15		80.54 ± 15.59		4.95 ± 0.93		5.89 ± 2.27		0.37 ± 0.12		20.09 ± 8.11		0.53 ± 0.17		34.43 ± 12.65		0.11 ± 0.06
Sclerotinia sclerotiorum (*Sclero*)	-	4 dpi	0.68 ± 0.05	4 dpi	0.14 ± 0.06	4 dpi	n.d. ± 0.0	3 dpi	0.34 ± 0.04	3 dpi	n.d. ± 0.0	3 dpi	n.d. ± 0.0	3 dpi	n.d. ± 0.0	3 dpi	n.d. ± 0.0	4 dpi	n.d. ± 0.0
	+		1.76 ± 0.35		8.89 ± 0.80		0.42 ± 0.001		3.91 ± 0.13		0.11 ± 0.03		0.04 ± 0.009		0.05 ± 0.007		27.09 ± 11.05		0.23 ± 0.07
Botrytis cinerea (*Bcin*)	-	5 dpi	0.12 ± 0.05	5 dpi	0.76 ± 0.47	3 dpi	n.d. ± 0.0	3 dpi	0.12 ± 0.06	3 dpi	n.d. ± 0.0	3 dpi	n.d. ± 0.0	3 dpi	n.d. ± 0.0	3 dpi	0.2 ± 0.29	3 dpi	0.01 ± 0.006
	+		0.18 ± 0.02		3.90 ± 1.77		0.20 ± 0.14		1.96 ± 1.12		0.09 ± 0.05		0.66 ± 0.34		0.12 ± 0.14		34.78 ± 24.91		0.29 ± 0.16

0 – 0.2 µg/g FW | 0.2 – 1 µg/g FW | 1 – 10 µg/g FW | 10 – 100 µg/g FW | 100 – ∞ µg/g FW

ICA amounts that were detected in *Psm* infected leaves were detected in leaves that were infected with *Sclero* (4 dpi) or *Bcin* (3 dpi) (Table 1). Approximately half of the ICA amounts

that were detected in *Sclero* or *Bcin* infected leaves were detected in leaves that were infected with *Hpa* (9 dpi) or *Chig* (10 dpi) (Table 1). These results indicate an ICA and camalexin accumulation in *A. thaliana* after the infection with *Hpa*, *Psm*, *Chig*, *Sclero* or *Bcin* with tendencies of a lifestyle specific degree of accumulation.

3.2.3. The NHP induced resistance in *Arabidopsis thaliana* against pathogens with various lifestyles

Recent studies have demonstrated the resistance inducing effect of NHP in mono- and dicotylous plant after an infection with biotrophic or hemibiotrophic bacteria and fungi (Holmes et al. 2019, Schnake et al. 2020, Zhang et al. 2021). However, if NHP induces resistances in plants against infections with necrotrophic pathogens has not been studied yet. To investigate the NHP effect in *A. thaliana* on pathogens with a necrotrophic lifestyle and compare it to the resistance inducing effect against biotrophic and hemibiotrophic pathogens, four- to five-week-old *A. thaliana* plants were watered with a 1 mM NHP solution or H_2O as a control treatment and afterwards infected with the biotrophic oomycete *Hpa*, hemibiotrophic *Psm* bacteria, the hemibiotrophic fungi *Chig* and *Sclero* and the necrotrophic fungi *Bcin*. Samples were taken 6 dpi with *Hpa*, 2 dpi with *Psm lux*, 7 dpi with *Chig*, 3 dpi with *Sclero* and 2 dpi with *Bcin* to assess the *A. thaliana* resistance. Additionally, the progression of the pathogen induced symptoms on *A. thaliana* leaves were documented photographically. The NHP induced resistance in *A. thaliana* after an infection with *Sclero* was only investigated once while the NHP induced resistance after an infection with *Hpa*, *Psm*, *Chig* and *Bcin* were investigated at least 3 times with similar results.

To assess the *A. thaliana* resistance against *Hpa*, H_2O and NHP pretreated and *Hpa* inoculated leaves were stained with trypan blue whereby the oomycetes infection structures were visualized in planta and the length of IH was quantified. The H_2O pretreated plant revealed a mean IH length of 636 mm per cm^2 and in the macroscopic analyses downy white patches were observed on the leaves (Figure 26.A, 26.F). After a pretreatment with NHP and an infection with *Hpa* of *A. thaliana* no IH were observed in the inoculated leaves and no downy white patches were visible on the leaves (Figure 26.A, 26.F). Hence, the statistical analyses revealed significantly higher length of IH in plants that were pretreated with H_2O than in plants that were pretreated with NHP (Figure 26.A).

The *A. thaliana* resistance against hemibiotrophic *Psm lux* bacteria was assessed by measuring the luminescence of the bacteria in a luminometer. The number of quantified *Psm lux* bacteria in the leaves was approximately 16 times higher in H_2O than in NHP pretreated plants which was determined as a significant difference between the pretreatments (Figure 26.B). Macroscopically, H_2O pretreated leaves seemed dehydrated and showed chlorosis, while NHP pretreated leaves only showed slight chlorosis or no infection symptoms (Figure 26.F).

To assess the *A. thaliana* resistance against *Chig*, *Sclero* and *Bcin* the mean necrotic area per inoculation site was determined on the leaves of H_2O and NHP pretreated plants in mm^2 (Figure 26.C, 26.D, 26.E). On NHP pretreated and *Chig* inoculated leaves a significantly smaller necrotic area per inoculation site was measured than on H_2O pretreated and *Chig* inoculated leaves whereat the measured necrotic area on NHP pretreated leaves (3.07 mm^2) was only half the size of the measured necrotic area on H_2O pretreated leaves (5.67 mm^2) (Figure 26.C). While on H_2O pretreated and *Chig* inoculated leaves necrotic lesions were observed at the 4 sites of droplet inoculation on the leaves, after NHP pretreatment and *Chig* inoculation smaller necrotic lesions and sometimes only water-soaked lesions were observed at the sites of inoculation (Figure 26.F).

The quantified necrotic area on NHP pretreated and *Sclero* inoculated leaves (9.17 mm^2) was almost half the size of the measured necrotic area on H_2O pretreated and *Sclero* inoculated leaves (15.82 mm^2) and thereby a significantly larger necrotic area was measured in H_2O pretreatments than in NHP pretreatments (Figure 26.D). This effect was verified visually. At the two *Sclero* droplet inoculation sites of NHP pretreated leaves smaller necrotic area were observed than on H_2O pretreated leaves (Figure 26.F). The investigation of the NHP induced resistance in *A. thaliana* after an infection with the necrotrophic *Bcin* revealed significantly smaller necrotic lesions on leaves of NHP pretreated plants compared to the lesion size on leaves of H_2O pretreated plants (Figure 26.E). The necrotic lesion size on leaves on H_2O pretreated and *Bcin* inoculated leaves was with 5.39 mm^2 approximately twice as large as the necrotic lesions that were measured on leaves of NHP pretreated plants (2.45 mm^2) (Figure 26.E). Macroscopically this NHP resistance inducing effect against *Bcin* was verified since NHP pretreated plants showed smaller necrotic lesions than H_2O pretreated plants (Figure 26.F). Additionally, the necrotic lesions caused by *Bcin* showed clear edges on leaves of H_2O treated

plants while after NHP pretreatments the edges of the necrotic lesions seemed blurred (Figure 26.F).

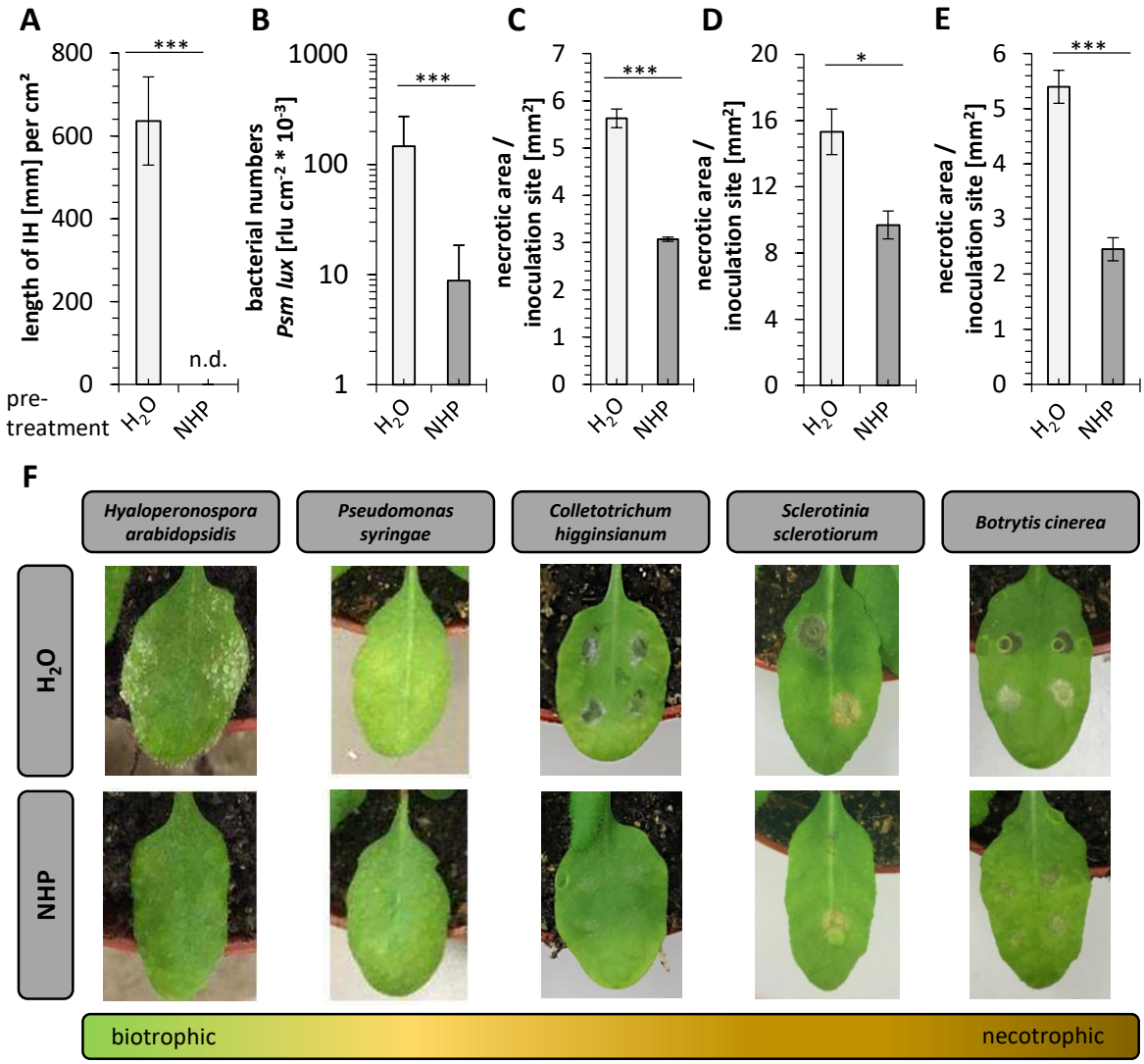

Figure 26: The NHP induced resistance in *Arabidopsis thaliana* against pathogens of various lifestyles. Four- to five-week-old Col-0 wildtype plants pre-treated with NHP or H_2O via the soil. One day later three fully grown leaves were inoculated with *Hyaloperonospora arabidopsidis* (*Hpa*) (50 spores/µl) via spray inoculation (n = 6), with *Pseudomonas syringae* lux (*Psm lux*) (OD = 0.001) via infiltration (n ≥ 6), with *Sclerotinia sclerotiorum* (*Sclero*) via spray inoculation (n = 5), or with *Botrytis cinerea* (*Bcin*) (50 spores/µl) via droplet inoculation (n = 8). Droplet inoculation with *Colletotrichum higginsianum* (*Chig*) (500 spores/µl) were performed 4 hours after the NHP or H_2O pre-treatments (n = 8). The resistance of *A. thaliana* plants was assessed (**A**) via the determination of length of internal hyphae (IH) of *Hpa* in leaves in mm 6 dpi, (**B**) via the determination of the number of *Psm lux* bacteria in a leave with a luminometer in relative luminescence units (rlu) 2 dpi, or via measurements of the necrotic area per inoculation site in mm^2 on the leaves (**C**) 7 dpi with *Chig*, (**D**) 3 dpi with *Sclero* and (**E**) 2 dpi with *Bcin* infections. Bars represent mean values ± standard deviations (A, B) or ± standard error of the mean (C, D, E). Statistical differences were investigated with a two-tailed *t* test and asterisks (p = * < 0.05, ** < 0.01, *** < 0.001) are indicated above bars. (**F**) Pictures were taken of NHP and H_2O pre-treated plants which were leave-inoculated with biotrophic *Hpa*, hemibiotrophic *Psm*, *Chig* or *Sclero* and necrotrophic *Bcin* pathogens to visualize immune inducing effects of NHP on the plant.

In Summary, the NHP resistance inducing effect in *A. thaliana* was observed to be effective against the infection with the investigated biotrophic, hemibiotrophic and necrotrophic

pathogens. The degree of effective resistance induction by NHP in *A. thaliana* however may rely on pathogen specific lifestyle strategies. To investigate the involvement of defense associated signaling pathways in the *A. thaliana* NHP induced resistance against hemibiotrophic and necrotrophic fungi, the effect of a NHP pretreatment and a *Chig* or *Bcin* infection was studied in mutants with defects in the SA, NHP, JA, ABA and phytoalexin biosynthesis pathways and compared to the Col-0 wildtype.

Although the role of EDS1 and PAD4 in plant defense against pathogens is not fully elucidated, studies have shown their direct interaction and activation of camalexin, tocopherol, SA and NHP biosynthesis (Feys et al. 2001, Stahl et al. 2019, Hartmann et al. 2018). After a H_2O pretreatment and a *Chig* infection, *A. thaliana eds1* and *pad4* mutants showed a significantly larger necrotic lesion size than Col-0 plants (Figure 27.A). In comparison to H_2O pretreated and *Chig* infected *eds1*, *pad4* and Col-0 plants, a significantly smaller necrotic lesion size was measured on NHP pretreated plants of these investigated genotypes (Figure 27.A). After a *Bcin* infection, Col-0, *eds1* and *pad4* plants that were pretreated with NHP similarly showed significantly smaller necrotic area than H_2O pretreated plants of the respective genotype (Figure 28.A). After a H_2O pretreatment and a *Bcin* infection an equal necrotic lesion size was observed on the Col-0 wildtype and the *eds1* and *pad4* mutant plants (Figure 28.A).

To further investigate the influence of the interaction of the SA and NHP signaling pathways influence on the NHP induced resistance in *A. thaliana* the *sid2*, *fmo1* mutants and the double mutant *sid2/fmo1* were challenged with NHP and infected with *Chig* or *Bcin*. The assessment of resistance revealed a similar necrotic lesions size on H_2O pretreated and *Chig* infected Col-0 and *sid2* plants which was significantly smaller than the detected necrotic lesion size on H_2O pretreated an *Chig* infected *fmo1* and *sid2/fmo1* plants (Figure 27.B). The NHP pretreated and *Chig* infected Col-0, *fmo1* and *sid2/fmo1* plants however showed a significantly smaller necrotic lesion size than the H_2O pretreated and *Chig* infected plants of the respective genotype (Figure 27.B). In *sid2* mutant plants, NHP pretreatments only resulted in slightly, but statistically not significant smaller necrotic lesions compared to the H_2O pretreatments after *Chig* infections (Figure 27.B). The assessment of the *A. thaliana* resistance against a *Bcin* infection revealed significantly smaller necrotic lesions on NHP pretreated Col-0, *sid2*, *fmo1* and *sid2/fmo1* plants than on the H_2O pretreated and *Bcin* infected plants of these genotypes (Figure 28.B). Although the necrotic area on H_2O pretreated and *Bcin* infected *sid2*, *fmo1* and

sid2/fmo1 plants seemed to be slightly smaller than the observed necrotic area on Col-0 plants, no significant differences were determined between the genotypes (Figure 28.B).

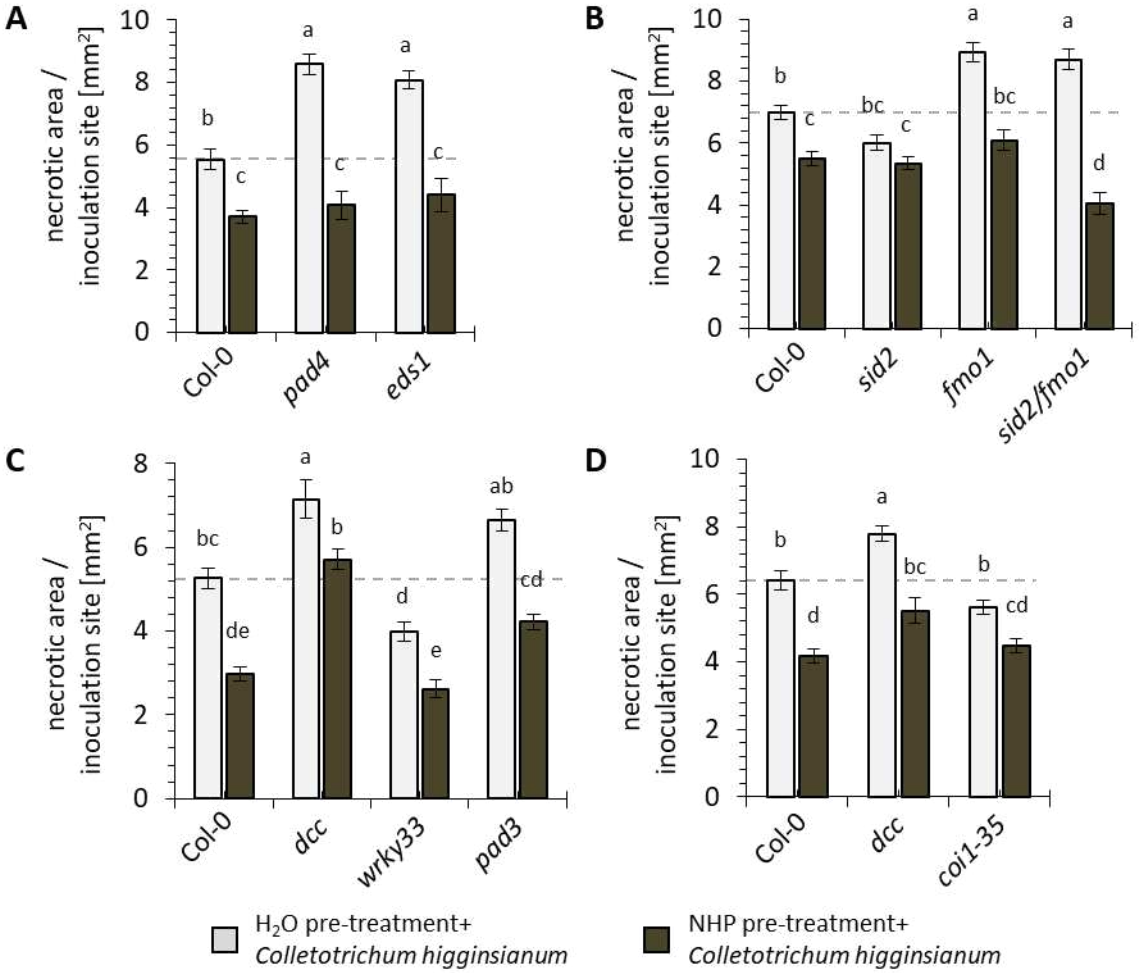

Figure 27: The NHP induced resistance in *Arabidopsis thaliana* mutants with defects in defense related signaling pathways against *Colletotrichum higginsianum* (*Chig*). 4,5-week-old *A. thaliana* Col-0 wildtype plants were watered with 1 mM NHP or H_2O and were one day later droplet inoculated with a *Chig* solution (500 spores/µl). In independent experiments, NHP and H_2O pre-treatments of Col-0 were compared to NHP and H_2O pre-treatments of (**A**) the *pad4* and *eds1* mutants; (**B**) the *sid2*, *fmo1* and *sid2/fmo1* mutants; (C) the *dcc*, *wrky33* and *pad3* mutants, and (**D**) the *dcc* and *coi1-35* mutants. Sampling was performed 2 dpi and the size of necrotic area per inoculation site in mm^2 was determined 5 dpi with *Chig* (n = 8) using ImageJ. Bars represent mean values ± standard error of the mean for the quantified necrotic area. Kruskal-Wallis test performed in SPSS was used to determine statistical differences between the pre-treatments and results are indicated with letters above bars.

The influence of indole derived phytoalexins on the *A. thaliana* basal and NHP induced resistance was investigated with the *cyp79b2/cyp79b3* (*dcc*) double mutant and the *pad3* mutant. In the biosynthesis of phytoalexins like camalexin and ICA, CYP79B2 and CYP79B3 facilitate the first step from Trp to IOAx and PAD3 catalyzes the last synthesis step from DHCA to camalexin (Stahl et al. 2019). A knock-out mutant of the transcription factor WRKY33 was as well studied in this matter since it has been shown that WRKY33 has a positive influence on the PAD3 activity (Thomma et al. 1999). However, transcriptional analyses revealed that the

WRKY33 transcription factor influences several other signaling pathways and thereby regulates the accumulation of SA, JA, ET and ABA (Liu et al. 2015). In this study, NHP treated and *Chig* infected *A. thaliana dcc*, *pad3* and *wrky33* mutants showed significantly smaller necrotic lesions than H_2O pretreated and *Chig* plants of the respective genotypes like the wildtype Col-0 (Figure 27.C). After a H_2O pretreatment and *Chig* infection *A. thaliana dcc* and *pad3* mutants developed an equal size of necrotic lesion. However, the statistical analyses revealed a significantly larger necrotic area on H_2O pretreated and *Chig* infected *dcc* plants than on H_2O pretreated and *Chig* infected Col-0 plants while the detected necrotic area in H_2O pretreated and *Chig* infected Col-0 and *pad3* plants was statistically determined as equal (Figure 27.C). The *wrky33* mutants showed significantly smaller necrotic lesion sizes after a H_2O treatment and a *Chig* infection than the Col-0 wildtype and the *dcc* and *pad3* mutants after the same treatments (Figure 27.C).

After a *Bcin* infection NHP pretreated Col-0, *wrky33*, *pad3* and *coi1-35* plants showed significantly smaller necrotic area than H_2O pretreated and *Bcin* infected plants (Figure 28.C). In H_2O pretreated and *Bcin* infected plants the largest necrotic area was measured on leaves of *wrky33* plants, which was significantly larger than the quantified necrotic area on leaves of Col-0, *dcc, coi1-35* and *pad3* plants (Figures 28.C, 28.D). The quantified necrotic lesion size on leaves of H_2O pretreated and *Bcin* infected *dcc* mutant plants was significantly smaller than the detected lesions on *wrky33* plants, but significantly larger than the detected lesion size on leaves of Col-0 plants (Figure 28.D). On leaves of H_2O pretreated and *Bcin* infected *pad3* plants significantly smaller necrotic lesions were observed than on Col-0 and *wrky33* plants (Figure 28.C).

To investigate the influence of the JA signaling on the NHP induced resistance in *A. thaliana* against *Chig*, the NHP resistance inducing effect was tested in the *coi1-35* mutant. COI1 is part of the JA receptor complex which enables the induction of JA dependent gene expression in *A. thaliana* (Feys et al. 1994, reviewed in Staswick 2008). Compared to the quantified necrotic area on H_2O pretreated and *Chig* infected *coi1-35* plants, after NHP treatments *coi1-35* plants showed a wildtype-like reduction of necrotic area (Figure 27.D). After H_2O treatments and *Chig* infections Col-0 and *coi1-35* plants showed an equal necrotic lesion size which were significantly smaller than the quantified necrotic lesion size on H_2O pretreated and *Chig* infected *dcc* mutants (Figure 27.D). After a Bcin infection NHP pretreated Col-0 and *coi1-35* plants showed significantly smaller necrotic area than H_2O pretreated and *Bcin* infected plants

of the respective genotypes (Figure 28.C). The leaves of H_2O pretreated and *Bcin* infected *coi1-35* plants showed significantly larger necrotic lesions than leaves of H_2O pretreated and *Bcin* infected Col-0 plants but significantly smaller necrotic lesions than leaves of H_2O pretreated and *Bcin* infected *wrky33* plants (Figure 28.C).

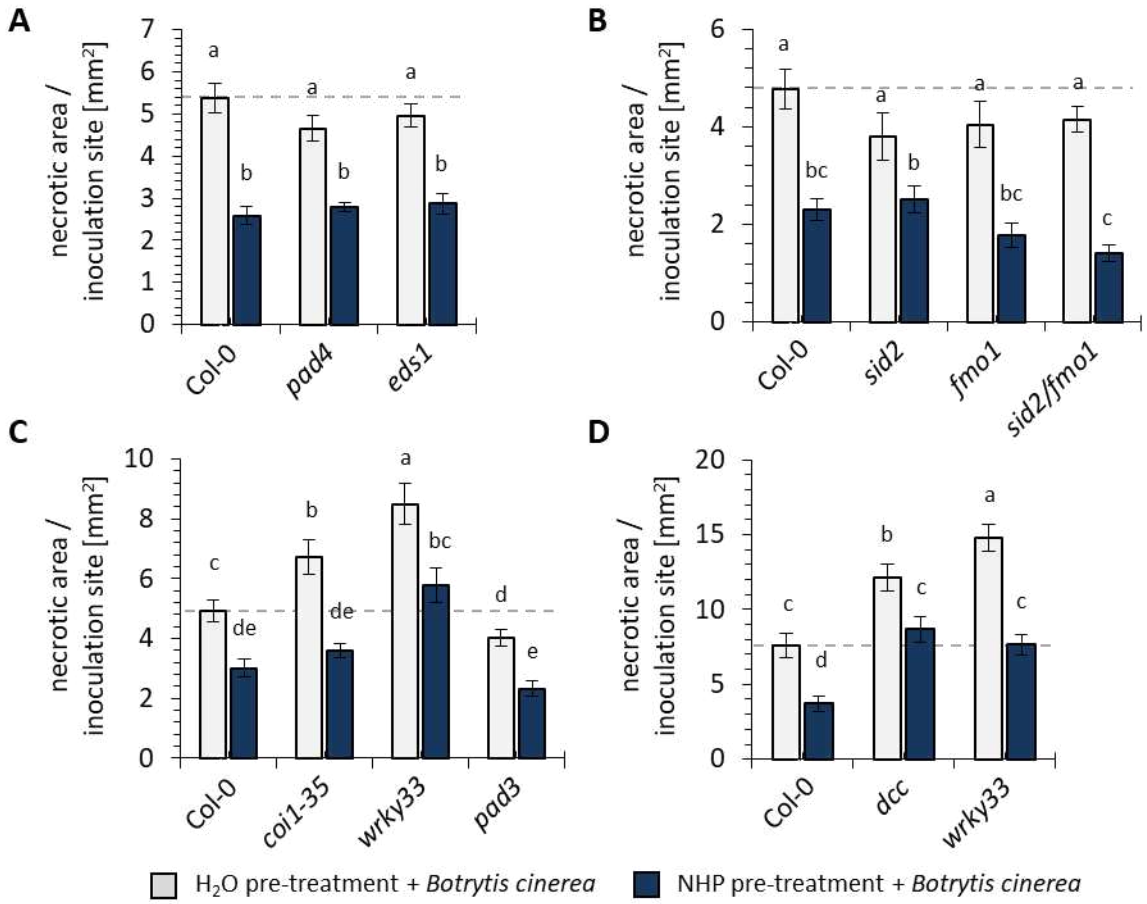

Figure 28: The NHP induced resistance in *Arabidopsis thaliana* mutants with defects in defense related signaling pathways against *Botrytis cinerea* (*Bcin*). Plants (4,5-week-old) were watered with 1 mM NHP or H_2O and were droplet inoculated with a *Bcin* solution (50 spores/µl) one day later. In independent experiments, NHP and H_2O pre-treatments of Col-0 WT plants were compared to NHP and H_2O pre-treatments of (**A**) the *pad4* and *eds1* mutants; (**B**) the *sid2*, *fmo1* and *sid2/fmo1* mutants; (**C**) the *coi1-35*, *wrky33* and *pad3* mutants; and (**D**) the *dcc* and *wrky33* mutants. Samples were taken 2 dpi and the size of necrotic area per inoculation site was quantified in mm^2 2 dpi with *Bcin* (n = 8) using ImageJ. Mean values ± standard error of the mean were calculated for the quantified necrotic area and are represented by the bars. Statistical differences were determined with a Kruskal-Wallis test in SPSS and are indicated above bars.

3.2.4. Toxicological effects of NHP on *Ascomycetes*

To verify that NHP induces resistance in planta and thereby reduces disease symptoms of *Ascomycetes* in *A. thaliana*, the toxicological effect of NHP on the investigated *Ascomycetes* was tested. Therefore, Mathur's agar plugs with grown *Chig* or *Bcin* mycelium were grown on

fresh Mathur's agar plates supplemented with NHP or with NH_4Cl + HCl as control. After 3 days the radial mycelium growth was quantified.

The radial *Chig* mycelium growth remained equal on NHP and NH_4Cl + HCl supplemented Mathur's agar plates after 3 days of growth. On plates with both supplements approximately 5.5 cm^2 mycelium were observed (Figure 29.A). On Mathur's agar plates which contained NHP or NH_4Cl + HCl a similar radial *Bcin* mycelium growth of approximately 13 cm^2 was observed (Figure 29.B). No statistical differences in the radial growth of *Chig* and *Bcin* was determined between NHP and NH_4Cl + HCl supplemented plates (Figure 29). These results indicate, that NHP has no direct toxicological effect on the investigated *Ascomycetes Chig* and *Bcin*.

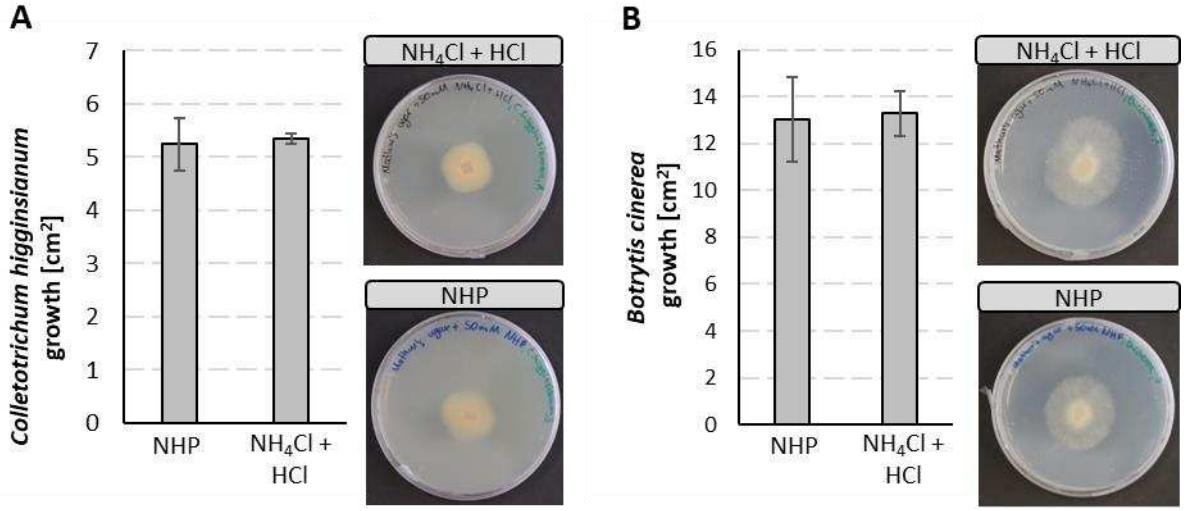

Figure 29: Toxicological effects of NHP on Ascomycetes. Mathur's agar plugs with 10 days grown (**A**) *Colletotrichum higginsianum* (*Chig*) or (**B**) *Botrytis cinerea* (*Bcin*) mycelium were propagated on fresh Mathur's agar plates supplemented with NHP or with NH_4Cl + HCl as control. After 3 days the radial mycelium growth was measured and mean values ± standard deviations were calculated in cm^2. For each tested medium and pathogen three replicates were performed (n = 3). Statistical differences were investigated with a two-tailed *t*-test (p = * < 0.05, ** < 0.01, *** < 0.001).

3.2.5. Chemical induction of callose deposition in *Arabidopsis thaliana*

It has been demonstrated that SA treatments induce callose deposition at plasmodesmata in *A. thaliana* and pathogen growth might thereby be hindered (Wang et al. 2013). To investigate if the NHP resistance priming in *A. thaliana* relies on similar mechanisms, the deposition of callose was investigated. For NHP priming experiments prior to *Chig* infections, *A. thaliana* plants were pretreated with H_2O and NHP and four hours later inoculated with a *Chig* spore solution or were mock treated with H_2O. Samples were taken 2 dpi and de-stained from chlorophyl. For NHP priming experiments prior to *Bcin* infections, *A. thaliana* plants were

pretreated with H_2O and NHP and one day later inoculated with a *Bcin* spore solution or were mock treated with liquid Mathur's medium. Samples were taken 1 dpi with *Bcin* and likewise de-stained from chlorophyl. All bleached leaf samples were stained with aniline blue and callose deposits were visualized via fluorescence microscopy.

The quantified fluorescent area in leaves of NHP pretreated *A. thaliana* plants was significantly larger than the quantified fluorescent area in H_2O pretreated plants independent of a following mock, *Chig* or *Bcin* inoculation (Figure 30, ZB). However, after a H_2O pretreatment and a H_2O mock control inoculation (0.19 $\mu m^2/mm^2$) a significantly smaller fluorescent area was detected compared to the quantified fluorescent area after a H_2O pretreatment and a *Chig* inoculation (1.91 $\mu m^2/mm^2$) (Figure 30.B). After NHP pretreatments likewise a significantly smaller fluorescent area was quantified in H_2O mock control inoculated leaves (27.19 $\mu m^2/mm^2$) than in *Chig* inoculated leaves (58.03 $\mu m^2/mm^2$) (Figure 30.B). These results agree with the visual observations under the microscope of small fluorescent dots in the leaves which were rare in H_2O pretreated and mock inoculated leaves, a few fluorescent dots were observed on leaves of H_2O pretreated and *Chig* inoculated plants, some more were observed on leaves of NHP pretreated and mock inoculated leaves and the most fluorescent dots were visible on leaves of NHP pretreated and *Chig* inoculated plants (Figure 30.A).

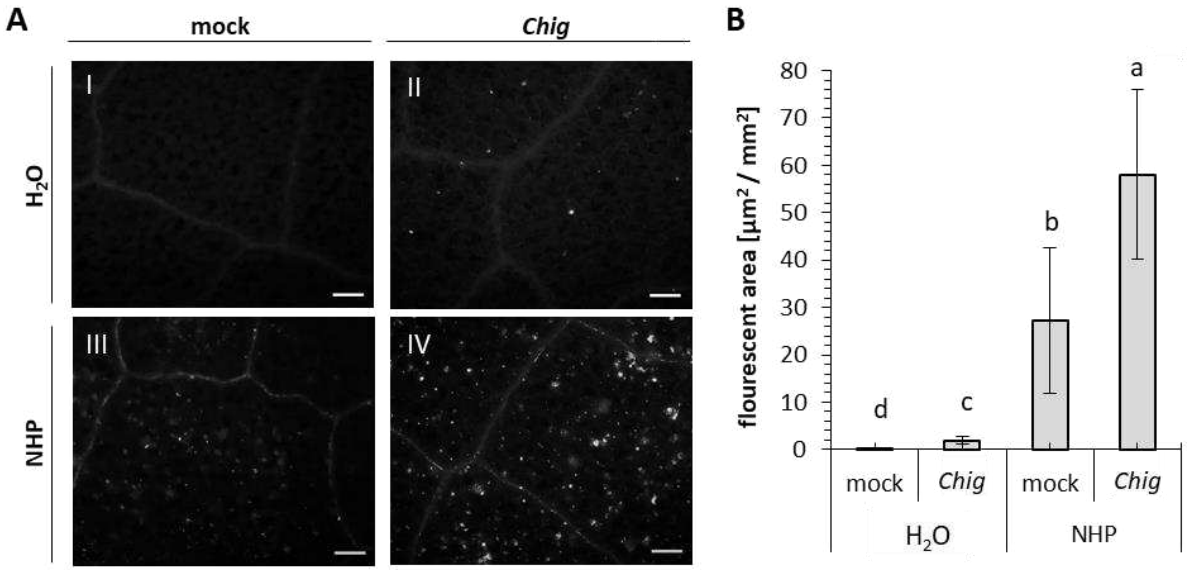

Figure 30: The induction of callose deposition in NHP primed and *Colletotrichum higginsianum* (*Chig*) infected *Arabidopsis thaliana* plants. 4,5-week-old plants were watered with a 1 mM NHP solution (III, IV) or H_2O (I, II) as control treatment. *Chig* (500 spores/µl) (II, IV) and H_2O control (I, III) droplet inoculations were performed 4 h after the pre-treatments and samples were taken 2 dpi (n = 4). (**A**) Leaf samples were stained with aniline blue and callose deposits were visualized at the site of inoculation via fluorescence microscopy and the Zen Software. (**B**) Using ImageJ, fluorescent areas were quantified per mm^2. Statistical differences between the treatments were calculated with the Kruskal-Wallis Test in SPSS and are indicated above bars. Bars indicate mean values ± standard deviations.

After a H_2O pretreatment and a *Bcin* inoculation a significantly larger fluorescent area was quantified than in leaves of H_2O pretreated and mock (Mathur's medium) inoculated plants (Figure 31.B). Similarly, NHP pretreatment and a *Bcin* inoculated plants showed a significantly larger fluorescent area compared to the quantified fluorescent area in leaves of NHP pretreated and mock inoculated plants (Figure 31.B). The microscopical visual analyses supports these results and revealed small fluorescent dots in the leaves. The fewest fluorescent dots were observed in leaves of H_2O pretreated and mock inoculated plants, some more were observed on leaves of NHP pretreated and mock inoculated leaves, even more fluorescent dots were visible on leaves of H_2O pretreated and *Bcin* inoculated plants and the most fluorescent dots were observed on leaves of NHP pretreated and *Bcin* inoculated plants (Figure 31.A). Summarizing these results indicate an induction of callose deposition after an NHP treatment. Moreover, these results suggest that callose depositions are also induced by the attacking pathogens *Chig* and *Bcin*.

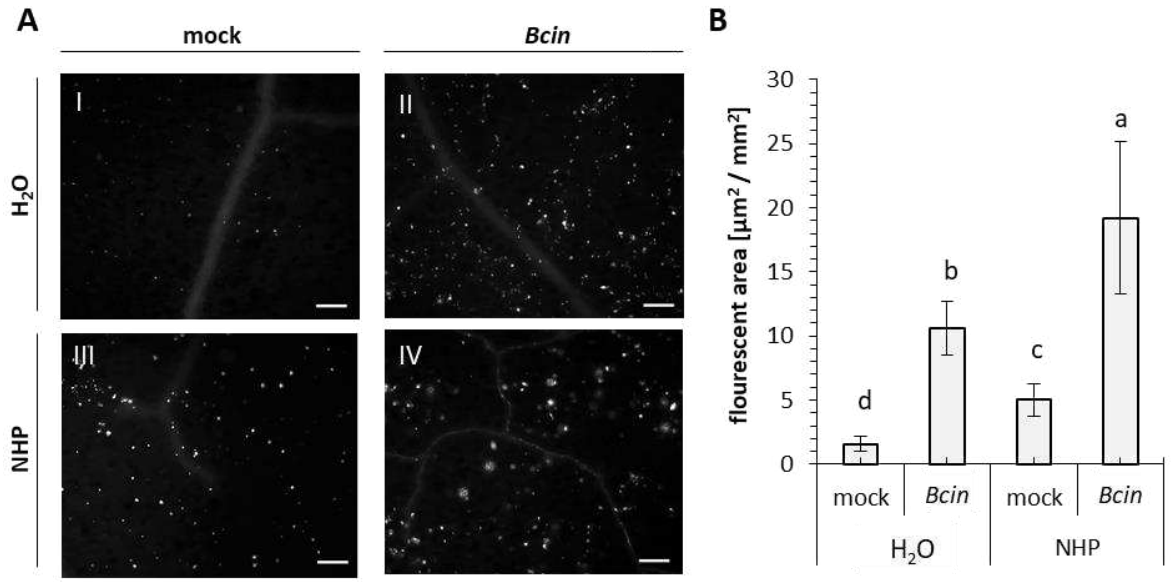

Figure 31: The induction of callose deposition in NHP primed and *Botrytis cinerea* (*Bcin*) infected *Arabidopsis thaliana* plants. 4,5-week-old plants were watered via the soil with a 1 mM NHP solution (III, IV) or H_2O (I, II) as control treatment. Droplet infections with *Bcin* (50 spores/µl) (II, IV) or Mathur's medium (I, III) as control treatment were performed one day after the pre-treatments and samples were harvested 1 dpi (n = 3). (**A**) Samples were stained with aniline blue and callose deposits were evaluated at the site of inoculation using a fluorescence microscope and the Zen Software. (**B**) Fluorescent areas were quantified per mm^2 using ImageJ and statistical differences between the treatments were determined with the Kruskal-Wallis Test in SPSS. Bars indicate mean values ± standard deviations and statistical results are indicated with letters above bars.

3.2.6. SAR induction by biotrophic, hemibiotrophic and necrotrophic pathogen in *Arabidopsis thaliana*

The induction of SAR in *A. thaliana* by and against the hemibiotrophic bacteria *Psm* is widely studied but only little is known about the SAR induction in *A. thaliana* by and against fungi with hemibiotrophic and necrotrophic lifestyles. To gain further insight into the mechanisms of SAR in *A. thaliana*, plants were challenge inoculated (1° leaf) with the hemibiotrophic bacteria *Psm*, the hemibiotrophic fungi *Chig*, the necrotrophic fungi *Bcin* or a respective control solution used in the inoculum preparation. Systemic leaves (2° leaf) of *Psm* or mock control challenged plants were inoculated with the biotrophic oomycete *Hpa*, *Psm*, *Chig* or *Bcin*. The systemic leaves (2° leaf) of *Chig* or *Bcin* or mock control challenged plants were inoculated with *Psm lux*, *Chig* or *Bcin*. The *A. thaliana* resistance in systemic leaves was assessed with pathogen specific methods. The length of internal Hyphae (IH) was measured to assess the *A. thaliana* resistance against *Hpa*. To assess the *A. thaliana* resistance against *Psm lux* bacterial numbers were quantified in the inoculated systemic leaves via luminometer, while the resistance of *A. thaliana* against *Chig* and *Bcin* was determined by the quantification of the necrotic area per inoculation site.

The presented results revealed that *Hpa* developed significantly longer IH in systemic leaves of mock control ($MgCl_2$) than in systemic leaves of *Psm* challenged *A. thaliana* plants (Figure 32.A). Likewise, a significantly higher number of *Psm lux* bacteria was determined in systemic leaves of mock control than in systemic leaves of *Psm* challenged *A. thaliana* plants (Figure 32.B). Furthermore, the quantified necrotic area on systemic *Chig* or *Bcin* inoculated leaves of mock control challenged plants was significantly larger than the quantified necrotic area on systemic *Chig* or *Bcin* inoculated leaves of *Psm* challenged plants (Figures 32.C, 32.D). These results indicate that a local *Psm* challenge can induce resistance in systemic leaves against *Hpa*, *Psm*, *Chig* and *Bcin* in *A. thaliana*.

A. thaliana plants that were challenged with a mock control solution (H_2O) revealed a significantly higher number of *Psm lux* bacteria in systemic leaves compared to the detected number of bacteria in the systemic leaves of *Chig* inoculated local leaves (Figure 32.E). The mock challenge inoculated plants also showed larger necrotic area on the systemic *Chig* or *Bcin* inoculated leaves than the systemic *Chig* or *Bcin* inoculated leaves of *Chig* challenged local *A. thaliana* leaves (Figure 32.F, 32.G). Summarizing these results might indicate that a local *Chig* inoculation induces resistance against *Psm*, *Chig* and *Bcin* in *A. thaliana*.

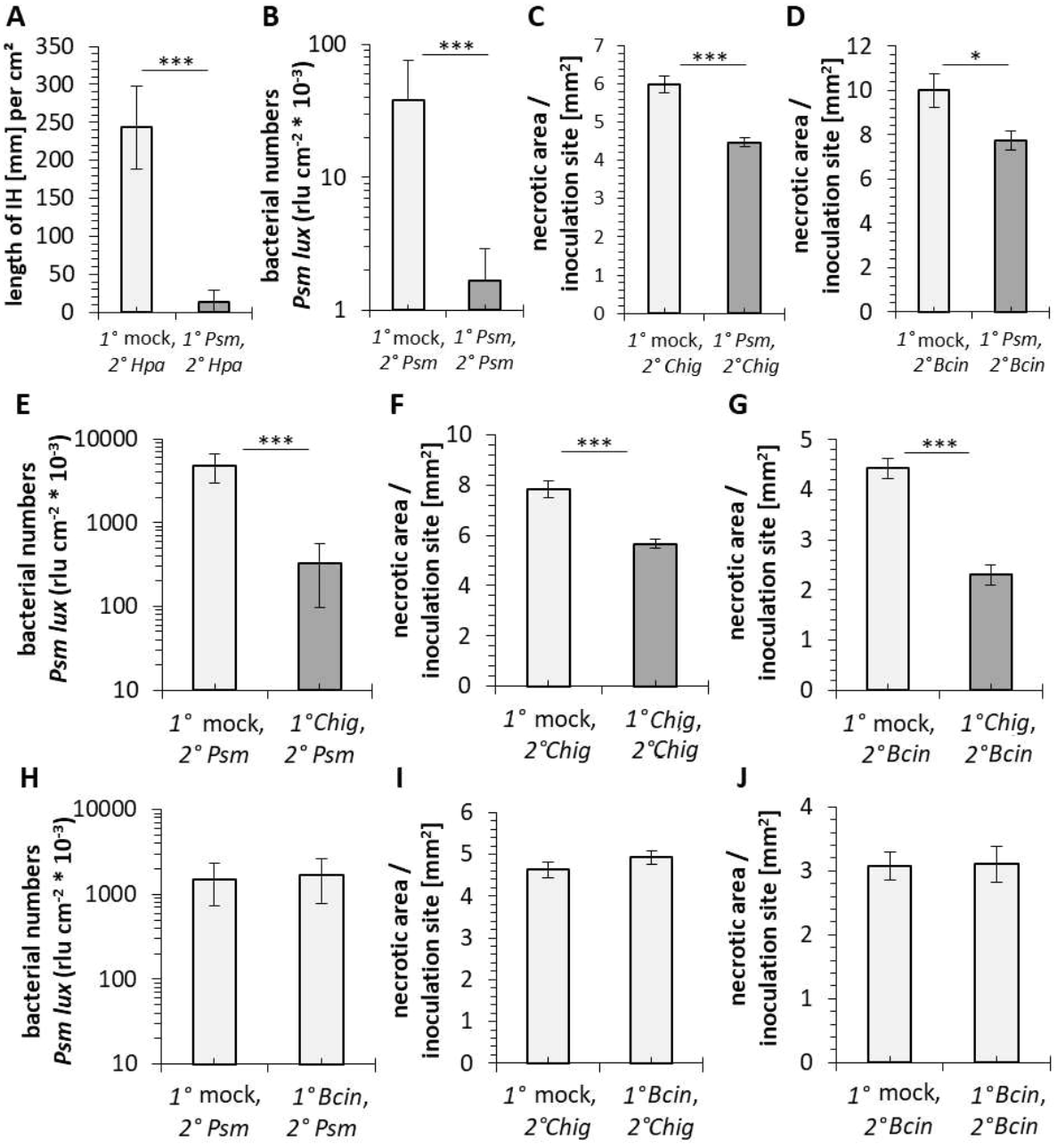

Figure 32: The *Psm*, *Chig* and *Bcin* induced SAR in *A. thaliana* against pathogens with various lifestyle strategies. Local leaves of five- week-old *A. thaliana* Col-0 wildtype plants were challenge infiltrated with *Psm* (OD_{600} = 0.005) or 10 mM $MgCl_2$ as mock treatment and systemic leaves were (**A**) spray inoculated with a *Hpa* spore solution (50 spores/µl), (**B**) infiltrated with *Psm lux* (OD_{600} = 0.001), droplet inoculated with (**C**) a *Chig* spore solution (500 spores/µl) or (**D**) a *Bcin* spore solution (50 spores/µl) two days later. For the *Chig* induced SAR, local leaves of five-week-old *A. thaliana* Col-0 plants were challenged with a *Chig* (500 spores/µl) or mock (H_2O) droplet inoculation and five days later systemic leaves were (**E**) infiltrated with *Psm lux* (OD_{600} = 0.001), droplet inoculated with (**F**) a *Chig* spore solution (500 spores/µl) or (**G**) a *Bcin* spore solution (50 spores/µl). To induce SAR with *Bcin*, local leaves of five- week-old *A. thaliana* Col-0 plants were challenged with a *Bcin* (50 spores/µl) or mock (Mathur's medium) droplet inoculation and two days later systemic leaves were (**H**) infiltrated with *Psm lux* (OD_{600} = 0.001), droplet inoculated with (**I**) a *Chig* spore solution (500 spores/µl) or (**J**) a *Bcin* spore solution (50 spores/µl). The Hpa growth in *A. thaliana* was quantified via measurements of the length of IH in mm/cm² 7 dpi and mean values are given with SD. The luminescence of *Psm lux* bacteria in systemic leaves was determined in cfu 2 dpi (n = 6) and mean values and SD were calculated for detected bacterial numbers. The size of necrotic area per inoculation site on systemic inoculated leaves was quantified in mm² 7 dpi with *Chig* (n = 6) and 2 dpi with *Bcin* (n = 6) and mean values and SEMs were calculated for the quantified *Chig* and *Bcin* caused necrotic area on *A. thaliana* leaves. Grey bars mark significant reduction of pathogen growth in comparison to the respective control treatment of a genotype determined with a two-tailed *t* test (p = * < 0.05, ** < 0.01, *** < 0.001).

In contrast to that, after a local *Bcin* or respective mock control treatment an equal number of *Psm lux* bacteria was measured in systemic leaves (Figure 32.H). Likewise, the *Chig* or *Bcin* mediated necrotic area in systemic leaves was similar in size after a local *Bcin* or mock inoculation (Figures 32.I, 32.J). These results indicate that a local *Bcin* inoculation in contrast to a local *Psm* or *Chig* inoculation cannot induce resistance in systemic *A. thaliana* leaves against *Psm*, *Chig* or *Bcin*.

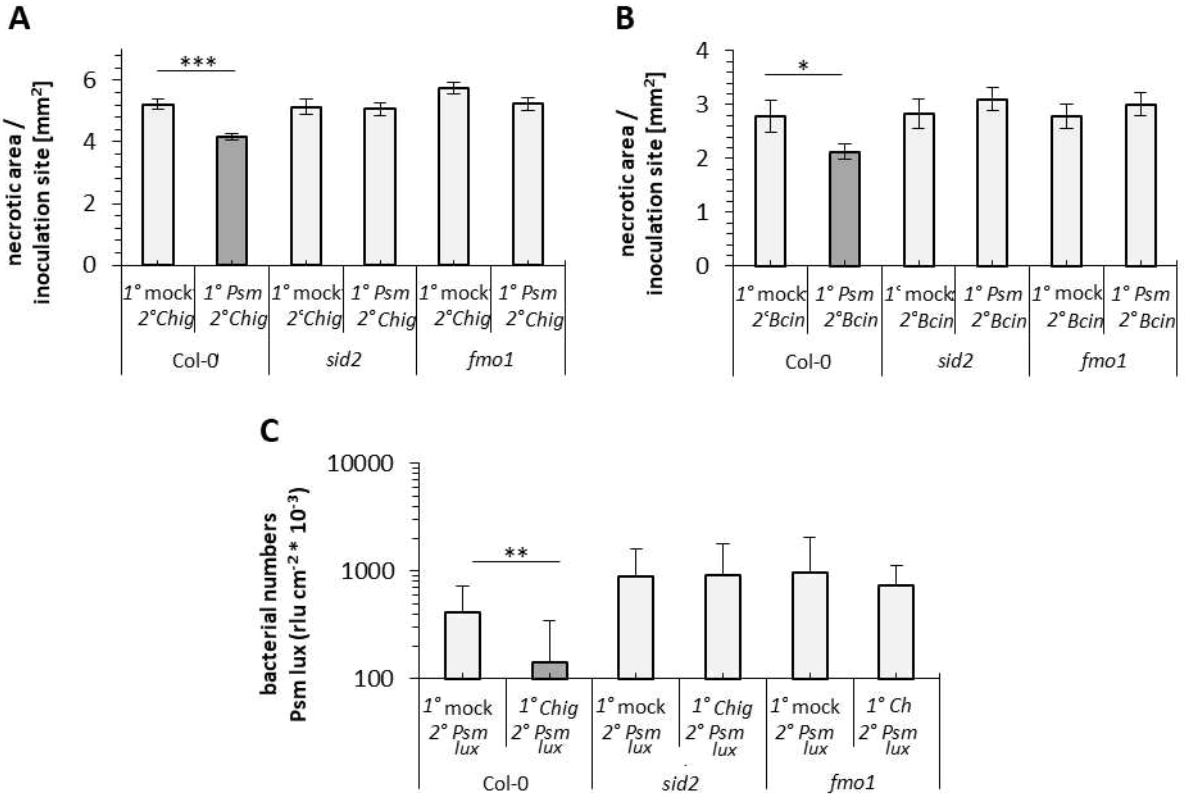

Figure 33: The influence of SA and NHP signaling defects on the *Psm* and *Chig* induced systemic acquired resistance against hemibiotrophic and necrotrophic fungal pathogens. Local leaves of five- week-old *A. thaliana* Col-0, *sid2* and *fmo1* plants were challenge infiltrated with *Psm* (OD_{600} = 0.005) or 10 mM $MgCl_2$ as mock treatment and systemic leaves were droplet inoculated with (**A**) a *Chig* spore solution (500 spores/µl) or (**B**) a *Bcin* spore solution (50 spores/µl) two days later. The size of necrotic area per inoculation site on inoculated leaves was quantified seven dpi with *Chig* (n = 6) and two dpi with *Bcin* (n = 6). Mean values and SEMs were calculated for the quantified *Chig* and *Bcin* caused necrotic area on *A. thaliana* leaves. (**C**) Local leaves of five-week-old *A. thaliana* Col-0 WT and *sid2* and *fmo1* mutant plants were challenged with a *Chig* or H_2O droplet inoculation and 5 dpi systemic leaves were infiltrated with *Psm lux* (OD_{600} = 0.001). The luminescence of *Psm lux* bacteria in systemic leaves was determined two days later (n = 6). Mean values and SD were calculated for detected bacterial numbers. Statistic differences between the challenge inoculations were determined with a two-tailed *t* test (p = * < 0.05, ** < 0.01, *** < 0.001). Grey bars mark significant reduction of pathogen growth in comparison to the respective control treatment of a genotype.

The mechanisms of the indicated resistance inducing effect in systemic leaves after a local *Psm* or *Chig* infection were further investigated. Using the *A. thaliana sid2* and *fmo1* mutants the influence of the SA and NHP signaling on the *Psm* induced SAR against *Chig* and *Bcin*, and the *Chig* induced SAR against *Psm lux* was studied.

The *Psm* challenged *A. thaliana* Col-0 plants showed significantly smaller necrotic area on systemic *Chig* infected leaves than mock ($MgCl_2$) challenged and *Chig* infected Col-0 plants (Figure 33.A). On systemic *Chig* infected leaves of mock and *Psm* challenged *sid2* and *fmo1* mutant plants, area of necrosis equal in size were detected (Figure 33.A). Similarly, systemic *Bcin* infected leaves of *Psm* challenged Col-0 plants revealed significantly smaller necrotic area than the systemic *Bcin* infected leaves of mock challenged Col-0 plants, but the quantified necrotic area on systemic *Bcin* infected leaves of mock or *Psm* challenged *sid2* and *fmo1* mutant plants were statistically equal in size (Figure 33.B). However, systemic *Bcin* infected leaves of *Psm* challenged *sid2* and *fmo1* plants developed slightly larger necrotic area than the systemic *Bcin* infected leaves of mock challenged *sid2* and *fmo1* plants.

After a *Chig* challenge of *A. thaliana* Col-0 plants systemic *Psm lux* infected leaves showed a significant lower number of bacteria than the systemic leaves of mock (H_2O) challenged Col-0 plants (Figure 33.C). In contrast, an equal number of bacteria was measured in systemic *Psm lux* infected leaves of *Chig* and mock challenged *sid2* and *fmo1* plants (Figure 33.C). In summary, these results show an induction of SAR by a local infection with *Psm* or *Chig* against hemibiotrophic and necrotrophic pathogens in the Col-0 wildtype, but not in the *sid2* and *fmo1* mutants. This indicates a dependency of the *Psm* and *Chig* induced SAR in *A. thaliana* on a functional SID2 and FMO1 protein.

3.3. Discussion

3.3.1. NHP is an important mediator of resistance towards infections with pathogens of various lifestyles in *Arabidopsis thaliana*

A. thaliana serves as a model organism in understanding plants defense responses like SAR against pathogens (Meinke et al. 1998). In the last years the small metabolite NHP was found to accumulate in local and systemic *A. thaliana* leaves after an infection with hemibiotrophic *Psm* bacteria and that this systemic NHP accumulation is essential for SAR establishment (Hartmann and Zeier 2019, Zeier 2021). Furthermore, an exogenous treatment with NHP was sufficient to induce resistance in *A. thaliana* towards infections with the biotrophic oomycete *Hpa* and the hemibiotrophic bacterium *Psm* (Hartmann et al. 2018). About the role of NHP in defense responses against necrotrophic pathogen however little is known yet. A recent study suggests NHP might play a role in *A. thaliana* defense responses against necrotrophic pathogens since the establishment of an egg extract induced SAR against infections with the necrotrophic *Bcin* was observed to be *fmo1* dependent (Alfonso et al. 2021).

This study shows the accumulation of NHP and its metabolic precursor Pip in *A. thaliana* upon the infections with the biotrophic oomycete *Hpa*, the hemibiotrophic bacterium *Psm,* the hemibiotrophic fungi *Chig* and *Sclero* and the necrotrophic fungi *Bcin* in time course analyses (Table 1). Additionally, the here presented exogenous treatments of *A. thaliana* plants with NHP induced resistance against infections with the same pathogens (Figure 26). These results further support a role for NHP in defense responses against necrotrophic pathogens. Consistently, a recent study demonstrated that infections in peanut seeds with the fungus *Aspergillus flavus*, which is described as necrotrophic fungus (Liu et al. 2021), induce Pip accumulation in seeds of resistant peanut varieties but not in seeds of susceptible varieties (Sharma et al. 2021), indicating that high Pip levels are associated with resistance to the necrotrophic pathogen. The same study additionally showed that exogenous Pip and lysine treatments of peanut seeds induced resistance towards *A. flavus* infections (Sharma et al. 2021), further supporting a role for the NHP biosynthesis metabolite in resistance of plants against necrotrophs. In agreement, Zhang and colleagues (2020) revealed that Pip treatments of tomato plants confer an enhanced resistance against infections with the necrotrophic fungi *Bcin*. In *A. thaliana* Pip likewise induces resistance against *Psm*, but this Pip induced resistance is dependent on a functional *fmo1* gene, revealing NHP as the resistance mediating metabolite

and not Pip (Bernsdorff et al. 2016). It is hence likely that NHP and not Pip induces the in previous studies observed resistance in plants against necrotrophic pathogens as demonstrated in this study by the NHP induced resistance against *Bcin* infections in *A. thaliana*.

Detected NHP and Pip levels only slightly varied in *A. thaliana* plants infected with *Hpa*, *Chig*, *Sclero* and *Bcin* whereat in infections with *Psm* the highest levels of all investigated metabolites in this study were detected (Table 1). These differences might be caused by the used application method for the respective inoculum in the infections. Since the full leave was infiltrated with a *Psm* solution but in droplet inoculations with *Chig*, *Sclero* and *Bcin* or spray inoculations with *Hpa* only small parts of a leaf were initially infected, the area in the leave that responds to infections and produces defense related metabolites was thus not uniform in the infections with different pathogens. On the other hand, NHP derivates, such as NHPG and NHPGE, accumulated in all five tested infection systems. Given that NHPG and NHPGE are thought to control the NHP homoeostasis in *A. thaliana* (Mohnike et al. 2021) and significantly higher NHPG and NHPGE amounts were detected in *Hpa*, *Psm*, *Chig*, *Sclero* and *Bcin* infected leaves than in the respective mock control leaves, a low cellular NHP level might be sufficient to activate NHP dependent defense responses. In the systemic leaves of *Psm* infected *A. thaliana* plants NHP amounts between 1 and 4 µg g^{-1} FW have been detected in this (Figure 22) and previous studies 2 dpi (Yildiz et al. 2021, Hartmann et al. 2018). Noticeably, at this infection stage a local *Psm* infection is sufficient to induce SAR in *A. thaliana* (Figure 32, Bernsdorff et al. 2016) and it has been demonstrated that these low amounts of NHP trigger resistance responses like the expression of PR genes (Yildiz et al. 2021). Furthermore, these low levels of NHP in systemic leaves of *Psm* infected *A. thaliana* plants induced the expression of the *UGT76B1* gene, which encodes for the enzyme that converts NHP to NHPG (Yildiz et al. 2021, Bauer et al. 2021). The rapid conversion of systemically accumulating NHP into NHP derivates based on NHP homeostasis indicates that even smaller amounts of in planta accumulating NHP than detected in systemic leaves of *Psm* infected plants are sufficient to induce defense responses in *A. thaliana*. In support, *Chig* infections of *A. thaliana* leaves induced SAR in systemic leaves, whereat in local *A. thaliana* leaves maximal detected NHP amount of 0,37 µg seemed to be efficient to induce SAR (Figures 23, 32).

The total NHP amounts (NHP + NHPG + NHPGE) that were triggered by a pathogen in *A. thaliana* leaves however seem to be lifestyle dependent since higher amounts of total NHP were detected in leaves infected with biotrophic and hemibiotrophic pathogens, like *Hpa*, *Psm* and *Chig* than in leaves that were infected with pathogens that exhibit a rather necrotrophic lifestyle like *Sclero* or *Bcin* (Table 1). The hemibiotrophic *Sclero* represents an exception since it maintains a biotrophic and necrotrophic phase in parallel and is to assume that necrotrophy occurs early in the infection of *A. thaliana* plants (Kabbage et al. 2015). In agreement, NHP deficient *fmo1* mutants are more susceptible to hemibiotrophic *Chig* infections than the Col-0 wildtype, while *A. thaliana* leaves of Col-0 and *fmo1* plants that were infected with the necrotrophic *Bcin* revealed similar disease symptoms (Figure 27). In infections with the necrotrophic *Bcin* accumulating NHP hence does not mediate effective immune responses against the spread of the *Bcin* infection, while it likely does against *Chig* infections. However, an exogenous pretreatment of *A. thaliana* plants with NHP was sufficient to induce resistance towards *Chig* and *Bcin*, indicating that NHP primes the plant for defense responses that effectively reduces the growth of both fungi.

In infection time courses of A. *thaliana* with the here investigated biotrophic and hemibiotrophic pathogens SA and NHP accumulated in leaves in parallel (Figure 20.T). This is in line with the parallel accumulation of SA and NHP after the infection with biotrophic or hemibiotrophic pathogens in several plant species like cucumber, tobacco or tomato (Schnake et al. 2020). In contrast, only NHP but no SA accumulation was observed in *A. thaliana* leaves infected with the necrotrophic *Bcin* (Figure 25). In infections with *Sclero*, which maintains a biotrophic and necrotrophic phase in parallel (Kabbage et al. 2015), a significant SA accumulation was only detected in later infection stages (4 dpi) in *A. thaliana* leaves, but NHP accumulation was observed 2 dpi already (Figure 24). This agrees with previous studies that showed that the JA signaling is activated in response to necrotrophic and SA signaling to biotrophic and hemibiotrophic pathogens (Glazebrook 2005, Wasternack and Hause 2013). Following the rules of the SA-JA antagonism, SA signaling is suppressed in plants that are infected with pathogens that exhibit a predominantly necrotrophic lifestyle (Glazebrook 2005). Since SA and NHP trigger the expression of each other's biosynthesis genes (Hartmann and Zeier 2019), NHP accumulation might be supported in infections with biotrophic and hemibiotrophic pathogens that show SA accumulation and vice versa. The presented results

however suggest that the infection with true necrotrophic fungi like *Bcin* successfully suppress SA accumulation in *A. thaliana*.

This suppression of SA accumulation in *Bcin* infected *A. thaliana* leaves is further supported by the accumulation of the SA derivates in the performed infection time course. The accumulation of SAG and SGE in parallel with SA was observed in *A. thaliana* leaves after the infection with the investigated biotrophic and hemibiotrophic pathogens, whereat the SA derivates likely accumulate to achieve SA homeostasis. SA homeostasis is critical for responses against pathogens of *A. thaliana* plants and is achieved by chemical modification of SA, including the formation of SAG and SGE (Dempsey et al. 2011). After *Bcin* infections however no SA and only a slight SAG and SGE accumulation was observed, indicating that bioactive accumulation SA is converted into its inactive derivate forms to achieve complete suppression. Furthermore, total SA levels in *A. thaliana* leaves were lower after *Bcin* infections than after infections with all other tested pathogens, indicating a suppression of the SA biosynthesis pathway (Figure 25). In support, it was shown that infections with necrotrophic pathogens activate the JA signaling pathway in plants and that accumulating JA induces the modification of SA to support the SA-JA antagonism by depleting the pool of bioactive SA (Wasternack and Hause 2013, Koo et al. 2007). The activation of the JA signaling is moreover associated with a more effective defense against necrotrophic pathogens than the SA signaling (Spoel et al. 2007). In agreement, this study shows that JA mediated defense responses contribute to *A. thaliana* defense responses against *Bcin* since the JA signaling mutant *coi1-35* revealed higher disease symptoms than Col-0 or the SA deficient mutant *sid2* after *Bcin* infections (Figure 28).

3.3.2. Mechanisms of the NHP induced resistance against hemibiotrophic and necrotrophic fungi in *Arabidopsis thaliana*

This study demonstrates the accumulation of NHP after the infection with hemibiotrophic *Chig* and necrotrophic *Bcin* fungi (Table 1). Additionally, the resistance inducing effect of NHP in *A. thaliana* plants was shown to significantly reduce the infection symptoms caused by *Chig* and *Bcin* (Figure 26). To gain further insight into the mechanisms of the NHP induced resistance towards these hemibiotrophic and necrotrophic fungi, NHP was applied to *A. thaliana* Col-0 and mutant plants with defects in resistance associated signaling pathways

via the soil. Noticeably, NHP induced resistance in all tested NHP, SA, JA and indole signaling mutants (Figures 27, 28), indicating that the mechanisms of the NHP induced resistance are not disrupted by these signaling pathways in *A. thaliana*.

The response of unprimed Col-0 and mutant plants however reveled pathogen specific responses to the defects of defense associated signaling pathways. *A. thaliana fmo1* plants for example revealed a susceptibly towards infections with *Chig* when compared to the infection symptoms of Col-0 plants, indicating that the accumulating NHP in response to the hemibiotrophic fungi is contributing to *A. thaliana* immune responses against it (Figure 27). Since the *fmo1* mutation in *A. thaliana* plants does not affect the susceptibility towards *Bcin* (Figure 28), it is unlikely that the in the metabolite analyses detected accumulation of NHP after *Bcin* infections contribute to defense responses against the necrotroph. However, the exogenous treatment of *A. thaliana* plants with NHP seems to reduce the growth of the necrotrophic *Bcin* in planta in comparison to control treated plants. To rule out that NHP has a direct toxicological effect on the here investigated ascomycetes, *Chig* and *Bcin* were grown on plates supplemented with NHP and control plates. The toxicological assay demonstrated similar growth of both fungi on NHP and control plates (Figure 29). Thus, NHP has no direct effect on the growth of *Chig* and *Bcin* and induces resistance in the plant.

The immune inducing effect of NHP in *A. thaliana* plants against hemibiotrophic pathogens has previously been demonstrated in infections with *Psm* (Hartmann et al. 2018). After a *Psm* infection, NHP and SA accumulation at the site of infection is crucial to activate defense responses in *A. thaliana* and *fmo1* and *sid2* plants are highly susceptible to *Psm* infections (Hartmann and Zeier 2019). In this study the SA deficient *sid2* mutant though revealed wildtype like disease symptoms after infections with the hemibiotrophic *Chig* (Figure 27), indicating that a SA accumulation in *A. thaliana* leaves does not initiate efficient defence responses against *Chig* infections. In contrast, previous studies described the susceptibility of *A. thaliana sid2* mutants against infections with two other *Chig* pathovars (Liu et al. 2007, Gebauer et al. 2017). The *Chig* strain WT063A used in this study was not investigated in this matter before and therefore might show deviant results.

It was further demonstrated that SA and NHP support the transcriptional activation of each other's biosynthesis genes and are partially regulated by the same set of genes, including *pad4* and *eds1* (Hartmann and Zeier 2019). Hence, *A. thaliana pad4* and *eds1* mutants are

insufficient in SA and NHP accumulation and therefore more susceptible to infections with the hemibiotrophic *Psm* (Feys et al. 2001, Jing et al. 2011, Rietz et al. 2011, Hartmann et al. 2018, Zeier et al. 2021). In infections with *Chig*, *A. thaliana pad4* and *eds1* mutants likewise showed an increased susceptibility when compared to the Col-0 wildtype (Figure 27). In agreement with these results, the increased susceptibility of *A. thaliana pad4* (Liu et al. 2007, Hiruma et al. 2011) and *eds1* (Birker et al. 2009) mutants towards *Chig* was demonstrated before and was mainly associated with defects in SA biosynthesis and signaling. In the here investigated *A. thaliana* - *Chig* infection system, defects in the SA biosynthesis did however not affect the growth of *Chig* in planta and the susceptibility of *pad4* and *eds1* plants can therefore only be explained by defects in the NHP signaling in *pad4* and *eds1* mutants. In agreement, *pad4*, *eds1*, *fmo1* mutants and the double mutant *sid2/fmo1* revealed a similar degree of susceptibility towards *Chig* when compared to Col-0 plants.

In *A. thaliana* infections with *Bcin*, the SA and NHP signaling mutants *sid2*, *fmo1*, *sid2/fmo1*, *pad4* and *eds1* showed comparable or even slightly decreased disease symptoms in comparison to *Bcin* infected Col-0 plants (Figure 28). Hence, the SA and NHP signaling pathways do not seem to contribute to efficient defense reactions of *A. thaliana* to the necrotrophic fungi. Although, an exogenous NHP treatment was sufficient to prime the plants resistance against a *Bcin* infection, indicating that NHP activates mechanisms in *A. thaliana*, that confer resistance to the necrotroph. A recent study demonstrated that exogenous NHP treatments of wheat plants prime for callose deposition and induces resistance against infections with hemibiotrophic *F. graminearum* fungi (Zhang et al. 2021). In line with these recent results, this study shows that NHP treatments of *A. thaliana* plants induce the deposition of callose and induces resistance towards hemibiotrophic *Chig* and necrotrophic *Bcin* fungi (Figures 30, 31). These results further suggest that NHP induced callose accumulation contribute to the *A. thaliana* resistance against these hemibiotrophic and necrotrophic fungi.

Callose deposition have been demonstrated to be pathogen induced but can also be induced by treatments with priming substances like SA (Wang et al. 2021). Previous studies revealed that exogenous SA treatments induce callose deposition in Arabidopsis, and mutants impaired in SA biosynthesis, consistently show reduced defense responses associated with callose deposition (Wang et al. 2013). Since NHP accumulation promotes the SA biosynthesis

(Hartmann and Zeier 2019) it is imaginable that this phenomenon induced the here presented callose accumulation after NHP treatments. However, the NHP induced resistance against *Chig* and *Bcin* in *A. thaliana* is independent on mutations in the SA biosynthesis pathway, demonstrating that this induction of resistance by NHP is SA-independent. In agreement, in the results of previous performed transcriptome analyses of *A. thaliana* Col-0 plants that were exogenously treated with NHP, the upregulation of the *A. thaliana CALLOSE SYNTHASE1* (*CALS1*) gene was observed in comparison to control treatments (Yildiz et al. 2021). Likewise, *CALS1* is upregulated in systemic leaves of *Psm* challenged *A. thaliana* plants (Bernsdorff et al. 2016). In exogenous treatments with SA, *A. thaliana cals1* mutants showed no induction of callose deposition at plasmodesmata, indicating that SA mediated callose accumulation is CALS1 dependent (Cui and Lee 2016). Since accumulating SA and NHP promote the transcriptional activation of each other's biosynthesis genes (Hartmann and Zeier 2019), it is however possible that *cals1* mediated callose accumulation is SA and NHP induced or only NHP-induced by an SA promotion of the NHP biosynthesis. Future studies of A. thaliana sid2 mutants might be able to clarify the role of SA in the NHP induced deposition of callose.

Independent of the conducted pre-treatments *Bcin* infection induced noticeably higher amounts off callose in *A. thaliana* leaves than *Chig* infection (Figures 27, 28). When *A. thaliana* plants were treated with NHP and one of the pathogens an additive effect in the callose accumulation was observed (Figures 27, 28). In fact, previous studies have shown the induction of callose deposition by *Bcin* and *Chig* infections (You et al. 2010, Shimada et al. 2007). Further, Shimada and colleagues presented evidence that the penetration of plants' epidermis cells by avirulent Colletotrichum isolates triggers callose formation underneath the infection peg to prevent infection. In comparison, virulent Colletotrichum isolates, like the here used *Chig* pathovar, triggered a reduced deposition of callose and it is hypothesized that plants induce callose formation by the recognition of PAMPs (Shimada et al. 2007). Likewise, in infections of tomato with *Bcin*, a correlation between the induction of resistance and the level of callose accumulation was observed recently (Oukala et al. 2021). Hence, the level of pathogen induced callose deposition in a plant seem to be dependent on the specific plant-pathogen interaction.

In support, avirulent *P. syringae* strains were found to induce callose deposition in *A. thaliana*, while virulent strains, like the here used *Psm*, do not. These virulent *P. syringae* strains exhibit

an effector protein which was identified to suppress the deposition of callose to achieve unhindered growth (Hauk et al. 2003). Moreover, the *Phytophthora brassicae* RxLR3 effector was identified to inhibit plant induced callose deposition at plasmodesmata to promote cell-to-cell trafficking (Tomczynska et al. 2020). In *A. thaliana* infections with haustoria forming pathogens it was likewise demonstrated that adapted pathogens like *Hpa* induce less callose deposition in host plants than non-adapted pathogens like *B. graminis*. In the defence against haustoria forming pathogens callose encasements have been observed to form around haustoria, indicating this structural barrier might block the pathogens nutrient resource (Meyer et al. 2009). This demonstrates that plants induce callose deposition as a defense response against bacteria, oomycete and fungi of diverse lifestyles, but the level of callose accumulation in a plant is dependent on the virulence of the attacking pathogen. Since pathogens exhibit mechanisms to interrupt these defense responses, callose formation seems to be a crucial factor in the establishment of the host plant's resistance. However, the pathogen induced accumulation of callose in *A. thaliana* is facilitated by several callose synthases, which are regulated by different signaling pathways in the immune response (Nishimura et al. 2003, Jacobs et al. 2003, Cui and Lee 2016). Hence, the role of NHP in the defense associated induction of callose deposition has to be elucidated. Moreover, cell wall based defense is in addition to callose depositions also achieved by lignification or suberination in plants (Prasannath 2017) and it is not clear how NHP affects these cell wall based responses or how they contribute to the *A. thaliana* resistance. Thus, the contribution of NHP induced callose deposition to the observed NHP induced resistance in *A. thaliana* should be further investigated in the future.

3.3.3. Infections with hemibiotrophic pathogens trigger SAR in *Arabidopsis thaliana*, but an infection with the necrotrophic *Botrytis cinerea* does not

An infection of *A. thaliana* leaves with hemibiotrophic *Psm* bacteria has been demonstrated to confer resistance to systemic leaves against a following pathogenic attack (Mishina and Zeier 2007) which is a phenomenon broadly referred to as SAR. Previous research demonstrated that the Pseudomonas induced SAR in *A. thaliana* is sufficient to induce systemic resistance against biotrophic and hemibiotrophic pathogens like *Hpa* and *Psm* (Hartmann et al. 2018). SAR is predicted to be an effective defense response to infections of

biotrophic and hemibiotrophic pathogens, whereas it is thought to play no role in defenses against necrotrophic pathogens (Glazebrook 2005). However, in tomato plants a mycorrhiza inoculation establishes sufficient defense responses against following infections with necrotrophic *Bcin* fungi (Sanmartín et al. 2020). Additionally, a recent study showed that treatments of *A. thaliana* leaves with egg extract induces SAR in systemic leaves against a *Bcin* infection, indicating SAR is sufficient to induce resistance against necrotrophic pathogens. In agreement, this study demonstrates that a challenge inoculation with hemibiotrophic *Psm* bacteria and hemibiotrophic *Chig* fungi of *A. thaliana* leaves enhance the resistance in systemic leaves against infections with the necrotroph *Bcin* significantly (Figure 32). These results finally show proof that SAR is sufficient to induce resistance against necrotrophic pathogens.

In the *Psm* induced SAR against biotrophic and hemibiotrophic pathogens in *A. thaliana* the accumulation of SA and NHP in systemic leaves is essential for the full establishment of systemic resistance (Hartmann and Zeier 2019, Zeier 2021). In support, this study demonstrates that the establishments of the *Psm* induced SAR in *A. thaliana* against *Chig* and *Bcin* fails in *sid2* and *fmo1* mutants. Moreover, the *Chig* induced SAR against *Psm lux* failed in *sid2* and *fmo1* mutants, verifying the crucial role for SA and NHP in SAR. This is further in line with the observed accumulation of SA and NHP after infections with *Psm* and *Chig* in *A. thaliana* leaves in the metabolite analyses (Table 1). In contrast, no SA accumulation and only a weak NHP accumulation was observed after *Bcin* infections in *A. thaliana* leaves (Figure 25). Consequently, *A. thaliana* challenge infections with the necrotrophic *Bcin* did not establish SAR against a following *Psm*, *Chig* or *Bcin* infections (Figure 32). In fact, the failing establishment of SAR in plants like *A. thaliana* after challenge inoculations with *Bcin* was previously revealed in several studies (Govrin and Levine 2002, de Cremer et al. 2013).

The compare the *Psm* induced SAR effect on the infection with pathogens of different lifestyles, systemic leaves were infected with *Hpa*, *Psm*, *Chig* and *Bcin*. The comparison demonstrated that the pathogen induced SAR is more effective against the biotrophic oomycete *Hpa* and hemibiotrophic *Psm* infections than against infections with hemibiotrophic *Chig* or necrotrophic *Bcin* fungi. Similar effects were observed in this study when *A. thaliana* plants were pretreated with NHP and infected with same pathogens and *Sclero* (Figure 26). The measured bacterial numbers in *Psm* infected leaves of H_2O pre-treated *A. thaliana* plants

were 16 times higher than in *Psm* infected leaves of NHP pre-treated plants. In *Chig*, *Sklero* or *Bcin* infection NHP treatments only reduced the necrotic area on leaves 1.5 - 2-fold in comparison to the H_2O control pre-treatments (Figure 26). These results indicate that the immune responses activated by NHP in Arabidopsis are more effective against the infection strategies of *Hpa* and *Psm* than against the infection strategies of the here investigated hemibiotrophic *Chig* and *Sclero*, and necrotrophic *Bcin* fungi. Similarly, a study by Lenk and her team (2019) discovered that the Pip induced systemic resistance in barley is more sufficient in the defense against biotrophic *B. graminis* fungi and hemibiotrophic *Xtra* bacteria than against necrotrophic *P. teres* fungi.

Yildiz et al. (2021) demonstrated that SAR and NHP priming activate the same set of genes in *A. thaliana*, explaining these similar after SAR and NHP priming experiments. Since the here observed establishment of SAR against these biotrophic, hemibiotrophic and necrotrophic pathogens requires FMO1, NHP seems to mediate defense responses in *A. thaliana* more effective against *Hpa* or *Psm* than against the fungal infections. *Hpa* and *Psm* have been demonstrated to be SA sensitive pathogens in previous studies (Hartmann et al. 2018), whereas defects in the SA signaling did not influence the *A. thaliana* resistance against the here used *Chig* and *Bcin* isolates (Figures 27, 28). Since NHP promotes the SA biosynthesis (Hartmann and Zeier 2019, Zeier 2021), the NHP induced resistance and SAR is likely more effective in the defense against the SA sensitive pathogens *Hpa* and *Psm*. In addition to these SA dependent defense responses, NHP seems to induce SA independent defense responses that facilitate the induction of resistance in local and systemic leaves against SA insensitive pathogens like *Chig* and *Bcin*. Moreover, the *A. thaliana sid2* mutant failed to establish the *Psm* induced SAR against *Bcin*, indicating that the systemic SA amplification loop (Hartmann and Zeier 2019) is required to promote the NHP biosynthesis and establish defense responses.

3.3.4. Indolic compounds reveal pathogen specific roles in the *Arabidopsis thaliana* resistance against *Colletotrichum higginsianum* and *Botrytis cinerea*

In the defence against attacking pathogens plants rapidly accumulate secondary metabolites to mediate defence responses (Glazebrook 2005). In *A. thaliana* this pathogen induced accumulation of secondary metabolites includes Trp derived indolic compounds such as camalexin or ICA (Stahl et al. 2016). Previous studies demonstrated that the accumulation of

the phytoalexin camalexin and other small indolic metabolites like ICA in *A. thaliana* is triggered by the infections of a broad spectrum of pathogens including bacteria, fungi and oomycetes with diverse lifestyles (Glawischnig 2007, Stahl et al. 2016). In agreements, in this study an accumulation of camalexin and ICA was detected in *A. thaliana* leaves after the infection with the biotrophic oomycete *Hpa*, hemibiotrophic *Psm* bacteria, the hemibiotrophic fungi *Chig* and *Sclero*, and the necrotrophic fungi *Bcin*. The conducted growth assays however indicate a different role for the accumulating indolic compounds in *A. thaliana* defenses against hemibiotrophic *Chig* and necrotrophic *Bcin* fungi (Figure 27, 28).

In *A. thaliana* infections with *Chig* the *dcc* and *pad3* mutants were observed to be more susceptible to the infection than Col-0 plants, while *wkry33* mutants showed wildtype like disease symptoms (Figure 27). In *A. thaliana* infections with *Bcin* in contrast, *dcc* and *wrky33* mutants were more susceptible to *Bcin* infections compared to wildtype plants, while leaves of *pad3* mutants revealed Col-0 like symptoms (Figure 28). The *dcc* mutant exhibits defects in the CYP79B2 and CYP79B3 enzymes, which catalyse the first steps of the secondary indolic metabolism and the *dcc* mutant can therefore not accumulate indolic compounds including camalexin and ICA (Müller et al. 2010). The *pad3* mutant plants in contrast is only disabled in the last step of the camalexin biosynthesis and hence show no pathogen induced camalexin accumulation (Schuhegger et al. 2006). Since growth assays showed a higher susceptibility of *dcc* mutants compared to Col-0 plants after *Chig* and *Bcin* infections, it is to assume that indolic compounds are crucial factors in the *A. thaliana* defence against both pathogens. A camalexin deficiency however only increases the susceptibility of *A. thaliana* plants against *Chig* infections, but not against *Bcin* infections, indicating camalexin is involved in defence reactions against *Chig* but not *Bcin*. This further suggests that other indolic compounds than camalexin have to be involved in the *A. thaliana* defence against *Bcin* potentially involving ICA, since ICA accumulation after *Bcin* infection in *A. thaliana* was observed.

Although several studies report the relevance of camalexin in *A. thaliana* defence responses against necrotrophic pathogens (Thomma et al. 1999, Bohman et al. 2004, Ferrari et al. 2007, Schlaeppi et al. 2010), it was demonstrated that *Bcin* isolates show differing sensitivity to camalexin (Kliebenstein et al. 2005). Camalexin-insensitive *Bcin* isolates produce wildtype like lesions on camalexin-deficient *A. thaliana* plants like *pad3* mutants demonstrating no effect of camalexin on the propagation of these camalexin insensitive isolates (Kliebenstein et al.

2005). Stefanato et al. (2009) classified the used *Bcin* isolate B05.10 in this study as a moderately to highly virulent, which rather points to a camalexin insensitivity. Consistently, the same study showed that *A. thaliana pad3* mutants are not significantly more susceptible to this *Bcin* isolate than wildtype plants (Stefanato et al. 2009), which supports the here presented results. Hence, it is to assume that this *Bcin* isolate is rather insensitive to camalexin and other indolic compounds that are not produced in the *dcc* mutant are responsible for this mutant's susceptibility. In *A. thaliana* infections with *Chig*, in contrast, the *dcc* and *pad3* mutants revealed a similar level of increased susceptibility compared to Col-0 plants, indicating that camalexin is the indolic compound with the most effects on resistance responses against *Chig* (Figure 27). The increased susceptibility of *pad3* mutants against *Chig* infections was previously observed in several studies (Chanda et al. 2008, Narusaka et al. 2004). In the *A. thaliana* resistance against non-adapted Colletotrichum species camalexin has been shown to be involved in post-invasive defense reactions that confer resistance (Hiruma et al. 2011, Hiruma et al. 2013). However, *dcc* mutants showed an even more severe susceptibility than *pad3* mutants in infections with non-adapted *Colletotrichum gloeosporioides* fungi indicating that in the *A. thaliana* resistance against Colletotrichum species yet unknown Trp derived compounds are crucial (Hiruma et al. 2013, Kosaka and Takano 2018, Schmidt et al. 2020). It was further hypothesized that ICAs might play a role in the *A. thaliana* resistance against Colletotrichum species (Schmidt et al. 2020). Noticeably, the detected ICA amounts in *A. thaliana* after *Chig* infections were lower than after *Bcin* infections, which might indicate that the infection with the adapted *Chig* isolate suppresses ICA accumulation. Thus, camalexin might contribute majorly to the defense responses of *A. thaliana* against the here investigated *Chig* isolate, but resistance can not be established since Trp derived metabolites like ICA are not efficiently produced by *A. thaliana* Col-0 plants. Previous studies reported the accumulation of ICA in the exudates of Arabidopsis roots infected with the necrotrophic oomycete *Pythium sylvaticum* and in local and systemic *A. thaliana* leaves after a Pseudomonas infection (Bednarek et al. 2005, Stahl et al. 2016), but the role of ICA in the defense against pathogens is not enlightened yet. The here presented additional accumulation of ICA in *A. thaliana* after the infection with biotrophic, hemibiotrophic and necrotrophic pathogens, indicates that ICA may play a role in *A. thaliana* defense reactions against these pathogens. ICA is for example thought to be esterified to

plants cell walls (Forcat et al. 2010) and might thereby serve as structural barrier against invading pathogens of all lifestyles.

The last step of the camalexin biosynthesis mediated by PAD3, has been demonstrated to be regulated by the WRKY33 transcription factor (Mao et al. 2011). Noticeably, the *A. thaliana wrky33* mutant revealed an increased susceptibility towards *Bcin*, but not towards *Chig* infections when compared to Col-0 plants (Figures 27, 28). However, WRKY33 is a regulator of several defense pathways and is also involved in the pathogen induced accumulation of SA, NHP, JA, ET and ROS (Birkenbihl et al. 2012, Liu et al. 2015, Sham et al. 2017, Wang et al. 2018). Furthermore, in the *wrky33* mutant enhanced ABA levels were observed in comparison to wildtype plants demonstrating a negative regulation of ABA by WRKY33 (Liu et al. 2015, Sham et al. 2017). A strong ABA accumulation, as observed in *wrky33* mutants, results in impaired regulation of the SA and JA signaling, which leads to a hypersensitivity against necrotrophic pathogens (Sham et al. 2017). Thus, the here observed susceptibility of *A. thaliana wrky33* mutants against *Bcin* infections is likely based on high ABA levels and not on the impaired transcriptional activation of the camalexin biosynthesis in this mutant. This is further supported by the wildtype like disease symptoms of *pad3* mutants after *Bcin* infections.

In contrast, *wrky33* mutants were observed to be slightly more resistant towards *Chig* infections than Col-0 wildtype plants (Figure 27). The accumulation of ABA in *wrky33* mutants was demonstrated to be crucial for the *A. thaliana* resistance against *Bcin* (Liu et al. 2015) and likewise high ABA concentrations have been observed to promote the infection of *Chig* species in their hosts (Svoboda et al. 2021). However, the interaction of *A. thaliana* with the here for infections used *Chig* isolate has not been investigated in this matter yet and ABA plays different roles in plants interactions with biotrophic and necrotrophic pathogens. *A. thaliana* mutants with defects in ABA signaling were shown to have an enhanced resistance against biotrophic and hemibiotrophic pathogens like *Hpa* and *Pst* (Mohr and Cahill 2003), while they are more susceptible to infections with necrotrophic pathogens like *P. irregulare* (Adie et al. 2007). Thus, the enhanced resistance of *wrky33* mutants towards *Chig* infections might be based on high ABA levels in this mutant. However, further research is needed to confirm this assumption.

3.3.5. Conclusion

This study shows that NHP accumulates in *A. thaliana* after the infection with biotrophic, hemibiotrophic and necrotrophic pathogens and induces resistance to the same pathogens. It was demonstrated that exogenous NHP treatments prime for enhanced callose deposition, which might contribute to the NHP induced elevated resistance state in *A. thaliana*. SA accumulation in *A. thaliana* leaves was, in contrast to NHP accumulation, only observed after infections with biotrophic and hemibiotrophic pathogens, but not after infections with necrotrophic pathogens. Since NHP and SA are both required to establish SAR (Zeier 2021), SAR was established after a challenge inoculation with hemibiotrophic *Psm* bacteria and *Chig* fungi, but SAR establishment failed after challenge inoculations with necrotrophic *Bcin* fungi. This SAR response triggered by hemibiotrophic bacteria or fungi was able to induce resistance in systemic leaves against the necrotroph *Bcin*, serving proof that SAR can confer resistance against necrotrophic pathogens. Noticeably, SAR establishment against hemibiotrophic and necrotrophic pathogens was found to be dependent on a functional *fmo1* gene, indicating that NHP triggers systemic immune responses that induce resistance to pathogens of all lifestyles. The *sid2* mutants did also fail to establish SAR against hemibiotrophic and necrotrophic pathogens, demonstrating that the systemic SA-NHP amplification loop is required for the systemic accumulation of NHP that activates defense responses against those pathogens. SAR and NHP treatments additionally showed a higher induction of resistance against SA-sensitive pathogens like *Hpa* and *Psm* than against rather SA-insensitive pathogens like *Chig*, *Sclero* or *Bcin*. This mechanism shows that the categorization of *A. thaliana* defense responses depending on the lifestyle of the invading pathogen might not be suitable 2nd pathogen specific adaptions and virulence mechanism in the interactions must be considered. Moreover, it was demonstrated that indolic compounds, like camalexin, that accumulate after the infection with *Chig* and *Bcin* have pathogen-specific effects on the spread of disease symptoms in *A. thaliana* leaves.

4. PART III: NPR1: A potential NHP receptor in *Arabidopsis thaliana*

4.1. Introduction

4.1.1 The interaction of NPR1 with SA in the activation of immune responses in plants

Defense responses in plants against biotrophic and hemibiotrophic pathogens require the accumulation of the small metabolite SA (Hartmann et al. 2018, Hartmann and Zeier 2019). The pathogen induced accumulation of SA was shown to induce the expression of *PR* genes, which encode for small proteins that can reduce disease in pathogen infected host plants (van Loon et al. 2006, Bernsdorff et al. 2016, Hartmann and Zeier 2019). In a forward genetic screening *NPR1* was identified as regulator of the SA induced PR gene expression, since transgenic plants did not show *PR* gene expression upon treatments with the SA analog 2,6-dichloro-isonicotinic acid (INA) (Cao et al. 1994). An equilibrium dialysis further demonstrated that NPR1 binds SA but does not bind SA analogs like INA (Wu et al. 2012), revealing NPR1 as the SA receptor in *A. thaliana* that transmits SA dependent defense responses. These results were verified in several independent studies using different experimental setups (Ding et al. 2018, Manohar et al. 2015, Nair et al. 2021) which raised the interest in the structural mechanism by which NPR1 facilitates the binding of SA.

It was found that NPR1 exists as an oligomer in uninduced *A. thaliana* plants, while a pathogen infection and thereby the accumulation of SA causes a redox shift which results in a monomerization of NPR1 (Mou et al. 2003). Mou and colleagues (2003) further suggested that monomerized NPR1 is translocated to the nucleus due to an intrinsic nuclear localization sequence (NLS), where it activates the transcription of *PR* genes. To gain insight into the mechanism of the SA activated defense gene expression via NPR1, several residues in the *A. thaliana* NPR1 amino acid sequence were investigated. In this matter, the mutation of the residues 521 and 529 to cysteine in NPR1 were shown to disrupt its binding to a cupper ion in SA molecules (Wu et al. 2012). The binding to this copper ion in the NPR1 wildtype protein

was found to cause a conformation change that allows the protein to function as activator of transcription (Wu et al. 2012).

Ding and colleagues (2018) further reported that the mutation of the NPR1 residue 432 from arginine to glutamine disrupts the SA binding but not the interaction with TGACG BINDING FACTOR (TGA) transcription factors. Since the NPR1 protein does not posses a DNA binding domain, its transcriptional activation of genes is dependent on the interaction with transcription factors like the TGA transcription factors (Kinkema et al. 2000, Zhou et al. 2000). In *A. thaliana* several TGAs were identified, including TGA2, TGA5 and TGA6 which were shown to have redundant functions in the positive regulation of SA mediated expression of *PR* genes (Zhang et al. 2003). Other TGAs, like TGA1, however act independent of NPR1 (Shearer et al. 2012). Moreover, recent studies revealed that the NPR1 protein exhibits close structural similarities to two paralogs, NPR3 and NPR4, which like NPR1 interact with TGA transcription factors and are bona fide SA receptors (Zhang et al. 2006, Ding et al. 2018). Defects in the *A. thaliana NPR3* and *NPR4* gene, result in an elevated *PR* gene expression and resistance, demonstrating that NPR3 and NPR4 function as negative regulators of the of SA-induced *PR* gene expression (Zhang et al. 2006, Ding et al. 2018).

4.1.2 The interplay of NPR1 and NHP in SAR

The NPR1 protein is an essential component for the full establishment of SAR (Ding et al. 2020, Zeier 2021). Previous research demonstrated that *A. thaliana npr1* knock-out mutants are unable to induce SAR upon the exogenous treatments with NHP or its metabolic precursor Pip (Návarová et al. 2012, Yildiz et al. 2021, Liu et al. 2020). Additionally, the treatment of *sid2* mutant leaves with NHP resulted in an impaired but modest establishment of SAR while *npr1* mutants and *sid2/npr1* double mutants completely failed to establish the SAR response in systemic leaves (Yildiz et al. 2021). These findings suggest that the NHP induced SAR state is mostly dependent on SA and NPR1. However, the *A. thaliana npr1* and *sid2/npr1* mutants revealed that for the full establishment of the NHP induced SAR state SA-independent reactions of a functional NPR1 protein are crucial. Since the exogenous NHP and Pip treatments induced an increased expression of *NPR1* transcripts in *A. thaliana*, it was further proposed that NHP mediated defense responses that are dependent on NPR1 are mediated by the NHP induced activation of *NPR1* transcription (Yildiz et al. 2021, Zeier 2021). However,

basal level of NPR1 transcripts were able to fully establish SAR, demonstrating that the NHP promotion of the NPR1 transcription is not necessary for SAR (Ding et al. 2020). Hence, other and yet unknown mechanisms for those NHP induced mechanisms in SAR which are dependent on NPR1 but independent on SA have to be existent. Another explanation for NHP induced NPR1 dependent defense reactions in SAR could be a direct interaction of NHP and NPR1 (Zeier 2021). Since SA and NHP exhibit structural similarities in regard of the arrangement of the carboxylic acid and hydroxyl group and NPR1 is a bona fide receptor of SA, it is imaginable that NPR1 serves as in planta receptor for NHP as well. Detailed information about parallels in the SA and NHP metabolism are given in 1.4.3.

4.1.3. Aims

The establishment of local and systemic defense responses of plants like the plant model organism *A. thaliana* against pathogens requires the interplay of the small metabolites SA and NHP (Hartmann et al. 2018, Hartmann and Zeier 2018). The binding of SA by NPR1 has been demonstrated in several studies (Wu et al. 2012, Manohar et al. 2015, Ding et al. 2018, Nair et al. 2021). This study aimed to investigate a possible interaction of NHP with NPR1 in a similar experimental approach as the aforementioned studies. Therefore, binding reactions with purified, heterologously expressed, Strep-tagged NPR1-protein were performed in the presence or absence of NHP, using SA as positive control. Afterwards binding reactions mixtures including respective controls were applied to size-exclusion chromatography (SEC) columns and the flowthrough was analyzed via GC-MS to detect and quantify NPR1 bound SA or NHP amounts. NPR1 bound SA or NHP were compared to input controls to estimate the amounts bound SA or NHP. Additionally, this study intended to gain further insight into a potential NPR1 binding to NHP. Therefore, the $NPR1^{R432Q}$ mutant which is not able to bind SA was generated, and the binding was investigated with the established experimental pipeline.

4.2. Results

4.2.1. Cloning of *Arabidopsis thaliana NPR1* into the pET52b(+) plasmid

To investigate the binding of NPR1 to possible ligands, the *A. thaliana NPR1* sequence was cloned into the pET52b(+) plasmid. Therefore, the plasmid was digested with XmaI and SacI restriction enzymes and digestion procedures were evaluated on a 1% agarose gel (Figure 34.A). The calculated size for the double digested plasmid is 5197 bp, which was visually verified by the gel. The undigested circular pET52b(+) plasmid was visible above the 10 kb marker of the ladder, verifying that the plasmid was undigested before digestion procedures. However, since no super-coiled form of the undigested plasmid was identified, it is to expect that the undigested plasmid was observed in the nicked, circular form where a single-stranded break in the DNA occurs which can be observed frequently during the purification process. To assure the activity of both used restriction enzymes the digestion was additionally performed with only one of the restriction enzymes (Figure 34.A). The XmaI and SacI single digestions resulted in a product size between 5 and 6 kb which corresponds to the estimated size of 5227 bp for the single digested plasmid (Figure 34.A). Hence, the XmaI and SacI single digestion scenarios resulted in linearized pET52b(+) plasmids, confirming the sufficient digestion of both used restriction enzymes. The performed agarose gels of the single and double digestion reactions further show the presence of two bands, revealing that parts of the circular plasmid template were not digested in the reactions (Figure 34.A). The upper, less prominent band thereby corresponds to the circular plasmid and the lower band to the digested, linearized plasmid (Figure 34.A). For further cloning procedures the lower band was cut from the agarose gel and nucleic acids were purified (Figure 34.A).

For cloning purposes, the full-length *A. thaliana* NPR1 coding sequence (AT1G64280; NCBI nucleotide database entry NM_105102.3) was amplified by PCR from a *Psm* induced *A. thaliana* Col-0 cDNA sample (Supplementary Suppl. Figure 8). In the PCR reaction nuclease free H_2O was used as a negative control. PCR reactions and controls were evaluated on a 1% agarose gel and revealed a band between 1.5 kb and 2 kb in two tested samples which corresponds to the estimated *NPR1* product size of 1782 bp (Figure 34.B). The performed water control (negative control) reaction in contrast did not reveal a band on the gel, demonstrating that no amplification occurred (Figure 34.B). The amplified *NPR1* products were purified from the gel for further cloning procedures.

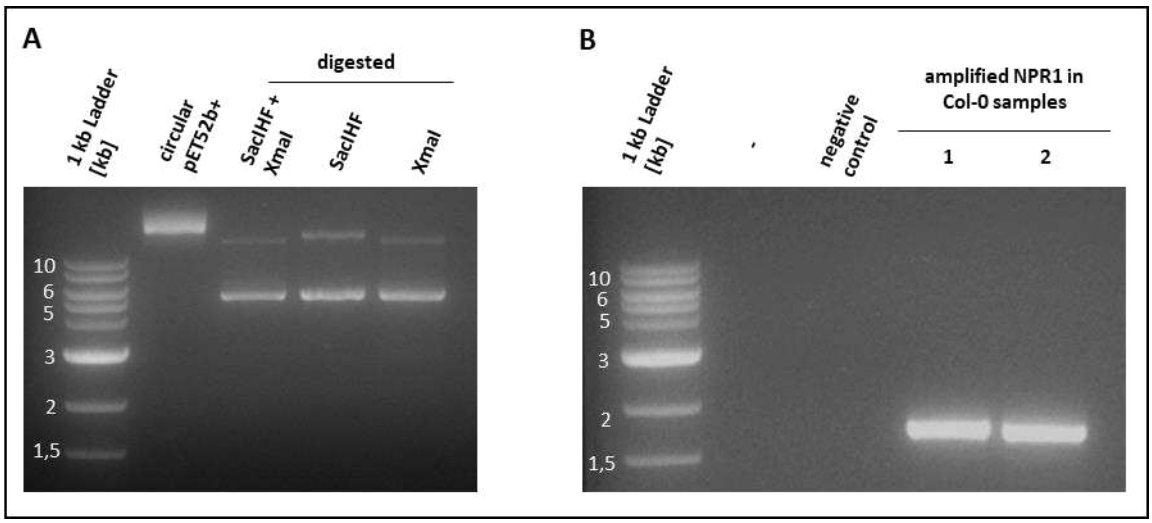

Figure 34: Visualization of the linearized pET52b(+) plasmids and the PCR amplified *Arabidopsis thaliana NPR1* sequence on agarose gels prior to cloning procedures. (**A**) The pET52b(+) plasmid was digested with SacIHF and XmaI. To assure the activity of both restriction enzymes the digestion was performed with only one of the restriction enzymes and the circular plasmids was used as a control of the template. (**B**) The *A. thaliana NPR1* sequence (1782 bp) required for cloning was amplified by PCR from a cDNA sample which was extracted from a *A. thaliana* Col-0 plant. In the PCR reaction nuclease free H_2O was used as a negative control. Digested plasmids and PCR products were applied to 1 % agarose gels and a 1 kb ladder was used as marker. The gels were run at 90 V for at least one hour in a gel chamber. DNA fragments were visualized under UC-light.

Cloning reactions were then performed with the linearized pET52b(+) plasmid and the amplified *NPR1* insert using the In-fusion HD cloning Kit (Takara, Kusatsu, Japan), and the resulting plasmids were transformed into competent *E. coli* Stellar cells. After plating potentially positive *E. coli* transformants, grown on LB medium with appropriate selection markers, were further tested for the presence of the NPR1 insert by PCR with primers specific for the pET52b+ T7 promotor and terminator regions (Table 5, Figure 35.A, ZF.C). The amplified PCR products were visualized on a 1 % agarose gel (Figure 35). The estimated size of the desired PCR band was 2047 bp, since additionally to the *NPR1* sequence of 1782 bp the T7 primers amplify parts of the pET52b(+) plasmid including the sequence for different fusion tags and the multiple cloning site (Figure 35.C). In the PCR reaction, nuclease free H_2O was used as a negative control. The agarose gel showed bands of approximately 2 kb length of several samples of potentially positive clones but did not show any bands in the negative control (Figure 35.B). PCR products of approximately 2 kb were purified from the gel to verify correct, in-frame cloning via subsequent sequencing. For the sequencing procedure T7 forward and reverse primers were used in combination with an additional primer which starts the amplification at position 718 of the NPR1 sequence (Table 6).

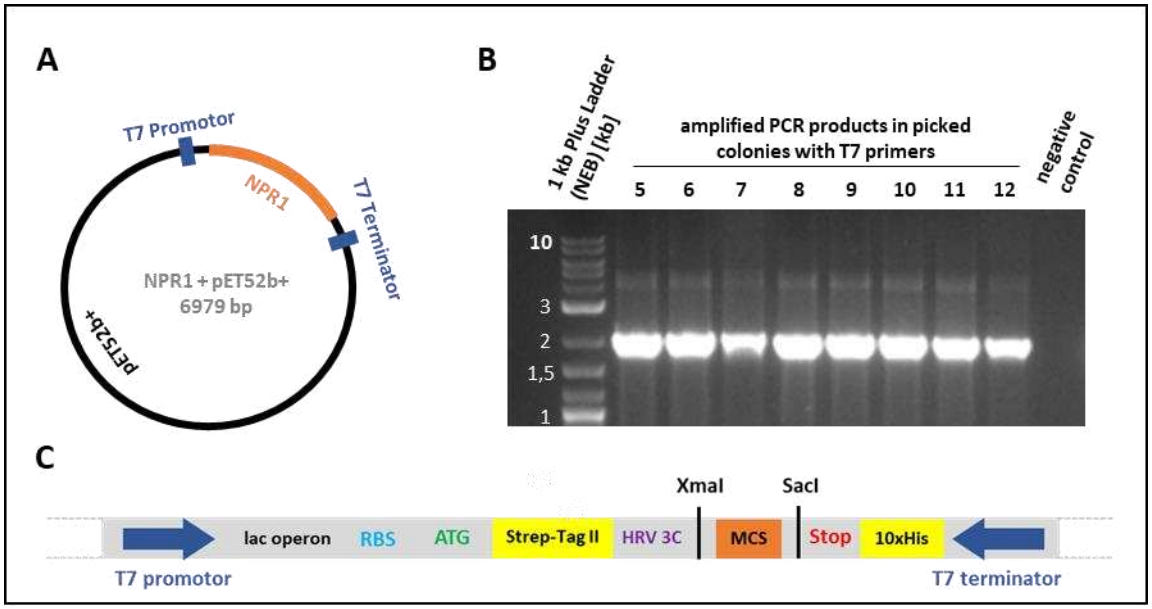

Figure 35: Schematic overview and verification of the cloning of the *Arabidopsis thaliana* NPR1 sequence in the pET52b(+) plasmid. (**A**) The pET52b(+) plasmid with the inserted *A. thaliana NPR1* sequence is 6979 bp in length and the correct cloning procedure was verified with PCRs using primers for the T7 promotor and terminator region. (**B**) Potentially positive PCR clones were picked after cloning and transformation procedures, DNA was purified and PCRs using T7 primers were performed to confirm the correct integration of the *A. thaliana NPR1* sequence in the pET52b(+) plasmid. As negative control nuclease free H_2O was used in PCR reactions. PCR products and 1 kb plus ladder were applied to a 1 % agarose gel and the gels were run at 90 V for at least one hour in a gel chamber. DNA fragments were visualized using UV-light. (**C**) The T7 promotor and terminator region boarder the lac operon, a ribosome-binding site (RBS), the start codon (ATG), the strep-tag, a protease cleavage site of Human rhinovirus (HRV-3C), digestion motifs like the used XmaI and SacI, the multiple cloning site, a stop codon (Stop), and a 10x His tag. Hence, PCR products with T7 primers of positive NPR1 clones with a length of 2047 bp were expected.

4.2.2. Expression of the *Arabidopsis thaliana* NPR1 protein in *Escherichia coli* Lemo21 cells

To test the binding of NPR1 to SA and NHP, the expression of positive tested NPR1 clones was established in *E. coli* Lemo21 cells. Bacterial cultures containing heterologously expressed Strep-NPR1 proteins were lysed by sonification and the further purification of Strep-NPR1 proteins was performed with an ÄKTA protein purification system via the Strep-tag. The NPR1 expression was visually verified via SDS PAGE, wherefore samples were collected throughout the expression and purification process. To verify the successful IPTG induction of NPR1 expression in *E. coli* cells, a control culture was assessed to which no IPTG was added. The performed SDS PAGE revealed that in the sonicated IPTG induced lysate, the expression of protein slightly smaller than 70 kDa was induced which showed only weak abundance in the IPTG uninduced culture (Figure 36.A). As the predicted size of the Strep-NPR1 fusion protein is 67 kDa, the presence of these bands in IPTG-induced samples strongly suggested the

successful expression and purification of Strep-NPR1.The nature of the purified band was later unequivocally confirmed in subsequent immunodetection assays, described in the following section. During the ÄKTA purification process samples of the flowthrough (FT), wash fraction (WF) and three elution fractions (EF1, EF2, EF3) were taken for the SDS-PAGE analyses. In all fractions the 67 kDa band was identified on the SDS PAGE (Figure 36.A). The detected Strep-NPR1 in the FT indicates that high amounts of the proteins did not bind to the used column which might be due to high expression in the here used bacterial culture. Further the SDS PAGE of the WF sample indicates that fractions of the NPR1 did not bind efficiently to the column. Since all three elution fractions, in particular EF2, showed a high abundance of the 67 kDa Strep-NPR1 band on the SDS-PAGE the purification process was successful (Figure 36.A).

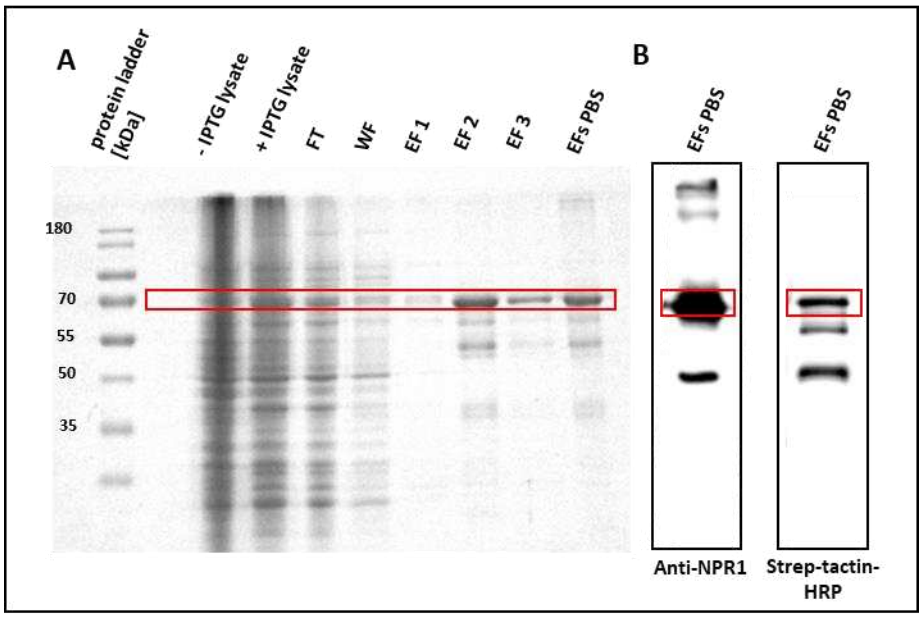

Figure 36: Verification of *Arabidopsis thaliana* NPR1 expression in *Escherichia coli* Lemo21 cells via antibody detection of the protein or the cloned Strep-tag. (**A**) The *Arabidopsis thaliana* NPR1 protein expression was induced in starter cultures with IPTG in *E. coli* Lemo21 cells and uninduced control culture was prepared. Induced and uninduced cultures were incubated over night at 16°C for expression and afterwards pelleted by centrifugation. Pellets were resuspended in lysis buffer, sonicated for cell lysis and centrifuged. Aliquots of the supernatant for the SDS gel were taken (- IPTG lysate, + IPTG lysate). To the supernatant, avidin was added for biotin blocking and the sample was centrifuged again. The NPR1 proteins were purified from the resulting supernatant using an ÄKTA protein purification system. Aliquots of the flowthrough (FT), wash fraction (WF) and three elution fractions (EF1, EF2, EF3) were taken for subsequent SDS-PAGE analyses. The elution fraction 1-3 were pooled, rebuffered in PBS and concentrated for further analyses. An aliquot of each of the elution fractions in PBS (EFs PBS) was prepared for the SDS-PAGE analyses. Collected aliquots for the SDS PAGE were combined with 5 x SDS-PAGE loading buffer, incubated at 95°C for 5 min and applied to an SDS gel consisting of a 5 % stacking gel and a 12 % separating gel. A prestained protein ladder was used as size marker. Samples were run on the gel and visualized by Coomassie blue staining (**B**) To visualize the tagged proteins and their potential degradation products on the SDS-PAGE, western blots were performed with an antibody for the NPR1 protein (Anti-NPR1) and a strep-tactin horse radish peroxidase conjugate (strep-tactin-HRP) which binds the N-terminal cloned strep-tag. Western blots were evaluated by chemiluminescence. Results are shown for the pooled and concentrated EFs. Red boxes indicate the presence of the NPR1 protein with a size of 67 kDa in the SDS-PAGE and western blots.

The EF1, EF2 and EF3 were pooled, rebuffered in PBS and concentrated for further analyses. However, all investigated EFs revealed contaminations with mostly smaller proteins, suggesting a partial digestion of the expressed NPR1 protein due to undesired proteolytic activity during the purification procedure (Figure 36.A).

To visualize the tagged proteins and their potential degradation products on the SDS-PAGE, western blots were performed with an antibody for the NPR1 protein (Anti-NPR1) and a strep-tactin horse radish peroxidase conjugate (strep-tactin-HRP) which binds to the C-terminal cloned Strep-tag. Western blots were evaluated by chemiluminescence and verified the approximately 67 kDa band detected in the SDS-PAGE analyses as Strep-NPR1 protein since the NPR1 antibody as well as the strep-tactin-HRP bound to this protein (Figure 36.B). Further, western blots showed a band between 50 kDa and 55 kDa, indicating an N-terminal fragment of the Strep-NPR1 caused by digestion (Figure 36.B). Other possible digestion products or contaminants observed in the SDS-PAGE analyses were either detected by the NPR1 antibody or by the strep-tactin-HRP, indicating that those detections might be unspecific (Figure 36.B). The purified, PBS buffered, and concentrated proteins were finally used to test the Strep-NPR1 binding to SA or NHP.

4.2.3. Strep-NPR1 binding studies via size exclusion chromatography

The NPR1 protein binds SA which allows the protein to function as co-activator of SA-transmitted signaling in pathogen related defense of plants (Wu et al. 2012, Wang et al. 2020, Fu and Dong 2013). However, the lack of SA molecules in plants leads to restricted establishment for SAR while the lack NPR1 proteins leads to a complete failure of SAR establishment (Yildiz et al. 2021). These findings suggest that other molecules are involved in the full establishment of NPR1 dependent defense reactions in SAR. Since NHP and SA molecules share similar hydroxyl and carboxyl group arrangements and NHP is a central player in SAR as well as SA it is suggested that NHP interacts with NPR1 in the same manner as SA (Zeier et al. 2021). Therefore the NPR1 binding to NHP was investigated in this thesis.

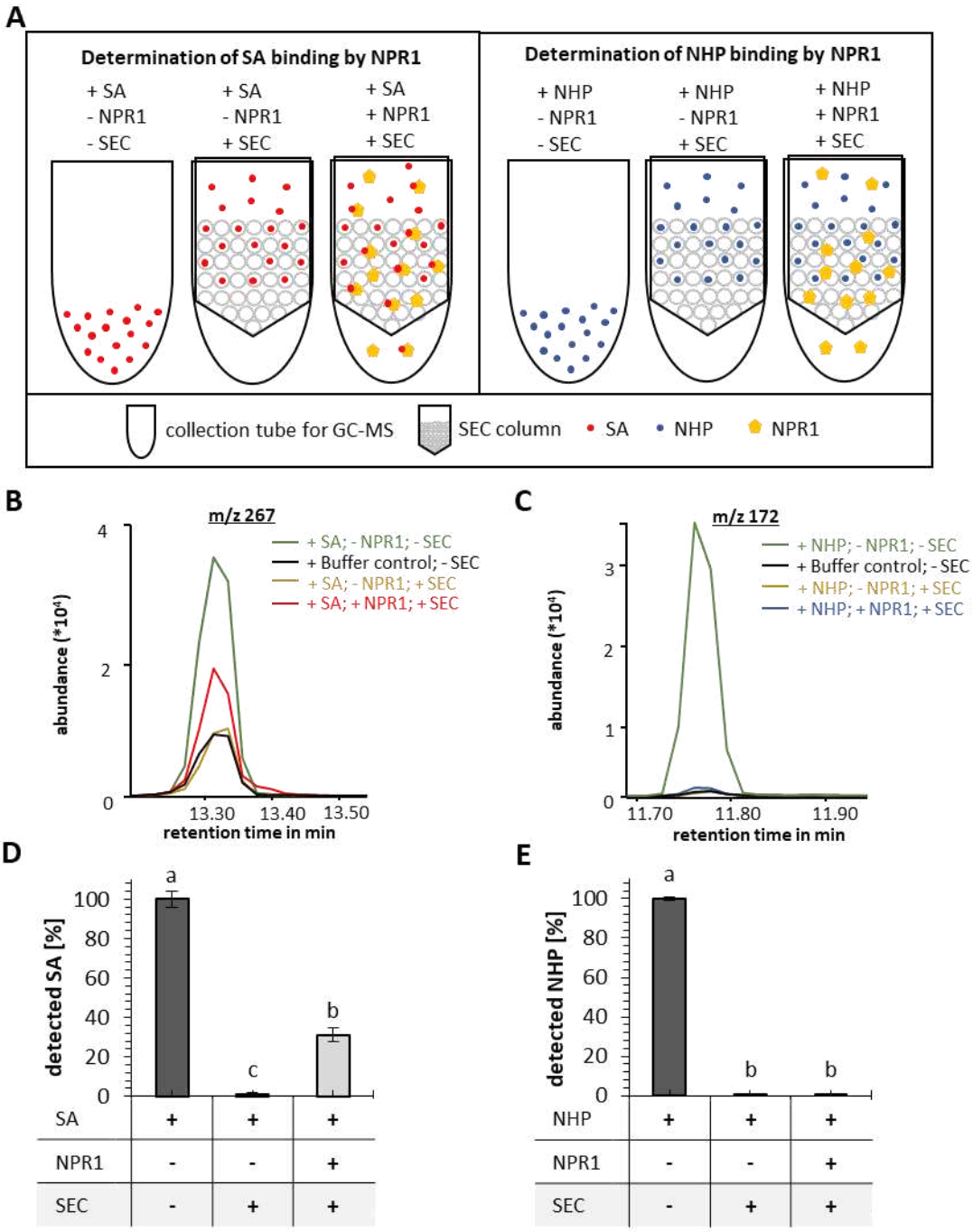

Figure 37: The *Arabidopsis thaliana* NPR1 protein binds SA, but not NHP under the chosen experimental conditions. Binding reactions were performed in 50 µl 1 x PBS containing 50 µg of the purified, PBS buffered NPR1 protein and 200 nM SA or NHP. Two control reactions without NPR1 protein and only SA or NHP input were performed. Binding and control reactions were incubated for 1 hour at 4 °C and afterwards applied to SEC columns. (**A**) In the SEC process small molecules like SA will remain in the columns after a centrifugation step while larger molecules like NPR1 or SA bound to NPR1 will pass the column and will be collected for the GC-MS analyses. To compare the potentially NPR1 bound SA or NHP in the collection tube with the input one of the two prepared control samples is not applied to SEC column and directly analyzed via GC-MS. The other control sample which is applied to the SEC column assures correct separation of the SEC columns. Buffer containing D4 labeled SA and D9 labeled NHP was added to all binding and control samples before they were analyzed via GC-MS. A buffer control was additionally run in the GC-MS analyses (+Buffer control; - SEC). (**B**) In the selected ion chromatogram of m/z 267 of SA-NPR1 binding assays, SA peaks were identified at a retention time (RT) of 13.32 min in the buffer control (+ Buffer control; - SEC), the SEC control (+ SA; - NPR1; + SEC), the SA input control (+ SA; - NPR1; - SEC) and the SA-NPR1 binding reaction samples (+ SA; + NPR1; + SEC).

(**C**) In the selected ion chromatogram of m/z 172 of NHP-NPR1 binding assays, NHP peaks were identified at a RT of 11.77 min in the buffer control (+ Buffer control; - SEC), the SEC control (+ NHP; - NPR1; + SEC), the NHP input control (+ NHP; - NPR1; - SEC) and the NHP-NPR1 binding reaction samples (+ NHP; + NPR1; + SEC). (**D**) (**E**) Total amounts of SA or NHP were quantified using the added internal standards and detected amounts were expressed relative to the SA or NHP input, respectively in percent (%). Tables below diagrams indicate the addition of SA/NHP and the NPR1 protein to a reaction and if the samples were applied to a SEC column (grey background). Bars indicate the mean values ± standard deviations of at least two replicates per reaction combination. Letters above bars indicate the statistical differences investigated between the reaction combinations with an ANOVA in SPSS.

To test the binding of the here expressed Strep-NPR1 protein with SA or NHP, a size exclusion chromatography (SEC) based experimental setup was established, similar to NPR1 binding experiments performed by Liu et al. (2020) and Ding et al. (2018) with a following GC-MS analyses to detect bound SA or NHP. Binding reactions were performed in 50 µl 1 x PBS buffer and contained 50 µg of purified and PBS buffered Strep-NPR1 protein and 200 nM SA or NHP. For each binding reaction with SA or NHP two control reactions without protein were performed. Binding reactions were performed for one hour at 4°C and the reactions were stopped by the application to a SEC column (exclusion limit 5000 M_r). Due to the SEC process small molecules like SA will remain in the columns after a centrifugation step while larger molecules like NPR1 or SA bound to NPR1 will pass the column and will be collected for the GC-MS analyses (Figure 37.A). To compare the collected NPR1 bound SA or NHP with the SA or NHP input one of the two prepared control samples without protein is not applied to SEC column. After applying the TMS-based derivatization protocol as described in section 5.17. all samples were analyzed via GC-MS.

The other SA or NHP control sample without protein is applied to the SEC column to assure correct separation of the molecules by the SEC columns. For SA and NHP quantification, buffer containing D4 labeled SA and D9 labeled NHP was added to all collected samples and a buffer control was additionally prepared for the GC-MS run. The buffer control assured that no NHP or SA residues included in the buffer leads to a misinterpretation of the results. Finally, all binding reactions, input controls, SEC controls and buffer controls were analyzed via GC-MS and SA and NHP amounts were quantified.

In SA binding experiments, in the performed buffer control (+ Buffer control; - SEC) and the SEC control (+ NHP; - NPR1; + SEC) samples similar amounts of SA were detected,

demonstrating that the used buffer which contains the deuterated internal standards for SA and NHP quantification contains small amounts of non-labeled SA. To estimate the correct amounts of Strep-NPR1 bound SA, detected SA in the buffer control were hence subtracted from the detected amounts in all other investigated SA samples. In the selected ion chromatogram (m/z 267) of SA binding experiments the highest SA peaks at an RT of 13.32 min were detected in the SA input control (+ NHP; - NPR1; - SEC) that was not applied to a SEC sample and between this input and the SEC column control the peak of Strep-NPR1 bound SA (+ NHP; + NPR1; + SEC) was observed (Figure 37.B). This indicates a sufficient binding of SA by the here expressed Strep-NPR1. It was further calculated that approximately 31% of the 200 nM SA input were bound in the reaction (Figure 37.D). In the flowthrough of the SEC column control sample, only containing SA, minor amounts of SA which correspond to 1,26% of the SA input were detected, indicating a small but neglectable error rate of the SEC columns. In NHP binding experiments in contrast, the selected ion chromatogram (m/z 172) revealed peaks of similar height at an RT of 11.77 min in the buffer control (+ Buffer control; - SEC), the SEC control (+ NHP; - NPR1; + SEC) and the NPR1-NHP binding (+ NHP; + NPR1; + SEC) samples (Figure 37.C). Only in the NHP input controls, which were not applied to a SEC column, NHP was detected, indicating that the expressed Strep-NPR1 does not bind NPR1 (Figure 37.C, 37.E). Since small amounts of NHP were detected in the buffer control, these amounts were subtracted from the NHP amounts detected in all other samples to estimate the correct amounts of Strep-NPR1 bound NHP.

To gain further insight into the binding of SA to the expressed Strep-NPR1 protein, the binding of SA to the above mentioned generated Strep-NPR1^{R432Q} mutant was investigated. Prior to the binding experiments, the generation of the desired Strep-NPR1^{R432Q} mutant was verified by sequencing of the complete NPR1 coding region (Figure 38.A). Sequences obtained from putative mutant clones were aligned to the mutagenesis primers, the *A. thaliana* wildtype NPR1 sequence, the predicted NPR1^{R432Q} mutant sequence to identify the correctly amplified and mutagenized Strep-NPR1^{R432Q} mutants (Figure 38.A). To assure the successful expression and purification of the Strep-NPR1^{R432Q} mutant SDS-PAGE with following western blots were performed (Figure 38.C).

Binding assays were performed as described in the previous section with 50 µg Strep-NPR1, Strep-NPR1^{R432Q} or Bovine serum albumin (BSA) and 500 nM SA. The BSA reaction was set up

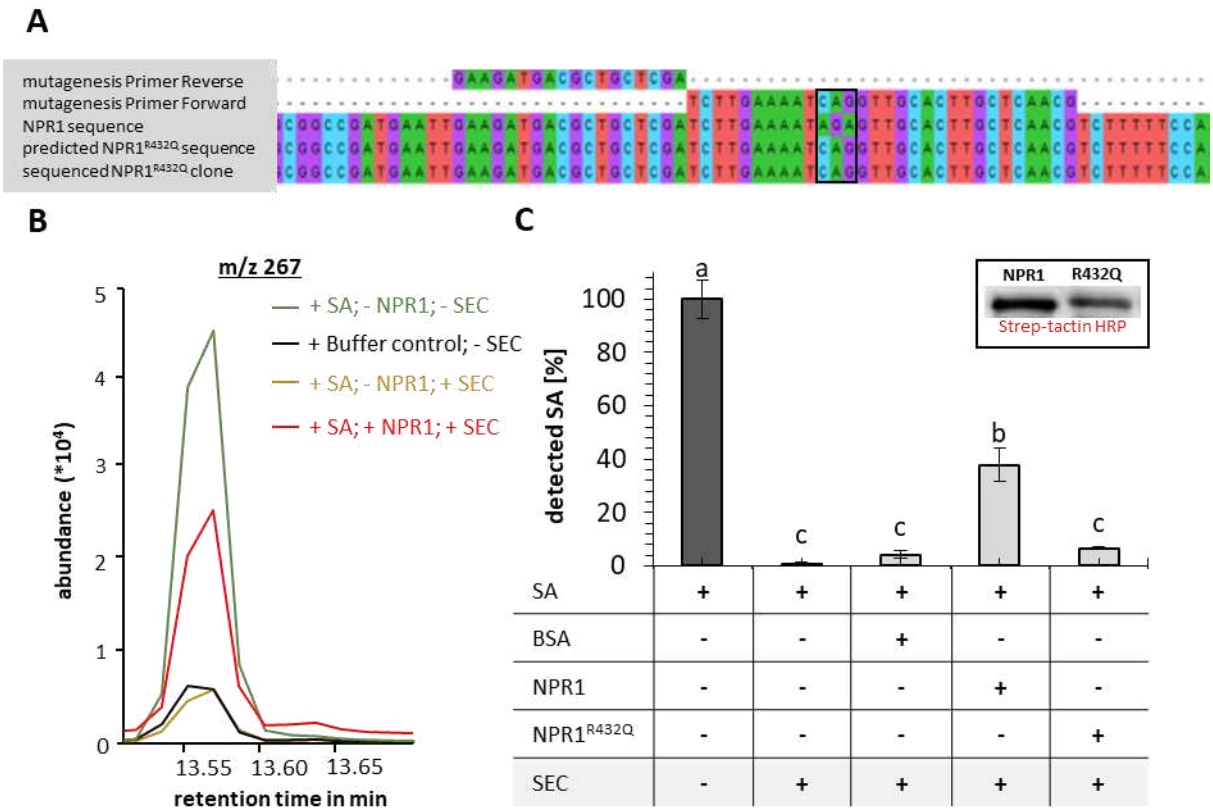

Figure 38: The direct interaction of SA and Strep-tagged NPR1 is disrupted in the generated NPR1^{R432Q} mutant. (**A**) Generated Strep-NPR1^{R432Q} mutant clones were sequenced and aligned to the used mutagenesis Primers, the *A. thaliana* NPR1 WT sequence and the predicted NPR1^{R432Q} mutant sequence to verify the correct mutagenesis. (B) Binding assays with 500 nM SA and Strep-NPR1 or the Strep-NPR1^{R432Q} mutant or bovine serum albumin (BSA) were performed and analysed via GC-MS as described in Figure 37 with the respective buffer, input and SEC column controls. In the selected ion chromatogram of m/z 267 of performed binding assays, SA peaks were identified at a retention time (RT) of 13.57 min in the buffer control (+ Buffer control; - SEC), the SEC control (+ SA; - NPR1; + SEC), the SA input control (+ SA; - NPR1; - SEC) and the SA-protein binding reaction samples (+ SA; + NPR1; + SEC, + SA; + R432Q; + SEC, + SA; + BSA; + SEC). (C) Total SA amounts were quantified using the added D4-SA standards and detected amounts were expressed relative to the SA input in percent (%). Bars indicate the mean values ± standard deviations of two replicates per reaction combination. Letters above bars indicate the statistical differences investigated between the reaction combinations with an ANOVA in SPSS. The table 2elow diagrams indicates the combination of SA and Strep-NPR1, Strep-NPR1^{R432Q} or BSA proteins in a reaction and indicates if the samples was applied to a SEC column (grey background) before GC-MS analyses. The black lined box shows the results of a western blot analyses of Strep-NPR1 and Strep-NPR1^{R432Q}, which was performed as described in Figure 36 with Strep-tacti HRP for the detection of the used Strep-tag.

to investigate unspecific binding of SA molecules to proteins. In the selected ion chromatogram of m/z 267 of NPR1-SA binding assays, SA peaks were identified at an RT of 13.57 min (Figure 38.B). The highest amounts were thereby detected in GC-MS runs of the SA input control (+ SA; - NPR1; - SEC) (Figure 38.B) and the lowest amounts in the runs of buffer control (+ Buffer control; - SEC) and the SEC control (+ SA; - NPR1; + SEC). To estimate the correct amounts of protein bound SA, the amount of SA detected in the buffer controls (+SA/+SEC) was subtracted from the respective, detected amounts of SA in the other samples. By comparing the selected ion chromatograms of the SA-specific m/z 267, the overall trends

of the SA-binding experiment can already be observed: The SEC control peak, representing the total amount of SA in the binding reactions, was the highest peak as expected, while the peak for SA in the Strep-NPR1 and SA binding reaction was still very prominent, suggesting that a significant amount of SA was bound to NPR1, whereas the SA input control peaks were significantly smaller. These observations were confirmed after calculating the total amounts of SA in the respective assays (Figure 38.B). Detected SA amounts in BSA and Strep-NPR1^{R432Q} binding reactions were comparable and much lower than Strep-NPR1 binding assays with SA (Figure 38.C). It was finally estimated that approximately 40 % of the 500 nM SA in the reaction was bound by the Strep-NPR1 protein, while the Strep-NPR1^{R432Q} mutant only bound 6.5 % of the 500 nM SA (Figure 38.C). In the BSA control reaction 4 % of the 500 nM input SA were bound, demonstrating a similar affinity of BSA and the Strep-NPR1^{R432Q} mutant to SA when compared to the Strep-NPR1 wildtype protein (Figure 38.C). In the SEC control reaction 0.8 % of the 500 nM input SA were detected, indicating a minor but negatable error rate of the used SEC columns (Figure 38.C). In summary, these results indicate Strep-NPR1 binding of SA but the generated Strep-NPR1^{R432Q} mutant shows unspecific binding to SA similar to the control protein BSA.

4.3. Discussion

4.3.1. NPR1 is not an NHP receptor

The interplay of SA and NHP is crucial for the full establishment of SAR (Hartmann and Zeier 2019). After an infection with a pathogen, plants like *A. thaliana* accumulate SA and NHP at the site of infection (Hartmann et al. 2018). As mobile SAR signal, NHP is translocated to systemic plant parts where it promotes the transcriptional response of its owns biosynthesis genes and via the mutual amplification loop of NHP and SA induces the transcriptional response of SA biosynthesis genes (Yildiz et al. 2021, Zeier 2021). The systemic accumulation of SA results in the transcription of PR genes, which mediate resistance in plants like *A. thaliana* (van Loon et al. 2006, Bernsdorff et al. 2016, Hartmann and Zeier 2019). The perception of SA is thereby facilitated by direct binding to the bona fide SA receptor NPR1 (Wu et al. 2012, Manohar et al. 2015, Ding et al. 2018, Nair et al. 2021). It was further demonstrated that the NHP induced SAR is mostly dependent on NPR1 and SA, however a minor part of the NHP induced systemic immune responses was observed to be independent of SA and dependent on NPR1 (Yildiz et al. 2021). Until today it is not known how the interplay between NHP and NPR1 is mediated. Given that SA and NHP exhibit structural similarities, it was recently suggested that NPR1 might serve as NHP receptor (Zeier 2019, Nair et al. 2021).

To investigate the binding affinity of NPR1 to NHP, the *A. thaliana NPR1* sequence was cloned into the pET52b(+) plasmid and the construct was transformed into and expressed in *E. coli* Lemo21 cells (Figure 34 – 36). To verify the binding efficiency of the expressed NPR1 protein, SA binding assays were performed in parallel with NHP binding assays. Binding reactions were performed in 50 µl PBS buffer, containing 50 µg of the purified NPR1 protein and 200 nM SA or NHP. As controls two reactions without NPR1 protein and only SA or NHP input were performed. After one hour reaction time, binding reactions and performed controls were applied to SEC columns and the flowthrough was analyzed via GC-MS to detect NPR1 bound SA or NHP amounts.

NPR1 bound SA or NHP were compared to input controls to estimate the amounts bound SA or NHP. In the SEC process small molecules like SA will remain in the columns after a centrifugation step while larger molecules like NPR1 or SA bound to NPR1 will pass the column and will be collected for the GC-MS analyses (Figure 37.A). To compare the potentially NPR1

bound SA or NHP in the collection tube with the input, one of the two prepared control samples is not applied to SEC column and directly analyzed via GC-MS. The other control sample which is applied to the SEC column assures correct separation via the SEC columns. For SA and NHP quantification, buffer containing deuterium-labeled SA and NHP was added to all binding and control samples before they were analyzed via GC-MS.

The here conducted binding assays revealed that the expressed Strep-NPR1 protein is not able to bind NHP but does bind SA (Figure 37, 38). To further investigate the potential binding of NPR1 to NHP, the Strep-NPR1^{R432Q} mutant was generated by PCR using primers with the R432Q mutational change (Table 5). The binding of SA to the Strep-NPR1^{R432Q} protein was disrupted as demonstrated in previous studies (Figure 38, Ding et al. 2018). The generated mutant is not able to bind SA but can still interact with TGA transcription factors (Ding et al. 2018). However, the first binding assays revealed no binding of NHP by unmodified Strep-NPR1 proteins and a further investigation of this interaction was not prioritized.

In parallel with this study, the binding of NHP by NPR1 was investigated by two different research groups. Liu et al. (2020) performed mutual binding assays of *E. coli* expressed NPR1 with 200 nM [^{3}H] labeled SA and a 10 000-fold excess amount of unlabeled SA or NHP. Binding assays were performed for one hour and applied to SEC columns as described in this study previously. In the flowthrough tritium-labeled SA was by scintillation counting measured and the results showed that unlabeled SA is not bound by NPR1 in the presence of SA but is bound in the presence of NHP (Liu et al. 2020). Hence, the NPR1 protein bound SA but not NHP in the presence of [^{3}H] labeled SA. These experiments, however, do not completely rule out the binding of NHP by NPR1, since NHP levels in the flowthrough were not quantified. Additionally, the NPR1 protein was expressed with a histidine (His) tag and a maltose binding protein (MBP) tag (Liu et al. 2020), which both combined roughly have a size of 45 kDa. Since NPR1 has a size of 66 kDa, it is questionable if this tag hinders the binding of NPR1 to a ligand. To minimize the risk of an interference of the NPR1 binding by a large tag, the used NPR1 protein in this study was fused to a Strep-tag for purification, which is only eight amino acids long and roughly 1 kDa in size. Furthermore, the here presented NPR1 binding assays were conducted in individual reactions with SA or NHP without the competitive addition of labeled SA as performed in recent studies (Ding et al. 2018, Liu et al. 2020) which demonstrates that even without competing SA, NPR1 does not bind NHP.

In support a second study that was performed in parallel and cooperation to this work with the group of Prof. Dr Christiane Gatz (Georg-August-Universität Göttingen), which investigated the NPR1 binding to SA and NHP with a similar experimental setup to this work in which unmodified SA and NHP do not compete with labeled SA in the NPR1 binding assays. Using state-of-the-art technology, Nair et al. (2021) and I used isothermal titration calorimetry (ITC) to demonstrate in saturation binding assays that insect-cell-expressed Strep-MBP-NPR1 protein is able to bind SA with an equilibrium dissociation constant (K_D) of 7.9 ± 0.5 µM. However, the insect cell expressed NPR1 protein did not show any activity to the NHP provided by our group (AG Zeier) (Nair et al. 2021). In previous studies *E. coli* expressed His-MBP-NPR1 showed a K_D of 0.2213 ± 0.03885 µM (Ding et al. 2018), indicating that insect cell and *E. coli* expressed NPR1 proteins exhibit a high binding affinity to SA. However, the *E. coli* expressed His-MBP-NPR1 showed a much stronger binding affinity than the insect cell expressed Strep-MBP-NPR1 protein. Since a basal level of around 1.4 µM SA was detected in *A. thaliana* leaves, the previously reported high binding affinity of *E. coli* expressed His-MBP-NPR1 would lead to a saturation of binding at basal SA levels (Kong et al. 2016, Nair et al. 2021). NPR1 dependent immune responses in *A. thaliana* are however inducible and therefore a constitutive saturation of NPR1 binding of SA is unlikely (Kong et al. 2016, Nair et al. 2021). Nair and his team (2021) thus suggested that the used SEC method in previous studies might not be accurate enough to estimate realistic binding affinities of NPR1 proteins. Given that two independent studies revealed that NHP is not bound by NPR1 during the conduction of this study, the binding affinity of the here expressed Strep-NPR1 protein was not investigated. However, the established binding assay revealed that the expressed Strep-NPR1 protein is able to bind 31 % SA at a 200 nM SA input and 40 % at a 500 nM SA input, indicating that the NPR1 binding is not saturated at these concentrations. This agrees with the results of the saturation binding assays performed by Ding and colleagues (2018).

Based on a molar 1:1 binding ratio of NPR1 and SA molecules, Nair and his team (2021) were able to measure that 10% – 14% of Strep-MBP tagged protein bound a SA molecule in independent binding experiments, while Ding and co-workers (2018) detected that only 0.02% of the His-MBP-NPR1 protein bound a SA molecule. In this study 1.2% - 3.8% of the *E. coli* expressed Strep-NPR1 protein bound a SA molecule (see Suppl. Figure 10 for calculations). This shows, that when expressed in *E. coli*, a higher fraction of Strep-tagged NPR1 molecules binds SA molecules than His-MBP-tagged NPR1 proteins (Ding et al. 2018), which might be

caused be an interference of the NPR1 binding mechanisms by the large His-MBP tag. Furthermore, the insect cell expressed Strep-MBP tagged NPR1 protein showed a much higher ability to bind SA than the Strep-tagged protein in this study (Nair et al. 2021). This might be based on the fact that the tested *A. thaliana* NPR1 protein originates from a eukaryotic organism and the expression in eukaryotic insect cells might be closer to the original than the expression in procaryotic *E. coli* bacteria. In summary, the by Nair and co-workers (2021) performed ITC binding assay with insect cell expressed NPR1 proteins hence seem to predict a much more accurate binding affinity of NPR1. Nonetheless the binding assays performed by Lui et al. (2020), Ding et al. (2018) and in this study are still sophisticated enough to identify interaction partners of NPR proteins. Since in Strep-tagged NPR1 proteins expressed in *E. coli* however show that a higher percentage of Strep-tagged NPR1 binds SA molecules than His-MBP tagged NPR1 in previous studies, it would be interesting to test an insect cell expressed Strep-tagged NPR1 protein in this matter. Thereby it could be verified if a large tag interferes with the NPR1 binding of SA that caused abbreviating molar binding ratios of NPR1 and SA molecules in this and previous studies.

3.3.2. NHP induces SA-independent NPR1-mediated immune responses

Previous studies have demonstrated that the SA deficient *A. thaliana sid2* mutant shows a modest NHP induced SAR against the infection with *Psm* bacteria, but NHP treatments did not induce systemic resistance in *npr1* knock-out mutants (Yildiz et al. 2021). Since this and previous studies (Liu et al. 2020, Nair et al. 2021) demonstrated that heterologously expressed NPR1 does not directly interact with NHP, indirect mechanisms must exist by which NHP mediates the SA-independent activation of NPR1 mediated defense responses in *sid2* mutants. Yildiz and her team hypothesized that NHP treatments might elevate NPR1 levels and thereby enhance the perception of SA. Consequently, NHP treatments of *sid2* mutants would result in the systemic activation of NPR1-dependent immune responses by basal SA levels. This hypothesis however has to be validated by future research. Since NPR1 is regulated by a redox shift which is mediated by SA (Mou et al. 2003), Nair and colleagues (2021) suggested NHP could similarly activate SA-independent NPR1-mediated immune responses by the induction of a redox shift. However, *sid2* mutants that were treated with NHP did not indicate a redox shift in their performed experiments and recommended to investigate this

issue with more suitable experimental setups (Nair et al. 2021). Thus, it remains unknown how NHP contributes to the activation of NPR1 in the absence of SA and further research is needed to validate current hypotheses in this matter.

4.3.3. Conclusion

This study supports that the *A. thaliana* NPR1 protein is a bona fide SA receptor in the mediation of defense responses against pathogens. Since SA and NHP exhibit similar structural characteristics and NHP was demonstrated to induce SA-independent NPR1 activation it was investigated if a Strep-NPR1 protein expressed in *E. coli* can bind NHP by the same mechanisms as it binds SA. As previously shown by Lui et al. (2020) and Nair et al. (2021) this study demonstrated that NPR1 does not bind NHP under the chosen experimental conditions. This suggests the existence of yet unknown mechanisms in the NHP induced activation of SA-independent NPR1 mediated immune responses that have to be investigated in future studies. In comparison to previously used methods in the investigation of potential NPR protein interaction partners, the here established SEC based binding assay with a following GC-MS detection is a suitable method to identify and exclude NPR1 ligand partners.

5. Material and Methods

5.1. Cultivation of plants

All plants were grown in environmentally controlled growth chambers on a mixture of soil (Substrat BP3, Klasmann-Deilmann), vermiculite and sand (8:1:1), if not stated otherwise. The plants were watered three times a week with tap water. To ensure equal growth conditions the positions of the individual plant pots was rotated regularly. The described growth conditions for plants were maintained after all below described treatments, if not stated otherwise.

Arabidopsis thaliana

A. thaliana plants were cultivated in a controlled plant growth room with a 10-h day (21°C) and 14-h-night (18°C) cycle. The relative humidity was adjusted to 60 %. Depending on the pathogen treatment experiments were performed with four- to five-week-old *A. thaliana* plants.

The following *A. thaliana* lines were used in this study: Col-0 (Nottingham Arabidopsis Stock Centre [NASC] ID: N1092), *fmo1* (Mishina and Zeier 2006), *sid2-1* (*sid2*; Nawrath and Métraux 1999, Bernsdorff et al. 2016), *sid2/fmo1* (Löwe et al. 2023), *coi1-35* (Staswick and Tiryaki 2004), wrky33-2 (*wrky33*; Zheng et al. 2006), *pad4-1* (*pad4*; Jirage et al. 1999), *eds1-2* (*eds1*; Bartsch et al. 2006), *cyp79b2 cyp79b3* (*dcc*; Zhao et al. 2002), *pad3-1* (*pad3*; Glazebrook and Ausubel 1994)

Nicotiana tabacum

Nicotiana tabacum cv. Xanthi, *Nicotiana tabacum* cv. Xanthi and were grown in single pots with a 16 h light (23 °C) and 8 h darkness (20 °C) day-night-cycle. The relative humidity in the growth chamber was adjusted to 60%.

Cucumis sativus

Cusumis sativus cv. Wisconsin SMR58 plants were grown with a 16 h light period (25 °C) and an 8 h darkness period (23 °C) cycle and the relative humidity was set to 60%.

Brachypodium distachyon

Brachypodium distachyon cv. Bd21 seeds were surface sterilized (10 min in bleach, three times in sterile H_2O for 30 sec). Seeds were placed on agar plates containing 0.5 % MS and 0.8 %

agar incubated for 3 days in darkness at 4 °C. Six-days-old seedlings were grown in single pots on a mixture of soil (Substrat BP3, Klasmann-Deilmann), sand, vermiculite, and gravel (4:2:1:1) under 16 h light (25°C) and 8 h darkness (23°C) long day conditions with a relative humidity of 60%.

Hordeum vulgare

The cultivation of *Hordeum vulgare* cv. Ingrid was performed by Dr. Ulrich Schaffrath (Department of Plant Physiology, RWTH Aachen University, Germany). Seeds were pre-germinated for 24 h on wet filter paper. Germlings were then transferred to pots filled with standard soil (type ED73, Balster Einheitserdewerk GmbH, Froendenberg, Germany). *H. vulgare* plants were grown under a 16 h light (20 °C) and an 8 h darkness (20°C) day-night-cycle and the relative humidity was set to 65 %.

5.2. Cultivation of pathogens

***Pseudomonas syringae* (*Psm, Psm lux, Psl, Pstb*)**

The *Pseudomonas* strains *Pseudomonas syringae* pv. *maculicola* ES4326 (*Psm*) (Hartmann et al. 2018), a modified *Pseudomonas syringae* pv. *maculicola* strain carrying the *Photorhabdus luminescens* luxCDABE operon (*Psm lux*) (Hartmann et al. 2018), *Pseudomonas syringae* pv. *lachrymans* (*Psl*) (Grzegorz Bartoszewski, Warsaw University of Life Sciences) and *Pseudomonas syringae* pv. *tabaci* (DSM 1856) (*Pstb*) were grown in King's B medium (20 g l^{-1} Bacto Peptone, 1.5 g l^{-1} K_2HPO_4 x 3 H_2O, 10 g l^{-1} Glycerol, pH = 7.2) containing the appropriate antibiotics (*Psm*: 50 µg/ml rifampicin; *Psm lux*: 50 µg/ml rifampicin, 25 µg/ml kanamycin; *Psl* and *Pstb*: no antibiotics). The *Psm*, *Psm lux* and *Psl* were grown at 28°C and *Pstb* was grown at 18°C in King's B medium containing no antibiotics.

***Xanthomonas translucens* (*Xtra*)**

The *Xanthomonas translucens* strain DSM 18974 (*Xtra*) was cultivated on peptone-sucrose agar (PSA) (20 g l^{-1} sucrose, 5 g l^{-1} peptone, 0.5 g l^{-1} K_2HPO_4, 0.25 g l^{-1} $MgSO_4x7H_2O$, 15 g l^{-1} agar) at 28°C.

***Magnaporthe grisea* (*Mgri*)**

The *Magnaporthe grisea* strain Guy11 (*Mgri*) (provided by Nick Talbot, The Sainsbury Laboratory, Norwich, United Kingdom) was grown at 18 °C (9 light hours) on cornmeal agar

(CMA) (15 g cornmeal/L) supplemented with a nitrate salt solution (6 g l^{-1} $NaNO_3$, 0.5 g l^{-1} KCl, X $MgSO_4$, 1.5 g l^{-1} KH_2PO_4) as described by Parker et al. (2008).

***Magnaporthe oryzae* (*Mory*)**

The *Magnaporthe oryzae* isolate TH6772 (Institute of Biochemistry, Tamagawa University, Machida-shi, Tokyo, Japan) (*Mory*) was grown at 23°C in the dark on oat-meal agar plates (20 g l^{-1} agar, 2 g l^{-1} yeast extract, 10 g l^{-1} starch, 30 g l^{-1} oatflakes). The cultivation of *Mory* was performed by Ulrich Schaffrath in the Department of Plant Physiology at RWTH Aachen University (Aachen, Germany).

***Botrytis cinerea* (*Bcin*)**

The *Botrytis cinerea* strain B05.10 (*Bcin*) was grown on Mathur's agar (2.8 g/l glucose, 1.22 g/l $MgSO_4*7H_2O$, 2.72 g/l KH_2PO_4, 2.18 g/l mycological peptone, 30 g/l agar) in a controlled growth chamber with a 10-h-d (21°C)/14-h-night (18°C) cycle.

***Colletotrichum higginsianum* (*Chig*)**

The *Colletotrichum higginsianum* isolate WT063A (*Chig*) was grown on Mathur's agar as well. However, plates were incubated at 25°C in the dark.

***Hyaloperonospora arabidopsidis* (*Hpa*)**

The *Hyaloperonospora arabidopsidis* isolate Noco2 (*Hpa*) was propagated every week to fresh two-week-old *A. thaliana* Col-0 seedlings (50 - 100 seedlings/pot). Spores were washed from inoculated seedlings 7 dpi with tab water. Fresh two-week-old seedlings were then spray inoculated with the spore suspension without quantifying the number of spores. The inoculated seedlings were incubated in sealed trays with transparent lids at 18 °C (9 light hours).

***Sclerotinia sclerotiorum* (*Sclero*)**

Sclerotinia sclerotiorum (*Sclero*) was cultivated by Dr. Ulrike Steiner at the institute of Crop Science and Resource Conservation at the Rheinische Friedrich-Wilhelms-Universität Bonn. For long term stocks, *Sclero* sclerotia were grown on potato-dextrose-agar (PDA, 1.5 g/l) in petri dishes for 14 days at 20°C with day-night light conditions. Grown sclerotia were harvested from the plates and were stored at -20°C until further use. To prepare a *Sclero* inoculum frozen sclerotia were transferred to fresh PDA plates and mycelium was grown under the before described conditions until they were completely grown with fresh *Sclero* mycelium. For one inoculum, ten circular discs

(1 cm radius) were stamped out of plates that were completely grown with fresh *Sclero* mycelium and were transferred to 500 ml liquid PSA medium (24 g PSA / l) in a schikane flask. The flask was incubated on a shaker at 80 rpm for eight days. Afterwards the grown culture was homogenized in a blender, supernatant PSA medium was decanted, and the total volume of the inoculum was adjusted to 500 ml. The density of the *Sclero* inoculum was not determined but it was aimed to reach a similar cloudiness for each prepared inoculum.

5.3. Plant inoculations with bacteria

For experiments, log-phase cultures of the bacteria were grown over night under permanent shaking (240 rpm). The cultures were washed three times with 10 mM $MgCl_2$ and were diluted to the required final OD_{600} levels for leaf inoculations as indicated in the experiments. Unless stated otherwise mock controls were inoculated likewise with a 10 mM $MgCl_2$ solution.

Five-week *A. thaliana* and four- to five-week-old *N. tabacum* plants were carefully pressure infiltrated from the abaxial side of the leaves with a *Pstb*- or *Psm*-solution using a needleless syringe. For metabolite analyses of *Psm* (OD_{600} = 0.001) and mock inoculated *A. thaliana* plants samples were taken 1, 2 and 3 days post inoculation (dpi), frozen in liquid nitrogen and stored at -80°C (n = 4). To induce SAR in *A. thaliana* plants, local leaves were challenge inoculated with a *Psm* solution of OD_{600} = 0.005. For resistance assays systemic *A. thaliana* leaves were infiltrated with *Psm lux* OD_{600} = 0.001 (n ≥ 6) and the luminescence of *Psm lux* was measured in the luminometer 2.5 dpi, when visible infection symptoms started to develop.

For the metabolite analyses of four- to five-week-old *N. tabacum* plants, fully grown leaves were pressure infiltrated with *Pstb* OD_{600} = 0.005 and were harvested 1, 2 and 3 dpi. The samples were frozen in liquid nitrogen and stored at -80°C (n = 5). For resistance assays *N. tabacum* leaves were infiltrated with a *Pstb* solution of OD_{600} = 0.001 (n = 4) or a *Psm* solution of OD_{600} = 0.001 (n ≥ 5) and growth assays were performed 3 dpi to determine bacterial growth.

Three-week-old *C. sativus* plants were spray-inoculated with *Psl* OD_{600} = 0.2 (0.005 % silwet) from the abaxial side of the first true leave. To collect *C. sativus* phloem sap, filter paper (1 cm x 1 cm) was prepared, and the weight was determined using a precision scale. After removing the local, inoculated leaf the escaping sap was soaked up with the filter paper at the site of

the petiole and weighted again. The filter paper was then transferred into 100 µl MeOH/H_2O (80:20, v/v). The process was repeated for the systemic leaf. Leaf samples were collected in form of leaf discs that were stamped out of a leaf immediately after it was removed from the plant. Leaf and phloem sap samples for the metabolite analyses were taken 1 dpi, 3 dpi and 5 dpi, frozen in liquid nitrogen and stored at -80°C (n = 5). *C. sativus* plants were harvested for resistance assays 3 dpi (n = 4) and 6 dpi (n = 4) and pictures were taken 6 dpi.

To analyze metabolite levels of five-week-old *B. distachyon* plants post pathogen infection, leaves were pressure infiltrated with *Xtra* (OD_{600} = 0.05). Local inoculated and systemic untreated leaved were sampled 1 dpi, 3 dpi and 5 dpi (n = 3) for metabolite analyses. At this growth stage *B. distachyon* developed three tillers. The oldest leaf of each tiller was determined as local leaf and the youngest leaf as systemic leaf (Abb. H.C). The leaf samples were frozen in liquid nitrogen and stored at -80°C. For resistance assays three-week old Brachypodium plants were inoculated with a bacterial solution of OD_{600} = 0.005. The assessment of resistance was performed 3 dpi (n = 9) and pictures of *Xtra* inoculated leaves were taken 3 dpi and 8 dpi. In both experimental setups a needleless syringe was used to pressure infiltrate the bacterial solution from the adaxial site of the leaves.

5.4. Plant inoculation with fungi and an oomycete

To inoculate *B. distachyon* with *Mgri*, spores were isolated within 15 days of growth on plate by washing the mycelium with sterile H_2O. To increase the spore yield they were scraped of the plate using a coverslip. The resulting solution was filtered using Miracloth (Merck Millipore, Billerica, MA, USA) and centrifuged for 4 min (4000 rpm). The spore pellet was resuspended in 3 ml sterile H_2O and the spore concentration was determined using a Neubauer chamber (NanoEnTek. Inc., Seoul, Korea). For the inoculation of *B. distachyon* with *Mgri* the spore suspension was adjusted to 50 spores/µl and applied to three- to four-week-old plants in the 3-leaf-stage. The spore solution was applied by spray inoculation with an airbrush until the leaves were evenly covered with fine droplets. Mock control plants were treated in the same manner with autoclaved water. As described by Parker et al. (2008) *B. distachyon* plants were maintained hermitically sealed in autoclave bags after inoculation. To study the changes in metabolite levels in *B. distachyon* upon fungal inoculation per sample

one plant was harvested 2 dpi, 3 dpi and 4 dpi (n ≥ 4), frozen in liquid nitrogen and stored at -80°C. To assess the *B. distachyon* resistance against *Mgri* the area of necrosis was measured 4 dpi as described below and pictures of *B. distachyon* leaves were taken 4 dpi (n = 4).

Mory was grown on oat-meal agar plates and sporulation was induced by incubating under black light for two weeks. Spores were harvested in H_2O prior to *H. vulgare* inoculations and the spore suspension containing 1 g l^{-1} gelatin, 0.5 ml l^{-1} Tween was adjusted to 250 spores/µl. The plants were kept for 24 h at 24° C and 100% relative humidity in the dark after spray inoculation and were then transferred to growth chamber conditions with the afore mentioned conditions. Mock control plants were treated likewise with H_2O containing 1 g l^{-1} gelatin, 0.5 ml l^{-1} Tween. For metabolite analyses the spray inoculated *H. vulgare* leaves were sampled 5 dpi (n = 3), frozen in liquid nitrogen and stored at – 80°C. Treatments of barley plants were performed by Ulrich Schaffrath in the Department of Plant Physiology at RWTH Aachen University (Aachen, Germany).

For *A. thaliana* inoculations with *Bcin*, spores were washed within 10 days of growth on plate by washing the mycelium with 5 – 8 ml sterile Mathur's medium (2.8 g/l glucose, 1.22 g/l $MgSO_4*7H_2O$, 2.72 g/l KH_2PO_4, 2.18 g/l myc. peptone). The resulting *Bcin* spore suspension was filtered through Miracloth (Merck Millipore, Billerica, MA, USA) and the number of spores was quantified using a Neubauer improved counting chamber (C-Chip, NanoEnTek. Inc., Seoul, Korea). Three leaves of 4.5-week-old *A. thaliana* plants were inoculated with four 3 µl droplets of a *Bcin* spore suspension with an adjusted spore concentration of 50 spores/µl. The droplets were placed at the right and left side of the middle vein, two in the lower part of the leaves and two in the lower parts of the leaves. Mock control plants were treated likewise with sterile Mathur's medium. All plants were maintained at 18 °C (9 light hours) in sealed trays with transparent lids. For metabolite analysis the three inoculated leaves of one plant represented one replicate and samples were taken 1 dpi, 3 dpi and 5 dpi (n = 4). To assess the *A. thaliana* resistance against *Bcin* lesions measurements were performed 2 dpi (n = 8) whereat two leaves of one plant represented one replicate.

To investigate the *A. thaliana* infections with *Chig*, spores were harvested within 14 days of growth on 100 ml Mathur's agar in a 250 ml Erlenmeyer flask by washing the mycelium with 5 – 8 ml sterile water. This spore suspension was filtered through Miracloth (Merck Millipore, Billerica, MA, USA), the *Chig* spore concentration was measured in an improved counting

chamber (C-Chip, NanoEnTek. Inc., Seoul, Korea) and adjusted to 500 spores/ul. Three leaves of four- to five-week-old *A. thaliana* plants were inoculated with four 5 µl droplets of the *Chig* spore suspension as described for inoculations with *B. cinerea*. Mock control plants were treated in the same manner with sterile water. The infected and control plants were maintained in sealed trays with transparent lids at 18°C with a 9 h light – 15 h darkness cycle in an environmentally controlled growth chamber. For metabolite analysis the three inoculated leaves of one plant represented one replicate, but for resistance assays two leaves of one plant represented one replicate. Samples were taken 2 dpi, 4 dpi, 6 dpi, 8 dpi and 10 dpi for metabolite analyses (n = 4). Resistance assays were performed 7 dpi (n = 8) and in parallel to the infection time course of the metabolite analysis (n = 3) to evaluate disease progression.

For *A. thaliana* infections with *Hpa*, spores were washed from *Hpa* infected two-week-old *A. thaliana* seedlings 7 dpi with tab water and the resulting spore solution was filtered through Miracloth (Merck Millipore, Billerica, MA, USA). The number of spores was quantified using a Neubauer improved counting chamber (C-Chip, NanoEnTek. Inc., Seoul, Korea) and adjusted to 50 spores/µl. Four-week-old *A. thaliana* plants were spray inoculated with the *Hpa* spore suspension until fine droplets covered all leaves. Mock control plants were treated likewise with tab water. The inoculated plants were maintained in sealed trays with transparent lids at 18 °C (9 light hours). For metabolite analyses samples were harvested 3 dpi, 6 dpi and 9 dpi (n = 4) whereat three leaves of one plant represent one replicate. Resistance assays were performed 6 dpi (n = 6).

The *Sclero* inoculum was set up by Dr. Ulrike Steiner (The Institute of Crop Science and Resource Conservation, Rheinische Friedrich-Wilhelms-University Bonn) and provided by Philip Bischof. Three leaves of Five-week-old *A. thaliana* plants were inoculated at the middle vein of the leaf with two 3 µl droplets of a *Sclero* suspension (one in the middle of the top half of the leaf and one at the middle of bottom half of the leaf). Mock control plants were treated in the same manner with tab water. To examine the changes in metabolite levels in *A. thaliana* upon a *Sclero* infection, infected and control leaves per plant were harvested 1, 2, 3 and 4 dpi (n = 3). The leaves of one plant represent one replicate. The resistance of A. thaliana against *Sclero* was evaluated 3 dpi (n = 5).

All samples harvested for metabolite analysis frozen in liquid nitrogen and stored at – 80°C until further processing.

5.5. Plant treatments with N-Hydroxypipecolic acid

The chemical synthesis of N-hydroxypipecolic acid was performed as described by Hartmann et al. (2018). Aqueous NHP solutions were always freshly prepared at the day of the experiment using H_2O as solvent.

Treatments with NHP of *N. tabacum* and different *A. thaliana* Genotypes were performed following the established procedure described in Schnake et al. 2020. Individually cultivated plants were watered with 10 ml of a 1 mM solution of NHP by pipetting. As a control treatment 10 ml H_2O were applied to the soil by pipetting. The inoculation of *N. tabacum* with *Pstb* or *Psm* and the inoculation of *A. thaliana* with *Hpa*, *Psm*, *Bcin* and *Sclero* were performed 24 h after the application of the pretreatment. The inoculation of *A. thaliana* with *Chig* was performed 4 h after the application of the pretreatment.

To test the effect of NHP on the immunity of *C. sativus* in a subsequent pathogenic attack, using a syringe with a needle approximately 1 ml of a 1 mM NHP solution was directly injected into the plant stem. Injection of sterile H_2O served as a control. The spray inoculation of all true *C. sativus* leaves with a *Psl* solution was performed 24 h later.

For the NHP treatment of *B. distachyon* plants, a 1 mM NHP solution was infiltrated thoroughly from the adaxial site into the leaves using a syringe. *B. distachyon* plants were inoculated with *Xtra* or *Mgri* 24 h after the application of the pretreatment. As control treatment plants were infiltrated in the same manner with H_2O.

5.6. Establishment of systemic acquired resistance

To investigate the ability of a pathogen to trigger SAR in *A. thaliana*, three fully grown leaves of five-week-old Col-0 plants were challenge inoculated with *Psm*, *Chig* or *Bcin* as described before or were treated likewise with the respective mock solution (see 5.4. - 5.5.). Systemic leaves of *Psm* (n = 6) and mock (n = 6) challenged plants were 2 dpi in individual experiments inoculated with *Hpa*, *Psm*, *Chig* or *Bcin* as described before. The systemic leaves of Chig and

mock pretreated plants were 2 dpi inoculated with *Psm*, *Chig* or *Bcin* in individual experiments. These *Psm*, *Chig* and *Bcin* inoculations were also performed on systemic leaves of *Bcin* or mock challenged Col-0 plants 2 days post the *Bcin* or mock pretreatment.

To investigate the influence of defects in the SA and NHP signaling pathways on the establishment of SAR in *A. thaliana* against pathogens with a necrotrophic lifestyle, Col-0 wildtype and mutant plants were either challenge inoculated with *Psm* and systemic leaves were inoculated with *Psm* or *Chig*, or wildtype and mutant plants were challenge inoculated with *Chig* and the systemic leaves were inoculated with *Psm* as described above for the wildtype. The *A. thaliana* resistance was assessed for each pathogen as described below (see 5.7) to investigate differences between the pathogen and mock control pretreatments.

To test the establishment of SAR in the monocot gras *B. distachyon*, the first and second grown leave of three-week-old seedlings, which did not start to tiller yet (see Figure 17.A), were pressure infiltrated with an *Xtra* solution (OD_{600} = 0.05) (n = 6) or 10 mM $MgCl_2$ (n = 6) as a control using a needles syringe. Two days after the *Xtra* challenge the youngest fully grown systemic leaf of each plant was infiltrated with *Xtra* (OD_{600} = 0.005) (Figure 17.A). The *B. distachyon* resistance of mock and *Xtra* pretreated plants was determined in systemic leaves three days later as described below (see 5.7).

5.7. Assessment of resistance

Growth assays were used to determine the infection level in the differently treated plants allowing conclusion about the degree of infection and therefore the effect of NHP or SAR on plant resistance.

To assess the resistance of *A. thaliana* against *Hpa* infections harvested plants were incubated at 37°C in a trypan blue staining solution (trypan blue (1 mg/ml), 25 % lactic acid, 25 % phenol, 25 % glycerol) while shaking at 200 rpm overnight. The next day the trypan blue solution was replaced with a chloral hydrate solution (2.5 g/ml). The leaves were incubated at 37°C while shaking at 200 rpm overnight again to destain the trypan blue stained leaves. The destaining procedure was repeated at one more time but, if necessary, until the destaining was sufficient. For further analysis the leaves were stored in 50 % glycerol and fixated on glass slides. Pictures

of the stained leaves on glass slides were taken on a light table 2nd the length of internal hyphae (IH) was quantified in ImageJ.

To determine the resistance of *A. thaliana* against *Psm lux* which carries the *Photorhabdus luminescens* luxCDABE operon the luminescens was quantified in leaf discs of infected *A. thaliana* plants using a luminometer as described by Hartmann et al. (2018). To assess the *A. thaliana* resistance against *Chig*, *Bcin* and *Sclero* the infected leaves were harvested in 50 % Glycerol and pictures of the disease symptoms were taken of planar leaves on a light table. The necrotic leaf area was measured for all infection sites using ImageJ and the mean necrotic area was determined for each leaf individually. Afterwards the mean and the standard error of the mean (SEM) were calculated with the mean values of the necrotic area of each leaf. Significant differences were determined using the students t-test in experiment with Col-0 only whereas an ANOVA was performed using SPSS for the statistical analysis of more than one genotype in an experiment.

To determine bacterial growth in *N. tabacum*, *C sativus* and *B. distachyon*, leaf discs were cut out of inoculated leaf material and homogenized in 10 mM $MgCl_2$. Each sample was diluted to an appropriate ratio and plated on solid medium. For *Pstb* and *Psl* growth assays KB plates was used, whereas PSA plates was used in *Xtra* growth assays. The plates were incubated for two to four days at 28 °C before the number of bacterial colonies was counted and significant differences between both treatments were determined using the students t-test.

To test whether NHP has an immunity enhancing effect on *B. distachyon* against infections with *Mgri* the youngest, fully grown leaf at the time of inoculation was removed and bleached in an ethanol-chloroform-solution (4:1) containing 1.5 % trichloroacetic acid. After at least two days of incubation at room temperature the bleaching solution was replaced with H_2O and the leaves were photographed on a light table. Using ImageJ, the percentage of the necrotic area of the leaf was quantified. To determine significant differences between pretreatments the students t-test was used.

5.8. Toxicological assays

To investigate a potential direct toxicological effect of NHP on *Chig* or *Bcin* during the NHP induced resistance in *A. thaliana*, toxicological assays were performed. Therefore, Mathur's

agar plates containing 50 mM NHP or 50 mM NH_4Cl + HCl were prepared. Since NH_4Cl + HCl are generated in the chemical biosynthesis of NHP in equimolar amounts to NHP, NH_4Cl + HCl supplemented plates were used as controls. Agar plugs of equal sizes were taken from fully grown *Chig* or *Bcin* Mathur's agar plates and placed on fresh Mathur's agar plates supplemented with 50 mM NHP or 50 mM NH_4Cl + HCl. Radial mycelium growth on these plates was documented photographically 3 days later and quantified using ImageJ.

5.9. Aniline blue staining and quantification of callose deposits in *Arabidopsis thaliana*

To determine if NHP induces callose deposition in *A. thaliana* and thereby increases resistance, 4,5-week-old plants were watered with a 1 mM NHP solution or H_2O as control treatment. The *Chig* infections and water control treatments of three fully grown leaves were performed 4 h after the pretreatment and samples were taken 2 dpi. Infections with *Bcin* and Mathur's medium control treatments of three fully grown leaves were performed one day after the pretreatment and samples were harvested 1 dpi. Sampled leaves were destained from chlorophyll in an acetic acid / ethanol (1:3) solution. Transparent leaves were washed in 150 mM K_2HPO_4 for 30 min 24 h later. Afterwards the leaves were stained with an anillin blue staining solution (150 mM K_2HPO_4, 0.01 % anillin blue) over night at darkness while shaking (240 rpm). The stained leaves were washed in 150 mM K_2HPO_4 for 30 min to remove the staining solution. Callose deposits were evaluated via fluorescence microscopy (Zeiss Axiophot light microscope, Filter-Set Cyan GFP, F31-044) using the Zen Software. Fluorescent areas per mm^2 were quantified using ImageJ and statistical differences between the treatments were determined with the Kruskal-Wallis Test in SPSS.

5.10. Analysis of plant metabolites by gas chromatography-mass spectrometry

A GC-MS-method based on trimethylation of carboxyl-, hydroxyl- and amino-groups of the sample analytes was used to quantify the accumulation of the targeted plant metabolites (Pip, NHP and SA) upon pathogen attack as previously described in Hartmann et al. (2018).

Therefore, 40-60 mg pulverized frozen leaf tissue were extracted with 1 ml MeOH/H_2O (80:20, v/v) or MeOH/NaPO4 (pH = 6) (80:20, v/v) extraction buffer supplemented with internal standards, including D9-NHP (1 µg) for the quantification of NHP, D9-Pip (1 µg) for the quantification of Pip and D4-SA (0.5 µg) for the quantification of SA. During the extraction step the samples were mixed thoroughly with the extraction buffer by vortexing for 30 sec and then incubated in a shaker at 4 °C for at least 5 min. The samples were then centrifuged (4 min, 14000 rpm) and the resulting pellet was extracted with 1 ml MeOH/H_2O (80:20, v/v) extraction buffer without internal standards. The extraction step was repeated, and the supernatants of both extraction steps were pooled. Aliquots of 400 µL of the extract were evaporated (ScanSpeed vacuum centrifuge, Labogene ApS, Denmark) and dried for subsequent derivatisation. The derivatisation was started by adding 20 µl Pyridine, 20 µl N-Methyl-N-trimethylsilyltrifluoroacetamide (MSTFA) and mixing the samples thoroughly after pipetting. The samples were diluted with 60 µl N-hexane and incubated at 70 °C for 30 min. After cooling (to room temperature) for 30 min the samples were 1:5 diluted with N-hexane and transferred into GC-vials.

Due to liquid raw material in the metabolite analyses of *C. sativus* phloem sap, the extraction and derivatisation methods were adjusted. Metabolite extraction from *C. sativus* phloem sap samples was performed as described above using 500 µl MeOH/H_2O (80:20, v/v) extraction buffer supplemented with internal standards and 400 µl MeOH/H_2O (80:20, v/v) extraction buffer without internal standards. The resulting 1 ml phloem sap extract was evaporated, and derivatisation was performed as describes with minor exception. Instead of 60 N-hexane, 20 ul N-hexane were used in the derivatisation procedure. For GC-MS analyses samples were 1:2 and 1:3 diluted with N-hexane and transferred to GC-vials.

In a gas chromatograph (GC 7890A; Agilent Technologies) 2 µl samples were separated using a silica capillary column (Phenomenex ZB-35; 30 m x 0.25mm x 0.25mm). The following GC oven program was used: initial temperature of 70 °C for 2 min, followed by a gradient to 320 °C at a rate of 10 °C/min, followed by final hold time of 5 min. For the detection of Pip, NHP and SA ion fragments, the mass spectrometer (5975C mass spectrometric detector; Agilent Technologies) was set to electron-ionisation (EI) mode. For the quantification of the individual metabolites peaks from selected chromatograms of a specific m/z ratio were integrated and quantified by relating their peak areas to the peak area of the corresponding internal standard

using the MSD ChemStation software version E.02.01.1177 (Agilent Technologies). Analyzed metabolites and internal standards are summarized in table 2.

Table 2: List of analysed metabolites with retention time, analyzed masses (m/z), and correction factors (CF) for the used internal standard (IST).

Metabolit / **IST**	Retention time	m/z	Used IST	CF
D9-Pip	9.15	165	x	x
Pip	9.24	156	D9-Pip	0.8
D9-NHP	10.4	181	x	x
NHP	10.49	172	D9-NHP	0.82
D4-SA	11.75	271	x	x
SA	11.77	267	D4-SA	0.54
Salicin	21.05	268	x	x
NHPG	21.15	172	salicin	1*
NHPGE	21.54	172	salicin	1*
SAG	21.87	267	salicin	0.68
SGE	21.93	193	salicin	0.18
Camalexin	21.24	272	salicin	0.25
2,x-2,X-DHBA-Gly1	27.30	267	salicin	1*
2,x-2,X-DHBA-Gly2	27.64	267	salicin	1*
IPA	18.38	202	x	x
ICA	17.98	246	IPA	0,49
Norvaline	7.41	144	x	x
Serotonin (3 TMS)	22.68	290	norvaline	1*
Serotonin (4 TMS)	24.83	290	norvaline	1*
PBTS	16.36	293	norvaline	1*

*CFs were not calculated and since were set to 1. For these metabolites thus a relative quantification was performed.

5.11. RNA extraction and cDNA synthesis

To study the influence of a *Psl* infection in *C. sativus* on the *C. sativus ALD1* and *FMO1* gene expression in semi-quantitative PCRs RNA extractions, following cDNA synthesizes were performed with the same frozen leaf material that was used for metabolite analyses. RNA

extractions and cDNA synthesizes were performed with *Psm* inoculated *A. thaliana* leaves sampled 2 dpi to provide a template for the NPR1 cloning procedure.

The frozen leaf material was ground in a beat mill (Tissuelyser II, Qiagen, Hilden, Gemany) and approximately 70 mg of pulverized leaf material was used for the subsequent RNA extraction. The frozen leave material was solved in 1 ml RNAMagic buffer (Bio-Budget Technologies, Krefeld, Germany) by vortexing and incubated at RT for 4 min. Afterwards 200 µl pre-cooled chloroform were added and the samples was shaken by hand for 15 sec and centrifuged for 15 min (12 000 rpm, 4°C) for phase separation. The upper phase was mixed with 500 µl pre-cooled isopropanol by inverting and incubated at RT for 10 min to precipitate the RNA. After another 10 min centrifugation step (12 000 rpm, 4°C) the resulting RNA Pellet was washed two times with 1 ml 75 % Ethanol by vortexing for 15 sec and subsequent centrifugations (5 min, 12 000 rpm, 4°C). The supernatant was discarded, and the RNA Pellet was dried in a Speedvac for 5 min and then incubated in 50 µl RNase and nuclease free water at 58°C to resolve the pellet. To evaluate the quality of the extracted RNA, all samples were incubated with RNA loading buffer and evaluated on an agarose gel (0.5 x TAE Puffer, 1% Agarose, 5 µl Midori Green/100 ml) (Supp. Fig. 1).

RNA concentrations were determined with a Nanodrop 2000 (Thermo Scientific, Massachusetts, USA) and 1000 ng were aliquoted for cDNA Synthesis. The RNA samples were treated with DNase I for 30 min at 37°C to avoid contamination with genomic DNA. The DNase was inactivated with an incubation at 70°C for 15 min with 1 µl 25 mM EDTA. The cDNA was synthesized using the GoScript Reverse Transcription Kit (Promega, Wisconsin, USA) according to instructions. Therefore, per reaction 4 µl Nuclease-Free Water, 4 µl GoScript™ Reaction Buffer, Oligo(dT) and 2 µl GoScript™ Enzyme Mix were combined to a master max of which 10 µl were added to each DNase treated 1000 ng sample aliquot. The reactions were mixed by pipetting and incubated in a thermocycler at 25°C for 5 min for annealing of the primers, at 42°C for 60 min for cDNA extension, at 70°C for 15 min for enzyme inactivation and were then cooled to 4°C. All cDNA samples were diluted in a 1:10 ratio with nuclease free water for subsequent procedures.

5.12. PCR

To confirm the cDNA synthesis control PCRs with the *A. thaliana* housekeeping gene *POLYPYRIMIDINE TRACT-BINDING PROTEIN 1* (*PTB*, At3g01150) or the *C. sativus* housekeeping gene *ACTIN (ACT,* Csa_2G301530) housekeeping genes were performed using the 2 x GoTaq® Green Master Mix (Promega). PCR reaction consisted of 10 µl 2 x GoTaq® Green Master Mix, 1 µl of 10 µM upstream primer, 1 µl of 10 µM downstream primer, 1 µl DNA template (100 ng) and 7 µl nuclease free water. For amplification by PCR the DNA was initially denaturized for 2 min at 95°C. Subsequent PCR cycles were performed with 30 sec denaturation at 95°C, 30 sec annealing at specific temperatures (Table 3) and 1 min extension for every kb at 72°C. Finial extension of the PCR products was achieved at 72°C for 5 min. Afterwards the samples were cooled at 4 °C and evaluated on a 1 % agarose gel.

To study the *ALD1* (Csa_4G179090) and *FMO1* (Csa_018944) gene expression in *C. sativus* in an infection time course with *Psl*, semi-quantitative PCRs were performed with the 2 x GoTaq® Green Master Mix (Promega). The light intensity was measured for each band using ImageJ and relative light intensities to the highest band intensity were calculated. Mean values were visualized in Excel.

To amplify the *A. thaliana* NPR1 (AT1G64280) sequence for subsequent cloning or sequencing procedures PCRs were performed using Phusion Polymerase (NEB, Massachusetts, USA). The 20 µl reactions consisted of 4 µl 5x Phusion HF Buffer, 0.4 µl 10 mM dNTPs, 0.2 µl Phusion DNA Polymerase, 100 ng cDNA template, 1 µl 10 µM Forward Primer and 1 µl 10 µM Reverse Primer (Table 4). Thermocyclers were programmed for an initial denaturation for 30 sec at 98°C. The following PCR cycles were performed with 10 sec denaturation at 98°C, 15 sec annealing at specific temperatures (Table 4) and 30 sec extension for every kb at 72°C. The finial extension of the PCR products was performed at 72°C for 5 min. The samples were cooled at 4 °C in the thermocycler until further visual evaluation on a 1 % agarose gel.

Table 3: Primer sequences and PCR conditions for investigated *Cucumis sativus* and *Arabidopsis thaliana* genes in this study. PCR cycles were repeated 35 times for *PTB*, *ACT* and *FMO1* amplification and 33 times for *ALD1* amplification.

Primer name	Organism	Primer sequence (5´- 3´)	Primer length [bp]	Annealing temperature [C°]	Product length [bp]
*PTB*_for	*A. thaliana*	GATCTGAATGTTAAGGCTTTTAGCG	25	55	61
*PTB*_rev	*A. thaliana*	GGCTTAGATCAGGAAGTGTATAGTCTCTG	29		
*ACT*_for	*C. sativus*	GCATCGCTCAGTACCTTCCA	20	60	189
*ACT*_rev	*C. sativus*	GACCCGTATCTGAGCTCAACC	21		
*FMO1*_for	*C. sativus*	GACTATGCGAAGCTCGACCA	20	59	266
*FMO1*_rev	*C. sativus*	AGGAGGCCTTGATTAGGGGT	20		
*ALD1*_for	*C. sativus*	CCAAATTCGCTGGCTTCACC	20	59	168
*ALD1*_rev	*C. sativus*	TGGAAAGGCAAGCAAGACCA	20		

5.13. Cloning of NPR1

Cloning of NPR1 (AT1G64280, NCBI nucleotide database entry NM_105102.3) into the pET52b(+) plasmid (Novagen, Madison, Wisconsin, USA) was performed with the In-fusion HD cloning Kit (Takara, Kusatsu, Japan) according to manufacturer's instructions. For in-frame cloning the XmaI and SacI restriction sites of the plasmid were chosen for introduction of the *A. thaliana* NPR1 gene. The 50 µl digestion reaction consisted of 1 ug plasmid DNA, 5 µl 10X rCutSmart Buffer (New England Biolabs, Massachusetts, USA), 10 units or 1 µl XmaI (New England Biolabs, Massachusetts, USA), 20 units or 1 µl SacI (New England Biolabs, Massachusetts, USA) and nuclease free water. The digestion was performed at 37°C for 30 min and the restriction enzyme were afterwards heat inactivated at 65°C for 29 min. The digestion was visually verified on a 1% agarose gel. The calculated size for the double digested plasmid is 5197 bp and 5227 bp for the single digested plasmid, which was visually verified by the gel. The XmaI+SacI digested plasmid was purified from the gel using QIAquick Gel Extraction Kit (Qiagen, Hilden, Gemany).

To amplify the *A. thaliana NPR1* gene, five-week-old *A. thaliana* plants were infected with *Psm* OD_{600} = 0.001 as described before. Leaf samples were harvested 2 dpi, shock frozen in liquid nitrogen and stored at -80°C. RNA extractions and cDNA synthesis was performed as described. The *NPR1* Primers were designed using the provided Takara online primer design tool (https://www.takarabio.com/learning-centers/cloning/primer-design-and-other-tools, Table 4).

Table 4: Primer sequences used for NPR1 cloning. Primer design was performed with the Takara online primer design tool. PCR cycles were repeated 35 times.

Primer name	Primer sequence (5´- 3´)	Length [bp]	Annealing Temperature [°C]
npr1_F1_Inf	CGTGGCACCAGAGCGAGCTCATGGACACCACCATTGATGGATTCG	45	64
npr1_R1_Inf	CTTTCAGGGACCCGGGTCACCGACGACGATGAGAGAG	37	64

The PCR was performed using Phusion polymerase as described above. The NPR1 PCR fragments with a predicted length of 1812 bp (15 bp for each overhang created by the primers and 1782 bp for NPR1) were purified from a 1% agarose gel using the QIAquick Fel Extraction Kit (Qiagen, Hilden, Gemany).

Ligation using the In-fusion HD Cloning Kit

The ligation was performed using the In-fusion HD cloning Kit (Takara, Kusatsu, Japan) according to the manufacturer's instructions. To ligate the purified NPR1 PCR product and the linearized pET52b(+) plasmid the In-fusion cloning procedure was performed as recommended in a 2:1 ratio using 100 ng of purified PCR product and 50 ng of linearized pET52b(+) plasmid. The purified PCR product and linearized plasmid were combined with 2 µl of the provided 5x In Fusion HD Enzyme Premix and the reaction volume was filled up to 10 µl with deionized water. A positive control with a in the kit provided control insert and control plasmid and negative control was performed without an insert but with the linearized pET52b(+) plasmid. All reactions were incubated at 50°C for 15 min. The resulting ligated plasmids were stored on ice and transformed immediately.

Transformation

The ligated plasmids were transformed into competent E. coli Stellar cells (Takara). The cells were removed from the -80°C freezer and thawed on ice for 5-10 min before use. In fresh sterile tubes 50 µl of the thawed cells and 2.5 µl of the ligation mix was combined, mixed by flicking and incubated on ice for 30 min. Subsequently the cells were exposed to a heat shock at 42°C for exactly 45 sec and placed on ice for 1-2 min. SOB-Medium (Takara, Kusatsu, Japan) was prewarmed at 37°C and 450 µl were added to each reaction. Afterwards the transformation reactions were incubated at 37°C while shaking at 200 rpm for 1 h and plated on LB plates containing chloramphenicol (35 µg/ml) to select for the pET52b(+) plasmid and

ampicillin (50 µg/ml) to select for the competent Stellar cells. The control reactions were plated on LB containing only ampicillin since the control plasmid carries an ampicillin resistance. The plates were incubated at 37°C overnight and colonies were visible on the NPR1-pET52b(+) transformant and the positive control, while no colonies were observed on the negative control plates.

Colonies of were picked and grown in LB (35 µg/ml chloramphenicol, 50 µg/ml ampicillin) overnight while shaking (240 rpm). On the next day the plasmids were purified using the PureYield™ Plasmid Miniprep System (Promega, Wisconsin, USA) and concentration were measured using a Nanodrop 2000 (Thermo Scientific, Massachusetts, USA). To determine the presence of an insert PCRs using T7 primers were performed (Figure 6) using the Phusion polymerase as described.

Afterwards a 1 % agarose gel was prepared to evaluate the PCR results. Bands of the size of NPR1 (1782 bp) were purified from the gel, the concentration was determined using a Nanodrop 2000 (Thermo Scientific, Massachusetts, USA) and the PCR products were sent for sequencing at Eurofins Genomics (Ebersberg, Germany). Alignments of the sequencing results with the NPR1 Sequence identified plasmids with the desired inserted sequence.

5.14. Mutagenesis of NPR1

To generate a point mutation in the cloned NPR1 sequence at the residue 432 which results in an amino acid change of arginine to glutamine and thereby disrupts SA binding of NPR1 (Ding et al. 2018) the Q5 site directed mutagenesis kit (New England Biolabs, Massachusetts, USA) was used with minor adjustments to the manufacturer's instructions. The initial PCR reaction was performed as recommended. Back-to-back primers carrying the desired point mutation were designed using the NEBaseChanger (nebasechanger.neb.com) tool (Table 5).

Table 5: Primer Sequences for the mutagenesis of the residue 432 of the *A. thaliana NPR1* sequence from arginine to glutamine. Primer designed was performed using the NEBaseChanger (nebasechanger.neb.com) tool.

Primer name	Primer sequence (5'-3')	Length [bp]	Annealing Temperature [°C]
$NPR1^{R432Q}$_F	TCTTGAAAATCAGGTTGCACTTGCTCAACG	30	62
$NPR1^{R432Q}$ _R	TCGAGCAGCGTCATCTTC	18	62

The 25 µl PCR reaction consisted of 12.5 µl Q5 Hot Start High-Fidelity 2X Master Mix, 1.25 µl 10 µM forward primer, 1.25 µl 10 µM reverse primer, 10 ng in 1 µl template plasmid DNA, and nuclease-free water. For amplification the initial denaturation was achieved at 98°C for 30 sec, following PCR cycles were repeated 25 times and had a denaturation at 98°C for 10 sec, an annealing temperature of 62°C for 30 sec, and an extension at 72°C for 30 sec for each amplified kb. The final extension was performed at 72°C for 2 min. The resulting PCR products is the linearized plasmid carrying the desired $NPR1^{R432Q}$ point mutation which was stored at 4°C until further use.

To result a circular plasmid and to eliminate the wildtype NPR1 plasmid a KLD (Kinase, Ligase, DpnI) treatment of the PCR product was performed. The 10 µl reactions consisted of 1 µl PCR product, 5 µl 2 x KLD Reaction Buffer, 1 µl 10 x KLD Enzyme Mix and nuclease-free water. To phosphorylate the linearized point mutation carrying plasmid, ligate it and remove the wildtype *NPR1* plasmid the reactions were incubated at room temperature for 5 minutes and then directly transformed into competent *E. coli* Stellar cells as described before. The $NPR1^{R432Q}$ point mutation in the *NPR1* Sequence was verified via sequencing.

5.15. Verification of correct cloning

To verify correct cloning of the *A. thaliana* NPR1 sequence in the pET52b(+) plasmid, 50 µl Phusion PCRs were performed as described with primers for the T7 promotor and terminator of the plasmid (Figure 35, Table 6). For documentation and to assure the amplified fragments are of the expected size of 2047 bp, 5 µl of the PCR products were evaluated on a 1% agarose gel. The other 45 µl were evaluated on another 1% agarose gel and the bands of 2047 bp size were cut out of the gel on a light table using as little UV-light as possible to avoid DNA damage.

Table 6: Primer sequences of primers used for *A. thaliana NPR1* (wildtype and mutant) sequencing.

Primer name	Primer sequence (5'-3')	Length [bp]	Annealing Temperature [°C]
T7term	CTAGTTATTGCTCAGCGGT	19	58
T7-pET-mod	CCCGCGAAATTAATACGACTCAC	23	58
NPR1_Seq_FW-718	TCATTGCCGGAAGAGCTTGT	20	58

The gel slices were weighted, and the DNA was extracted from the gel using the QIAquick Gel Extraction Kit (Qiagen, Hilden, Gemany). DNA concentrations were determined with a Nanodrop 2000 (Thermo Scientific, Massachusetts, USA). For sequencing 15 µl (10 ng/µl) aliquots were prepared for each sample and 2 µl of a 10 µM primer was added. The primers for the T7 promotor and terminator were used for sequencing as well as third primer which started sequencing the middle of the NPR1 (Table 6). The performed $NPR1^{R432Q}$ Mutagenesis was verified in the same manner.

5.16. Expression and purification of Strep tagged NPR1 protein

To induce protein expression, a starter culture of a single positive Lemo21 clone was grown overnight at 37°C while shaking in 3 ml LB medium (chloramphenicol (35 µg/ml), ampicillin (50 µg/ml)). Of the grown culture 1 ml was added to 400 ml fresh LB medium containing 1 % Ethanol, chloramphenicol (35 µg/ml) and ampicillin (50 µg/ml) in 2 l Erlenmeyer flask. The culture was grown until OD_{600} = 0.5 at 37°C while shaking at 240 rpm when the culture was stored on ice to induce protein expression by adding 400 µM Isopropyl-β-D-thiogalactopyranosid (IPTG). As a control, a second culture was not treated with IPTG and was further treated as described for the IPTG induced culture. Proteins were expressed overnight at 16°C while shaking at 240 rpm. The bacterial pellets were collected by centrifuging the culture at 3 220 g for 15 min at 4°C in a swing bucket centrifuge (Eppendorf 5810R). The resulting pellet was resuspended in 8 ml Lysis Buffer and sonicated (Digital Sonifier W-250 D, Branson Ultrasonic Corporation) for 2 min (10% amplitude 20 sec impulse, 20 sec pause) to lyse the *E. coli* cells. The cell lysate was then centrifuged at 25 000 g for 30 min. At this point aliquots of the IPTG induced an uninduced lysate were taken for a SDS gel and the uninduced lysate was not used in the further described purification process. For biotin blocking 1 U Avidin / µg estimated biotin in the lysate (*E. coli* = 1.75 µg / [l/OD]) was added and the lysate was centrifuged at 25 000 g for 30 min again. Afterwards the soluble protein in the supernatant was filtered through a low protein binding 0.22 µm nylon filter and then purified using a 1 ml Strep-Tactin™XT Superflow™ High Capacity Cartridge (IBA Lifesciences, Göttingen, Germany) connected to a Biorad NGC system (Bio-Rad Laboratories, Hercules, California, USA). The cartridge was connected with the chromatography workstation and washed with 5 column volumes (CV) wash buffer (W: 100 mM Tris/HCl pH 8.0, 150 mM NaCl,

1 mM EDTA) with a flowrate of 1 ml/min. The cell lysate was applied to the column afterwards with a flow rate of 0.5 ml/min and the flowthrough was collected for SDS-PAGE analysis. The Strep-tactin column with bound recombinant protein was washed with 5 CV wash buffer until A_{280} was stable 2nd all fractions were collected for SDS-PAGE analysis as well. To elute the protein from the column a gradient of 2 CV elution buffer (EB: 100 mM Tris/HCl, pH 8.0, 150 mM NaCl, 1 mM EDTA, 2.5 mM biotin) from 0 - 100% was applied prior to 5 CV EB and elution fractions were collected for SDS-PAGE analysis. Aliquots of all collected fractions in the purification process were mixed with 5 x SDS-PAGE loading buffer (250 mM Tris, pH 7, 0.5 % (w/v) Bromphenolblue, 10 % (w/v) SDS, 50 % (v/v) glycerin, 25 % (v/v) ß-Mercaptoethanol) and incubated at 95°C for 5 min immediately to break all the disulfide bonds and denature the protein. Samples were stored on ice or were stored at -80°C until they were loaded on the SGS-PAGE gel.

The elution fractions containing the protein (fraction 1-3) were combined and centrifuged in a 5 ml 30 kDA cut-off concentrator (Vivaspin 6, Sartorius Stedim Lab Ltd, Stonehouse, United Kingdom) according to the manufacturer's instructions at 4000 g at 4°C until the volume of the protein solution was reduced to 0.5 ml. The protein solution was transferred to a 0.5 ml 30 kDA cut-off Millipore's Amicon® Ultra-0.5 centrifugal filter (Merck Millipore, Burlington, Massachusetts, USA) and centrifuged at 14 000 g at 4°C until the volume was reduced to 100 µl. For buffer exchange 400 µl 1 x PBS buffer pH = 7.4 was added to the 0.5 ml concentrator which was subsequently centrifuged at 14 000 g at 4 °C until the volume was reduced to approximately 100 µl. To the 0.5 ml concentrator 400 µl 1 x PBS buffer are added again and the procedure is repeated 5 times to assure a sufficient buffer exchange. An aliquot of the concentrated and rebuffered elution fractions was mixed with 5 x SDS-PAGE loading buffer and incubated at 95°C for 5 min.

The total protein concentration of the concentrated and rebuffered elution fractions was determined with a Bradford assay. Therefore, 10 µl of protein sample was diluted with 200 µl Bradford Reagent (Sigma-Aldrich, Missouri, USA) and absorptions were measured with a Tecan infinite m200 pro (Tecan Group, Männedorf, Switzerland) at 595 nm. To verify the NPR1 expression, an SDS-polyacrylamide gel was prepared consisting of a 5 % stacking gel (5 % polyacrylamide [v/v], 0.5 M Tris pH = 6.8, 0.4 % SDS [w/v], 0.1 % ammonium persulfate (APS) [w/v], 1 µl ml^{-1} Tetramethylethylendiamin (TEMED)) and a 12 % separating gel

(12 % polyacrylamide [v/v], 1.5 M Tris pH = 8.8, 0.4 % SDS [w/v], 0.1 % APS [w/v], 1 µl ml^{-1} TEMED). Protein samples (5 µl) were loaded onto the SDS-PAGE and run in a gel chamber for 30 min at 90 V and 1 h for 150 V in SDS running buffer (0.025 M Tris pH = 8.8, 0.193 M glycine, 0.1 % SDS [w/v]). SDS-PAGE were finally washed with water for three times and afterwards stained with coomassie blue for at least 30 min while shaking using Fastgene Q stain buffer (Nippon Genetics Europe GmbH, Düren, Germany).

Western Blot

To visualize the tagged proteins and their potential degradation products on the SDS-PAGE, western blots were performed with an antibody for the NPR1 protein and a Strep-Tactin horse radish peroxidase conjugate which binds the C-terminal cloned Strep tag. The proteins were blotted to a Hybond-P 0.45 µm PVDF membrane (Amersham Biosciences, Amersham, England) which was incubated for 10 min in 100 % Ethanol before use. The electrotransfer of the protein from the SDS gel to the membrane was performed for 1 h at 70 V in transfer buffer (25 mM Tris, 192 mM Glycerin, 15 % Methanol). Afterwards the membrane showed the transferred pre-stained ladder and was blocked for 30 min in 5% milk powder in TBST (50 mM Tris-HCl, 150 mM NaCl, 0,05 % Tween20, pH = 7.5). The strep-tactin horse radish peroxidase conjugate (IBA Lifesciences, Göttingen, Germany) was then applied for 1 h in a 1:1000 dilution in 2.5 % milk powder in TBST. The incubation with the antibody was followed by four wash streps with TBST. For direct detection of the NPR1 protein the membrane was incubated with 1 : 1000 diluted rabbit anti - NPR1 antibody (Agrisera, Vännäs, Sweden) in 2.5 % milk powder in TBST for 1 h and then washed four 4 times in TBST. Subsequently the membrane was incubated in 1 : 100 000 diluted Anti-rabbit IgG Antibody (Peroxidase Antibody produced in goat, Sigma-Aldrich, Missouri, USA) in 2.5 % milk powder in TBST for 1 h. To remove the antibody the membrane was washed four times with TBST. Before chemiluminescent detection of the antibody bound NPR1 protein or Strep-tag the membrane was incubated for 5 min with ECL Prime Western Blotting Detection Reagent (Amersham Biosciences, Amersham, England) and the luminescence was measured in a FlourChem Q (Proteinsimple™, SanJose, CA, USA). The visible bands were finally analyzed using the Alpha View Software (Proteinsimple™, SanJose, CA, USA).

5.17. NPR1 binding assays

The NPR1 protein binds SA which allows the protein to function as co-activator of SA transmitted signaling and system acquired resistance (Wu et al.2012, Fu and Dong 2013). Since the NHP and SA molecules share similar hydroxyl and carboxyl group arrangements and NHP is a central player in SAR as well as SA the NPR1 binding to NHP was investigated. To gain further insight into the binding of SA to NPR1, the binding of SA to the generated $NPR1^{R432Q}$ mutant was tested.

To test the NPR1 binding to SA and NHP, binding reactions were performed in 50 µl 1 x PBS (pH = 7.4) in 1.5 ml tubes. Each binding reaction contained 50 µg of the purified and PBS buffered NPR1 protein and 200 µM SA or NHP. For each binding reaction a SA or NHP control without protein was performed. To compare the SA binding of NPR1 to the SA binding of the generated $NPR1^{R432Q}$ mutant, binding reactions were performed in 50 µl 1 x PBS (pH = 7.4) in 1.5 ml tubes as well. To test unspecific binding of SA to proteins a BSA control was included. The binding reactions contained 50 µg of the purified and PBS buffered NPR1, $NPR1^{R432Q}$ protein or BSA and 500 µM SA. Additionally, a control reaction with 500 µM SA without protein was set up.

All binding reactions were carefully spined down with a tabletop mini-centrifuged and incubated at 4°C for one hour. In the meantime, PD MiniTrap G-25 (GE Healthcare Bio-Sciences AG, Uppsala, Sweden) were equilibrated with 1 x PBS (pH = 7.4) by washing the columns 5 times with 400 µl 1 x PBS Puffer (pH = 7.4) and intermediate centrifugation steps for 1 min at 800 g (4°C) as recommended. After one hour of incubation the binding reaction and described controls were applied to the center of the size-exclusion columns (SEC) and the columns were immediately centrifuged for 2 min at 750 g (4°C). For each NPR1 binding reaction a SA or NHP control reaction without protein was set up and not applied to a SEC to calculate the percentage of bound SA to the SA input. The SA or NHP control reaction without protein that was applied to the column assures the efficiency of the SEC method and verified in every scenario that applied SA or NHP without a protein remained in the column after centrifugation.

To quantify the amounts SA and NHP in the binding and control reactions via GC-MS a 50 µl MeOH/H_2O (80:20, v/v) buffer with 1 µg/ml D9-NHP and 0.5 µg/µl D4-SA was added to each

sample and all liquids were evaporated in a ScanSpeed vacuum centrifuge (LaboGene ApS, Denmark). For TMS derivatization 10 µl Pyridine and 10 µl MSTFA/(1%)TCMS were added to each sample and afterwards the samples were vortexed for at least 30 sec. To collect the liquids in the tube all samples were centrifuged at max. speed for 30 sec. The samples were incubated at 70 °C for 30 min and subsequently the tubes were centrifuged at max. speed for 30 sec again. The remaining 12 – 15 µl liquid in tube were transferred to a GC-vail and mixed with 50 µl N-hexane.

The binding reactions and control scenarios were finally analyzed in a gas chromatograph (GC 7890A; Agilent Technologies), which separated 2 µl samples using a silica capillary column (Phenomenex ZB-35; 30 m x 0.25mm x 0.25mm) with the before described oven program. For the detection of NHP and SA ion fragments, the mass spectrometer (5975C mass spectrometric detector; Agilent Technologies) was set to single ion mode (SIM). Only fragments ions with the m/z of 172, 181, 267 and 271 were detected. Peaks were quantified as described before using the MSD ChemStation software version E.02.01.1177 (Agilent Technologies). For quantification ratios between NHP (m/z 172) and its internal standard D9-NHP (m/z 181) and SA (m/z 267) and its internal standard D4-SA (m/z 271) were calculated. Statistical differences were determined with an ANOVA in SPSS.

5.18. Statistical analyses

In this study the number of biological replicates as well as the type of performed statistical tests are indicated in the respective figure legends. The indicated two-tailed Student's *t*-tests were performed in Microsoft Excel, for pairwise comparisons of two distinct treatments. For comparisons of multiple groups, ANOVA or Kruskal-Wallis tests were performed using the SPSS statistical software version 26 (IBMVR Corporation, Armonk, NY USA). Comparisons of multiple groups in growth assays were executed by an analysis of variance (ANOVA) and a post hoc Tukey's HSD test (significance level $p < 0.05$). The comparison of multiple groups in metabolite analyses, quantifications of Callose deposition and NPR1 binding assays were performed with a nonparametric one-way ANOVA according to Kruskal–Wallis with a stepwise step-down comparison (significance level $p < 0.05$). The here presented experiments were repeated at least two times showing reproducible results. Only *H. vulgare* infections with *Mory*

and *A. thaliana* infections with *Sclero* were, in cooperation with other research groups, just performed once.

6. References

Abeles, F. B., Morgan, P. W., & Saltveit Jr, M. E. (2012). *Ethylene in plant biology*. Academic press.

Abeysekara, N. S., Swaminathan, S., Desai, N., Guo, L., & Bhattacharyya, M. K. (2016). The plant immunity inducer pipecolic acid accumulates in the xylem sap and leaves of soybean seedlings following *Fusarium virguliforme* infection. *Plant Science*, *243*, 105-114.

Adie, B. A., Pérez-Pérez, J., Pérez-Pérez, M. M., Godoy, M., Sánchez-Serrano, J. J., Schmelz, E. A., & Solano, R. (2007). ABA is an essential signal for plant resistance to pathogens affecting JA biosynthesis and the activation of defenses in Arabidopsis. *The Plant Cell*, *19*(5), 1665-1681.

Ahuja, I., Kissen, R., & Bones, A. M. (2012). Phytoalexins in defense against pathogens. *Trends in plant science*, *17*(2), 73-90.

Alfonso, E., Stahl, E., Glauser, G., Bellani, E., Raaymakers, T. M., Van den Ackerveken, G., ... & Reymond, P. (2021). Insect eggs trigger systemic acquired resistance against a fungal and an oomycete pathogen. *New Phytologist*, *232*(6), 2491-2505.

Amselem, J., Cuomo, C. A., van Kan, J. A., Viaud, M., Benito, E. P., Couloux, A., ... & Dickman, M. (2011). Genomic analysis of the necrotrophic fungal pathogens *Sclerotinia sclerotiorum* and *Botrytis cinerea*. *PLoS genetics*, *7*(8), e1002230.

Anderson, J. P., Badruzsaufari, E., Schenk, P. M., Manners, J. M., Desmond, O. J., Ehlert, C., ... & Kazan, K. (2004). Antagonistic interaction between abscisic acid and jasmonate-ethylene signaling pathways modulates defense gene expression and disease resistance in Arabidopsis. *The Plant Cell*, *16*(12), 3460-3479.

Arnold, D. L., & Preston, G. M. (2019). *Pseudomonas syringae*: Enterprising epiphyte and stealthy parasite. *Microbiology*, *165*(3), 251-253.

Ashfield, T., Ong, L. E., Nobuta, K., Schneider, C. M., & Innes, R. W. (2004). Convergent evolution of disease resistance gene specificity in two flowering plant families. *The Plant Cell*, *16*(2), 309-318.

Auh, C. K., & Murphy, T. M. (1995). Plasma membrane redox enzyme is involved in the synthesis of O2-and H2O2 by Phytophthora elicitor-stimulated rose cells. *Plant Physiology*, *107*(4), 1241-1247.

Bailey, K., Çevik, V., Holton, N., Byrne-Richardson, J., Sohn, K. H., Coates, M., ... & Tör, M. (2011). Molecular cloning of ATR5Emoy2 from *Hyaloperonospora arabidopsidis*, an avirulence

determinant that triggers RPP5-mediated defense in Arabidopsis. *Molecular plant-microbe interactions*, *24*(7), 827-838.

Bajwa, V. S., Shukla, M. R., Sherif, S. M., Murch, S. J., & Saxena, P. K. (2015). Identification and characterization of serotonin as an anti-browning compound of apple and pear. *Postharvest Biology and Technology*, *110*, 183-189.

Bartsch, M., Bednarek, P., Vivancos, P. D., Schneider, B., von Roepenack-Lahaye, E., Foyer, C. H., ... & Parker, J. E. (2010). Accumulation of isochorismate-derived 2, 3-dihydroxybenzoic 3-O-β-D-xyloside in Arabidopsis resistance to pathogens and ageing of leaves. *Journal of Biological Chemistry*, *285*(33), 25654-25665.

Bartsch, M., Gobbato, E., Bednarek, P., Debey, S., Schultze, J. L., Bautor, J., & Parker, J. E. (2006). Salicylic acid–independent ENHANCED DISEASE SUSCEPTIBILITY1 signaling in Arabidopsis immunity and cell death is regulated by the monooxygenase FMO1 and the nudix hydrolase NUDT7. *The Plant Cell*, *18*(4), 1038-1051.

Bauer, S., Mekonnen, D. W., Hartmann, M., Yildiz, I., Janowski, R., Lange, B., ... & Schäffner, A. R. (2021). UGT76B1, a promiscuous hub of small molecule-based immune signaling, glucosylates N-hydroxypipecolic acid, and balances plant immunity. *The Plant Cell*, *33*(3), 714-734.

Baxter, L., Tripathy, S., Ishaque, N., Boot, N., Cabral, A., Kemen, E., ... & Tyler, B. M. (2010). Signatures of adaptation to obligate biotrophy in the *Hyaloperonospora arabidopsidis* genome. *science*, *330*(6010), 1549-1551.

Bednarek, P. (2012). Chemical warfare or modulators of defence responses–the function of secondary metabolites in plant immunity. *Current opinion in plant biology*, *15*(4), 407-414.

Bednarek, P., & Osbourn, A. (2009). Plant-microbe interactions: chemical diversity in plant defense. *Science*, *324*(5928), 746-748.

Bednarek, P., Schneider, B., Svatos, A., Oldham, N. J., & Hahlbrock, K. (2005). Structural complexity, differential response to infection, and tissue specificity of indolic and phenylpropanoid secondary metabolism in Arabidopsis roots. *Plant physiology*, *138*(2), 1058-1070.

Bellés, J. M., Garro, R., Fayos, J., Navarro, P., Primo, J., & Conejero, V. (1999). Gentisic acid as a pathogen-inducible signal, additional to salicylic acid for activation of plant defenses in tomato. *Molecular plant-microbe interactions*, *12*(3), 227-235.

Bender, J., & Celenza, J. L. (2009). Indolic glucosinolates at the crossroads of tryptophan metabolism. *Phytochemistry Reviews*, *8*(1), 25-37.

Berens, M. L., Berry, H. M., Mine, A., Argueso, C. T., & Tsuda, K. (2017). Evolution of hormone signaling networks in plant defense. *Annual review of phytopathology*, *55*, 401-425.

Bernsdorff, F., Döring, A. C., Gruner, K., Schuck, S., Bräutigam, A., & Zeier, J. (2016). Pipecolic acid orchestrates plant systemic acquired resistance and defense priming via salicylic acid-dependent and-independent pathways. *The Plant Cell*, *28*(1), 102-129.

Beßer, K., Jarosch, B., Langen, G., & Kogel, K. H. (2000). Expression analysis of genes induced in barley after chemical activation reveals distinct disease resistance pathways. *Molecular Plant Pathology*, *1*(5), 277-286.

Birkenbihl, R. P., Diezel, C., & Somssich, I. E. (2012). Arabidopsis WRKY33 is a key transcriptional regulator of hormonal and metabolic responses toward *Botrytis cinerea* infection. *Plant physiology*, *159*(1), 266-285.

Birker, D., Heidrich, K., Takahara, H., Narusaka, M., Deslandes, L., Narusaka, Y., ... & O'Connell, R. (2009). A locus conferring resistance to *Colletotrichum higginsianum* is shared by four geographically distinct Arabidopsis accessions. *The Plant Journal*, *60*(4), 602-613.

Bleecker, A. B., & Kende, H. (2000). Ethylene: a gaseous signal molecule in plants. *Annual review of cell and developmental biology*, *16*(1), 1-18.

Block, A., Schmelz, E., Jones, J. B., & Klee, H. J. (2005). Coronatine and salicylic acid: the battle between Arabidopsis and Pseudomonas for phytohormone control. *Molecular Plant Pathology*, *6*(1), 79-83.

Bohman, S., Staal, J., Thomma, B. P., Wang, M., & Dixelius, C. (2004). Characterisation of an Arabidopsis–*Leptosphaeria maculans* pathosystem: resistance partially requires camalexin biosynthesis and is independent of salicylic acid, ethylene and jasmonic acid signalling. *The Plant Journal*, *37*(1), 9-20.

Bolwell, G. P., & Daudi, A. (2009). Reactive oxygen species in plant–pathogen interactions. In *Reactive oxygen species in plant signaling* (pp. 113-133). Springer, Berlin, Heidelberg.

Boutrot, F., & Zipfel, C. (2017). Function, discovery, and exploitation of plant pattern recognition receptors for broad-spectrum disease resistance. *Annual review of phytopathology*, *55*, 257-286.

Bussell, J. D., Reichelt, M., Wiszniewski, A. A., Gershenzon, J., & Smith, S. M. (2014). Peroxisomal ATP-binding cassette transporter COMATOSE and the multifunctional protein abnormal INFLORESCENCE MERISTEM are required for the production of benzoylated metabolites in Arabidopsis seeds. *Plant Physiology*, *164*(1), 48-54.

Cao, H., Bowling, S. A., Gordon, A. S., & Dong, X. (1994). Characterization of an Arabidopsis mutant that is nonresponsive to inducers of systemic acquired resistance. *The Plant Cell*, *6*(11), 1583-1592.

Catanzariti, A. M., Dodds, P. N., & Ellis, J. G. (2007). Avirulence proteins from haustoria-forming pathogens. *FEMS microbiology letters*, *269*(2), 181-188.

Chanda, B., Venugopal, S. C., Kulshrestha, S., Navarre, D. A., Downie, B., Vaillancourt, L., ... & Kachroo, P. (2008). Glycerol-3-phosphate levels are associated with basal resistance to the hemibiotrophic fungus *Colletotrichum higginsianum* in Arabidopsis. *Plant physiology*, *147*(4), 2017-2029.

Chang, M., Zhao, J., Chen, H., Li, G., Chen, J., Li, M., ... & Fu, Z. Q. (2019). PBS3 protects EDS1 from proteasome-mediated degradation in plant immunity. *Molecular plant*, *12*(5), 678-688.

Chen, F., D'Auria, J. C., Tholl, D., Ross, J. R., Gershenzon, J., Noel, J. P., & Pichersky, E. (2003). An *Arabidopsis thaliana* gene for methylsalicylate biosynthesis, identified by a biochemical genomics approach, has a role in defense. *The Plant Journal*, *36*(5), 577-588.

Chen, H. Y., & Li, X. (2017). Identification of a residue responsible for UDP-sugar donor selectivity of a dihydroxybenzoic acid glycosyltransferase from Arabidopsis natural accessions. *The Plant Journal*, *89*(2), 195-203.

Chen, Y. C., Holmes, E. C., Rajniak, J., Kim, J. G., Tang, S., Fischer, C. R., ... & Sattely, E. S. (2018). N-hydroxy-pipecolic acid is a mobile metabolite that induces systemic disease resistance in Arabidopsis. *Proceedings of the National Academy of Sciences*, *115*(21), E4920-E4929.

Chezem, W. R., Memon, A., Li, F. S., Weng, J. K., & Clay, N. K. (2017). SG2-type R2R3-MYB transcription factor MYB15 controls defense-induced lignification and basal immunity in Arabidopsis. *The Plant Cell*, *29*(8), 1907-1926.

Chinchilla, D., Bauer, Z., Regenass, M., Boller, T., & Felix, G. (2006). The Arabidopsis receptor kinase FLS2 binds flg22 and determines the specificity of flagellin perception. *The Plant Cell*, *18*(2), 465-476.

Chini, A., Fonseca, S. G. D. C., Fernandez, G., Adie, B., Chico, J. M., Lorenzo, O., ... & Solano, R. (2007). The JAZ family of repressors is the missing link in jasmonate signaling. *Nature*, *448*(7154), 666-671.

Clarke, J. D., Volko, S. M., Ledford, H., Ausubel, F. M., & Dong, X. (2000). Roles of salicylic acid, jasmonic acid, and ethylene in cpr-induced resistance in Arabidopsis. *The Plant Cell*, *12*(11), 2175-2190.

Coates, M. E., & Beynon, J. L. (2010). *Hyaloperonospora arabidopsidis* as a pathogen model. *Annual review of phytopathology*, *48*, 329-345.

Cui, W., & Lee, J. Y. (2016). Arabidopsis callose synthases CalS1/8 regulate plasmodesmal permeability during stress. *Nature plants*, *2*(5), 1-9.

De Cremer, K., Mathys, J., Vos, C., Froenicke, L., Michelmore, R. W., CAMMUE, B. P. A., & De Coninck, B. (2013). RNA seq-based transcriptome analysis of *Lactuca sativa* infected by the fungal necrotroph *Botrytis cinerea*. *Plant, cell & environment*, *36*(11), 1992-2007.

De Silva, D. D., Crous, P. W., Ades, P. K., Hyde, K. D., & Taylor, P. W. (2017). Life styles of Colletotrichum species and implications for plant biosecurity. *Fungal Biology Reviews*, *31*(3), 155-168.

Dean, J. V., & Delaney, S. P. (2008). Metabolism of salicylic acid in wild-type, ugt74f1 and ugt74f2 glucosyltransferase mutants of *Arabidopsis thaliana*. *Physiologia plantarum*, *132*(4), 417-425.

Dean, R., Van Kan, J. A., Pretorius, Z. A., Hammond-Kosack, K. E., Di Pietro, A., Spanu, P. D., ... & Foster, G. D. (2012). The Top 10 fungal pathogens in molecular plant pathology. *Molecular plant pathology*, *13*(4), 414-430.

Delaney, T. P., Uknes, S., Vernooij, B., Friedrich, L., Weymann, K., Negrotto, D., ... & Ryals, J. (1994). A central role of salicylic acid in plant disease resistance. *Science*, *266*(5188), 1247-1250.

Dempsey, D. M. A., Vlot, A. C., Wildermuth, M. C., & Klessig, D. F. (2011). Salicylic acid biosynthesis and metabolism. *The Arabidopsis book/American Society of Plant Biologists*, *9*.

Dempsey, D., & Klessig, D. F. (2017). How does the multifaceted plant hormone salicylic acid combat disease in plants and are similar mechanisms utilized in humans?. *BMC biology*, *15*(1), 1-11.

Desikan, R., Hancock, J. T., Bright, J., Harrison, J., Weir, I., Hooley, R., & Neill, S. J. (2005). A role for ETR1 in hydrogen peroxide signaling in stomatal guard cells. *Plant physiology*, *137*(3), 831-834.

Ding, L. N., Yang, G. X., Yang, R. Y., Cao, J., & Zhou, Y. (2016). Investigating interactions of salicylic acid and jasmonic acid signaling pathways in monocots wheat. *Physiological and Molecular Plant Pathology*, *93*, 67-74.

Ding, Y., Sun, T., Ao, K., Peng, Y., Zhang, Y., Li, X., & Zhang, Y. (2018). Opposite roles of salicylic acid receptors NPR1 and NPR3/NPR4 in transcriptional regulation of plant immunity. *Cell*, *173*(6), 1454-1467.

Ding, Y., Sun, T., Ao, K., Peng, Y., Zhang, Y., Li, X., & Zhang, Y. (2018). Opposite roles of salicylic acid receptors NPR1 and NPR3/NPR4 in transcriptional regulation of plant immunity. *Cell*, *173*(6), 1454-1467.

Dixon, R. A. (2001). Natural products and plant disease resistance. *Nature*, *411*(6839), 843-847.

Djamei, A., Schipper, K., Rabe, F., Ghosh, A., Vincon, V., Kahnt, J., ... & Kahmann, R. (2011). Metabolic priming by a secreted fungal effector. *Nature*, *478*(7369), 395-398.

Du Fall, L. A., & Solomon, P. S. (2013). The necrotrophic effector S n T ox A induces the synthesis of a novel phytoalexin in wheat. *New Phytologist*, *200*(1), 185-200.

Duan, L., Liu, H., Li, X., Xiao, J., & Wang, S. (2014). Multiple phytohormones and phytoalexins are involved in disease resistance to *Magnaporthe oryzae* invaded from roots in rice. *Physiologia plantarum*, *152*(3), 486-500.

Ellis, C., Karafyllidis, I., & Turner, J. G. (2002). Constitutive activation of jasmonate signaling in an Arabidopsis mutant correlates with enhanced resistance to *Erysiphe cichoracearum*,

Pseudomonas syringae, and *Myzus persicae*. *Molecular Plant-Microbe Interactions*, *15*(10), 1025-1030.

Ferrari, S., Galletti, R., Denoux, C., De Lorenzo, G., Ausubel, F. M., & Dewdney, J. (2007). Resistance to *Botrytis cinerea* induced in Arabidopsis by elicitors is independent of salicylic acid, ethylene, or jasmonate signaling but requires PHYTOALEXIN DEFICIENT3. *Plant physiology*, *144*(1), 367-379.

Ferrari, S., Plotnikova, J. M., De Lorenzo, G., & Ausubel, F. M. (2003). Arabidopsis local resistance to *Botrytis cinerea* involves salicylic acid and camalexin and requires EDS4 and PAD2, but not SID2, EDS5 or PAD4. *The Plant Journal*, *35*(2), 193-205.

Feys, B. J., Moisan, L. J., Newman, M. A., & Parker, J. E. (2001). Direct interaction between the Arabidopsis disease resistance signaling proteins, EDS1 and PAD4. *The EMBO journal*, *20*(19), 5400-5411.

Forcat, S., Bennett, M., Grant, M., & Mansfield, J. W. (2010). Rapid linkage of indole carboxylic acid to the plant cell wall identified as a component of basal defence in Arabidopsis against hrp mutant bacteria. *Phytochemistry*, *71*(8-9), 870-876.

Fujiwara, T., Maisonneuve, S., Isshiki, M., Mizutani, M., Chen, L., Wong, H. L., ... & Shimamoto, K. (2010). Sekiguchi lesion gene encodes a cytochrome P450 monooxygenase that catalyzes conversion of tryptamine to serotonin in rice. *Journal of Biological Chemistry*, *285*(15), 11308-11313.

Gaffney, T., Friedrich, L., Vernooij, B., Negrotto, D., Nye, G., Uknes, S., ... & Ryals, J. (1993). Requirement of salicylic acid for the induction of systemic acquired resistance. *Science*, *261*(5122), 754-756.

Gaige, A. R., Ayella, A., & Shuai, B. (2010). Methyl jasmonate and ethylene induce partial resistance in *Medicago truncatula* against the charcoal rot pathogen *Macrophomina phaseolina*. *Physiological and Molecular Plant Pathology*, *74*(5-6), 412-418.

Gamir, J., Pastor, V., Cerezo, M., & Flors, V. (2012). Identification of indole-3-carboxylic acid as mediator of priming against *Plectosphaerella cucumerina*. *Plant Physiology and Biochemistry*, *61*, 169-179.

Gamir, J., Pastor, V., Cerezo, M., & Flors, V. (2012). Identification of indole-3-carboxylic acid as mediator of priming against Plectosphaerella cucumerina. *Plant Physiology and Biochemistry*, *61*, 169-179.

Garcion, C., Lohmann, A., Lamodière, E., Catinot, J., Buchala, A., Doermann, P., & Métraux, J. P. (2008). Characterization and biological function of the ISOCHORISMATE SYNTHASE2 gene of Arabidopsis. *Plant physiology*, *147*(3), 1279-1287.

Glawischnig, E. (2007). Camalexin. *Phytochemistry*, *68*(4), 401-406.

Glazebrook, J. (2005). Contrasting mechanisms of defense against biotrophic and necrotrophic pathogens. *Annu. Rev. Phytopathol.*, *43*, 205-227.

Glazebrook, J., & Ausubel, F. M. (1994). Isolation of phytoalexin-deficient mutants of *Arabidopsis thaliana* and characterization of their interactions with bacterial pathogens. *Proceedings of the National Academy of Sciences*, *91*(19), 8955-8959.

Göhre, V., Spallek, T., Häweker, H., Mersmann, S., Mentzel, T., Boller, T., ... & Robatzek, S. (2008). Plant pattern-recognition receptor FLS2 is directed for degradation by the bacterial ubiquitin ligase AvrPtoB. *Current biology*, *18*(23), 1824-1832.

Govrin, E., & Levine, A. (2002). Infection of Arabidopsis with a necrotrophic pathogen, *Botrytis cinerea*, elicits various defense responses but does not induce systemic acquired resistance (SAR). *Plant molecular biology*, *48*(3), 267-276.

Gow, N. A. (1993). Nonchemical signals used for host location and invasion by fungal pathogens. *Trends in Microbiology*, *1*(2), 45-50.

Grant, M. R., Godiard, L., Straube, E., Ashfield, T., Lewald, J., Sattler, A., ... & Dangl, J. L. (1995). Structure of the Arabidopsis RPM1 gene enabling dual specificity disease resistance. *Science*, *269*(5225), 843-846.

Grant, M., Brown, I., Adams, S., Knight, M., Ainslie, A., & Mansfield, J. (2000). The RPM1 plant disease resistance gene facilitates a rapid and sustained increase in cytosolic calcium that is necessary for the oxidative burst and hypersensitive cell death. *The Plant Journal*, *23*(4), 441-450.

Grellet-Bournonville, C. F., Martinez-Zamora, M. G., Castagnaro, A. P., & Díaz-Ricci, J. C. (2012). Temporal accumulation of salicylic acid activates the defense response against Colletotrichum in strawberry. *Plant Physiology and Biochemistry*, *54*, 10-16.

Gruner, K., Griebel, T., Návarová, H., Attaran, E., & Zeier, J. (2013). Reprogramming of plants during systemic acquired resistance. *Frontiers in plant science*, 252.

Guo, X., & Stotz, H. U. (2007). Defense against *Sclerotinia sclerotiorum* in Arabidopsis is dependent on jasmonic acid, salicylic acid, and ethylene signaling. *Molecular Plant-Microbe Interactions*, *20*(11), 1384-1395.

Gupta, V., Willits, M. G., & Glazebrook, J. (2000). *Arabidopsis thaliana* EDS4 contributes to salicylic acid (SA)-dependent expression of defense responses: evidence for inhibition of jasmonic acid signaling by SA. *Molecular Plant-Microbe Interactions*, *13*(5), 503-511.

Hahlbrock, K., & Scheel, D. (1989). Physiology and molecular biology of phenylpropanoid metabolism. *Annual review of plant biology*, *40*(1), 347-369.

Halim, V. A., Eschen-Lippold, L., Altmann, S., Birschwilks, M., Scheel, D., & Rosahl, S. (2007). Salicylic acid is important for basal defense of *Solanum tuberosum* against *Phytophthora infestans*. *Molecular Plant-Microbe Interactions*, *20*(11), 1346-1352.

Handley, R., Ekbom, B., & Ågren, J. (2005). Variation in trichome density and resistance against a specialist insect herbivore in natural populations of *Arabidopsis thaliana*. *Ecological Entomology*, *30*(3), 284-292.

Hartmann, M., & Zeier, J. (2018). l-lysine metabolism to N-hydroxypipecolic acid: an integral immune-activating pathway in plants. *The Plant Journal*, *96*(1), 5-21.

Hartmann, M., & Zeier, J. (2019). N-hydroxypipecolic acid and salicylic acid: a metabolic duo for systemic acquired resistance. *Current opinion in plant biology*, *50*, 44-57.

Hartmann, M., Zeier, T., Bernsdorff, F., Reichel-Deland, V., Kim, D., Hohmann, M., ... & Zeier, J. (2018). Flavin monooxygenase-generated N-hydroxypipecolic acid is a critical element of plant systemic immunity. *Cell*, *173*(2), 456-469.

Hauck, P., Thilmony, R., & He, S. Y. (2003). A *Pseudomonas syringae* type III effector suppresses cell wall-based extracellular defense in susceptible Arabidopsis plants. *Proceedings of the National Academy of Sciences*, *100*(14), 8577-8582.

Henfling, J. W. D. M., Bostock, R., & Kuc, J. (1980). Effect of abscisic acid on rishitin and lubimin accumulation and resistance to *Phytophthora infestans* and *Cladosporium cucumerinum* in potato tuber tissue slices. *Phytopathology*.

Hiruma, K., Fukunaga, S., Bednarek, P., & Takano, Y. (2013). Glutathione and tryptophan metabolites are key players in Arabidopsis nonhost resistance against *Colletotrichum gloeosporioides*. *Plant signaling & behavior*, *8*(9), 9589-94.

Hiruma, K., Nishiuchi, T., Kato, T., Bednarek, P., Okuno, T., Schulze-Lefert, P., & Takano, Y. (2011). Arabidopsis ENHANCED DISEASE RESISTANCE 1 is required for pathogen-induced expression of plant defensins in nonhost resistance, and acts through interference of MYC2-mediated repressor function. *The Plant Journal*, *67*(6), 980-992.

Holmes, E. C., Chen, Y. C., Mudgett, M. B., & Sattely, E. S. (2021). Arabidopsis UGT76B1 glycosylates N-hydroxy-pipecolic acid and inactivates systemic acquired resistance in tomato. *The Plant Cell*, *33*(3), 750-765.

Horbach, R., Navarro-Quesada, A. R., Knogge, W., & Deising, H. B. (2011). When and how to kill a plant cell: infection strategies of plant pathogenic fungi. *Journal of plant physiology*, *168*(1), 51-62.

Hu, C., Ham, B. K., El-shabrawi, H. M., Alexander, D., Zhang, D., Ryals, J., & Lucas, W. J. (2016). Proteomics and metabolomics analyses reveal the cucurbit sieve tube system as a complex metabolic space. *The Plant Journal*, *87*(5), 442-454.

Huang, W., Wang, Y., Li, X., & Zhang, Y. (2020). Biosynthesis and regulation of salicylic acid and N-hydroxypipecolic acid in plant immunity. *Molecular Plant*, *13*(1), 31-41.

Huang, X. X., Zhu, G. Q., Liu, Q., Chen, L., Li, Y. J., & Hou, B. K. (2018). Modulation of plant salicylic acid-associated immune responses via glycosylation of dihydroxybenzoic acids. *Plant Physiology*, *176*(4), 3103-3119.

Huang, X., & Mazza, G. (2011). Application of LC and LC-MS to the analysis of melatonin and serotonin in edible plants. *Critical reviews in food science and nutrition*, *51*(4), 269-284.

Hückelhoven, R., Fodor, J., Preis, C., & Kogel, K. H. (1999). Hypersensitive cell death and papilla formation in barley attacked by the powdery mildew fungus are associated with hydrogen peroxide but not with salicylic acid accumulation. *Plant physiology*, *119*(4), 1251-1260.

Hwang, B. K., & Heitefuss, R. (1982). Induced resistance of spring barley to *Erysiphe graminis* f. sp. hordei. *Journal of Phytopathology*, *103*(1), 41-47.

Irieda, H., Inoue, Y., Mori, M., Yamada, K., Oshikawa, Y., Saitoh, H., ... & Takano, Y. (2019). Conserved fungal effector suppresses PAMP-triggered immunity by targeting plant immune kinases. *Proceedings of the National Academy of Sciences*, *116*(2), 496-505.

Ishihara, A., Hashimoto, Y., Tanaka, C., Dubouzet, J. G., Nakao, T., Matsuda, F., ... & Wakasa, K. (2008). The tryptophan pathway is involved in the defense responses of rice against pathogenic infection via serotonin production. *The Plant Journal*, *54*(3), 481-495.

Ishihara, A., Hashimoto, Y., Tanaka, C., Dubouzet, J. G., Nakao, T., Matsuda, F., ... & Wakasa, K. (2008). The tryptophan pathway is involved in the defense responses of rice against pathogenic infection via serotonin production. *The Plant Journal*, *54*(3), 481-495.

Jacobs, A. K., Lipka, V., Burton, R. A., Panstruga, R., Strizhov, N., Schulze-Lefert, P., & Fincher, G. B. (2003). An Arabidopsis callose synthase, GSL5, is required for wound and papillary callose formation. *The Plant Cell*, *15*(11), 2503-2513.

Jarvis, A. P., Schaaf, O., & Oldham, N. J. (2000). 3-Hydroxy-3-phenylpyruvic acidis an intermediate in the biosynthesis of benzoic acid and salicylic acid but benzaldehyde is not. *Planta*, *212*(1), 119-126.

Jing, B., Xu, S., Xu, M., Li, Y., Li, S., Ding, J., & Zhang, Y. (2011). Brush and spray: a high-throughput systemic acquired resistance assay suitable for large-scale genetic screening. *Plant Physiology*, *157*(3), 973-980.

Jirage, D., Tootle, T. L., Reuber, T. L., Frost, L. N., Feys, B. J., Parker, J. E., ... & Glazebrook, J. (1999). *Arabidopsis thaliana* PAD4 encodes a lipase-like gene that is important for salicylic acid signaling. *Proceedings of the National Academy of Sciences*, *96*(23), 13583-13588.

Jones, J. D., & Dangl, J. L. (2006). The plant immune system. *nature*, *444*(7117), 323-329.

Kabbage, M., Yarden, O., & Dickman, M. B. (2015). Pathogenic attributes of *Sclerotinia sclerotiorum*: switching from a biotrophic to necrotrophic lifestyle. *Plant science*, *233*, 53-60.

Katsir, L., Schilmiller, A. L., Staswick, P. E., He, S. Y., & Howe, G. A. (2008). COI1 is a critical component of a receptor for jasmonate and the bacterial virulence factor coronatine. *Proceedings of the National Academy of Sciences*, *105*(19), 7100-7105.

Keller, H., Hohlfeld, H., Wray, V., Hahlbrock, K., Scheel, D., & Strack, D. (1996). Changes in the accumulation of soluble and cell wall-bound phenolics in elicitor-treated cell suspension cultures and fungus-infected leaves of Solanum tuberosum. *Phytochemistry*, *42*(2), 389-396.

Kim, D. S., & Hwang, B. K. (2014). An important role of the pepper phenylalanine ammonia-lyase gene (PAL1) in salicylic acid-dependent signaling of the defence response to microbial pathogens. *Journal of experimental botany*, *65*(9), 2295-2306.

Kim, J. H., Lee, B. W., Schroeder, F. C., & Jander, G. (2008). Identification of indole glucosinolate breakdown products with antifeedant effects on *Myzus persicae* (green peach aphid). *The Plant Journal*, *54*(6), 1015-1026.

Kim, Y., Gilmour, S. J., Chao, L., Park, S., & Thomashow, M. F. (2020). Arabidopsis CAMTA transcription factors regulate pipecolic acid biosynthesis and priming of immunity genes. *Molecular Plant*, *13*(1), 157-168.

Kinkema, M., Fan, W., & Dong, X. (2000). Nuclear localization of NPR1 is required for activation of PR gene expression. *The plant cell*, *12*(12), 2339-2350.

Kliebenstein, D. J., Rowe, H. C., & Denby, K. J. (2005). Secondary metabolites influence Arabidopsis/Botrytis interactions: variation in host production and pathogen sensitivity. *The Plant Journal*, *44*(1), 25-36.

Kloek, A. P., Verbsky, M. L., Sharma, S. B., Schoelz, J. E., Vogel, J., Klessig, D. F., & Kunkel, B. N. (2001). Resistance to *Pseudomonas syringae* conferred by an *Arabidopsis thaliana* coronatine-insensitive (coi1) mutation occurs through two distinct mechanisms. *The Plant Journal*, *26*(5), 509-522.

Koch, E., & Slusarenko, A. (1990). Arabidopsis is susceptible to infection by a downy mildew fungus. *The Plant Cell*, *2*(5), 437-445.

Kogel, K. H., & Langen, G. (2005). Induced disease resistance and gene expression in cereals. *Cellular Microbiology*, *7*(11), 1555-1564.

Kogel, K. H., Ortel, B., Jarosch, B., Atzorn, R., Schiffer, R., & Wasternack, C. (1995). Resistance in barley against the powdery mildew fungus (*Erysiphe graminis* f. sp. hordei) is not associated with enhanced levels of endogenous jasmonates. *European Journal of Plant Pathology*, *101*(3), 319-332.

Kohler, A., Schwindling, S., & Conrath, U. (2002). Benzothiadiazole-induced priming for potentiated responses to pathogen infection, wounding, and infiltration of water into leaves requires the NPR1/NIM1 gene in Arabidopsis. *Plant Physiology*, *128*(3), 1046-1056.

Koo, Y. J., Kim, M., Kim, E. H., Song, J. T., Jung, C., Moon, J. K., ... & Choi, Y. D. (2007). Overexpression of salicylic acid carboxyl methyltransferase reduces salicylic acid-mediated pathogen resistance in *Arabidopsis thaliana*. *Plant molecular biology*, *64*(1), 1-15.

Kosaka, A., & Takano, Y. (2018). Nonhost resistance of *Arabidopsis thaliana* against Colletotrichum species. *Journal of General Plant Pathology*, *84*(5), 305-311.

Krasileva, K. V., Dahlbeck, D., & Staskawicz, B. J. (2010). Activation of an Arabidopsis resistance protein is specified by the in planta association of its leucine-rich repeat domain with the cognate oomycete effector. *The Plant Cell*, *22*(7), 2444-2458.

Kumar, M., Kesawat, M. S., Ali, A., Lee, S. C., Gill, S. S., & Kim, H. U. (2019). Integration of abscisic acid signaling with other signaling pathways in plant stress responses and development. *Plants*, *8*(12), 592.

Kunkel, B. N., & Brooks, D. M. (2002). Cross talk between signaling pathways in pathogen defense. *Current opinion in plant biology*, *5*(4), 325-331.

Latunde-Dada, A. O., O'Connell, R. J., Nash, C., Pring, R. J., Lucas, J. A., & Bailey, J. A. (1996). Infection process and identity of the hemibiotrophic anthracnose fungus (*Colletotrichum destructivum*) from cowpea (*Vigna unguiculata*). *Mycological Research*, *100*(9), 1133-1141.

Lawton, K. A., Potter, S. L., Uknes, S., & Ryals, J. (1994). Acquired resistance signal transduction in Arabidopsis is ethylene independent. *The Plant Cell*, *6*(5), 581-588.

Lee, H. Y., Byeon, Y., & Back, K. (2014). Melatonin as a signal molecule triggering defense responses against pathogen attack in Arabidopsis and tobacco. *Journal of Pineal Research*, *57*(3), 262-268.

Lefevere, H., Bauters, L., & Gheysen, G. (2020). Salicylic acid biosynthesis in plants. *Frontiers in plant science*, *11*, 338.

Lenk, M., Wenig, M., Bauer, K., Hug, F., Knappe, C., Lange, B., ... & Vlot, A. C. (2019). Pipecolic acid is induced in barley upon infection and triggers immune responses associated with elevated nitric oxide accumulation. *Molecular Plant-Microbe Interactions*, *32*(10), 1303-1313.

Lenk, M., Wenig, M., Mengel, F., Häußler, F., & Vlot, A. C. (2018). *Arabidopsis thaliana* immunity-related compounds modulate disease susceptibility in barley. *Agronomy*, *8*(8), 142.

Li, J., Brader, G., & Palva, E. T. (2004). The WRKY70 transcription factor: a node of convergence for jasmonate-mediated and salicylate-mediated signals in plant defense. *The Plant Cell*, *16*(2), 319-331.

Liu, G., Kennedy, R., Greenshields, D. L., Peng, G., Forseille, L., Selvaraj, G., & Wei, Y. (2007). Detached and attached Arabidopsis leaf assays reveal distinctive defense responses against hemibiotrophic Colletotrichum spp. *Molecular Plant-Microbe Interactions*, *20*(10), 1308-1319.

Liu, H., Wu, H., Wang, Y., Wang, H., Chen, S., & Yin, Z. (2021). Comparative transcriptome profiling and co-expression network analysis uncover the key genes associated withearly-stage resistance to *Aspergillus flavus* in maize. *BMC plant biology*, *21*(1), 1-18.

Liu, S., Kracher, B., Ziegler, J., Birkenbihl, R. P., & Somssich, I. E. (2015). Negative regulation of ABA signaling by WRKY33 is critical for Arabidopsis immunity towards *Botrytis cinerea* 2100. *Elife*, *4*, e07295.

Löwe, M., Jürgens, K., Zeier, T., Hartmann, M., Gruner, K., Müller, S., ... & Zeier, J. (2023). N-hydroxypipecolic acid primes plants for enhanced microbial pattern-induced responses. *Frontiers in Plant Science*, *14*.

Malamy, J., Carr, J. P., Klessig, D. F., & Raskin, I. (1990). Salicylic acid: a likely endogenous signal in the resistance response of tobacco to viral infection. *Science*, *250*(4983), 1002-1004.

Manabe, Y., Nafisi, M., Verhertbruggen, Y., Orfila, C., Gille, S., Rautengarten, C., ... & Scheller, H. V. (2011). Loss-of-function mutation of REDUCED WALL ACETYLATION2 in Arabidopsis leads to reduced cell wall acetylation and increased resistance to *Botrytis cinerea*. *Plant physiology*, *155*(3), 1068-1078.

Manohar, M., Tian, M., Moreau, M., Park, S. W., Choi, H. W., Fei, Z., ... & Klessig, D. F. (2015). Identification of multiple salicylic acid-binding proteins using two high throughput screens. *Frontiers in plant science*, *5*, 777.

Mao, G., Meng, X., Liu, Y., Zheng, Z., Chen, Z., & Zhang, S. (2011). Phosphorylation of a WRKY transcription factor by two pathogen-responsive MAPKs drives phytoalexin biosynthesis in Arabidopsis. *The Plant Cell*, *23*(4), 1639-1653.

Mauch-Mani, B., & Mauch, F. (2005). The role of abscisic acid in plant–pathogen interactions. *Current opinion in plant biology*, *8*(4), 409-414.

Meinke, D. W., Cherry, J. M., Dean, C., Rounsley, S. D., & Koornneef, M. (1998). *Arabidopsis thaliana*: a model plant for genome analysis. *Science*, *282*(5389), 662-682.

Melotto, M., Underwood, W., Koczan, J., Nomura, K., & He, S. Y. (2006). Plant stomata function in innate immunity against bacterial invasion. *Cell*, *126*(5), 969-980.

Métraux, J. P., Signer, H., Ryals, J., Ward, E., Wyss-Benz, M., Gaudin, J., ... & Inverardi, B. (1990). Increase in salicylic acid at the onset of systemic acquired resistance in cucumber. *Science*, *250*(4983), 1004-1006.

Meuwly, P., Molders, W., Buchala, A., & Metraux, J. P. (1995). Local and systemic biosynthesis of salicylic acid in infected cucumber plants. *Plant Physiology*, *109*(3), 1107-1114.

Meyer, D., Pajonk, S., Micali, C., O'Connell, R., & Schulze-Lefert, P. (2009). Extracellular transport and integration of plant secretory proteins into pathogen-induced cell wall compartments. The Plant Journal, 57(6), 986-999.

Meyerowitz, E. M. (1987). Arabidopsis thaliana. *Annual review of genetics*, *21*, 93-111.

Mishina, T. E., & Zeier, J. (2006). The Arabidopsis flavin-dependent monooxygenase FMO1 is an essential component of biologically induced systemic acquired resistance. *Plant physiology*, *141*(4), 1666-1675.

Mohnike, L., Rekhter, D., Huang, W., Feussner, K., Tian, H., Herrfurth, C., ... & Feussner, I. (2021). The glycosyltransferase UGT76B1 modulates N-hydroxy-pipecolic acid homeostasis and plant immunity. The Plant Cell, 33(3), 735-749.

Mohr, P. G., & Cahill, D. M. (2003). Abscisic acid influences the susceptibility of *Arabidopsis thaliana* to *Pseudomonas syringae* pv. tomato and *Peronospora parasitica*. *Functional Plant Biology*, *30*(4), 461-469.

Mou, Z., Fan, W., & Dong, X. (2003). Inducers of plant systemic acquired resistance regulate NPR1 function through redox changes. *Cell*, *113*(7), 935-944.

Müller, R., De Vos, M., Sun, J. Y., Sønderby, I. E., Halkier, B. A., Wittstock, U., & Jander, G. (2010). Differential effects of indole and aliphatic glucosinolates on lepidopteran herbivores. *Journal of chemical ecology*, *36*(8), 905-913.

Nafisi, M., Goregaoker, S., Botanga, C. J., Glawischnig, E., Olsen, C. E., Halkier, B. A., & Glazebrook, J. (2007). Arabidopsis cytochrome P450 monooxygenase 71A13 catalyzes the conversion of indole-3-acetaldoxime in camalexin synthesis. *The Plant Cell*, *19*(6), 2039-2052.

Nair, A., Goyal, I., Voß, E., Mrozek, P., Prajapati, S., Thurow, C., ... & Gatz, C. (2021). N-hydroxypipecolic acid-induced transcription requires the salicylic acid signaling pathway at basal SA levels. *Plant Physiology*, *187*(4), 2803-2819.

Nambara, E., & Marion-Poll, A. (2005). Abscisic acid biosynthesis and catabolism. *Annu. Rev. Plant Biol.*, *56*, 165-185.

Narusaka, M., Abe, H., Kobayashi, M., Kubo, Y., & Narusaka, Y. (2006). Comparative analysis of expression profiles of counterpart gene sets between Brassica rapa and Arabidopsis thaliana during fungal pathogen *Colletotrichum higginsianum* infection. *Plant biotechnology*, *23*(5), 503-508.

Narusaka, Y., Narusaka, M., Park, P., Kubo, Y., Hirayama, T., Seki, M., ... & Shinozaki, K. (2004). RCH1, a locus in Arabidopsis that confers resistance to the hemibiotrophic fungal pathogen *Colletotrichum higginsianum*. *Molecular Plant-Microbe Interactions*, *17*(7), 749-762.

Nawrath, C., & Métraux, J. P. (1999). Salicylic acid induction–deficient mutants of Arabidopsis express PR-2 and PR-5 and accumulate high levels of camalexin after pathogen inoculation. *The Plant Cell*, *11*(8), 1393-1404.

Ngou, B. P. M., Ding, P., & Jones, J. D. (2022). Thirty years of resistance: Zig-zag through the plant immune system. *The Plant Cell*.

Nishimura, M. T., Stein, M., Hou, B. H., Vogel, J. P., Edwards, H., & Somerville, S. C. (2003). Loss of a callose synthase results in salicylic acid-dependent disease resistance. *Science*, *301*(5635), 969-972.

Nobuta, K., Okrent, R. A., Stoutemyer, M., Rodibaugh, N., Kempema, L., Wildermuth, M. C., & Innes, R. W. (2007). The GH3 acyl adenylase family member PBS3 regulates salicylic acid-dependent defense responses in Arabidopsis. *Plant physiology*, *144*(2), 1144-1156.

O'Connell, R., Herbert, C., Sreenivasaprasad, S., Khatib, M., Esquerré-Tugayé, M. T., & Dumas, B. (2004). A novel Arabidopsis-Colletotrichum pathosystem for the molecular dissection of plant-fungal interactions. *Molecular plant-microbe interactions*, *17*(3), 272-282.

Oukala, N., Pastor-Fernández, J., Sanmartín, N., Aissat, K., & Pastor, V. (2021). Endophytic Bacteria from the Sahara Desert Protect Tomato Plants Against *Botrytis cinerea* Under Different Experimental Conditions. *Current Microbiology*, *78*(6), 2367-2379.

Pálfi, G., & Dézsi, L. (1968). Pipecolic acid as an indicator of abnormal protein metabolism in diseased plants. *Plant and Soil*, *29*(2), 285-291.

Pallas, J. A., Paiva, N. L., Lamb, C., & Dixon, R. A. (1996). Tobacco plants epigenetically suppressed in phenylalanine ammonia-lyase expression do not develop systemic acquired resistance in response to infection by tobacco mosaic virus. *The Plant Journal*, *10*(2), 281-293.

Pastor-Fernández, J., Pastor, V., Mateu, D., Gamir, J., Sánchez-Bel, P., & Flors, V. (2019). Accumulating evidences of callose priming by indole-3-carboxylic acid in response to *Plectospharella cucumerina*. *Plant signaling & behavior*, *14*(7), 1608107.

Pedras, M. S. C., Yaya, E. E., & Glawischnig, E. (2011). The phytoalexins from cultivated and wild crucifers: chemistry and biology. *Natural product reports*, *28*(8), 1381-1405.

Pei, Z. M., Murata, Y., Benning, G., Thomine, S., Klüsener, B., Allen, G. J., ... & Schroeder, J. I. (2000). Calcium channels activated by hydrogen peroxide mediate abscisic acid signalling in guard cells. *Nature*, *406*(6797), 731-734.

Pelagio-Flores, R., Ortíz-Castro, R., Méndez-Bravo, A., Macías-Rodríguez, L., & López-Bucio, J. (2011). Serotonin, a tryptophan-derived signal conserved in plants and animals, regulates root system architecture probably acting as a natural auxin inhibitor in *Arabidopsis thaliana*. *Plant and Cell Physiology*, *52*(3), 490-508.

Penninckx, I. A., Eggermont, K., Terras, F. R., Thomma, B. P., De Samblanx, G. W., Buchala, A., ... & Broekaert, W. F. (1996). Pathogen-induced systemic activation of a plant defensin gene in Arabidopsis follows a salicylic acid-independent pathway. *The Plant Cell*, *8*(12), 2309-2323.

Pfalz, M., Mikkelsen, M. D., Bednarek, P., Olsen, C. E., Halkier, B. A., & Kroymann, J. (2011). Metabolic engineering in *Nicotiana benthamiana* reveals key enzyme functions in Arabidopsis indole glucosinolate modification. *The Plant Cell*, *23*(2), 716-729.

Pieterse, C. M., Leon-Reyes, A., Van der Ent, S., & Van Wees, S. C. (2009). Networking by small-molecule hormones in plant immunity. *Nature chemical biology*, *5*(5), 308-316.

Pieterse, C. M., Leon-Reyes, A., Van der Ent, S., & Van Wees, S. C. (2009). Networking by small-molecule hormones in plant immunity. *Nature chemical biology*, *5*(5), 308-316.

Prasannath, K. (2017). Plant defense-related enzymes against pathogens: a review.

Qiu, D., Xiao, J., Ding, X., Xiong, M., Cai, M., Cao, Y., ... & Wang, S. (2007). OsWRKY13 mediates rice disease resistance by regulating defense-related genes in salicylate-and jasmonate-dependent signaling. *Molecular plant-microbe interactions*, *20*(5), 492-499.

Rasmussen, J. B., Hammerschmidt, R., & Zook, M. N. (1991). Systemic induction of salicylic acid accumulation in cucumber after inoculation with *Pseudomonas syringae* pv syringae. *Plant physiology*, *97*(4), 1342-1347.

Rekhter, D., Lüdke, D., Ding, Y., Feussner, K., Zienkiewicz, K., Lipka, V., ... & Feussner, I. (2019). Isochorismate-derived biosynthesis of the plant stress hormone salicylic acid. *Science*, *365*(6452), 498-502.

Riet, K. B., Ndlovu, N., Piater, L. A., & Dubery, I. A. (2016). Simultaneous analysis of defense-related phytohormones in *Arabidopsis thaliana* responding to fungal infection. *Applications in plant sciences*, *4*(8), 1600013.

Rietz, S., Stamm, A., Malonek, S., Wagner, S., Becker, D., Medina-Escobar, N., ... & Parker, J. E. (2011). Different roles of Enhanced Disease Susceptibility1 (EDS1) bound to and dissociated from Phytoalexin Deficient4 (PAD4) in Arabidopsis immunity. *New Phytologist*, *191*(1), 107-119.

Rogers, E. E., & Ausubel, F. M. (1997). Arabidopsis enhanced disease susceptibility mutants exhibit enhanced susceptibility to several bacterial pathogens and alterations in PR-1 gene expression. *The Plant Cell*, *9*(3), 305-316.

Rohde, A., Morreel, K., Ralph, J., Goeminne, G., Hostyn, V., De Rycke, R., ... & Boerjan, W. (2004). Molecular phenotyping of the pal1 and pal2 mutants of *Arabidopsis thaliana* reveals far-reaching consequences on phenylpropanoid, amino acid, and carbohydrate metabolism. *The Plant Cell*, *16*(10), 2749-2771.

Roychoudhury, A. (2021). Multifaceted roles of serotonin in plants. *Young Scientist-Tomorrow's Science Begins Today*, *5*(1).

Sanmartín, N., Pastor, V., Pastor-Fernández, J., Flors, V., Pozo, M. J., & Sánchez-Bel, P. (2020). Role and mechanisms of callose priming in mycorrhiza-induced resistance. *Journal of Experimental Botany*, *71*(9), 2769-2781.

Schlaeppi, K., Abou-Mansour, E., Buchala, A., & Mauch, F. (2010). Disease resistance of Arabidopsis to *Phytophthora brassicae* is established by the sequential action of indole glucosinolates and camalexin. *The Plant Journal*, *62*(5), 840-851.

Schmidt, A., Mächtel, R., Ammon, A., Engelsdorf, T., Schmitz, J., Maurino, V. G., & Voll, L. M. (2020). Reactive oxygen species dosage in Arabidopsis chloroplasts can improve resistance towards *Colletotrichum higginsianum* by the induction of WRKY33. *New Phytologist*, *226*(1), 189-204.

Schnake, A., Hartmann, M., Schreiber, S., Malik, J., Brahmann, L., Yildiz, I., ... & Zeier, J. (2020). Inducible biosynthesis and immune function of the systemic acquired resistance inducer N-hydroxypipecolic acid in monocotyledonous and dicotyledonous plants. *Journal of experimental botany*, *71*(20), 6444-6459.

Schuhegger, R., Nafisi, M., Mansourova, M., Petersen, B. L., Olsen, C. E., Svatos, A., ... & Glawischnig, E. (2006). CYP71B15 (PAD3) catalyzes the final step in camalexin biosynthesis. *Plant physiology*, *141*(4), 1248-1254.

Schumacher, J., & Tudzynski, P. (2012). Morphogenesis and infection in *Botrytis cinerea*. In *Morphogenesis and pathogenicity in fungi* (pp. 225-241). Springer, Berlin, Heidelberg.

Sewelam, N., Jaspert, N., Van Der Kelen, K., Tognetti, V. B., Schmitz, J., Frerigmann, H., ... & Maurino, V. G. (2014). Spatial H2O2 signaling specificity: H2O2 from chloroplasts and peroxisomes modulates the plant transcriptome differentially. *Molecular Plant*, *7*(7), 1191-1210.

Shah, J., Tsui, F., & Klessig, D. F. (1997). Characterization of a s alicylic a cid-i nsensitive mutant (sai1) of *Arabidopsis thaliana*, identified in a selective screen utilizing the SA-inducible expression of the tms2 gene. *Molecular Plant-Microbe Interactions*, *10*(1), 69-78.

Sham, A., Moustafa, K., Al-Shamisi, S., Alyan, S., Iratni, R., & AbuQamar, S. (2017). Microarray analysis of Arabidopsis WRKY33 mutants in response to the necrotrophic fungus *Botrytis cinerea*. *PLoS One*, *12*(2), e0172343.

Sharma, S., Choudhary, B., Yadav, S., Mishra, A., Mishra, V. K., Chand, R., ... & Pandey, S. P. (2021). Metabolite profiling identified pipecolic acid as an important component of peanut seed resistance against *Aspergillus flavus* infection. *Journal of Hazardous Materials*, *404*, 124155.

Shigenaga, A. M., & Argueso, C. T. (2016). No hormone to rule them all: Interactions of plant hormones during the responses of plants to pathogens. In *Seminars in Cell & Developmental Biology* (Vol. 56, pp. 174-189). Academic Press.

Shimada, C., Lipka, V., O'Connell, R., Okuno, T., Schulze-Lefert, P., & Takano, Y. (2006). Nonhost resistance in Arabidopsis-Colletotrichum interactions acts at the cell periphery and requires actin filament function. *Molecular Plant-Microbe Interactions*, *19*(3), 270-279.

Shine, M. B., Yang, J. W., El-Habbak, M., Nagyabhyru, P., Fu, D. Q., Navarre, D., ... & Kachroo, A. (2016). Cooperative functioning between phenylalanine ammonia lyase and isochorismate synthase activities contributes to salicylic acid biosynthesis in soybean. *New Phytologist*, *212*(3), 627-636.

Slusarenko, A. J., & Schlaich, N. L. (2003). Downy mildew of *Arabidopsis thaliana* caused by *Hyaloperonospora parasitica* (formerly *Peronospora parasitica*). *Molecular Plant Pathology*, *4*(3), 159-170.

Smith, T. A. (1977). Tryptamine and related compounds in plants. *Phytochemistry*, *16*(2), 171-175.

Smith-Becker, J., Marois, E., Huguet, E. J., Midland, S. L., Sims, J. J., & Keen, N. T. (1998). Accumulation of salicylic acid and 4-hydroxybenzoic acid in phloem fluids of cucumber during systemic acquired resistance is preceded by a transient increase in phenylalanine ammonia-lyase activity in petioles and stems. *Plant Physiology*, *116*(1), 231-238.

Sønderby, I. E., Geu-Flores, F., & Halkier, B. A. (2010). Biosynthesis of glucosinolates–gene discovery and beyond. *Trends in plant science*, *15*(5), 283-290.

Song, J. T., Lu, H., McDowell, J. M., & Greenberg, J. T. (2004). A key role for ALD1 in activation of local and systemic defenses in Arabidopsis. *The Plant Journal*, *40*(2), 200-212.

Soylu, E. M., & Soylu, S. (2003). Light and electron microscopy of the compatible interaction between Arabidopsis and the downy mildew pathogen *Peronospora parasitica*. *Journal of Phytopathology*, *151*(6), 300-306.

Spoel, S. H., Johnson, J. S., & Dong, X. (2007). Regulation of tradeoffs between plant defenses against pathogens with different lifestyles. *Proceedings of the National Academy of Sciences*, *104*(47), 18842-18847.

Stahl, E., Hartmann, M., Scholten, N., & Zeier, J. (2019). A role for tocopherol biosynthesis in Arabidopsis basal immunity to bacterial infection. *Plant physiology*, *181*(3), 1008-1028.

Staswick, P. E. (2008). JAZing up jasmonate signaling. *Trends in plant science*, *13*(2), 66-71.

Stefanato, F. L., Abou-Mansour, E., Buchala, A., Kretschmer, M., Mosbach, A., Hahn, M., ... & Schoonbeek, H. J. (2009). The ABC transporter BcatrB from *Botrytis cinerea* exports camalexin and is a virulence factor on *Arabidopsis thaliana*. *The Plant Journal*, *58*(3), 499-510.

Sticher, L., Mauch-Mani, B., & Métraux, A. J. (1997). Systemic acquired resistance. *Annual review of phytopathology*, *35*(1), 235-270.

Sugano, S., Sugimoto, T., Takatsuji, H., & Jiang, C. J. (2013). Induction of resistance to *Phytophthora sojae* in soyabean (Glycine max) by salicylic acid and ethylene. *Plant Pathology*, *62*(5), 1048-1056.

Sun, T., Busta, L., Zhang, Q., Ding, P., Jetter, R., & Zhang, Y. (2018). TGACG-BINDING FACTOR 1 (TGA 1) and TGA 4 regulate salicylic acid and pipecolic acid biosynthesis by modulating the expression of SYSTEMIC ACQUIRED RESISTANCE DEFICIENT 1 (SARD 1) and CALMODULIN-BINDING PROTEIN 60g (CBP 60g). *New Phytologist*, *217*(1), 344-354.

Sun, T., Huang, J., Xu, Y., Verma, V., Jing, B., Sun, Y., ... & Li, X. (2020). Redundant CAMTA transcription factors negatively regulate the biosynthesis of salicylic acid and N-hydroxypipecolic acid by modulating the expression of SARD1 and CBP60g. *Molecular Plant*, *13*(1), 144-156.

Sun, T., Zhang, Y., Li, Y., Zhang, Q., Ding, Y., & Zhang, Y. (2015). ChIP-seq reveals broad roles of SARD1 and CBP60g in regulating plant immunity. *Nature communications*, *6*(1), 1-12.

Sun, T., Zhang, Y., Li, Y., Zhang, Q., Ding, Y., & Zhang, Y. (2015). ChIP-seq reveals broad roles of SARD1 and CBP60g in regulating plant immunity. *Nature communications*, *6*(1), 1-12.

Svoboda, T., Thon, M. R., & Strauss, J. (2021). The role of plant hormones in the interaction of Colletotrichum species with their host plants. *International Journal of Molecular Sciences*, *22*(22), 12454.

Taheri, P., & Tarighi, S. (2010). Riboflavin induces resistance in rice against Rhizoctonia solani via jasmonate-mediated priming of phenylpropanoid pathway. *Journal of plant physiology*, *167*(3), 201-208.

Tariq, V. N., & Jeffries, P. (1984). Appressorium formation by *Sclerotinia sclerotiorum*: scanning electron microscopy. *Transactions of the British Mycological Society*, *82*(4), 645-651.

Thaler, J. S., & Bostock, R. M. (2004). Interactions between abscisic-acid-mediated responses and plant resistance to pathogens and insects. *Ecology*, *85*(1), 48-58.

Thaler, J. S., Humphrey, P. T., & Whiteman, N. K. (2012). Evolution of jasmonate and salicylate signal crosstalk. *Trends in plant science*, *17*(5), 260-270.

Thatcher, L. F., Cevik, V., Grant, M., Zhai, B., Jones, J. D., Manners, J. M., & Kazan, K. (2016). Characterization of a JAZ7 activation-tagged Arabidopsis mutant with increased susceptibility to the fungal pathogen Fusarium oxysporum. *Journal of Experimental Botany*, *67*(8), 2367-2386.

Thines, B., Katsir, L., Melotto, M., Niu, Y., Mandaokar, A., Liu, G., ... & Browse, J. (2007). JAZ repressor proteins are targets of the SCFCOI1 complex during jasmonate signaling. *Nature*, *448*(7154), 661-665.

Thomma, B. P., Nelissen, I., Eggermont, K., & Broekaert, W. F. (1999). Deficiency in phytoalexin production causes enhanced susceptibility of *Arabidopsis thaliana* to the fungus *Alternaria brassicicola*. *The Plant Journal*, *19*(2), 163-171.

Thomma, B. P., Nürnberger, T., & Joosten, M. H. (2011). Of PAMPs and effectors: the blurred PTI-ETI dichotomy. *The plant cell*, *23*(1), 4-15.

Thompson, A. M.G., Iancu, C. V., Neet, K. E., Dean, J. V., & Choe, J. Y. (2017). Differences in salicylic acid glucose conjugations by UGT74F1 and UGT74F2 from *Arabidopsis thaliana*. *Scientific Reports*, *7*(1), 1-11.

Tomczynska, I., Stumpe, M., Doan, T. G., & Mauch, F. (2020). A Phytophthora effector protein promotes symplastic cell-to-cell trafficking by physical interaction with plasmodesmata-localised callose synthases. *New Phytologist*, *227*(5), 1467-1478.

Tonnessen, B. W., Manosalva, P., Lang, J. M., Baraoidan, M., Bordeos, A., Mauleon, R., ... & Leach, J. E. (2015). Rice phenylalanine ammonia-lyase gene OsPAL4 is associated with broad spectrum disease resistance. *Plant molecular biology*, *87*(3), 273-286.

Torrens-Spence, M. P., Bobokalonova, A., Carballo, V., Glinkerman, C. M., Pluskal, T., Shen, A., & Weng, J. K. (2019). PBS3 and EPS1 complete salicylic acid biosynthesis from isochorismate in Arabidopsis. *Molecular plant*, *12*(12), 1577-1586.

Torres, M. A., Jones, J. D., & Dangl, J. L. (2005). Pathogen-induced, NADPH oxidase–derived reactive oxygen intermediates suppress spread of cell death in Arabidopsis thaliana. *Nature genetics*, *37*(10), 1130-1134.

Torres, M. A., Jones, J. D., & Dangl, J. L. (2006). Reactive oxygen species signaling in response to pathogens. *Plant physiology*, *141*(2), 373-378.

Ueno, Y., Yoshida, R., Kishi-Kaboshi, M., Matsushita, A., Jiang, C. J., Goto, S., ... & Takatsuji, H. (2015). Abiotic stresses antagonize the rice defence pathway through the tyrosine-dephosphorylation of OsMPK6. *PLoS pathogens*, *11*(10), e1005231.

Umemura, K., Satou, J., Iwata, M., Uozumi, N., Koga, J., Kawano, T., ... & Mitomi, M. (2009). Contribution of salicylic acid glucosyltransferase, OsSGT1, to chemically induced disease resistance in rice plants. *The Plant Journal*, *57*(3), 463-472.

van Loon, L. C., Geraats, B. P., & Linthorst, H. J. (2006). Ethylene as a modulator of disease resistance in plants. *Trends in plant science*, *11*(4), 184-191.

VanEtten, H. D., Mansfield, J. W., Bailey, J. A., & Farmer, E. E. (1994). Two classes of plant antibiotics: phytoalexins versus" phytoanticipins". *The Plant Cell*, *6*(9), 1191.

Vargas, W. A., Martín, J. M. S., Rech, G. E., Rivera, L. P., Benito, E. P., Díaz-Mínguez, J. M., ... & Sukno, S. A. (2012). Plant defense mechanisms are activated during biotrophic and necrotrophic development of *Colletotricum graminicola* in maize. *Plant physiology*, *158*(3), 1342-1358.

Vernooij, B., Friedrich, L., Morse, A., Reist, R., Kolditz-Jawhar, R., Ward, E., ... & Ryals, J. (1994). Salicylic acid is not the translocated signal responsible for inducing systemic acquired resistance but is required in signal transduction. *The Plant Cell*, *6*(7), 959-965.

Veronese, P., Nakagami, H., Bluhm, B., AbuQamar, S., Chen, X., Salmeron, J., ... & Mengiste, T. (2006). The membrane-anchored BOTRYTIS-INDUCED KINASE1 plays distinct roles in Arabidopsis resistance to necrotrophic and biotrophic pathogens. *The Plant Cell*, *18*(1), 257-273.

Vidal, S., de León, I. P., Denecke, J., & Palva, E. T. (1997). Salicylic acid and the plant pathogen *Erwinia carotovora* induce defense genes via antagonistic pathways. *The Plant Journal*, *11*(1), 115-123.

Vlot, A. C., Dempsey, D. M. A., & Klessig, D. F. (2009). Salicylic acid, a multifaceted hormone to combat disease. *Annual review of phytopathology*, *47*, 177-206.

Voegele, R. T., & Mendgen, K. (2003). Rust haustoria: nutrient uptake and beyond. *New Phytologist*, *159*(1), 93-100.

Vogel-Adghough, D., Stahl, E., Návarová, H., & Zeier, J. (2013). Pipecolic acid enhances resistance to bacterial infection and primes salicylic acid and nicotine accumulation in tobacco. *Plant signaling & behavior*, *8*(11), e26366.

Vorwerk, S., Somerville, S., & Somerville, C. (2004). The role of plant cell wall polysaccharide composition in disease resistance. *Trends in plant science*, *9*(4), 203-209.

Wan, J., Zhang, X. C., Neece, D., Ramonell, K. M., Clough, S., Kim, S. Y., ... & Stacey, G. (2008). A LysM receptor-like kinase plays a critical role in chitin signaling and fungal resistance in Arabidopsis. *The Plant Cell*, *20*(2), 471-481.

Wang, X., Sager, R., Cui, W., Zhang, C., Lu, H., & Lee, J. Y. (2013). Salicylic acid regulates plasmodesmata closure during innate immune responses in Arabidopsis. *The Plant Cell*, *25*(6), 2315-2329.

Wang, Y., Schuck, S., Wu, J., Yang, P., Döring, A. C., Zeier, J., & Tsuda, K. (2018). A MPK3/6-WRKY33-ALD1-pipecolic acid regulatory loop contributes to systemic acquired resistance. *The Plant Cell*, *30*(10), 2480-2494.

Wasternack, C., & Hause, B. (2013). Jasmonates: biosynthesis, perception, signal transduction and action in plant stress response, growth and development. An update to the 2007 review in Annals of Botany. *Annals of botany*, *111*(6), 1021-1058.

Wildermuth, M. C., Dewdney, J., Wu, G., & Ausubel, F. M. (2001). Isochorismate synthase is required to synthesize salicylic acid for plant defence. *Nature*, *414*(6863), 562-565.

Williamson, B., Duncan, G. H., Harrison, J. G., Harding, L. A., Elad, Y., & Zimand, G. (1995). Effect of humidity on infection of rose petals by dry-inoculated conidia of *Botrytis cinerea*. *Mycological Research*, *99*(11), 1303-1310.

Williamson, B., Tudzynski, B., Tudzynski, P., & Van Kan, J. A. (2007). *Botrytis cinerea*: the cause of grey mould disease. *Molecular plant pathology*, *8*(5), 561-580.

Wu, Y., Zhang, D., Chu, J. Y., Boyle, P., Wang, Y., Brindle, I. D., ... & Després, C. (2012). The Arabidopsis NPR1 protein is a receptor for the plant defense hormone salicylic acid. *Cell reports*, *1*(6), 639-647.

Xu, J., Audenaert, K., Hofte, M., & De Vleesschauwer, D. (2013). Abscisic acid promotes susceptibility to the rice leaf blight pathogen *Xanthomonas oryzae* pv oryzae by suppressing salicylic acid-mediated defenses. *PloS one*, *8*(6), e67413.

Xu, L., Zhao, H., Ruan, W., Deng, M., Wang, F., Peng, J., ... & Yi, K. (2017). ABNORMAL INFLORESCENCE MERISTEM1 functions in salicylic acid biosynthesis to maintain proper reactive oxygen species levels for root meristem activity in rice. *The Plant Cell*, *29*(3), 560-574.

Xu, Y. I., Chang, P. F. L., Liu, D., Narasimhan, M. L., Raghothama, K. G., Hasegawa, P. M., & Bressan, R. A. (1994). Plant defense genes are synergistically induced by ethylene and methyl jasmonate. *The Plant Cell*, *6*(8), 1077-1085.

Yan, Y., Yuan, Q., Tang, J., Huang, J., Hsiang, T., Wei, Y., & Zheng, L. (2018). *Colletotrichum higginsianum* as a model for understanding host–pathogen interactions: A review. *International Journal of Molecular Sciences*, *19*(7), 2142.

Yang, J. W., Yi, H. S., Kim, H., Lee, B., Lee, S., Ghim, S. Y., & Ryu, C. M. (2011). Whitefly infestation of pepper plants elicits defence responses against bacterial pathogens in leaves and roots and changes the below-ground microflora. *Journal of Ecology*, *99*(1), 46-56.

Yildiz, I., Mantz, M., Hartmann, M., Zeier, T., Kessel, J., Thurow, C., ... & Zeier, J. (2021). The mobile SAR signal N-hydroxypipecolic acid induces NPR1-dependent transcriptional reprogramming and immune priming. *Plant physiology*, *186*(3), 1679-1705.

You, M. K., Shin, H. Y., Kim, Y. J., Ok, S. H., Cho, S. K., Jeung, J. U., ... & Shin, J. S. (2010). Novel bifunctional nucleases, OmBBD and AtBBD1, are involved in abscisic acid-mediated callose deposition in Arabidopsis. *Plant physiology*, *152*(2), 1015-1029.

Yuan, Y., Zhong, S., Li, Q., Zhu, Z., Lou, Y., Wang, L., ... & He, Z. (2007). Functional analysis of rice NPR1-like genes reveals that OsNPR1/NH1 is the rice orthologue conferring disease resistance with enhanced herbivore susceptibility. *Plant biotechnology journal*, *5*(2), 313-324.

Zeier, J. (2021). Metabolic regulation of systemic acquired resistance. *Current opinion in plant biology*, *62*, 102050.

Zhang, E. T., Zhang, H., & Tang, W. (2021). Transcriptomic Analysis of Wheat Seedling Responses to the Systemic Acquired Resistance Inducer N-Hydroxypipecolic Acid. *Frontiers in microbiology*, *12*, 94.

Zhang, H., Qiu, Y., Li, M., Song, F., & Jiang, M. (2020). Functions of pipecolic acid on induced resistance against *Botrytis cinerea* and *Pseudomonas syringae* pv. tomato DC3000 in tomato plants. *Journal of Phytopathology*, *168*(10), 591-600.

Zhang, K., Halitschke, R., Yin, C., Liu, C. J., & Gan, S. S. (2013). Salicylic acid 3-hydroxylase regulates Arabidopsis leaf longevity by mediating salicylic acid catabolism. *Proceedings of the National Academy of Sciences*, *110*(36), 14807-14812.

Zhang, Y., Cheng, Y. T., Qu, N., Zhao, Q., Bi, D., & Li, X. (2006). Negative regulation of defense responses in Arabidopsis by two NPR1 paralogs. *The Plant Journal*, *48*(5), 647-656.

Zhang, Y., Tessaro, M. J., Lassner, M., & Li, X. (2003). Knockout analysis of Arabidopsis transcription factors TGA2, TGA5, and TGA6 reveals their redundant and essential roles in systemic acquired resistance. *The Plant Cell*, *15*(11), 2647-2653.

Zhang, Y., Zhao, L., Zhao, J., Li, Y., Wang, J., Guo, R., ... & Zhang, K. (2017). S5H/DMR6 encodes a salicylic acid 5-hydroxylase that fine-tunes salicylic acid homeostasis. *Plant Physiology*, *175*(3), 1082-1093.

Zhao, Y., Hull, A. K., Gupta, N. R., Goss, K. A., Alonso, J., Ecker, J. R., ... & Celenza, J. L. (2002). Trp-dependent auxin biosynthesis in Arabidopsis: involvement of cytochrome P450s CYP79B2 and CYP79B3. *Genes & development*, *16*(23), 3100-3112.

Zheng, Z., Qamar, S. A., Chen, Z., & Mengiste, T. (2006). Arabidopsis WRKY33 transcription factor is required for resistance to necrotrophic fungal pathogens. *The Plant Journal*, *48*(4), 592-605.

Zhou, J. M., Trifa, Y., Silva, H., Pontier, D., Lam, E., Shah, J., & Klessig, D. F. (2000). NPR1 differentially interacts with members of the TGA/OBF family of transcription factors that bind an element of the PR-1 gene required for induction by salicylic acid. *Molecular Plant-Microbe Interactions*, *13*(2), 191-202.

Zhu, Y., Guo, M. J., Song, J. B., Zhang, S. Y., Guo, R., Hou, D. R., ... & Huang, X. (2021). Roles of endogenous melatonin in resistance to Botrytis cinerea infection in an Arabidopsis model. *Frontiers in Plant Science*, *12*, 1031.

Zipfel, C., Kunze, G., Chinchilla, D., Caniard, A., Jones, J. D., Boller, T., & Felix, G. (2006). Perception of the bacterial PAMP EF-Tu by the receptor EFR restricts Agrobacterium-mediated transformation. *Cell*, *125*(4), 749-760.

7. Supplement

7.1 Part I

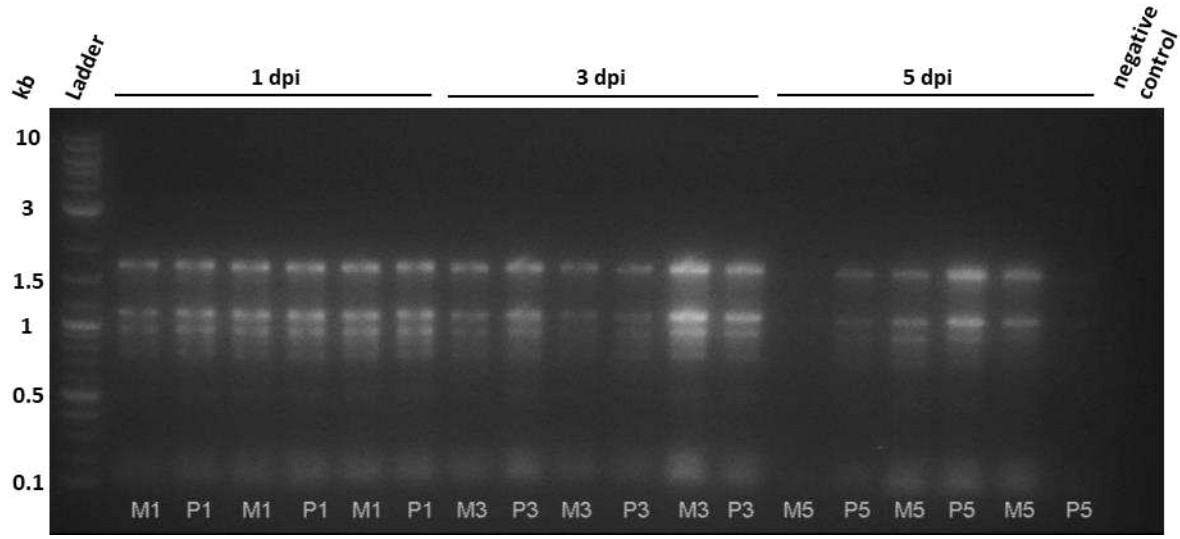

Suppl. Figure 1: Visual evaluation of extracted *Cucumis sativus* RNA quality. RNA was extracted from C. sativus leaves that were treated with a Psl (P) solution or MgCl2 (M) as control and were sampled 1 dpi, 3 dpi and 5 dpi. RNA was extracted using RNAmagic according to the manufacturer's instructions, RNA samples were mixed with loading buffer in a 1:1 ratio and incubated at 65°C for 5 min. All RNA samples were stored on ice for 5 min before they were loaded on a 1.5% agarose gel. The loading buffer without RNA served as negative control. The Quick-Load® Purple 1kb Plus DNA Ladder (New England BioLabs) was applied as size marker. Bands were visualized under UV-light.

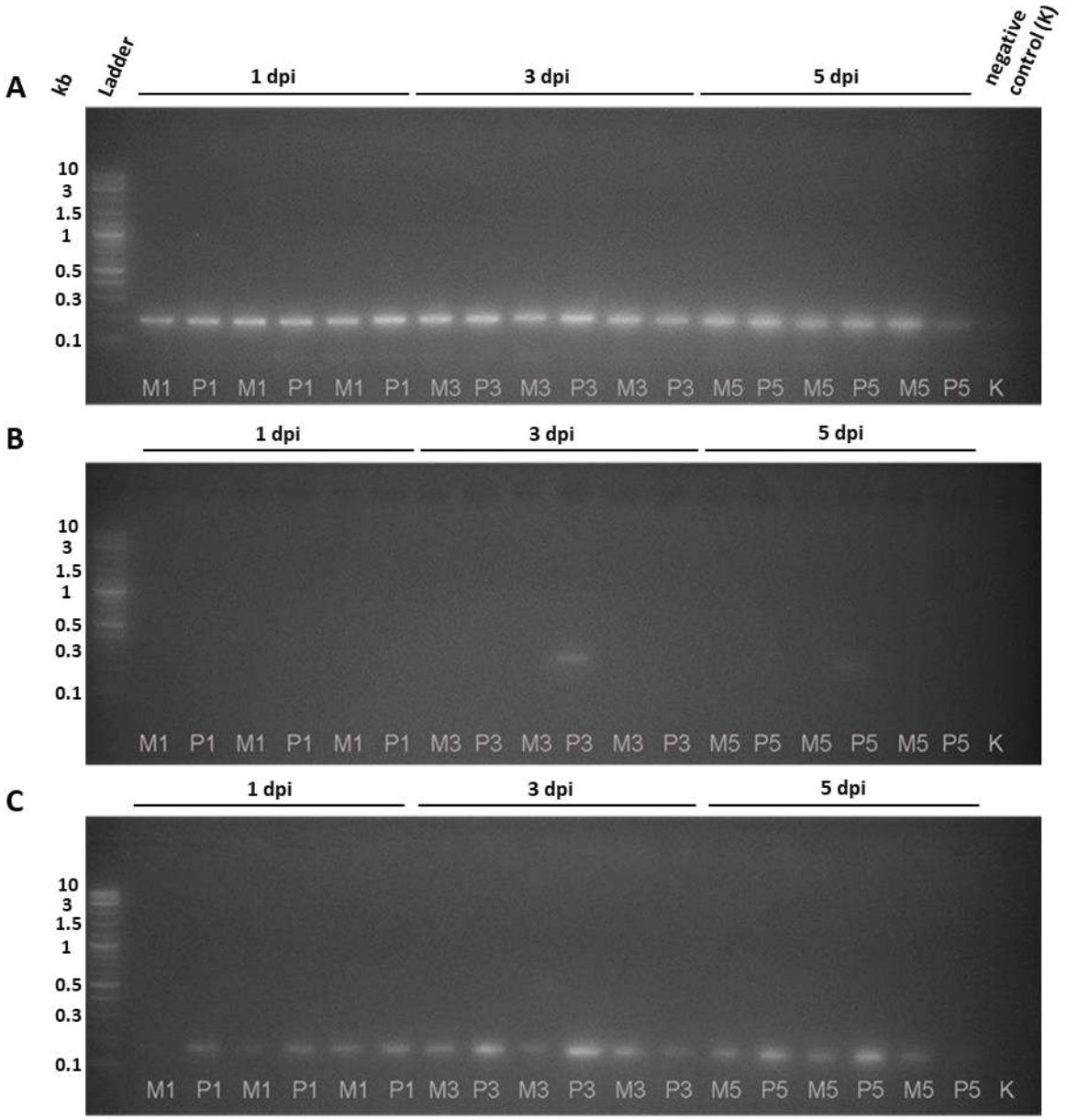

Suppl. Figure 2: Visual evaluation of *Cucumis sativus ACTIN*, *FMO1* and *ALD1* PCR products of *Psl* (P) infected and $MgCl_2$ (M) treatments. Sampling was performed 1 dpi, 3 dpi and 5 dpi, RNA was extracted, and cDNA syntheses were performed. (**A**) To ensure transcription, *C. sativus ACT* PCRs were performed. Additionally, PCRs for the *C. sativus* (**B**) *FMO1* and (**C**) *ALD1* genes were performed for semi-quantitative expression analyses. For each primer pair a negative control (K) was performed using water instead of cDNA as a template. All PCR products were evaluated on 2% agarose gels and visualized via UV-light. The Quick-Load® Purple 1kb Plus DNA Ladder (New England BioLabs) was used as size marker.

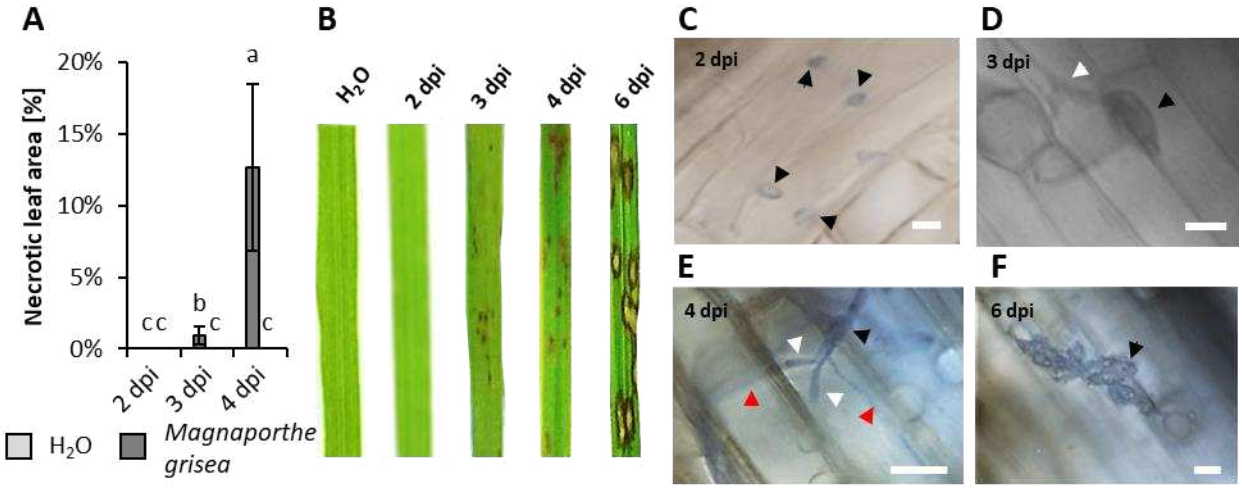

Suppl. Figure 3: Successful establishment of a *Magnaporthe grisea* (*Mgri*) infection in *Brachypodium distachyon*. Three-week-old *B. distachyon* plants were sprayed with a *Mgri* solution (50 spores/µl) or H_2O as a control treatment. (**A**) The *B. distachyon* resistance against *Mgri* was assessed in leaves 2, 3,4 and 6 dpi. Therefore, the leaves were destained from chlorophyl, pictures were taken, and the necrotic area was determined per leaf surface in %. For each investigated sampling timepoint and treatment five individual replicates were used. Mean values ± standard deviations are represented by bars. Letters above bars indicate the statistical differences investigated with an ANOVA in SPSS. (**B**) Pictures of the *Mgri* inoculated and control leaves of *B. distachyon* plants were additionally taken before the destaining processes to investigate the disease progression macroscopically. No necrotic lesions were observed on H_2O treated plants, but *B. distachyon* plants that were sprayed with *Mgri* spores developed brownish lesions with dark edges starting 3 dpi which spread until 6 dpi and in even later infection stages covered the hole leaf (**C-F**) After the *Mgri* infected and H_2O control leaves were destained and pictures were taken, leaves were stained with trypan blue to visualize *Mgri* infection structures microscopically in *B. distachyon* leaves (scale bar = 0.02mm). (**C**) In *Mgri* inoculated, trypan blue stained leaves that were sampled 2 dpi no disease symptoms were detected but the microscopic visualization of *Mgri* infection structures revealed that *Mgri* conidia (black arrows) covered the surface of the leaves. (**D**) In the *Mgri* sprayed leaves bulbous hyphae (white arrows) emerging from conidia (black arrows) were first observed 3 dpi. (**E**) Filamentous *Mgri* hyphae (red arrow) growing through cell walls were first observed 4 dpi. (**F**) Fully developed conidiophores were first observed in *Mgri* treated *B. distachyon* leaves 6 dpi, indicating *Mgri* has fulfilled its lifecycle in *B. distachyon*.

7.2 Part II

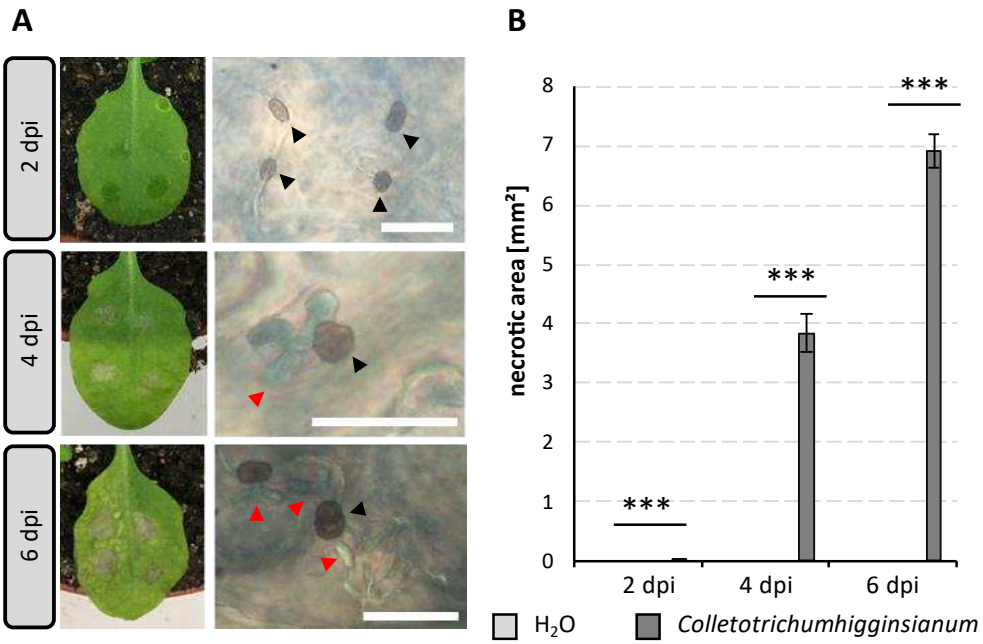

Suppl. Figure 4: Verification of a successful *Colletotrichum higginsianum* (*Chig*) infection *in Arabidopsis thaliana*. Micro- and macroscopic time-course analyses of the *Chig* infection in *A. thaliana*. 4,5-week-old plants were droplet infected with a *Chig* spore solution (500 conidia/µl) or H_2O as a control. (**A**) 2 dpi, 4 dpi and 6 dpi pictures of inoculated leaves were taken before and after sampling. (**B**) To determine the necrotic area of the leaves pictures of planar leaves which were taken after sampling were used. In *Chig* infected leaves the necrotic area increases while no necrosis was detected on control leaves at the same sampling time point indicating a successful *Chig* infection in the investigated *A. thaliana* leaves. (**A**) Harvested leaves were stained with trypan blue to visualize *Chig* infection structures in *A. thaliana* leaves (scale = 20 µm). At 2 dpi *Chig* conidia (black arrows) were observed on the leaves surface, 4 dpi biotrophic hyphae (red arrow) start to grow in the cell underneath a conidium (black arrow) and, 6 dpi necrotrophic hyphae (red arrows) start to grow intra- and intercellularly underneath a conidium (black arrow).

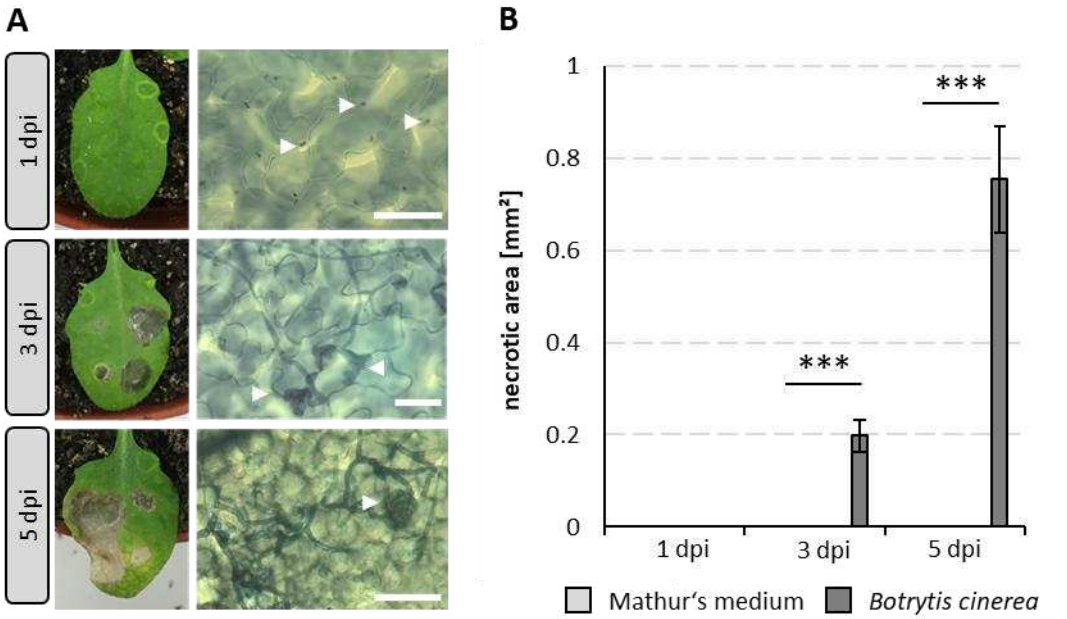

Suppl. Figure 5: Verification of a successful *Botrytis cinerea* (*Bcin*) infection in *Arabidopsis thaliana*. Micro- and macroscopic time-course analyses of the *Bcin* infection in *A. thaliana*. 4,5-week-old plants were droplet infected with a *Bcin* spore solution (50 conidia/µl) or Mathur's medium as a control. (**A**) Pictures of inoculated leaves were taken 1 dpi, 3 dpi and 5 dpi before and after sampling. (**B**) Pictures of planar leaves after sampling were used to determine the necrotic area of the leaves. In *Bcin* infected leaves the necrotic area is increasing while no necrosis was observed on control leaves at the same sampling time point indicating a successful *Bcin* infection in the investigated *A. thaliana* leaves. (**A**) Afterwards leaves were stained with trypan blue to visualize *Bcin* infection structures in *A. thaliana* leaves. At 1 dpi (scale = 50 µm) spores (arrows) were observed on the leaves surface, 3 dpi (scale = 100 µm) inter- and intracellular hyphae growth was visible (arrows) and, 5 dpi (scale = 100 µm) conidiophores carrying conidia (arrow) were spotted. Since no ascospores or sclerotia were identified in trypan blue stained leaves these results indicate that *Bcin* has full filled its asexual lifecycle in *A. thaliana* leaves within the observed 5 dpi.

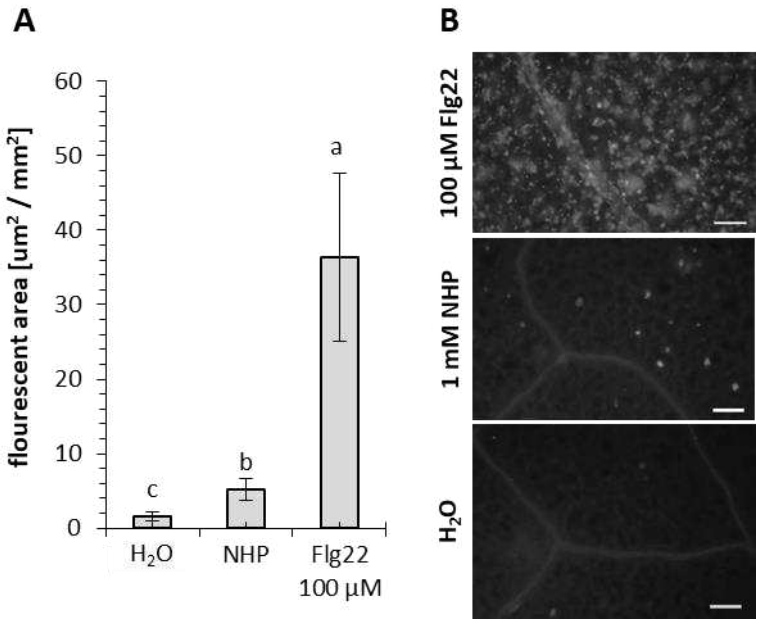

Suppl. Figure 6: The chemical induction of callose deposition in *A. thaliana*. 4,5-week-old plants watered with H_2O as control treatment, a 1 mM NHP solution or a 100 µM Flagellin 22 (Flg22) solution. Samples were taken 2 dpi (n = 3), stained with aniline blue and callose deposits were visualized via fluorescence microscopy and pictures were taken with Zen Software. Using ImageJ, fluorescent areas were quantified per mm^2 and statistical differences between the treatments were calculated with the Kruskal-Wallis Test in SPSS.

7.3 Part III

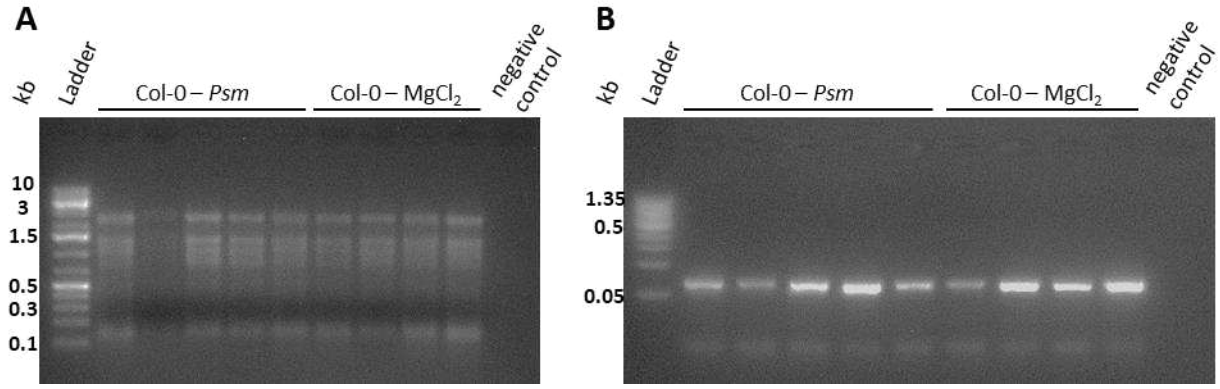

Suppl. Figure 8: Generation of an *Arabidopsis thaliana* DNA template for the NPR1 cloning procedure. 5-week-old *A. thaliana* plants were treated with *Pseudomonas syringae* pv. maculicola (*Psm*) bacteria or $MgCl_2$ as a control treatment and samples were taken 2 dpi (**A**) RNA was extracted, extracts were mixed with loading buffer and the RNA quality was evaluated on a 1.5% agarose gel. The loading buffer without RNA served as negative control. The Quick-Load® Purple 1kb Plus DNA Ladder (New England BioLabs) was applied as size marker. (**B**) cDNA syntheses were performed and to ensure transcription *PTB* PCRs were performed. The amplified PCR products were evaluated on a 1 % agarose gel. In the negative control water was used as a template instead of cDNA. Bands were visualized under UV-light.

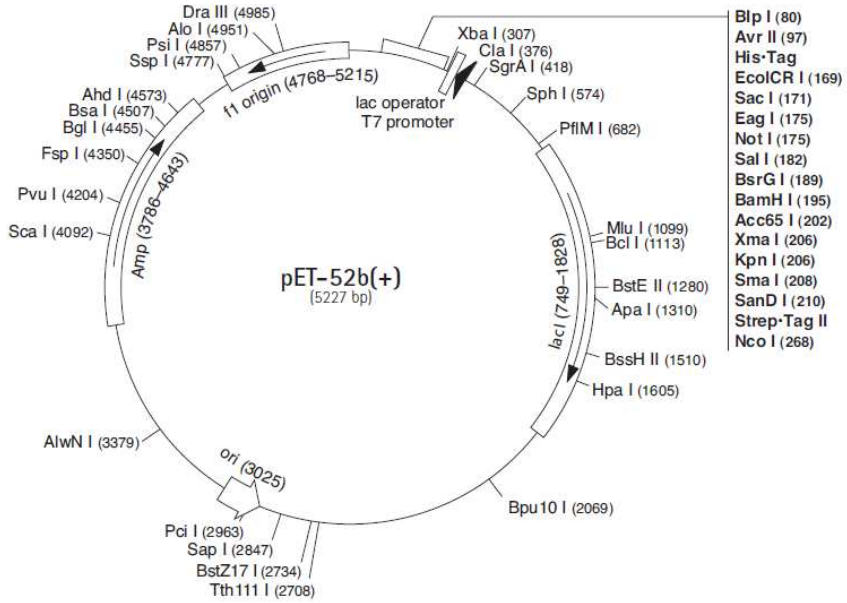

Suppl. Figure 9: The pET52b(+) vector structure. With a Xma I and Sac I digestion the vector was linearized for cloning. With primers for the T7 promotor sequence, positive clones were sequenced to ensure accurate cloning of the *A. thaliana* NPR1 sequence in frame.

A

NPR1

Molecular weight	66031	g/mol
	66.031	kDA
pmol/ug	15.14	pmol
pmol/50 ug	757.22	pmol
pmol/15 ug	252.41	pmol

SA

Molecular weight	138,12 g/mol
100 nM solution	0.1 pmol/ul
200 nM in 50 µl	10 pmol
500 nM in 50 µl	25 pmol

B

	NPR1 input [pmol]	SA input [pmol]	NPR1 bound SA [%]	NPR1 bound SA [pmol]	NPR1 protein able to bind SA [%]
Experiment 1 (Figure 37)	252.41	10	31.01	3.1	**1.23%**
Experiment 2 (Figure 38)	252.41	25	37.8	9.5	**3.76%**

Suppl. Figure 10: Calculation of the molar 1:1 binding ratio of NPR1 and SA. (**A**) To calculate the binding ratio of NPR1 and SA in this study the input of NPR1 and SA in SEC binding assays was calculated in pmol. To correct the input amount of NPR1 protein, the proportion of full-length protein in 50 µg purified NPR1 protein was measured visually on western blots. The relative abundance of the bands showed that one-third and thereby approximately 15 µg of 50 µg NPR1 protein input represent the full-length protein (for example Figure 36.B, Anti-HRP western blot). (**B**) Assuming, that only the full-length protein has full SA or NHP binding capacity the amount of 15 µg NPR1 protein input was set relative to the detected NPR1 bound SA. This calculation shows that in independent binding experiments in this study 1.2% - 3.8% of the *E. coli* expressed Strep-NPR1 protein bound a SA molecule.

8. Abbreviations

A.	*Arabidopsis*
AA	amino acids
ABA	abscisic acid
ALD1	AGD2-LIKE DEFENSE RESPONSE PROTEIN1
avir	*avirulence*
B.	*Brachypodium*
BA	benzoic acid
Bcin	*Botrytis cinerea* B05.10
bp	base pair
BSMT	salicylic acid/benzoic acid carboxyl methyltransferase
C.	*Cucumis*
CA	chorismic acid
cDNA	complementary DNA
cfu	colony forming units
Chig	*Colletotrichum higginsianum* WT063A
CM	chorismate mutase
CoA	coenzyme A
Col	Columbia
DHBA	dihydroxybenzoic acid
dpi	day post inoculation
EDS	ENHANCED DISEASE SUSCEPTIBILITY
EDTA	ethylendiaminetetraacetic acid

EIC	extracted ion chromatogram
ET	ethylene
ETI	effector-triggered immunity
FMO1	FLAVIN-DEPENDENT MONOOXYGENASE 1
FW	fresh weight
GFP	green fluorescent protein
Glc	glucose
h	hour
H.	*Hordeum*
Hpa	*Hyaloperonospora arabidopsidis* Noco2
hpi	hours post inoculation
HR	hypersensitive response
IAA	indole acetic acid, auxin
IC	isochorismic acid
ICA	indole-3-carboxylic acid
ICC	indole-3-carbaldehyde
ICS1	ISOCHORISMATE SYNTHASE 1
IR	induced resistance
JA	jasmonic acid
JA-Ile	jasmonoyl-isoleucine
LRR	leucine-rich repeat
M	$mol*l^{-1}$
m/z	mass-to-charge ratio
M+	molecular ion

MAMP	microorganism-associated molecular patterns
MAP	mitogen-activated protein
MAPK/MPK	mitogen activated protein kinase
MeOH	methanol
MeSA	methyl salicylate
Mgri	*Magnatporthe grisea* Guy11
min	minute
Mory	*Magnatporthe oryzae* TH6772
mRNA	messenger RNA
MSTFA	*N*-Methyl-*N*-(trimethylsilyl)trifluoroacetamide
MW	mass weight
N.	*Nicotiana*
n.d.	not detected
NahG	salicylate hydroxylase 191 from *Pseudomonas putida*
NB	nucleotide-binding site domain
NB-LRR	nucleotide-binding–leucine rich repeats
NDR1	NON RACE SPECIFIC DISEASE RESISTANCE 1
NHP	*N*-hydroxypipecolic acid
NLR	NB and LRR-containing protein
NPR1	NON-EXPRESSOR OF PR GENES 1
ON	overnight
OPDA	*cis-12-oxo-phytodienoic acid*
PAL	phenylalanine ammonia-lyase
PAMP	pathogen-associated molecular patterns

PBS3	AvrPphB SUSEPTIBLE 3
PCR	polymerase chain reaction
Pip	pipecolic acid
PR	pathogenesis-related
PRR	pattern recognition receptors
Psl	*Pseudomonas syringae* pv. lachrymans
Psm	*Pseudomonas syringae* pv. maculicola ES4326
Psm avir	*Pseudomonas syringae* pv. maculicola ES4326 avrRpm1
Psm lux	*Pseudomonas syringae* pv. maculicola luxCDABE
Pstb	*Pseudomonas syringae* pv. tabaci DSM 1856
PTI	PAMP-triggered immunity
pv.	pathovar
qPCR	quantitative PCR
R	resistance
rmp	rounds per minute
ROS	reactive oxygen species
RT	retention time
SA	salicylic acid
SAG	salicylic acid 2-*O*-ß-D-glucoside
SAGT	salicylic acid glucosyltransferases
SAR	systemic acquired resistance
SARD4	SAR-DEFICIENT 4
Sclero	*Sclerotinia sclerotiorum*
SD	standard deviation

SGE	salicyloyl glucose ester
SID	salicylic acid induction deficient
T3SS	bacterial Type-III secretion system
TAE	tris-acetate-ethylenediamine tetraacetic acid
*t*CA	*trans*-cinnamic acid
tDNA	transposable DNA
TIC	total ion chromatogram
TMCS	trimethylsilyl chloride
TMS	trimethylsilylation
TMV	tobacco mosaic virus
UGT	UDP-dependent glycosyltransferases
v/v	volume per volume
w/v	weight per volume
Xtra	*Xanthomonas translucens* DSM 18974
YFP	yellow fluorescent protein

9. APPENDIX

9.1 Curriculum vitae

Name of birth: Anika Schnake

Date and place of birth: 30.07.1990, Bremen, Germany

NON-ACADEMIC POSITSIONS

Costumer Solution Manager, MDx - Nordwest
QIAGEN GmbH, Hilden — July 2022 - today

ACADEMIC EDUCATION

Heinrich-Heine-University, Düsseldorf, Germany — July 2018 - today

PhD thesis: „The role of N-Hydroxypipecolic acid in plant resistance“
Supervisor: Prof. Dr. Jürgen Zeier, Institute for Molecular Ecophysiology of Plants, Heinrich-Heine-University, Düsseldorf, Germany

Heinrich-Heine-University, Düsseldorf, Germany — April 2016 -
(Dalhousie University, Halifax, Kanada) — October 2018
Degree: M.Sc. Biologie

Master thesis: “Establishment of the infection of peas with *Aphanomyces euteiches* and the expression of the small RNA biogenesis machinery during its infection”

Supervisor: Prof. Dr. Laura Rose, Institut for population genetics, Heinrich-Heine-University, Düsseldorf, Germany
Prof. Dr. Claudio Slamovits, Department of Biochemistry and Molecular Biology, Dalhousie University, Halifax, Canada

Heinrich-Heine-University, Düsseldorf, Germany — October 2010 -
Degree B.Sc. Biologie — April 2016

Bachelor thesis: “Analyses of *Phytophthora infestans* strain IPO-C infection success and life cycle in different tomato species“
Supervisor: Dr. Laura Rose, Institute for Population Genetics

ACADEMIC POSITIONS

Research Associate, Heinrich Heine University, Düsseldorf — July 2018 -
Under the supervision of Prof. Dr. Jürgen Zeier — December 2021
Institute for Molecular Ecophysiology of Plants

Research Assistant, Heinrich Heine University, Düsseldorf April – June 2018
Co-supervision of the master course " Plant-Environment Interaction".
Under the supervision of Prof. Dr. Jürgen Zeier
Institute for Molecular Ecophysiology of Plants

Research Assistant, Heinrich Heine University, Düsseldorf April – June 2017
Co-supervision of the master course " Plant-Environment Interaction".
Under the supervision of Prof. Dr. Jürgen Zeier
Institute for Molecular Ecophysiology of Plants

Student Assistent, Heinrich Heine University, Düsseldorf Mai – August 2016
Under the supervision of Prof. Dr. Laura Rose
Institute for Population Genetics

Research Intern, Malta Aquaculture Research Center, Marsaxlokk, Malta June 2014
Under the supervision of Dr. Robert Vassallo Agius

STIPENDS

Hedwig und Waldemar Hort Stipend 2017
Funding for a three-month internship abroad from the Society of Friends and Supporters of the University of Düsseldorf

TEACHING

Supervision of the master course " Plant-Environment-Interaction" August 2021
Institute of Molecular Ecophysiology of Plants, Heinrich-Heine University, Düsseldorf
2-week practical course to teach the basics of herbivory and wounding in plants

Supervision of the master course " Plant-Environment-Interaction" August 2020
Institute of Molecular Ecophysiology of Plants, Heinrich-Heine University, Düsseldorf
2-week practical course to teach the basics of herbivory and wounding in plants

Supervision of the master course " Plant-Environment-Interaction" June 2019
Institute of Molecular Ecophysiology of Plants, Heinrich-Heine University, Düsseldorf
1-week practical course to teach the basics of herbivory and wounding in plants

Supervision of bachelor and master students, Heinrich-Heine University, Düsseldorf: Jana Malik (B.Sc., 2019), Lisa Brahmann (B.Sc., 2020), Paula Luisa Timmermanns (B.Sc., 2021), Mona Strauss (B.Sc., 2021), Alexander Gerstel (B.Sc., 2021), Jana Malik (M.Sc., 2021)

PUBLICATIONS

(5) Hornbergs, J., Montag, K., Loschwitz, J., Mohr, I., Poschmann, G., **Schnake, A**., Gratz, R., Brumbarova T., Eutebach M., Angrand K., Fink-Straube C., Stühler K., Zeier J., Hartmann L., Strodel B., Ivanov R., Bauer, P. (2023). SEC14-GOLD protein PATELLIN2 binds IRON-REGULATED TRANSPORTER1 linking root iron uptake to vitamin E. Plant physiology, 192(1), 504-526.

(4) **Schnake, A**., Hartmann, M., Schreiber, S., Malik, J., Brahmann, L., Yildiz, I., von Dahlen, J., Rose, L.E., Schaffrath, U., Zeier, J. (2020). Inducible biosynthesis and immune function of the systemic

acquired resistance inducer N-hydroxypipecolic acid in monocotyledonous and dicotyledonous plants. *Journal of experimental botany*, *71*(20), 6444-6459.

(3) de Vries, S., von Dahlen, J. K., **Schnake, A**., Ginschel, S., Schulz, B., Rose, L. E. (2018). Broad-spectrum inhibition of *Phytophthora infestans* by fungal endophytes. *FEMS microbiology ecology*, *94*(4), fiy037.

(2) de Vries, S., Kukuk, A., von Dahlen, J. K., **Schnake, A**., Kloesges, T., Rose, L. E. (2018). Expression profiling across wild and cultivated tomatoes supports the relevance of early miR482/2118 suppression for *Phytophthora* resistance. *Proceedings of the Royal Society B: Biological Sciences*, *285*(1873), 20172560.

(1) de Vries, S., von Dahlen J.K., Uhlmann C., **Schnake A.**, Kloesges T., Rose L. E. (2017). Signatures of selection and host-adapted gene expression of the *Phytophthora infestans* RNA silencing suppressor PSR2. *Molecular Plant Pathology*, 18(1), 110-124.

9.2 Acknowledgements

Foremost, I would like to express my sincere gratitude to Professor Dr. Zeier, head of the Institute of Molecular Ecophysiology of Plants, for giving me the opportunity and support to conduct my doctoral thesis. I am very thankful for the guidance and encouragement in the last years. Very special thanks go out to Prof. Dr. Laura Rose, head of the Institute for Population Genetics, for her support as a mentor during my PhD and long before.

I also want to thank all former and recent group members of the Institute of Molecular Ecophysiology of Plants for the great time I had, working with you all. I want to thank Michael Hartmann for the patient guidance, support of my projects and for the great teamwork. A very special thanks also go out to Ipek Yildiz, for being the best colleagues one could ask for. I am really happy that we were able to share this experience. I would also like to thank Nicola Scholten for her support in the lab and with this thesis. Furthermore, I would like to thank Karin Kiefer for her kindness, support and openness in the last years. Additional thanks go to all the students I was able to work with and co-supervise: Jana Malik, Lisa Brahmann, Luisa Timmermanns, Mona Strauss and Alex Gerstel. I want to thank Elise Kerckhofs, Katharina Jürgens and Jessica Karasinski for not only being the best lab mates but also for becoming my best friends. I would also like to thank the Institute of Botany for the opportunity to perform my protein purifications in their lab. Special thanks go to Jannik Hornbergs, for his support in the botany lab and great conversations. To work with you all motivated me every day and without your support, I would not have been able to finish this thesis.

Finally, I want to thank my family and friends for their emotional support and considerateness in the last years.

9.3 Eidesstattliche Versicherung

Hiermit erkläre ich, dass ich die heute eingereichte Dissertation selbständig verfasst und keine anderen als die angegebenen Quellen und Hilfsmittel benutzt sowie Zitate kenntlich gemacht habe. Bei den vorliegenden Dissertationen handelt es sich um in Wort und Bild völlig übereinstimmende Exemplare.

Weiterhin erkläre ich, dass digitale Abbildungen nur die originalen Daten enthalten und in keinem Fall inhaltsverändernde Bildbearbeitung vorgenommen wurde.

Düsseldorf, den 14. März 2024

_____

Anika Schnake